Development of intracellular ligands and targeted protein degraders for chemokine receptors and histone deacetylases

Dissertation

zur

Erlangung des Doktorgrades (Dr. rer. nat.)

der

Mathematisch-Naturwissenschaftlichen Fakultät

der

Rheinischen Friedrich-Wilhelms-Universität Bonn

vorgelegt von

Silas Leander Wurnig

aus

Freiburg im Breisgau

Angefertigt mit Genehmigung der Mathematisch-Naturwissenschaftlichen Fakultät der Rheinischen Friedrich-Wilhelms-Universität Bonn

Gutachter/Betreuer: Prof. Dr. Finn K. Hansen

Gutachterin: Prof. Dr. Christa Müller

Gutacher. Prof. Dr. Radoslaw Nowak

Gutachterin: Prof. Dr. Evi Kostenis

Tag der Promotion: 22.08.2025

Erscheinungsjahr: 2025

The experimental part of this work was carried out at the pharmaceutical Institute of the Rheinischen Friedrich-Wilhelms-Universität Bonn, from January 2021 to January 2024, under the supervision of Prof. Dr. Finn K. Hansen.

This thesis was written in the style of a cumulative dissertation and the chapters 2, 3, 4, and 7 were already published.

Max E. Huber, Silas Wurnig, Lara Toy, Corinna Weiler, Nicole Merten, Evi Kostenis, Finn K. Hansen and Matthias Schiedel. Fluorescent Ligands Enable Target Engagement Studies for the Intracellular Allosteric Binding Site of the Chemokine Receptor CXCR2. *J. Med. Chem.* **2023**, *66*, 9916-9933.

Max E. Huber, Silas L. Wurnig, Aurélien F. A. Moumbock, Lara Toy, Evi Kostenis, Ana Alonso Bartolomé, Martyna Szpakowska, Andy Chevigné, Stefan Günther, Finn K. Hansen and Matthias Schiedel. Development of a NanoBRET assay platform to detect intracellular ligands for the chemokine receptors CCR6 and CXCR1. *ChemMedChem* **2024**, e202400284.

Silas L. Wurnig, Max E. Huber, Corinna Weiler, Hanna Baltrukevich, Nicole Merten, Isabel Stötzel, Yinshui Chang, René H. L. Klammer, Dirk Baumjohann, Eva Kiermaier, Peter Kolb, Evi Kostenis, Matthias Schiedel and Finn K. Hansen. A fluorescent probe enables the discovery of improved antagonists targeting the intracellular allosteric binding site of the chemokine receptor CCR7 *J. Med. Chem.* **2025**, *68*, 4, 4308–4333.

Silas L. Wurnig, Maria Hanl, Thomas M. Geiger, Shiyang Zhai, Ina Dressel, Dominika E. Pieńkowska, Radosław P. Nowak, Finn K. Hansen Light-Activatable Photochemically Targeting Chimeras (PHOTACs) Enable the Optical Control of Targeted Protein Degradation of HDAC6 *RSC Med. Chem.*, **2025**, Advance Article

This dissertation was supported by the University of Bonn and BIGS DrugS

Selbstständigkeitserklärung (Declaration of Originality)

Hiermit erkläre ich, dass die vorliegende Dissertation selbstständig und ohne unzulässige Hilfe angefertigt wurde. Ich habe keine anderen Quellen als die im Literaturverzeichnis angeführten genutzt. Sämtliche Textstellen wurden kenntlich gemacht, welche wörtlich oder sinngemäß aus veröffentlichten Schriften entnommen wurden, sowie alle Angaben, die auf mündlichen Auskünften beruhen. Des Weiteren sind alle von anderen Personen bereitgestellten Materialien oder erbrachten Dienstleistungen als solche gekennzeichnet. Unterstützungsleistungen bei der Auswahl und Auswertung des Materials, sowie bei der Erstellung der Manuskripte habe ich von Herrn, Prof. Dr. Finn K. Hansen (Universität Bonn) erhalten. Ich versichere, dass außer den in der Danksagung genannten Personen bei der geistigen Herstellung der vorliegenden Arbeit keine weiteren Personen, insbesondere kein Promotionsberater, beteiligt waren und dass weder unmittelbar noch mittelbar geldwerte Leistungen an Dritte vergeben wurden. Die vorgelegte Arbeit ist weder im Inland noch im Ausland in gleicher oder ähnlicher Form einer anderen Prüfungsbehörde zum Zweck einer Promotion oder eines anderen Prüfungsverfahrens vorgelegt worden. Ich habe keine früheren erfolglosen Promotionsversuche unternommen.

Bonn, der

Silas Leander Wurnig

Acknowledgments

First of all, I want to sincerely thank my mentor and supervisor Prof. Dr. Finn Hansen for his continuous support and encouragement throughout my four years at the University of Bonn.

Secondly, I want to thank Prof. Dr. Christa Müller, Prof. Dr. Evi Kostenis and Prof. Dr. Radosław Nowak for being part of my examining commission and the scientific collaborations that resulted in the papers presented in this dissertation.

Furthermore, I want to give a huge thank you to all (past or present) members of AK Hansen, AK, Bendas and the Assistants of the 7th semester that did the supervision together with me. I will never forgot the great talks and great parties we had together. You made my time at the institute so much better. I want to especially thank Heiko Weber, Felix Feller, Daniel Stopper, and Shiyang Zhai for being the best lab colleagues one could ask for. I will always remember the nice chats we had and the music we listened to.

Lastly, I want to give a huge thank you to my mum Uschi, my dad Karl-Heinz, my grandma Mimi, my aunt Dagmar, my uncle Peter, my cousins Melly and Sebastian and my girlfriend Chiara for always encouraging me to pursue my path. An especially great thank you goes out to my mum for making this all possible. Without you I would not be where I am today, and I will be forever grateful for that.

Sadly, you cannot read this anymore, but this is for you Mimi. I did it. I know that you look down from wherever you are now and you will smile.

Table of contents

List	t of abb	reviations	I
List	t of figu	res	XV
List	t of sch	emesX	VIII
List	t of tab	es	XIX
1	Intro	duction	2
	1.1	G protein-coupled receptors (GPCRs)	3
	1.1.1	GPCR-mediated signal transduction	5
	1.1.2	Chemokine receptors are members of the rhodopsin-like GPCR family	8
	1.1.3	The chemokine receptors CXCR1 and 2	. 10
	1.1.4	The chemokine receptor 6	. 12
	1.1.5	The chemokine receptor 7	14
	1.1.6	Chemokine receptors as drug targets	. 16
:	1.2	PROTACs	23
	1.2.1	PHOTACs: a new class of proximity-inducing tools	. 28
	1.3	Scope of the thesis	30
2.		escent ligands enable target engagement studies for the intracellular allosteric binding s mokine receptor CXCR2	
	2.1	Publication summary	
	2.1	Author contribution	
3.			34
		lopment of a NanoBRET assay platform to detect intracellular ligands for the chemokine CCR6 and CXCR1	. 36
3	3.1	Publication summary	36
3	3.2	Author contribution	. 39
4. allo		orescent probe enables the discovery of improved antagonists targeting the intracellular binding site of the chemokine receptor CCR7	
4	4.1	Publication summary	40
4	4.2	Author Contributions	. 42
5. (CC	•	nesis of novel squaramide-based CCR7 antagonists targeting the chemokine receptor 7	. 44
•	5.1	Design of novel squaramide-based CCR7 antagonists	
	5.1.1		
!	5.2	Biological evaluation of the novel CCR7 antagonists	
		p. = percentual competitive tracer displacement at given concentration	

5.2	2.1	SAR studies on the R ¹ and R ² positions	51
5.2	2.2	SAR studies on the R ³ position	51
5.3		Conclusion	51
5.5		Experimental section	52
5.5	5.1	General information and chemistry	52
5.5	5.2	Synthesis and compound characterization	53
6. De	vel	lopment of PROTACs targeting the chemokine receptor CCR7	74
6.1		Design of PROTACs targeting CCR7	74
6.1	1.1	Synthesis of the E3 ligase ligands	74
6.1	L.2	Synthesis of functionalized PROTAC-linker precursors	76
6.1	L.3	Final assembly of the CCR7 PROTACs	78
6.2		Biological evaluation of the CCR7 PROTACs	85
6.2	2.1	NanoBRET target engagement assays	85
^a Co	om	p. = percentual competitive tracer displacement at given concentration	86
6.2	2.2	ELISA assays	86
6.3		Conclusion	87
6.4		Experimental section	88
6.4	1.1	General information and chemistry	88
6.4	1.2	Synthesis and compound characterization	89
_		Activatable Photochemically Targeting Chimeras (PHOTACs) Enable the Opt	
7.1		Publication summary	114
7.2		Author contributions	116
8. Su	mn	nary and perspective	118
Referer	ice	S	122
Append	lix		142

List of abbreviations

Signs

°C degree Celsius

Numbers

2-CTC 2-chlorotritylchloride

Α

Å angstrom

α alpha, cooperativity

 $A_{2a}AR \hspace{1cm} A_{2a} \hspace{1cm} adenosine \hspace{1cm} receptor \hspace{1cm}$

AbTAC antibody-based targeting chimeras

ACKR1 atypical chemokine receptor 1

AcOH acetic acid

API active pharmaceutical ingredient

Arg arginine

Asp aspartate

ATP adenosine triphosphate

AUTAC autophagy-targeting chimeras

В

 β beta

 $\beta_2 AR$ β_2 adrenergic receptor

B cells bursa-derived cells

Boc *tert*-butyloxycarbonyl

BRD4 bromodomain-containing protein 4

BRET bioluminescence resonance energy transfer

C

C carbon

cAMP cyclic adenosine monophosphate

CCI19 C-C chemokine ligand 19

CCL20 C-C chemokine ligand 20

CCL21 C-C chemokine ligand 21

CCR C-C chemokine receptor

CCR1 C-C-chemokine receptor 1

CCR5 C-C chemokine receptor 5

CCR6 C-C chemokine receptor 6

CCR7 C-C chemokine receptor 7

CCR9 C-C chemokine receptor 9

CD Crohn's disease

CD4⁺ cluster of difference positive

Cdc42 cell division control protein 42 homolog

CDCl₃ deuterated chloroform

cGMP cyclic guanosine monophosphate

COPD chronic obstructive pulmonary disease

CRBN cereblon

Cu copper

CU colitis ulcerosa

CuAAC copper-catalyzed azide-alkyne cycloaddition

CuSO₄ copper sulfate

CXCL12 CXC chemokine ligand 12

CXCR1 CXC chemokine receptor 1

CXCR2 CXC chemokine receptor 2

CXCR4 CXC chemokine receptor 4

D

d doublet

D aspartic acid

Da dalton

DAG diacylglycerol

DCAF11 DDB1- and CUL4-associated factor 11

DCAF16 DDB1- and CUL4-associated factor 16

DCM dichloromethane

DIPEA *N,N*-diisopropylethylamine

DMF N,N-dimethylformamide

DMSO dimethylsulfoxide

DMSO-*d*₆ deuterated dimethylsulfoxide

dr diastereomeric ratio

Ε

E glutamic acid

ε absorption coefficient

E1 ubiquitin-activating enzyme

E2 ubiquitin-conjugating enzyme

E3 ubiquitin ligase

ECL extracellular loop

ELC EBI1-ligand chemokine

eq. equivalent

EtOH ethanol

F

F fluor

FDA Food and Drug Administration

FEM1B Fem-1 homolog 1B

Fmoc fluorenylmethoxycarbonyl

G

g gram

GAG glycosaminoglycan

GDP guanosine diphosphate

GTP guanosine triphosphate

GPCR G protein-coupled receptor

GRK G protein-coupled receptor kinase

GRO-alpha growth-related oncogene alpha

GRO-beta growth-related oncogene beta

Н

h hour

H proton

HBF₄ tetrafluoroboric acid

HATU hexafluorophosphate azabenzotriazole tetramethyluronium

HCI hydrochloric acid

HDAC histone deacetylase

HEK human embryonic kidney cells

hERG human ether-a-go-go-related gene

HEV high endothelial venules

HIV human immunodeficiency virus

HOBt hydroxybenzotriazole

HPLC high-performance liquid chromatography

HRMS-ESI high-resolution electrospray-ionization mass spectra

HyT hydrophobic tag

H₂O water

IABS intracellular allosteric binding site

IAP inhibitor of apoptosis protein

IC₅₀ half-maximal inhibitory concentration

ICL intracellular loop

IL-8 interleukin-8

Ile isoleucine

IMiD immunomodulatory imide drug

IP3 inositol triphosphate

ITC isothermal titration calorimetry

K

K₂CO₃ potassium carbonate

kDa kilodalton

 K_d dissociation constant

KEAP1 kelch-like ECH-associated protein 1

K_i inhibitory constant

K₃PO₄ potassium phosphate

L

 λ lambda

LRMS-ESI low-resolution electrospray-ionization mass spectra

LYTAC lysosome-targeting chimera

M

m multiplet

M molarity

MAPK mitogen-activated protein kinase

MDM2 mouse double minute 2 homolog

MHz megahertz

mL milliliter

MeOH methanol

mmol millimol

min minute

MIP-3α macrophage inflammatory protein 3α

MIP-3β macrophage inflammatory protein 3β

mp melting point

Ν

N asparagine, normality, nitrogen

Na₂CO₃ sodium carbonate

NaHCO₃ sodium hydrogencarbonate

NaNO₂ sodium nitrite

NaOAc sodium acetate

NLuc nanoluciferase

nM nanomolar

NMR nuclear magnetic resonance

0

O oxygen

Ρ

P proline

Pd/C palladium on carbon

 $Pd(dppf)Cl_2 \cdot CH_2Cl_2 \ bis(diphenylphosphino) ferrocene-palladium (II) dichloride-palladium (II) dichloride-palladium$

dichloromethane

Phe phenylalanine

PHOTAC photochemically-targeting chimeras

PKA protein kinase A

PKC protein kinase C

PLC phospholipase C

PIP2 phosphatidylinositol 4,5-bisphosphate

POI protein of interest

PPI protein-protein interaction

ppm parts per million

PROTAC proteolysis-targeting chimera

PyBRoP bromo-tris-pyrrolidino-phosphonium hexafluorophosphate Q quartet q R arginine R rheumatoid arthritis RARac Rho-related C3 botulinum toxin substrate Rf retention factor Rho Ras homolog Ras homolog family member A RhoA ring finger protein 114 RNF114 Rt, rt room temperature S singlet S S serine, sulfur

structure-activity relationship

SAR

Ser serine

Skp-1 S-phase kinase-associated protein

SLC secondary lymphoid-tissue chemokine

S_NAR nucleophilic aromatic substitution reaction

SnCl₂ tin(II) chloride

SPAAC strain-promoted azide alkyne cycloaddition

SPR surface plasmon resonance

T

TBTA tris(benzyltriazolylmethyl)amine

TFA trifluoroacetic acid

THF tetrahydrofuran

t triplet

TAMRA 5(6)-carboxytetramethylrhodamine

t_{1/2} half-life time

T cells thymus derived cells

Th17 helper T-cell 17

Thr threonine

TiO₂ titanium dioxide

Ti(OEt)₄ titanium ethoxide

TLC thin layer chromatography

TM transmembrane

TNBS 2,4,6-trinitrobenzenesulfonic acid

Tregs regulatory T-cells

Tyr tyrosine

U

Ub ubiquitin

UPS ubiquitin-proteasome system

UV ultraviolet

٧

V volume

Val valine

W

 $\omega \qquad \qquad \text{omega}$

Υ

γ gamma

μm micrometer

 μOR μ opioid receptor

Y tyrosine

List of figures

Figure 1 . Share of GPCR-based targets for drugs on the market. Reprinted with permission from Ma, F. and Zemmel, R. Value of Novelty? Nat. Rev. Drug Discov. 2002, 571-572 (2)
Figure 2. Illustration of a GPCR receptor in the lipid bilayer with the associated G proteins. Created with BioRender
Figure 3 Phylogenetric tree of GPCRs according to the GRAFS classification system. Reprinted with permission from Chen, Y. and Palczewski, K. Systems Pharmacology Links GPCRs with Retinal Degenerative Disorders. <i>Annu. Rev. Pharmacol. Toxicol.</i> 2016, 273-298
Figure 4 . Conformational changes in class A GPCRs upon activation. Three class A GPCRs captured in their crystallographic inactive and active conformations reveal similar conformational changes upon activation. TM6 is highlighted. M2 is the M2 muscarinic acetylcholine receptor and μ OR is the μ -opioid receptor. Reprinted with permission from Latorraca, N. A.; Venkatakrishnan, A. J. and Dror, R. O. GPCR Dynamics: Structures in Motion. Chem. Rev. 2017, 139-155
Figure 5. Outline of GPCR activation. Upon agonist binding to a GPCR the GDP bound to the $G\alpha$ subunit is replaced by GTP. This induces the dissociation of the α and the beta-gamma subunit and subsequent binding to the their effector proteins. Prolonged activation of a GPCR induces the activations of GRKs that phosphorylate serine and threonine residues at the intracellular side of the receptor. Binding of arrestin proteins to the phosphorylated receptor leads to clathrin-mediated internalization of the receptor. The internalized receptor is then either dephosphorylated and recycled or degraded. Reprinted with permission from Weis, W. I. and Kobilka, B. K. The Molecular Basis of G Protein-coupled Receptor Activation. <i>Annu. Rev. Biochem.</i> 2018, 897-919. (9)
Figure 6. The structure of chemokines and their respective receptors they can bind to. A) The CXC class chemokines and their receptors. B) The CC class chemokines and their receptors. C) The C class chemokines and their receptor. D) The CX3C class chemokine and its receptor. Reprinted with permission from Rostene, W.; Kitagbi, P. and Parsadaniantz, S. M. Chemokines: a new class of neuromodulator? <i>Nat. Rev. Neurosci.</i> 2007, 895-904 (92)
Figure 7. Physiological functions of CXCR1/2 and CXCL8. A) Binding of CXCL8 oligomers to GAGs establishes a chemokine gradient towards inflammed areas. B) Removal of non-immobilized CXCL8 by the scavenger receptor ACKR1 expressed on erythrocytes prevents systemic leukocyte activation. C) Translocation of immobilized CXCR1/2 expressing cells and GAG bound CXCL8 by transcytosis directs the immune reaction towards the inflammed areas. D) Synergy of CXCL8 and other chemoattractants to amplify the immune response. This figure is reprinted with the permission from Cambier, S.; Gouwy, M. and Proost, P. The chemokines CXCL8 and CXCL12: molecular and functional properties, role in disease and efforts towards pharmacological intervention. <i>Nat. Cell. Mol. Immunol.</i> 2023, 217-251 (275)
Figure 8. The CCR6 receptor controls the balance between Immunosuppression and inflammation through the CCL20/CCR6 axis with the help of the Treg and Th17 cells. Reprinted with permission from (122) CCR6 as a Potential Target for Therapeutic Antibodies for the Treatment of Inflammatory Diseases. <i>Antibodies</i> . 2023, 30
Figure 9 . The role of CCR7 in the immune system and breast tumor metastasis. A) The role of CCR7 in the immune system. Activation of CCR7 leads to the maturation of dendritic cells and T cells. Both chemokines CCL19 and CCL21 are able to display G-protein signaling but only CCL19 is able to recruit

activation of CCR7 promotes the enhanced survival and proliferation of cancer cells as well as their homing to lymphoid organs where they encounter supportive microenvironments. Reprinted with permission from Rizeq, B. and Malki, M. I. The Role of CCL21/CCR7 Chemokine Axis in Breast Cancer Progression. <i>Cancers</i> . 2020, 1036 (276)
Figure ${f 10.}$ Chemical structure of CCR1 antagonists with their respective K_i values towards CCR1 17
Figure 11. Chemical structures of CCR5 antagonists and their respective binding affinities 18
Figure 12. Chemical structures of CXCR4 antagonists and their respective binding affinities 18
Figure 13 . A) A 3D view of 00767013—CXCR2 interactions from the intracellular side. CXCR2 is shown in blue cartoon and shaded surface, and 00767013 is shown as yellow sticks. Reprinted with permission from Liu, K.; Wu, L.; Yuan, S.; Wu, M.; Xu, Y.; Sun, Q.; Li, S.; Zhao, S.; Hua, T. and Liu, ZJ. Structural basis of CXC chemokine receptor 2 activation and signaling. <i>Nature, 2020</i> , 135-140. (106). B) A 3D view of cmpd2105-CCR7 interactions from the intracellular side. CCR7 is shown in gray and important amino acid residues highlighted in color. Reprinted with permission from Jaeger, K. Bruenle, S.; Weinert, T.; Guba, W.; Muehle, J.; Miyazaki, T.; Weber, M.; Furrer, A.; Haenggi, N.; Tetaz, T.; Huang, CY.; Mattle, D.; Vonach, JM.; Gast, A.; Kuglstatter, A.; Rudolph, M. G.; Nogly, P.; Benz, J.; Dawson, R. J. P. and Standfuss, J. Structural Basis for Allosteric Ligand Recognition in the Human CC Chemokine Receptor 7. <i>Cell.</i> 2022, 1222-1230
Figure 14 . Chemical structures of intracellular CXCR2 antagonists and their respective binding affinities
Figure 15. Intracellular CCR7 antagonists and their respective binding affinites
Figure 16 . Structure of fluorescent tracers for CCR2 and CCR9 with their respective binding affinities.
Figure 17 . PROTAC-mediated degradation of a POI by ternary complex formation with the E2:E3 ubiquitination complex. Reprinted with permission from Sun, X., Gao, H., Yang, Y.; He, M.; Wu, Y.; Song, Y.; Tong, Y. and Rao, Y. PROTACs: great opportunities for academia and industry. <i>Sig Transduct Target Ther.</i> 2019, 64 (230)
Figure 18 . Chemical structures of the PROTACs ARV-110, ARV-417 and DT2216. The E3 ligase is highlighted in orange, the linker is black and the POI ligand is marked in blue
Figure 19 . Determination of cooperativity (α) as the thermodynamic value indicating the likelihood of ternary complex formation. Created with Biorender
Figure 20 . Illustration of the "hook effect". Increasing PROTAC concentrations saturate the E3 ligase and the POI pmpeding the formation of ternary complexes. Created with Biorender
Figure 21 . A) Depiction of the PHOTAC-mediated degradation mechanism. The PHOTAC can be switched between the inactive (orange) or active (red) conformation by irradiation with light. The active PHOTAC can then form ternary complexes with the E3 ligase and the POI to induce proteasomal degradation. Reprinted with permission from Ko, T.; Jou, C.; Grau-Perales, A. B.; Reynders, M. Fenton, A. A. and Trauner, D. Photoactivated Protein Degraders for Optical Control of Synaptic Function. <i>ACS Chem. Neurosci.</i> 2023, 3704-3713. (256) B) Switching of a PHOTAC from the <i>trans-</i> to the <i>cis-</i> state with the wavelengths necessary for the switch.
Figure 22 . Overview of the residues that will be modified during the synthesis of novel chemokine receptor antagonists

(red)
Figure 24 . Proposed six-membered cyclic transition state of the Grignard addition reaction with the Ellman's imine intermediate. (262)
Figure 25 . Common IMiDs and the novel CRBN phenylglutarimide template for the recruitment of the E3 ligase CRBN
Figure 26 . Commercially available thalidomide derivatives
Figure 27. Tested PROTACs do not induce a concentration-dependent reduction of CCR7 or CXCR2 receptor surface level under high cytomegalovirus (CMV)-driven expression per cell. (A) Intact CHO-Flp-In cells stably expressing human CCR7 (hCCR7) were labeled with mouse CCR7 antibody (MAB197). Surface hCCR7 was then visualized with FITC-conjugated goat anti-mouse IgG (green). No membrane fluorescence was observed in parental CHO-Flp-In cells. (B) hCCR7-CHO-Flp-In cells were incubated with vehicle (0.1% DMSO) or PROTAC at the indicated concentrations for 16 h. Plasma-membrane-resident receptor was measured in ELISA using mouse CCR7 antibody (MAB197) and anti-mouse HRP as secondary antibody (n=3 ± SEM, data generated by Max Huber). (C) Nonpermeabilized HEK293 cells stably transfected with human CXCR2 (hCXCR2) were labeled with mouse CXCR2 antibody (MAB331). Surface hCXCR2 was subsequently detected with FITC-conjugated goat anti-mouse IgG (green). No membrane-associated fluorescence was observed in parental HEK293 cells. Nuclei were stained with 4′,6-diamidin-2-phenylindole (DAPI, blue). (D) hCXCR2-HEK293 cells were treated with vehicle (0.1% DMSO) or protac at the indicated concentrations for 16 h. Plasma-membrane-localized receptor was detected in ELISA using mouse CXCR2 antibody (MAB331) and anti-mouse HRP as secondary antibody (n=3 ± SEM). Significant differences were determined by one-way ANOVA with Dunnett's multiple-comparison test. Scale bar is 10 μm
Figure 28. Overview of the most important compounds from chapters 2-7

List of schemes

Scheme 1 . Synthesis of the benzamide part. <i>Reagents and conditions</i> : (a) corresponding amine, PyBroP, DIPEA, DCM, rt, overnight; (b) SnCl ₂ ·H ₂ O, MeOH, reflux, 2 h45
Scheme 2. Synthesis of the primary amines. <i>Reagents and conditions</i> : (a) $Ti(OEt)_4$, DCM, rt, overnight. (b) corresponding alkyl magnesium chloride, tetrahydrofuran (THF), 0 °C to rt, 3 days, 18 - 54% yield over two steps. (c) HCl (in Et_2O), Et_2O , rt, 3 h, quantitative yield
Scheme 3 . Convergent synthesis of ligands targeting CCR7. <i>Reagents and conditions</i> : (a) anilines 4a-e , dimethyl squarate, MeOH, rt, overnight. (b) mono-substituted squaramides 10a-e , primary amine hydrochlorides 9a-d , DIPEA, MeOH, rt, 3 days
Scheme 4. Synthesis of E3 ligase ligands. <i>Reagents and conditions</i> : (a) NaOAc, AcOH, reflux, 4 h; (b) (4-hydroxyphenyl)boronic acid, K_3PO_4 , $Pd(dppf)Cl_2 \cdot CH_2Cl_2$, dioxane/ H_2O , 100 °C, 16 h; (c) <i>tert</i> -butyl bromoacetate, K_2CO_3 , DMF, rt, 4 h; (d) Pd/C , EtOH, rt, 16 h
Scheme 5. Synthesis of the 2-[2-(2-azidoethoxy)ethoxy]ethanamine based PROTAC-linker precursors. Reagents and conditions: (a) DIPEA, DMSO, reflux, 16 h; (b) TFA, DCM, rt, 4 h; (c) PyBroP, DIPEA, DCM, rt, overnight
Scheme 6. Synthesis of the PROTAC-linker precursors based on the 5,6-difluorothalidomide CRBN ligand. <i>Reagents and conditions</i> : (a) DIPEA, DMSO, reflux, 16 h
Scheme 7. Hypothesized mechanism of the CuAAC reaction. Modified from Worrel, Malik and Fokin. (278)78
Scheme 8. Assembly of CCR7 PROTACs using SLW089 as the POI ligand. <i>Reagents and conditions</i> : (+)-sodium L-ascorbate, CuSO ₄ , TBTA, H ₂ O, THF, rt, overnight
Scheme 9 . Assembly of CCR7 PROTACs using SLW007 as the POI ligand. <i>Reagents and conditions</i> : (a) (+)-sodium L-ascorbate, CuSO ₄ , TBTA, H ₂ O, THF, rt, 16 h
Scheme 10 . Synthesis of CCR7 PROTACs with variations in the linker region. <i>Reagents and conditions</i> : (a) TFA, DCM, rt, 4 h; (b) azidoacetic acid, PyBroP, DIPEA, DCM, rt, 16 h; (c) (+)-sodium L-ascorbate, CuSO ₄ , H ₂ O, TBTA, THF, rt, 16 h

List of tables

Table 1. Overview of the synthesized intermediates	. 45
Table 2. Overview of the synthesized furfurylamine intermediates	. 47
Table 3. Overview of the synthesized CCR7 ligands	. 48
Table 4 . Affinity data of the synthesized antagonists for the chemokine receptor CCR7	. 50
Table 5 . Overview of the synthesized PROTACs 25-32 .	. 81
Table 6 . Overview of the synthesized PROTACs based on the squaramide scaffold	. 84
Table 7 . Affinity data of the synthesized PROTACs towards CCR6, CCR7, CXCR1 and CXCR2 obtained by NanoBRET target engagement assays.	

1 Introduction

The transmission of information is one of the fundamental hallmarks in every complex system, whether it's within a living organism or, for instance, in a computer network. Information comes in various forms of encoding and transmission, such as language, images, electric currents, or molecules, especially in biological contexts. For information to be useful, it must be understandable, requiring perception and interpretation. Consequently, living cells necessitate structures to sense and process information in a variety of formats. Analogously, like a vintage tape recorder, there is a need for both a microphone to pick up sound and a tape to record it. A living cell therefore requires specific structures for the recognition and subsequent translation of these information. Without these structures, stimuli remain unused. For instance, unlike some animals like snakes and tilapia, the human body lacks sensory mechanisms for detecting infrared light. In multicellular organisms like humans, animals and fungi, G protein-coupled receptors (GPCRs) serve as crucial microsensors for extracellular stimuli such as small molecules, peptides, proteins, and photons. GPCRs play a pivotal role in signal transduction across cellular membranes, capturing chemical information from the extracellular environment and transmitting it intracellularly for further processing, integration, and cellular response. Upon ligand activation, the GPCR undergoes a conformational rearrangement that is detected by intracellular effectors, triggering a complex network of cellular responses. Given the importance of the GPCR-G protein axis in environmental perception, it is frequently targeted by drugs activating or inhibiting specific GPCRs by mimicking nonexistent information or blocking existing signals. This is highlighted by the fact that approximately 30% of FDA approved drugs currently on the market address GPCRs. (1) (2) Additionally, over 50% of marketed drugs worldwide target GPCRs.

The following introduction provides a general overview to GPCRs in the first part and to chemokine receptors in the second part to provide the fundamental understanding required to understand the published research articles and chapters in this thesis.



Figure 1. Share of GPCR-based targets for drugs on the market. Reprinted with permission from Ma, F. and Zemmel, R. Value of Novelty? Nat. Rev. Drug Discov. 2002, 571-572 (2)

1.1 G protein-coupled receptors (GPCRs)

GPCRs are the largest family of membrane-based proteins with over 800 genes in humans. (3) The common denominator of all GPCRs is their general structure consisting of seven transmembrane (TM1-TM7) helices that traverse the lipid bilayer of the cell membrane. (4) These helices are connected by three extra- and intracellular loops (ECLs and ICLs). The amino terminal end (*N*-terminus) of GPCRs is typically located at the extracellular side and the carboxy-terminal tail (*C*-terminus), is located intracellularly. (4) (5) Many GPCRs bear an eighth α -helix at the C-terminus. (4) (5) This arrangement of α -helices forms the typical barrel-like structure, creating a hydrophilic pocket within the cell membrane. (6) (7) In contrast to other classes of membrane proteins like ion channels or membrane receptors with an intrinsic enzymatic activity, GPCRs rely on interactions with other proteins. (8) According to their name the main intracellular signaling partner for GPCRs are the G proteins. These heterotrimeric guanine nucleotide-binding regulatory proteins consist of the three subunits α , β , and γ . (9) The β and γ subunits form a tightly associated dimer, that can be perceived as one functional signaling unit while the α subunit is capable of signal transduction by itself. (10) The general structure of a GPCR and the G proteins is shown in Figure 2.

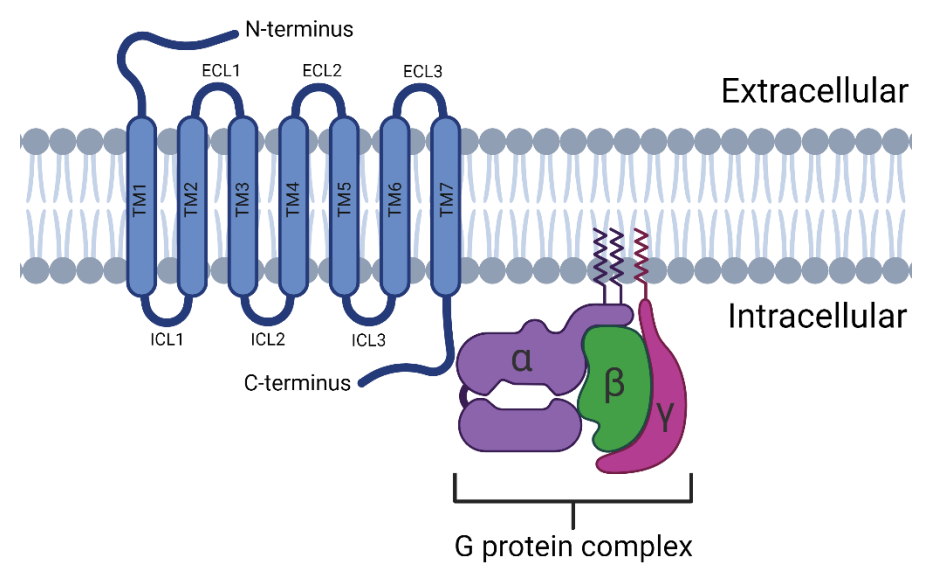


Figure 2. Illustration of a GPCR receptor in the lipid bilayer with the associated G proteins. Created with BioRender.

G proteins can be classified according to their sequence of the $G\alpha$ subtype and their corresponding function. Based on these aspects G proteins are divided into the four classes: $G\alpha_s$, $G\alpha_{i/o}$, $G\alpha_{q/11}$ and $G\alpha_{12/13}$. (11) (12) After binding to a ligand and subsequent activation of an GPCR distinct signaling patterns can occur since one GPCR can couple to several $G\alpha$ isoforms and each $G\alpha$ family is connected with a specific canonical signaling cascade. (13) (14) (15) Despite the vast amount of GPCRs, the family of G proteins encompasses only a small variety of different isotypes. (16) This becomes evident by the fact that all three subunits

are coded by a total of 33 genes. The $G\alpha$ subunit, encoded by 16 different genes, is the biggest class of G proteins. The $G\beta$ subunit with 5 genes and the $G\gamma$ subunit with 12 genes make up the rest. (17) (8) This is a strong indication that G protein activation is a highly conserved process among the GPCR family. This is further solidified by the comparably low diversity within the intracellular regions of the GPCRs, where G proteins typically bind. (18) (19)

GPCRs are clustered into five major classes based on their sequence similarity. Two of the main classification systems are the differentiation into the A-F classes or the **GRAFS** system. (20) (21) The phylogenetic tree of the **GRAFS** system is shown in Figure 3. This system is especially useful when human GPCRs are the main focus of the research. (21) The categories are as following:

- **G** metabotropic glutamate receptors
- R rhodopsin-like receptors
- A adhesion receptors
- F frizzled/taste 2 receptors
- S secretin-like receptors

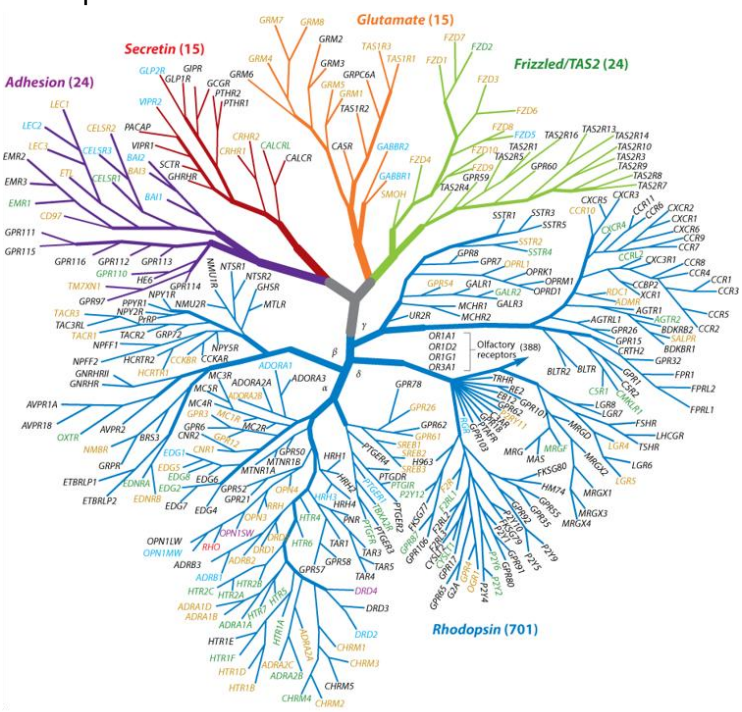


Figure **3** Phylogenetric tree of GPCRs according to the GRAFS classification system. Reprinted with permission from Chen, Y. and Palczewski, K. Systems Pharmacology Links GPCRs with Retinal Degenerative Disorders. *Annu. Rev. Pharmacol. Toxicol.* 2016, 273-298.

While the GPCR gene family stands out as the largest among membrane proteins, crucial residues remain highly conserved across the GPCR family. To facilitate comparison of structural elements across different receptors, the Ballesteros-Weinstein nomenclature for

residue labeling is employed. (22) In this system, the most conserved residue X within helix n is denoted as $X^{n.50}$, with N-terminal residues preceding $X^{n.50}$ labeled with decreasing numbers and C-terminal residues following $X^{n.50}$ labeled with increasing numbers. For instance, the DRY motif found in the adenosine A_{2A} receptor would be designated as $D^{3.49}$, $R^{3.50}$, and $Y^{3.51}$ rather than D101, R102, and Y103.

1.1.1 GPCR-mediated signal transduction

The signaling pathways associated with GPCRs present a greater level of complexity than what linear signaling pathways might suggest. This complexity arises from various factors such as the cross-talk between multiple intracellular signaling cascades, the receptor's adoption of multiple conformational states that cannot be simply classified as active or inactive, the ability of GPCRs to 1) form both homomeric and heteromeric complexes with other receptors, which results in altered signaling patterns and 2) the spatiotemporal compartmentalization of signaling proteins. (15) (23) (24) (25) (26) Consequently, a single compound acting on the same receptor subtype may elicit different effects in distinct cell types, tissues, and animal models. Therefore, it is crucial to carefully investigate the effects of each ligand on each individual receptor in every system. (27) While a detailed explanation of these pathways exceeds the scope of this introduction, a brief summary of the typical GPCR-mediated signal transduction pathways is provided to underscore the significant therapeutic implications of GPCRs. (28) (29)

When an agonist binds to the orthosteric binding site of the extracellular domain of the GPCR, it induces a conformational change in the receptor. (5) This can be best described with the analogy of a switch being flipped. The most prominent conformational change is the outward movement of transmembrane helix 6 (TM6) of the receptor. (30) (31) This creates a cavity at the intracellular side of the receptor and enhances interaction and activation of effector proteins. (32) Particularly noteworthy is the effect of G proteins on the displacement. In the presence of bound G proteins the displacement of TM6 is significantly increased, providing a structural basis for the stabilization of an active GPCR state. (33) These conformational changes are evolutionary conserved in microswitches. (34) (35) These include key motifs like the sodium binding pocket at D^{2.50} and S^{3.39}, the DRY motif and the NPxxY motif (N^{7.49}, P^{7.50}, Y^{7.53}). (36) (37) (38) These conserved microswitches transmit the signal from the ligand binding pocket through the receptor to the intracellular domain. The disruption of the ionic lock between

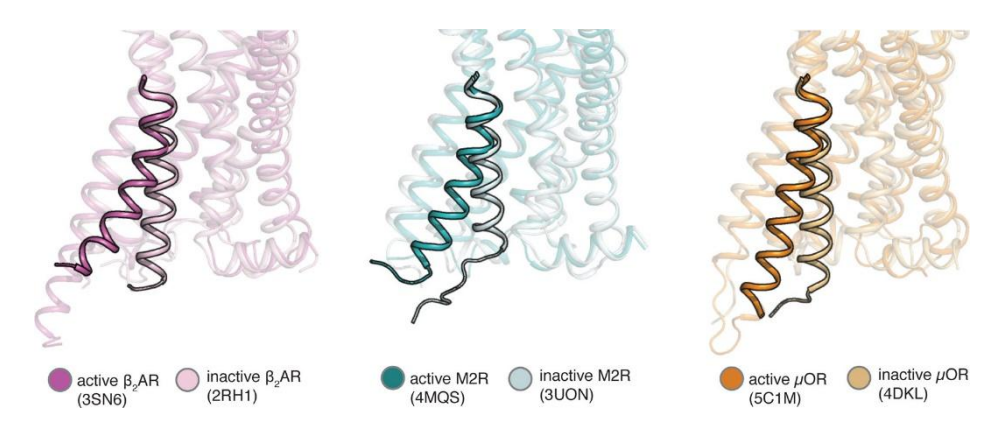


Figure 4. Conformational changes in class A GPCRs upon activation. Three class A GPCRs captured in their crystallographic inactive and active conformations reveal similar conformational changes upon activation. TM6 is highlighted. M2 is the M2 muscarinic acetylcholine receptor and μ OR is the μ -opioid receptor. Reprinted with permission from Latorraca, N. A.; Venkatakrishnan, A. J. and Dror, R. O. GPCR Dynamics: Structures in Motion. Chem. Rev. 2017, 139-155

R3.50 and E6.30 is the last step allowing the TM6 to move outwards by approximately 10 Å. (39) This mechanism is especially well understood for class A GPCRs and may differ from other non-class A GPCRs. These conformational changes promote the exchange of GDP (guanosine diphosphate) bound to the G α subunit to GTP (guanosine triphosphate) by means of an intra-protein network similar to GPCRs. (40) (41) The now active G α subunit dissociates from the G $\beta\gamma$ complex. (42) The activated G α -GTP and G $\beta\gamma$ subunits then interact with and modulate the activity of various effector proteins in the cell. (43) (44) The effect of the different G α subunits can be summarized as following:

- 1. $G\alpha_s$ proteins: $G\alpha_s$ proteins stimulate the production of the secondary messenger cyclic AMP (cAMP) by activating adenylate cyclase. This leads to the activation of protein kinase A (PKA) and subsequent phosphorylation of target proteins. (45) (46)
- 2. $G\alpha_{i/o}$ proteins: $G\alpha_{i/o}$ proteins inhibit the production of cAMP by inhibiting adenylate cyclase. They also activate potassium channels and inhibit calcium channels, leading to hyperpolarization and decreased intracellular calcium levels, respectively. (47) (48)
- 3. $G\alpha_{q/11}$ proteins: $G\alpha_{q/11}$ proteins activate phospholipase C (PLC), leading to the hydrolysis of phosphatidylinositol 4,5-bisphosphate (PIP₂) into inositol 1,4,5-trisphosphate (IP₃) and diacylglycerol (DAG). IP₃ triggers the release of calcium from intracellular stores, while DAG activates protein kinase C (PKC). (49) (50)
- Gα_{12/13} proteins: Gα_{12/13} proteins regulate cytoskeletal rearrangements and cell migration by activating Rho GTPases, such as RhoA, Rac, and Cdc42. They also modulate cell adhesion, apoptosis, and cell polarity. (51) (52)

Even though the $G\beta\gamma$ subunit does not have a catalytic site it still acts as a modulator of G protein signaling through tightly regulated protein-protein interactions *e.g.* protein kinases like mitogen-activated protein kinases (MAPKs) and G protein-coupled receptor kinases (GRKs). (53) (54) (55) (56)

The attenuation of the signaling cascade is mediated by two different pathways. The GRKs phosphorylate serine and threonine residues on the intracellular side of the GPCR. (57) This acts as a signal for the recruitment of Arrestins 1-4. (58) This 48kDa large family consists of four isoforms. Arrestin 1 and 4 are exclusively expressed in retinal cells, while the other two arrestins (2 and 3) are widely expressed in the human body. (59) β -Arrestins bind to the GPCRs phosphorylated by GRKs for example, therefore preventing the binding of further G-proteins by the active receptor. (60) (61) This promotes the clathrin-mediated internalization of the GPCR. (62) The second attenuation pathway lies in the intrinsic GTPase activity of G α proteins. This GTPase catalyzes the hydrolysis of GTP to GDP and inorganic phosphate (P_i). (63) (64) The GDP-bound G α protein can now reassociate with the beta-gamma subunit and is ready for a new cycle of activation. (65) The next section will focus on the chemokine receptors as members of the rhodopsin-like GPCRs.

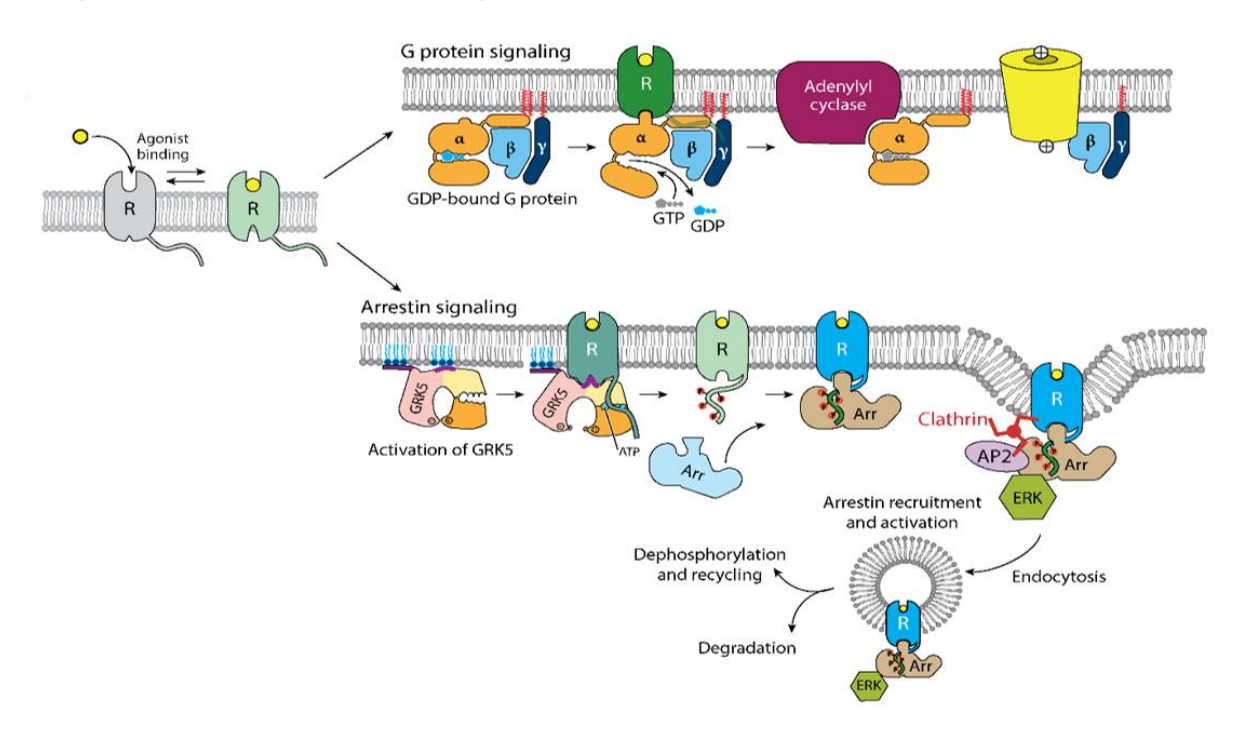


Figure **5.** Outline of GPCR activation. Upon agonist binding to a GPCR the GDP bound to the G α subunit is replaced by GTP. This induces the dissociation of the α and the beta-gamma subunit and subsequent binding to the their effector proteins. Prolonged activation of a GPCR induces the activations of GRKs that phosphorylate serine and threonine residues at the intracellular side of the receptor. Binding of arrestin proteins to the phosphorylated receptor leads to clathrin-mediated internalization of the receptor. The internalized receptor is then either dephosphorylated and recycled or degraded. Reprinted with permission from Weis, W. I. and Kobilka, B. K. The Molecular Basis of G Protein-coupled Receptor Activation. *Annu. Rev. Biochem.* 2018, 897-919. (9)

1.1.2 Chemokine receptors are members of the rhodopsin-like GPCR family

Chemokine receptors play an essential role in maintaining the homeostasis of the immune system. (66) This is done by orchestrating the trafficking and positioning of immune cells throughout the body. (67) Through interactions with their corresponding chemokine ligands, chemokine receptors regulate the recruitment, activation, differentiation, and survival of various immune cells such as T cells, B cells, dendritic cells, macrophages, and neutrophils. (68) (69) (70) Directing immune cells to specific sites of infection, inflammation, or damaged tissue, chemokine receptors ensure an effective immune response while minimizing collateral damage to healthy tissues. (71) (72) Importantly, chemokine receptors also govern the migration of hematopoietic stem cells from the bone marrow into the bloodstream and peripheral tissues. (73) This ensure the replenishment of immune cell population and the maintenance of immune cell homeostasis. (74) Dysfunction of chemokine receptors causes significant disruptions in immune function, contributing to the pathogenesis of various immunerelated diseases such as atherosclerosis, psoriasis, chronic obstructive pulmonary disease (COPD), asthma, and cancer progression. (75) (76) (77) (78) Additionally, these receptors can serve as entry targets for viruses like HIV, further underscoring their indispensability in immune regulation. (79)

Structurally, while chemokine receptors share similarities with other GPCRs of the rhodopsin-like family, including the hallmark seven transmembrane helices and the conserved DRY motific crucial for signal transduction, they exhibit distinct features reflective of their specialized functions. (80) (81) Notably, their pronounced variability at the N-terminal loop and elongated extracellular loops are important for facilitating interactions with chemokine ligands. (82) The complexity of chemokine-based signaling is underscored by the intricate interactions between the 45 chemokines, 18 chemokine receptors and the 4 atypical decoy receptors encoded by the human gene. (83) They are classified into the four families C, CC, CXC, and CX₃C, based on the characteristic pattern of cysteine residues in proximity to the amino acid terminus of the mature chemokine where X stands for any amino acid. (84) (67) Within a family of chemokines they are able to bind different chemokine receptors, while chemokine receptors can therefore be activated by different chemokines. (85) This is crucial due to the diverse and important functions of chemokine receptor within the homeostasis of the immune system. The decoy receptors, devoid of G protein activation structures, act as scavengers of chemokines and serve as regulators of immune responses, thereby modulating chemokine signaling. (86) (87)

Chemokines are the natural ligands of chemokine receptors. (88) They represent the largest group of the cytokine family. (89) These 7-12 kDa proteins share <30% sequence identity between the different classes but within the classes the sequence identity can be up to 99%. (90) Although the sequence identity is highly variable, the tertiary structure of chemokines is well conserved due to their intrinsic disulfide bridges between the cysteins. (91) This tertiary structure is highly important for their ability to bind to their receptors. (92) Recognition of chemokines by their receptor is believed to be a two-step mechanism. (93) Firstly, binding of the structured C-terminal end of the chemokine to the unstructured N-terminal end of the receptor and the extracellular loops allows the unstructured N-terminus of the chemokine to target the seven transmembrane helical bundle to stabilize the receptor in the active conformation that facilitates the intracellular signaling. (93) (94) Chemokines can exist as monomers, dimers, and oligomers. (95) Oligomers usually occur by the association of the antiparallel β-strands involving the residues near the N-terminal end including the cysteins. (83) (96) These oligomers are then able to bind to glycosaminoglycans (GAGs). While the chemokines are able to bind and activate the chemokine receptors as monomers, the association of chemokine oligomers to GAGs creates a localized chemokine gradient that

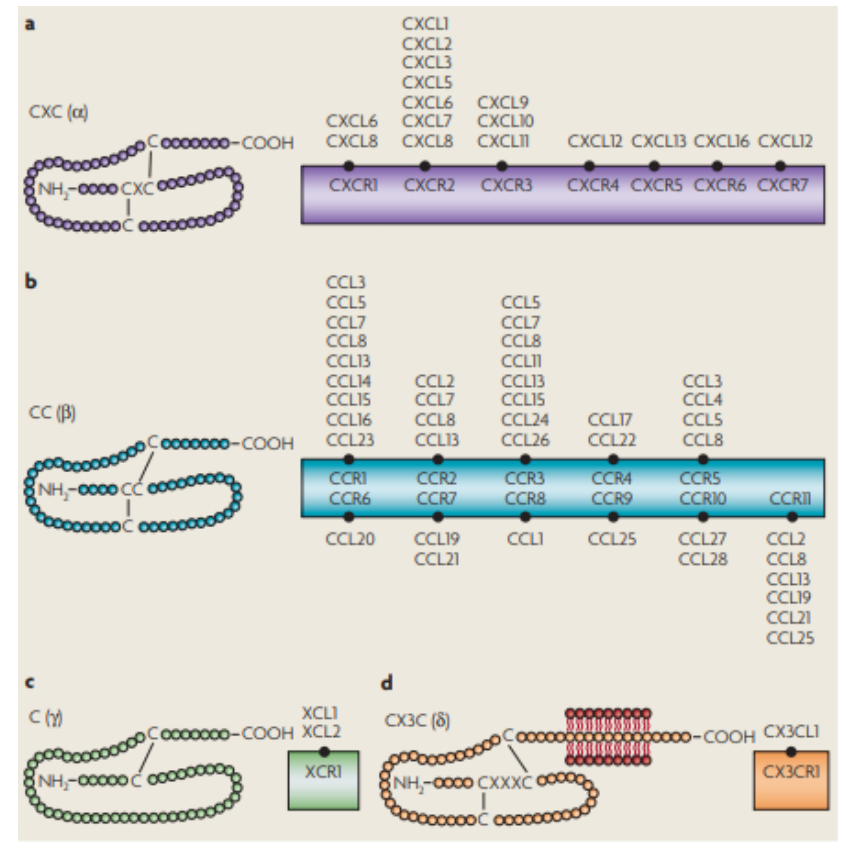


Figure **6.** The structure of chemokines and their respective receptors they can bind to. A) The CXC class chemokines and their receptors. B) The CC class chemokines and their receptors. C) The C class chemokines and their receptor. D) The CX3C class chemokine and its receptor. Reprinted with permission from Rostene, W.; Kitagbi, P. and Parsadaniantz, S. M. Chemokines: a new class of neuromodulator? *Nat. Rev. Neurosci.* 2007, 895-904 (92)

facilitates the recruitment of leukocytes to the desired areas. (97) (98) The next sections focus on the physiological function of the chemokine receptors CXCR1, CXCR2, CCR6 and CCR7 and their role in immune diseases and cancer.

1.1.3. The chemokine receptors CXCR1 and 2

The chemokine receptor CXCR1 reacts predominantly with the chemokine interleukin-8 (IL-8). (99) Interleukin-8 is a potent chemokine that is produced by numerous type of cells such as macrophages, epithelial cells, and endothelial cells as a response to inflammatory stimuli. (100) (101) Binding of IL-8 to CXCR1 triggers various downstream signaling cascades, leading to rearrangements of the cytoskeleton, the activation of integrin, and ultimately the promotion of migration and recruitment of neutrophils to the site of inflammation. (102) (103) This crucial process is needed for early infection response, as neutrophils are among the first responders to invade tissues and eradicate pathogens. (104) (105)

The CXCR2 receptors interacts, in contrast to the CXCR1 receptor, with multiple chemokines including IL-8 as well as the growth-related oncogenes alpha (GRO-alpha) and beta (GRO-beta). (106) (107) The activation of CXCR2 by those chemokines results in similar signaling events that promote chemotaxis and recruitment of various leukocytes to the inflamed tissue. (108) While CXCR1 activation is necessary for the first response towards inflammatory stimuli, the activation of CXCR2 is crucial in the amplification of the inflammatory cascade and the coordinated influx of immune cells to fight pathogens and repair damaged tissues. (109) (110)

Dysregulation of CXCR1 and CXCR2 has numerous implications in health and diseases. (111) Hyperactivation or aberrant signaling of these receptors plays a major role in various chronic inflammatory conditions such as rheumatoid arthritis (RA), where excessive neutrophil infiltration sustains inflammatory processes, causing damage to the joints. (112) Similarly, in chronic airway diseases like asthma and COPD, aberrant CXCR1 and CXCR2 signaling contributes to airway inflammation and hyperresponsiveness, leading to exacerbating respiratory symptoms. (113) Additionally, various types of cancer exploit CXCR1 and CXCR2 signaling to promote tumor growth, metastasis, and angiogenesis, resulting in poor cancer prognosis, thereby highlighting their role beyond the immune system. (114) (115) (116)

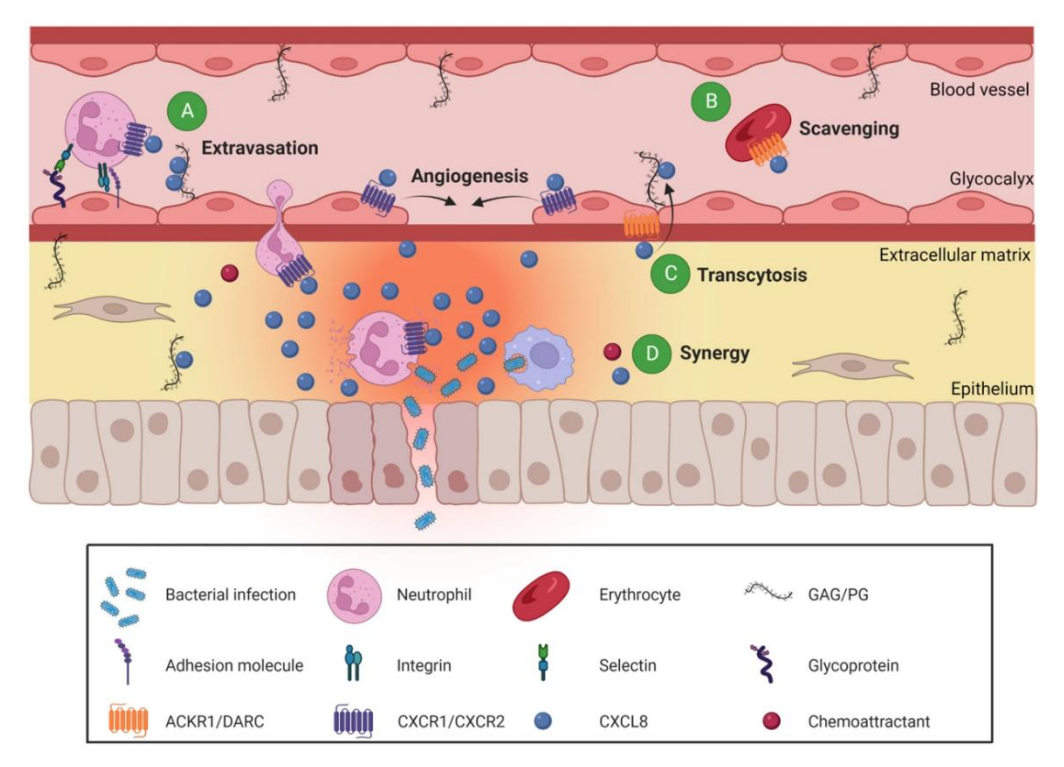


Figure 7. Physiological functions of CXCR1/2 and CXCL8. A) Binding of CXCL8 oligomers to GAGs establishes a chemokine gradient towards inflammed areas. B) Removal of non-immobilized CXCL8 by the scavenger receptor ACKR1 expressed on erythrocytes prevents systemic leukocyte activation. C) Translocation of immobilized CXCR1/2 expressing cells and GAG bound CXCL8 by transcytosis directs the immune reaction towards the inflammed areas. D) Synergy of CXCL8 and other chemoattractants to amplify the immune response. This figure is reprinted with the permission from Cambier, S.; Gouwy, M. and Proost, P. The chemokines CXCL8 and CXCL12: molecular and functional properties, role in disease and efforts towards pharmacological intervention. *Nat. Cell. Mol. Immunol.* 2023, 217-251 (275)

On the other hand, the loss of CXCR1 and CXCR2 signaling compromises innate immune responses, resulting in increased susceptibility to bacterial infections. (117) (118) As demonstrated in a mouse model, deficiency of CXCR2 has been associated with increased risks of *Staphylococcus aureus* induced septic arthritis. (119) Furthermore, dysregulation of CXCR1/2 function was associated with recurrent infections and a lowered immune response in humans. (120) (121)

In conclusion, the understanding of the physiological and pathophysiological functions of CXCR1 and CXCR2 in early and late-stage immune responses, as well as their involvement in the tightly controlled inflammation and tissue regeneration cycle after contact with pathogens is crucial in the development of targeted therapeutic inventions that modulate immune responses.

1.1.4 The chemokine receptor 6

The chemokine receptor CCR6 is another key player in the regulation of inflammatory responses, trafficking of immune cells, and maintenance of tissue homeostasis. (122) The receptor is mainly expressed on B cells, dendritic cells and certain T cells like the T helper cell Th17 and the regulatory T cells (Tregs). (123) (124)

The primary ligand of CCR6 is the chemokine ligand CCL20, also known as the macrophage inflammatory protein-3 alpha (MIP-3 α). (125) CCL20 is constitutively expressed in epithelial cells, intestinal epithelial cells, the lung, and the lymph nodes. (126) Additionally, macrophages and dendritic cells express CCL20 as a response to microbial invasion, inflammatory stimuli, or tissue damage. (127) Therefore, the CCL20/CCR6 axis plays a crucial role in immune surveillance and recruitment of immune cells. (128)

Activation of CCR6 by its chemokine ligand CCL20 triggers various intracellular signaling pathways that lead to cellular responses. These include chemotaxis, adhesion, and cytokine production. (129) This leads to the migration of immune cells to sites of infection or inflammation, particularly within mucosal tissues such as the gastrointestinal tract, the lungs, or skin. (130)

CCR6 plays a vital role in the presentation and initiation of the adaptive immune system. (131) Epithelial cells express CCL20 upon contact with pathogens. This leads to the phagocytosis of the pathogens by immature dendritic cells. (132) After phagocytosis the now mature dendritic cells travel into the lymph nodes where they act as antigen presenting cells for lymphocytes. (133)

Additionally, the CCR6 receptors play a significant role in the balance between regulatory Tregs and Th17 cells, two crucial subsets of CD4+ T cells bearing opposing functions in the regulation of immune responses. (134) The CCR6 receptor is expressed on both cell types and their interaction with the chemokine ligand CCL20 influences the migration of those cells within lymphoid organs and peripheral tissues like epithelial cells. (135) CCR6 expression on Tregs is associated with a potent immunosuppressive activity. (136) Migration towards inflamed tissue and activation of Tregs by CCL20 therefore reduces the immune response. On the other hand, expression of CCR6 on Th17 cells promotes their recruitment towards inflamed areas where they act as activators of the immune response to enhance the host defense against extracellular pathogens. (137) The balance between Treg and Th17 activation and migration is essential in the balance of immune homeostasis. (138)

Dysregulation of this balance has been implicated in various inflammatory and autoimmune disorders. (139) (140) For example, aberrant CCR6 signaling was observed in inflammatory bowel diseases such as Crohn's disease (CD) or Colitis Ulcerosa (CU) as well as in skin disorders like psoriasis. (141) This is attributed to excessive recruitment of Th17 cells that produce high amounts of pro-inflammatory cytokines that contribute to excessive tissue inflammation and damage. (142)

In summary, CCR6 plays a crucial role in the adaptive immune system, the trafficking of immune cells towards mucosal surfaces and inflamed tissues as well as the homeostasis of the immune response. Dysregulation of the CCR6/CCL20 axis results in uncontrolled balance between suppression and activation of the immune response at areas of inflammation leading to autoimmune diseases such as CD, CU or psoriasis. Understanding these mechanism holds promise for the development of targeted therapies for a range of immune associated diseases.

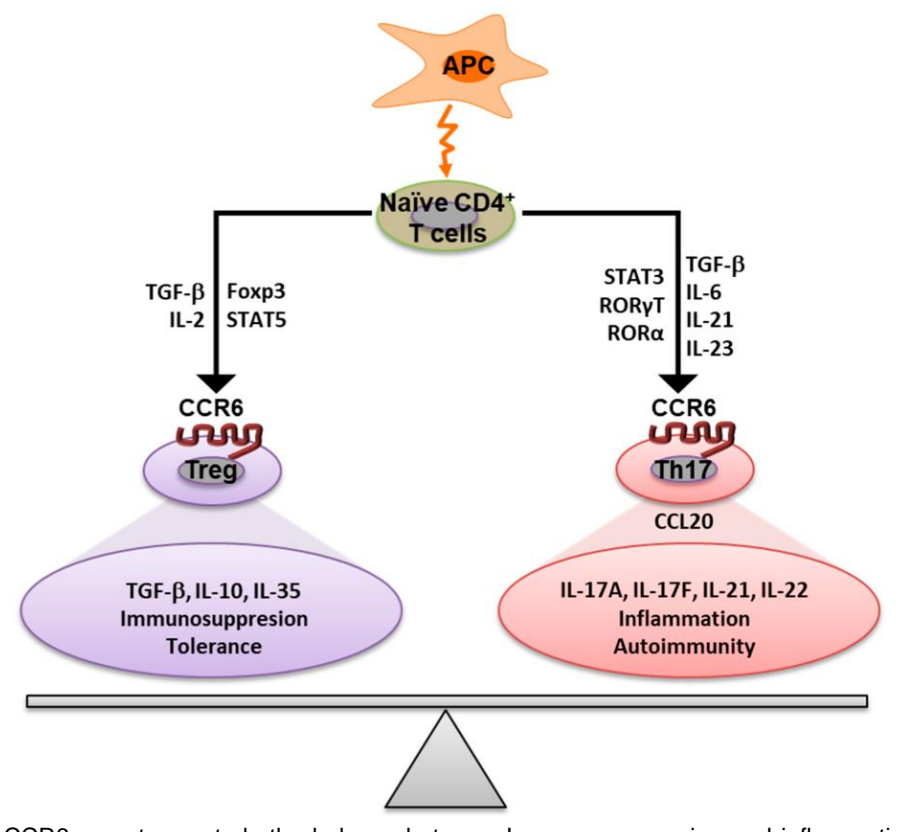


Figure **8.** The CCR6 receptor controls the balance between Immunosuppression and inflammation through the CCL20/CCR6 axis with the help of the Treg and Th17 cells. Reprinted with permission from (122) CCR6 as a Potential Target for Therapeutic Antibodies for the Treatment of Inflammatory Diseases. *Antibodies*. 2023, 30

1.1.5 The chemokine receptor 7

The chemokine receptor CCR7 is one of the main regulators of immune cell trafficking, especially in the homing of lymphocytes, therefore playing a key role in immune cell migration and immune surveillance. (143) CCR7 is expressed on a variety of immune cell subsets including B cells, mature dendritic cells as well as naïve and central memory T cells. (144)

The primary ligands for CCR7 are the chemokines CCL19 (also known as ELC or MIP-3 beta) and CCL21 (also known as SLC). (145) (146) Both chemokines are constitutively expressed in secondary lymphoid organs like the lymph nodes and the spleen. Additionally, high endothelial venules (HEVs) within lymphoid tissues express the chemokines CCL19 and CCL21. (147) Therefore, the interaction between CCR7 and its ligands is pivotal for the trafficking of immune cells between lymphoid organs and their peripheral tissues as well as the presentation of antigens and subsequent initiation of the adaptive immune response. (148)

Activation of CCR7 by CCL19 and CCL21 induces various intracellular signaling pathways, leading to cellular responses such as chemotaxis, adhesion, and cytoskeletal rearrangements. (149) As mentioned before immature dendritic cells bind to CCL20 expressed by epithelial cells after contact with pathogens. Phagocytosis of these pathogens by the immature dendritic cells triggers the downregulation of CCR6 and initiates the expression of CCR7 on the surface of these dendritic cells. (150) This maturing allows the homing of the mature dendritic cells to the lymph nodes where they are able to present the antigens to lymphocytes. (151) This illustrates the importance of the chemokine receptor CCR7 in the adaptive immune response.

Furthermore, CCR7-mediated signaling is particularly important for the trafficking of naïve T cells from peripheral tissues to secondary lymphoid organs. (152) Within lymph nodes, CCR7 directs the localization of T cells to specific microenvironments, such as the T cell zone and the paracortex. (153) This enables the interaction between T cells and other immune cells to regulate, activate, or amplify the immune response towards pathogens and foreign antigens. (154)

In addition to its role in the trafficking of immune cells, CCR7 is also involved in the development and maintenance of lymphatic vessel development as well as the formation of lymphoid tissue. (155) (156) During embryonic development, CCR7 signaling aids in the migration of dendritic cells and lymphocytes to the newly formed lymphoid tissues. (157)

The role of dysregulated CCR7 signaling in immune-related disorders such as rheumatoid arthritis and multiple sclerosis has been thoroughly investigated. (158) It has been shown that

aberrant expression of CCR7 and the respective chemokines CCL19 and CCL21 leads to unrestrained recruitment of T cells and dendritic cells contributing to excessive immune cell activation and subsequent exacerbating inflammation. (159) (160) (161)

Additionally, CCR7 (over)expression on tumor cells has been linked to high metastatic spread and poor prognosis in several types of cancer such as breast cancer, melanoma, and pancreatic cancer. (162) (163) (164) Tumors expressing CCR7 are able to migrate towards lymphoid organs, where they can thrive in supportive microenvironments and evade the immune surveillance. (165)

In summary, CCR7 plays a crucial role in the trafficking of immune cells towards the lymphoid organs and distribution throughout the body to aid in the initiation of the adaptive immune response. Dysregulation of CCR7 signaling plays an essential role in several autoimmune diseases and the metastasis of cancer. This highlights the importance of CCR7 as a potential target for the development of novel therapies for a range of immune-mediated and neoplastic diseases.

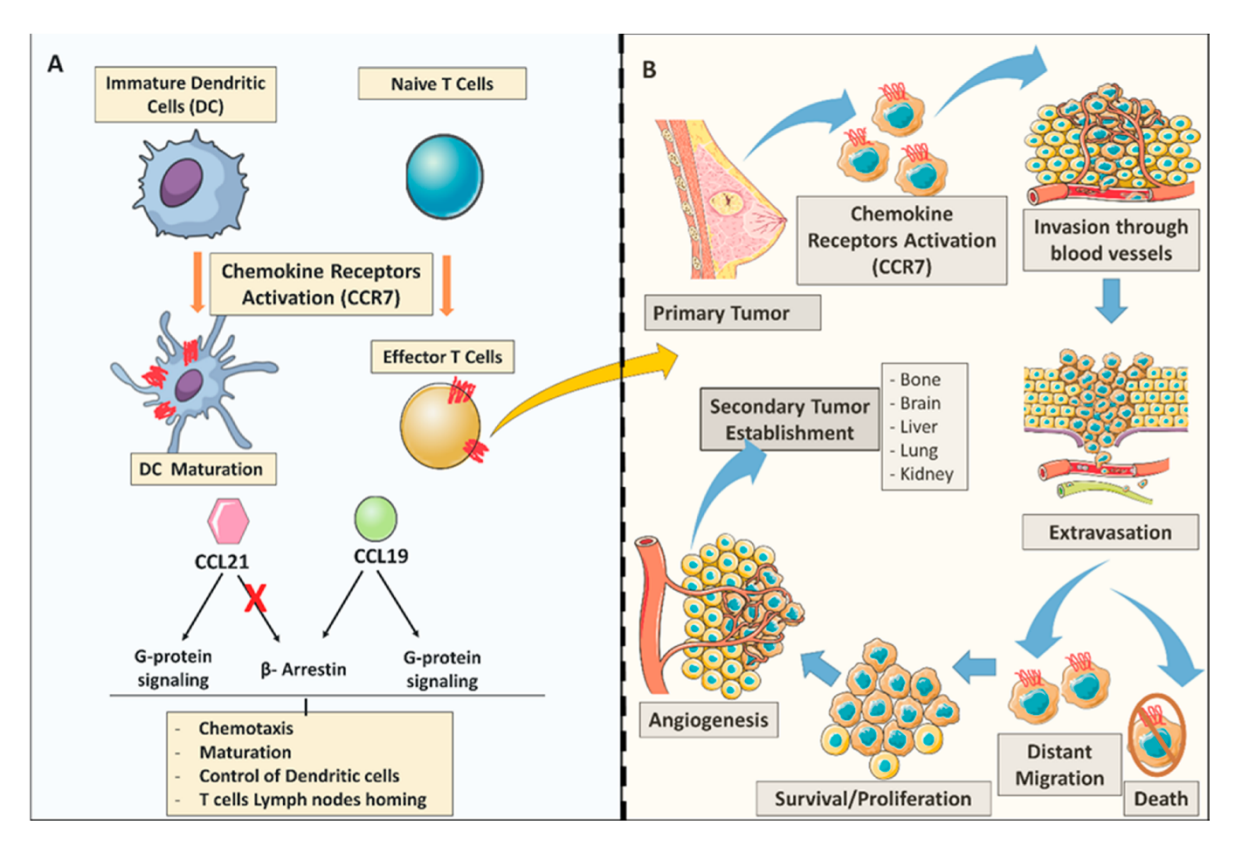


Figure **9**. The role of CCR7 in the immune system and breast tumor metastasis. A) The role of CCR7 in the immune system. Activation of CCR7 leads to the maturation of dendritic cells and T cells. Both chemokines CCL19 and CCL21 are able to display G-protein signaling but only CCL19 is able to recruit β-arrestin. B) CCR7 expression on tumor cells plays several roles in the dissemination of cancer. The activation of CCR7 promotes the enhanced survival and proliferation of cancer cells as well as their homing to lymphoid organs where they encounter supportive microenvironments. Reprinted with permission from Rizeq, B. and Malki, M. I. The Role of CCL21/CCR7 Chemokine Axis in Breast Cancer Progression. *Cancers*. 2020, 1036 (276)

1.1.6 Chemokine receptors as drug targets

Due to their involvement in a wide array of autoimmune diseases and cancer, modulation of chemokine receptor activity offers promising therapeutic avenues for the development of novel drugs. (166) Thus, intense efforts have been dedicated to the design, synthesis, and testing of new drug modalities. This section gives an overview on the current landscape of modulators and antagonists targeting selected chemokine receptors.

1.1.6.1 Targeting chemokine receptors at extracellular binding sites

The initial strides in developing chemokine receptor antagonists involved the systematic truncation at the N-terminal end of the natural chemokine ligands, yielding truncated chemokines capable of binding to their receptors without eliciting downstream signaling. (167) (168) This innovative approach has demonstrated remarkable therapeutic efficacy across a spectrum of chemokine receptors. However, the practical application of modified chemokines exhibits significant problems, particularly in their administration to patients. Unlike oral medications, such as capsules or tablets, antibodies and modified chemokines cannot be easily delivered orally as they get easily digested before they reach the target tissue. (169) Consequently, their administration usually requires intravenous injections, necessitating skilled medical personnel to mitigate risks of infection, thrombosis, or vascular damage. (170) Moreover, the potential for off-target effects on immune cells within the bloodstream poses a considerable concern, potentially resulting in severe adverse reactions. (171) Lastly, the inconvenience and discomfort associated with frequent injections has shown to be a major concern as it's impacting patients' daily routines and overall quality of life. (172) Recognizing these limitations, the imperative for the development of small molecules targeting the orthosteric binding site or allosteric binding sites on the extracellular site of the receptor emerged swiftly among researchers and pharmaceutical companies. This urgency is underscored by the rapid pace of progress, as evidenced by the large number of patents filed for small molecules targeting various chemokine receptors within a relatively short period of time since the identification of the first chemokine receptor merely a decade ago. (173)

To date, a number of small molecule antagonists for several chemokine receptors have entered clinical trials with two of them have been approved for the use in humans. (174) This section provides a short overview on the landscape of small molecule antagonists for certain chemokine receptors.

CCR1

Up to date eight CCR1 antagonists have entered clinical trials. (175) The first one was to enter clinical trials was BX 471 from Berlex Pharmaceutical Company. (176) The antagonist showed over 1000-fold selectivity for CCR1 with a reported K of 1.0 nM for human CCR1. (177) The compound showed an excellent safety profile and entered clinical trials. The major problem of this antagonist was its short biological half-life with $t_{1/2} \approx 2.3$ h. However, the problem could be solved by the formulation of an extended release tablet and BX 471 entered phase II trials for multiple sclerosis. (177) The drug showed no safety concerns and good tolerance but failed to show reduction in inflammatory lesions and was discontinued. (178) The same fate struck MLN3897, a pyridylbenzoxepine-based CCR1 antagonist from Millenium Health (owned by Takeda Oncology). (179) Despite good tolerance, high potency towards CCR1 ($IC_{50} = 3.4 \text{ nM}$), and effective inhibition of CCL3 induced immune cell recruitment in vivo, the compound failed to reach its clinical end point in a phase II trial. (180) CCX354 (Figure 10) from Chemocentryx (owned by Amgen) has completed Phase II trials and is the most promising CCR1 antagonist to date. (181) (182) This phenylpiperazine compound shows high affinity towards CCR1 (K =1.5 nM), good tolerance and was able to reach its end point in the reduction of disease score proinflammatory marker levels rheumatoid arthritis). (183)and in

Figure 10. Chemical structure of CCR1 antagonists with their respective K_i values towards CCR1.

CCR5

Although initially considered as a target for autoimmune diseases such as rheumatoid arthritis, CCR5 quickly attracted the attention of pharmaceutical companies when researchers found that CCR5 was used as an entry factor by macrophage-tropic HIV-1 strains. (184) This prompted intense efforts in the development of novel CCR5 antagonists for the treatment of HIV infections. (185) Maraviroc (Figure 11) is currently the only FDA approved CCR5 antagonist for the treatment of multidrug-resistant, CCR5-tropic HIV-1 infection. (186) It is administered in combination with other antiretroviral medications. (187) The CCR5 antagonists

showed low toxicity, a high affinity towards CCR5 ($IC_{50} = 3 \text{ nM}$), no activity against the hERG ion channel and a high efficacy in the treatment of a wide variety of HIV-1 derived enveloped pseudoviruses. (188) (189) The development of novel CCR5 antagonists such as SCH-C or aplaviroc was mostly terminated after clinical phases I or II due to their activity on the hERG channel or liver toxicity. (190) (191) However, the novel CCR5 antagonist cenicriviroc from Takeda Pharmaceuticals showed promising affinity and good tolerability without hERG channel activity. Cenicriviroc is now evaluated in clinical phase III trials for the oral treatment of nonalcoholic steatohepatitis (NASH) and COVID-19. (192) (193) (194) (195)

Figure 11. Chemical structures of CCR5 antagonists and their respective binding affinities.

CXCR4

CXCR4, like the chemokine receptor 5, is used by HIV-1 strains as an entry point. (194) This finding greatly accelerated the research on novel CXCR4 antagonists. The CXCR4 antagonist plerixafor was the first antagonists that went into clinical trials. It showed great efficacy *in vitro* but suffered from a lack in oral bioavailability and was discontinued. (195) The development of CXCR4 antagonists however took an entirely different reaction when researchers

Figure 12. Chemical structures of CXCR4 antagonists and their respective binding affinities.

found out that the CXCL12/CXCR4 axis plays a crucial role in the retention of hematopoietic stem cells. CXCL12 activated CXCR4 retains hematopoietic stem cells in the bone marrow. (196) Therefore, inhibition of CXCR4 leads to a rapid mobilization of stem cells from the bone marrow, allowing them to be harvested and given back to patients suffering from white blood cancers such as non-Hodgkin lymphomas. (197) This led to the FDA approval of plerixafor (Figure 12) in the treatment of non-Hodgkin lymphoma and multiple myeloma. (198) This success inspired the development of TG-0054 from TaiGen. The chemical structure has not yet been released by the company, but according to their patents, the compounds are based on polyamines. (199) The prototypical structure of these compounds is shown in Figure 12.

1.1.6.2 Targeting the intracellular allosteric binding site

In the past, the development of novel chemokine receptor antagonists was based on the premise that chemokine receptors exclusively interact with antagonists at their extracellular domains. However, groundbreaking research revealed the presence of an intracellular allosteric binding site (IABS) within chemokine receptors, fundamentally changing our understanding of chemokine receptor modulation. Up to date the IABS of several class A GPCRs like the Beta-2 adrenergic receptor (β₂AR) and the chemokine receptors CCR2, CCR7, CCR9 and CXCR2 have been disclosed with the help of X-ray crystallography. (200) (201) (202) (203) (204) (205) While the initial disclosure of the IABS occurred within class A GPCRs, a comparable site has been identified within class B GPCRs as well. (200) Furthermore, there is compelling evidence suggesting that the IABS could be a common feature across different GPCR classes. (206) (207) (208) The discovery of the IABS has paved the way for the emergence of novel therapeutic modalities for GPCRs, particularly chemokine receptors, where traditional extracellular antagonists have encountered limited success in clinical trials.

Targeting the IABS of chemokine receptors promises several advantages over traditional approaches focusing solely on their extracellular domains. Firstly, modulation of the intracellular allosteric binding sites provides the opportunity to modulate receptor activity in a highly specific manner, yielding highly selective antagonists for single chemokine receptors. (209) By direct interference in the intracellular signaling pathways, these modulators can fine-tune receptor function without interference in the binding of endogenous chemokine ligands, potentially minimizing off-target effects. (210) Additionally, the dynamic nature of intracellular allosteric binding sites allows for the development of drugs that can allosterically modulate receptor activity, offering a level of temporal and spatial control that may not be achievable with extracellular antagonists. (211) Furthermore, targeting intracellular binding sites may circumvent the limitations associated with the rapid turnover and clearance of extracellular

ligands, potentially prolonging the duration of therapeutic effects. (212) Overall, exploiting intracellular allosteric binding sites poses a promising avenue for the development of next-generation therapeutics targeting chemokine receptors, with the potential to enhance efficacy, selectivity, and safety profiles compared to traditional extracellular antagonists and modulators. This section will focus on the current research towards intracellular allosteric antagonists for several chemokine receptors.

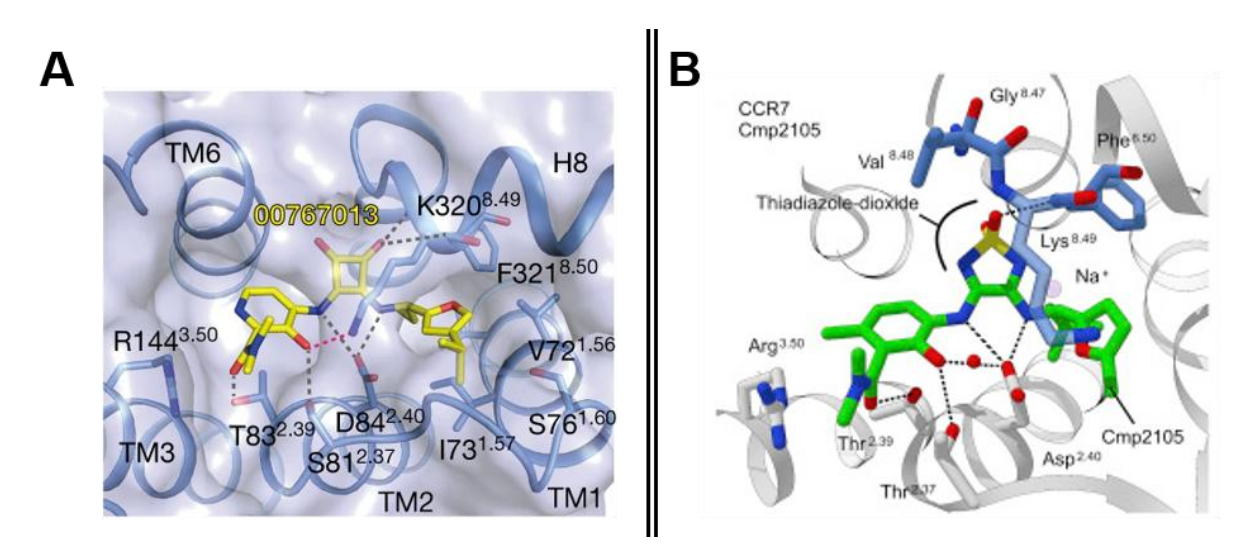


Figure 13. A) A 3D view of 00767013–CXCR2 interactions from the intracellular side. CXCR2 is shown in blue cartoon and shaded surface, and 00767013 is shown as yellow sticks. Reprinted with permission from Liu, K.; Wu, L.; Yuan, S.; Wu, M.; Xu, Y.; Sun, Q.; Li, S.; Zhao, S.; Hua, T. and Liu, Z.-J. Structural basis of CXC chemokine receptor 2 activation and signaling. *Nature, 2020,* 135-140. (106). B) A 3D view of cmpd2105-CCR7 interactions from the intracellular side. CCR7 is shown in gray and important amino acid residues highlighted in color. Reprinted with permission from Jaeger, K. Bruenle, S.; Weinert, T.; Guba, W.; Muehle, J.; Miyazaki, T.; Weber, M.; Furrer, A.; Haenggi, N.; Tetaz, T.; Huang, C.-Y.; Mattle, D.; Vonach, J.-M.; Gast, A.; Kuglstatter, A.; Rudolph, M. G.; Nogly, P.; Benz, J.; Dawson, R. J. P. and Standfuss, J. Structural Basis for Allosteric Ligand Recognition in the Human CC Chemokine Receptor 7. *Cell.* 2022, 1222-1230

CXCR2

The first proof of an intracellular binding pocket for CXCR2 was revealed by the co-crystal structure of CXCR2 with the antagonist 00767013. (106) This squaramide-based ligand binds to the a cytoplasmatic pocket formed by the ends of TM1, TM2, TM3, TM6 and the loop between the unstructured helix 8 and TM7. The two amino groups of the central cyclobutenedione scaffold forms hydrogen bonds with Asp84 while the conserved residues Lys320 and

Figure 14. Chemical structures of intracellular CXCR2 antagonists and their respective binding affinities.

Phe321 from hydrogen bonds with a carbonyl group. The isopropylfurfurylamine side chain forms extensive hydrophic interactions with the amino acid residues Val69, Val72 and Ile73, while the phenolic hydroxyl group and the carbonyl of the tertiary amide form hydrogen bonds with the amino acids Ser81 and Thr83. (204) This co-crystal structure provided evidence that the series of squaramide-based compounds, including the phase II clinical candidate navarixin, are indeed intracellular allosteric antagonists. Further investigations into novel scaffolds like the *N*,*N'*-diarylurea series led to the discovery of the hit compounds elubrixin and danirixin. (213) Both have been demonstrated to be intracellular allosteric modulators. However, similar to navarixin, all these compounds did not succeed in phase II clinical trials and the development was terminated. (214) (215) Despite the lack of successful clinical trials so far, research on intracellular allosteric antagonists of CXCR2 shows great promise for the development of novel drug modalities targeting the chemokine receptor CXCR2.

CCR7

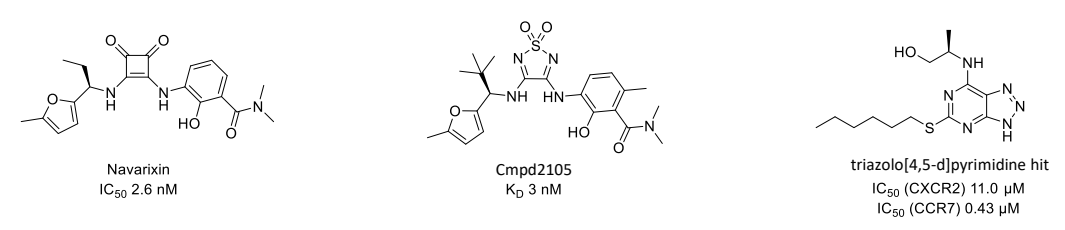


Figure 15. Intracellular CCR7 antagonists and their respective binding affinites.

The development of novel antagonists for CCR7 took a great stride with the elucidation of its crystal structure in a complex with cmpd2105. (205) This patented thiadiazole-1,1-dioxidebased compound was shown to bind to the IABS of CCR7. (216) Based on this discovery, a 3D shape similarity screening was performed, leading to the discovery that the CXCR2 antagonists navarixin can bind to CCR7 in a similar fashion. (205) The central thiadiazoledioxide scaffold interacts with conserved residues at the TM7 and helix 8 with its two oxygens, while the amino groups form hydrogen bonds with Asp94. The isopropylfurfurylamine side chain forms hydrophobic interactions with Val79, Thr82 and Phe86, The benzamide side chain on the other side of the molecule forms hydrogen bonds with Thr91, Thr93 and Arg154. These interactions are similar to the interactions between navarixin and CXCR2 which may explain why cmpd2105 and navarixin are capable of binding to both CCR7 and CXCR2. (205) While the discovery of the IABS of CCR7 represents a major step forward in the development of novel antagonists for CCR7, the challenge remains to optimize the selectivity towards CCR7. New research focused on the optimization of triazolo[4,5-d]pyrimidines as selective intracellular allosteric antagonists for CCR7. The initial hit of this study showed great affinity but lacked selectivity towards CCR7. Subsequent optimization studies were performed that led

to the discovery of the hit compound (Figure 15) with great overall potency and satisfying selectivity for CCR7 over CXCR2. (217)

CCR2 and CCR9

Recently the group of Prof. Dr. Matthias Schiedel established fluorescent probes for the IABS of CCR2 and CCR9. (218) (219) By modification of the intracellular allosteric antagonist SD-24 for CCR2 and vercirnon for CCR9, they synthesized fluorescent tracers based on a TAMRA fluorophore (Figure 16).(218) (219) These tools enable faster discovery of novel antagonists for the IABS of CCR2 and CCR9. This approach offers great potential and could serve as a powerful method for the discovery of intracellular antagonists for other chemokine receptors, for which the presence of an IABS has been proposed but not yet conclusively demonstrated.

Figure 16. Structure of fluorescent tracers for CCR2 and CCR9 with their respective binding affinities.

1.2 PROTACs

Small molecules have historically been invaluable tools in drug discovery, offering the ability to modulate the activity of dysfunctional proteins in various diseases. However, their effectiveness can be hindered by several factors. Firstly, small molecule inhibitors need intensive optimization in regard to affinity and specificity while adhering to the so-called rules of five by Lipinski. (220) Additionally, the development of resistance mechanisms by cells, such as the upregulation of protein production or mutation of the protein can render these inhibitors ineffective over time. (221) Lastly, most small molecules are designed to compete with endogenous ligands of the targeted protein, hence the druggable genome in humans is limited to the finite number of proteins with a specific drug-binding site like enzymes, receptors, transporters or ion channels. (222) Expansion of the druggable proteome was achieved by the development of monoclonal antibodies and oligonucleotides. (223) (224) In 2001, a paradigm shifting strategy was developed. This approach used bifunctional molecules called proteolysis targeting chimeras (PROTACs) hijacking the ubiquitin-proteasome system (UPS) to directly degrade the targeted protein. (225) The UPS is responsible for the degradation of misfolded or no longer required proteins in the course of natural protein homeostasis (226). Proteins are marked for degradation with the protein ubiquitin (Ub). (227) For this, ligases tag the desired proteins with ubiquitin residues as a form of post-translational modifications. (228) To this end, an ubiquitin-activating enzyme (E1) activates a carboxylic acid group of ubiquitin under hydrolysis of ATP to form an intermediate thioester bond between the ubiquitin and a cysteine side chain residue of the E1 ligase. Next, an ubiquitin-conjugating enzyme (E2) receives the ubiquitin residue by means of an transthioesterification reaction. When the ubiquitin-charged E2 protein approximates an ubiquitin ligase (E3) and the desired protein, the ubiquitin gets attached to a lysine side chain residue of the protein via an isopeptidic bond. This can happen multiple times to the same protein resulting in polymeric ubiquitin side chains with homogenous or branched characteristics. The fate of the ubiquitinated protein is regulated according to the specific pattern of ubiquitination. The adequately ubiquitinated protein is then recognized by the 26S proteasome followed by proteolytic degradation. (228) PROTACs hijack this degradation mechanism by combining a ligand for a protein of interest (POI) with an E3 ligase binding ligand that are connected by a linker. (229) The PROTAC induces the formation of a POI:PROTAC:E3 ligase ternary complex to induce proximity between the targeted protein and the E2:E3 ubiquitination complex resulting in the ubiquitination of the targeted POI. The ternary complex then dissociates with the polyubiquitinated-POI ready for degradation by the proteasome and the free PROTAC is ready to enter a new catalytic cycle. (229) This

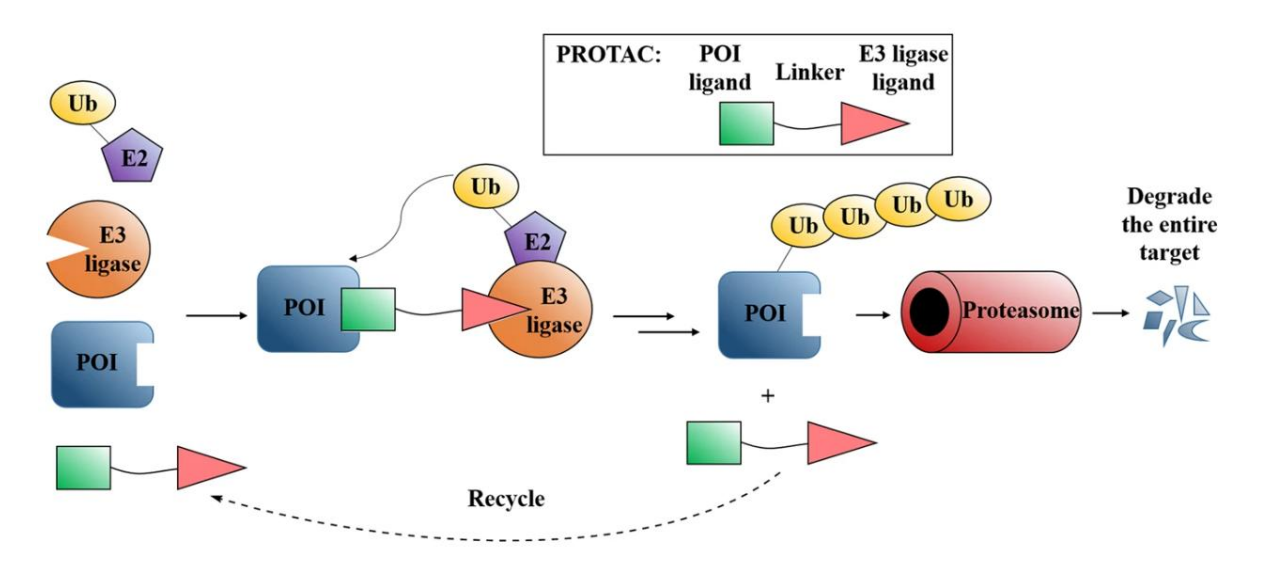


Figure 17. PROTAC-mediated degradation of a POI by ternary complex formation with the E2:E3 ubiquitination complex. Reprinted with permission from Sun, X., Gao, H., Yang, Y.; He, M.; Wu, Y.; Song, Y.; Tong, Y. and Rao, Y. PROTACs: great opportunities for academia and industry. *Sig Transduct Target Ther.* 2019, 64 (230)

mechanism of targeted protein degradation could be superior to the traditional small molecule inhibition approach. (230) This is due to the catalytic mechanism of PROTACs that often requires much lower concentrations for efficacy than small molecules. In addition, due to their catalytic nature, PROTACs do not necessarily require high affinity ligands at the active sites. (230) Furthermore, they expand the druggable proteome because the POI ligands used in PROTAC development do not inevitably have to bind to an active site, but can also target any binding site present on the POI. (231)

The first proof-of-concept PROTACs used a complex phosphopeptidic ligand as an E3 ligase ligand. (225) These PROTACs recruited the Skp-1-Cullin-F box. However, the initial success was tempered by the impracticality of these early prototypes, which required microinjections due to their poor permeability. To surmount this limitation, subsequent efforts pivoted towards the incorporation of cell-permeable polyarginine-containing peptide ligands, specifically targeting the von Hippel-Lindau (VHL) E3 ligase. (232) While this approach showcased promise, it primarily served as a proof-of-concept rather than a viable path towards novel therapeutics. Consequently, the focus of PROTAC research shifted towards the discovery of novel E3 ligases and the development of corresponding ligands. Notably, VHL and cereblon emerged as prominent targets, with the identification of cereblon as the primary molecular target of thalidomide marking a significant turning point in PROTAC development. (233) Thalidomide is best known for its tragic role as the root cause for a vast amount of birth defects, due to the teratogenic properties of the S-enantiomer. (234) The drug was used as the active pharmaceutical ingredient (API) in the sedative and antiemetic drug Contergan that was licensed as a drug for pregnant women with morning sickness. The drug was synthesized as

the R-enantiomer but unfortunately due to the chemical nature of the internal imide the drug can rapidly racemize in aqueous solution. (234) (235) This discovery, however, prompted intense efforts in the development of novel thalidomide analogues for the use in PROTAC synthesis. Up to date several other E3 ligases such as the mouse double minuted 2 homolog (MDM2), the DDB1- and CUL1-associated factor 11 (DCAF11) and 16 (DCAF16), the ring finger protein 114 (RNF114), the Kelch-like ECH-associated protein 1 (KEAP1), the Fem-1homolog B (FEM1B), and the inhibitor of apoptosis proteins (IAPs) have been targeted as E3 ligases in the development of PROTACs. (236) (237) The discovery of new targetable E3 ligases and the optimization of hit compounds for E3 ligases is therefore of utmost importance in the field of targeted protein degradation. The immense potential of PROTACs is highlighted by the fact that up to date at least 20 PROTACs have entered clinical trials. (238) Among the first PROTACs to enter clinical trials are ARV-110 and ARV-471 can be named which were developed in a cooperation between Arvinas and Pfizer with the latter being currently in phase III clinical trials. (239) These PROTACs aim for the degradation of estrogen and androgen receptors. Both of these receptors are well-established targets for the treatment of either breast or prostate cancer and offer a new therapeutic avenue in cancer treatment. (240) (241) All of the PROTACs that are currently evaluated in clinical trials are based on thalidomide as the E3

Figure 18. Chemical structures of the PROTACs ARV-110, ARV-417 and DT2216. The E3 ligase is highlighted in orange, the linker is black and the POI ligand is marked in blue.

ligase ligand except for DT2216. This PROTAC addresses VHL as the E3 ligase ligand and is now evaluated in phase I clinical trials for the treatment of hematological and solid tumors.

In contrast to the mechanism of action, the thermodynamics of ternary complex formation was a much more difficult area of research. The understanding on the thermodynamics of ternary complex formation however was jump-started by the first crystal structure of a ternary complex between the PROTAC MZ1, BRD4 and VHL. (242) Binding equilibria were then determined by methods such the isothermal titration calorimetry (ITC) or surface plasmon resonance (SPR) spectroscopy. (242) (243) These measurements allowed for the development of mathematical methods to understand the thermodynamics of ternary complex formation. The formation of ternary complexes is affected by the association and dissociation of PROTAC:POI or PROTAC:E3 binary complexes and subsequent association and dissociation of the binary complexes to the second protein to form the necessary ternary complex. The formation of ternary complexes can either be hindered or favored depending on the amount and nature of de novo formed protein-protein interactions (PPIs). (243) The ratio of dissociation constants for binary (K_D^{binary}) and ternary (K_D^{ternary}) complex formation allows for the calculation of the calculated cooperativity (α). (244) Positive cooperativity (α > 1) describes the preferred formation of ternary complexes rather than binary complexes, predicting a stable ternary complex that favors effective POI degradation. On the other hand, negative cooperativity (α < 1) hints at the existence of unfavorable PPIs between the E3 ligase and the POI, preventing ternary complex formation. (243) (244) However, the existence of positive cooperativity is not obligatorily necessary for successful PROTAC-mediated degradation. (245)

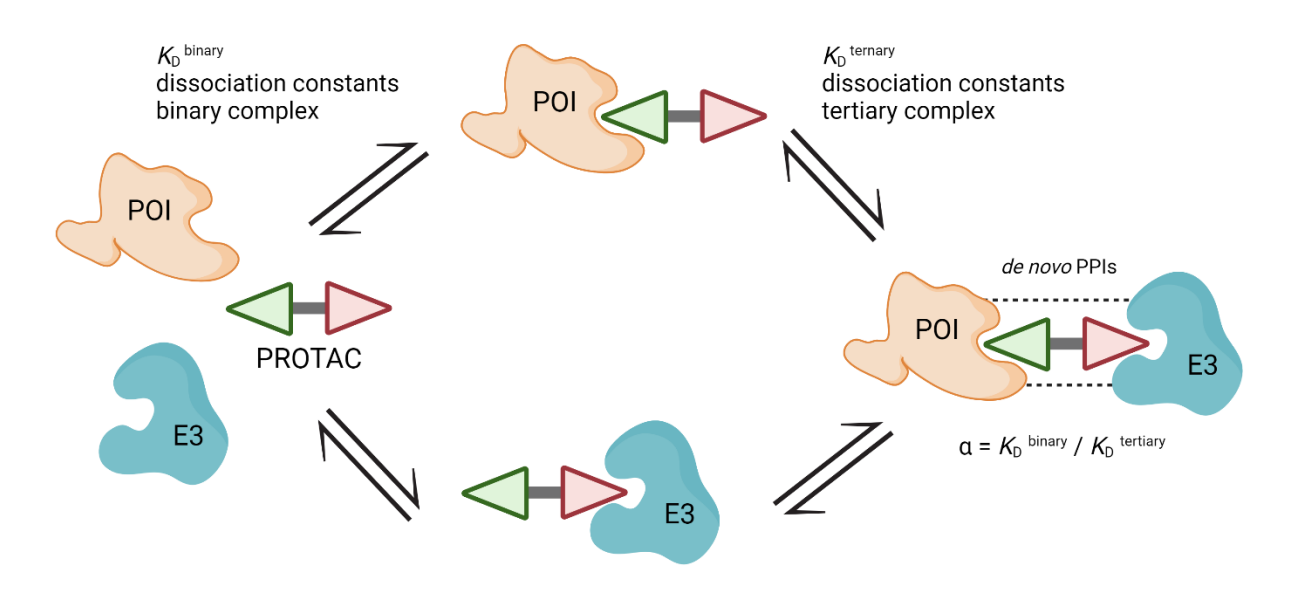


Figure 19. Determination of cooperativity (α) as the thermodynamic value indicating the likelihood of ternary complex formation. Created with Biorender.

In addition to the effect of cooperativity, the concentration of the PROTAC plays an important role as well. At lower concentrations, PROTAC molecules engage in a competitive interaction, vying for binding sites on both the E3 ligase and the POI. However, when the concentration of PROTACs becomes excessive, saturation occurs, impeding the formation of ternary complexes. This saturation effectively precludes further binding opportunities for both the E3 ligase and the POI, thereby hindering the formation of ternary complexes. Consequently, the full occupancy of binding sites on both targeted proteins results in a diminished capacity for ternary complex formation, ultimately compromising the efficiency of PROTAC-mediated protein degradation. This so-called "hook effect" can be visualized in a bell-shaped curve that illustrates the relationship between PROTAC concentration and the amount of ternary complexes formed. (246)

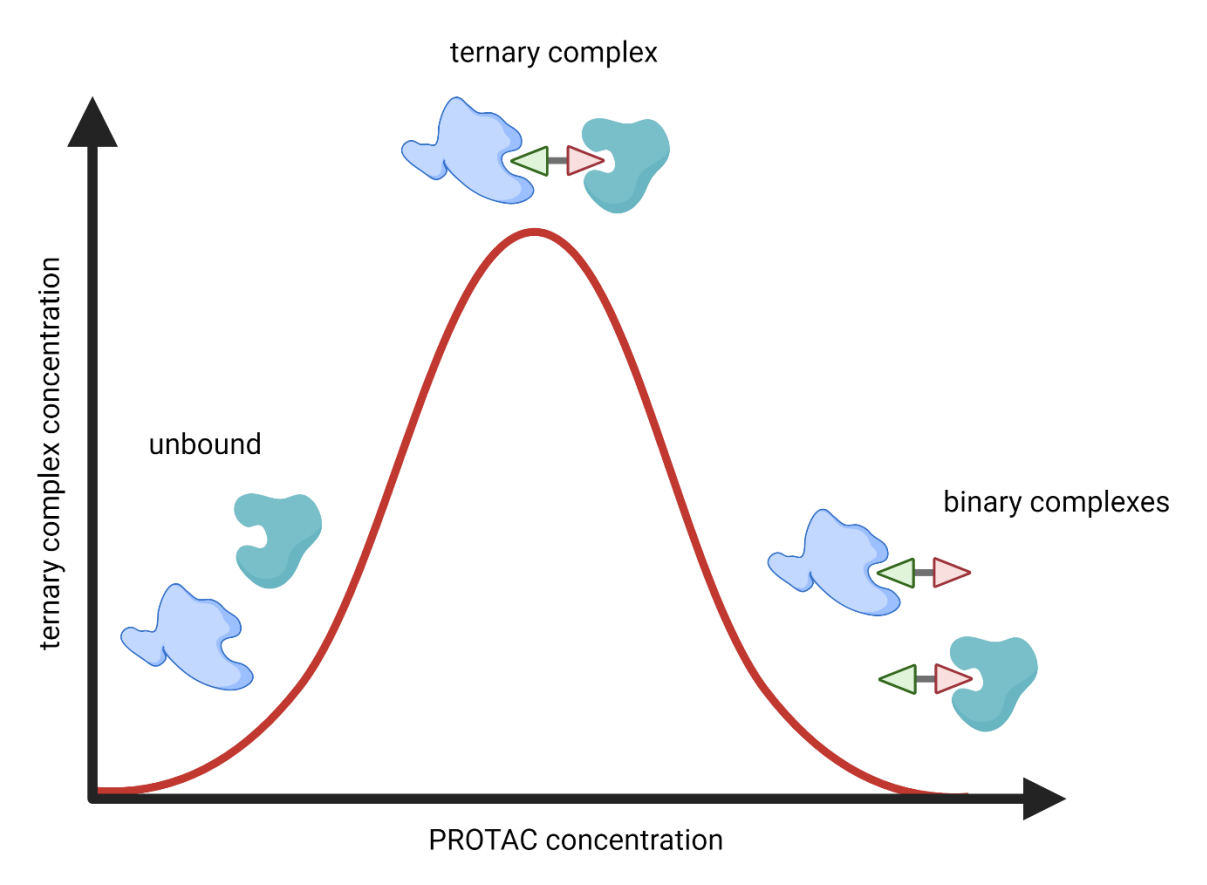


Figure **20**. Illustration of the "hook effect". Increasing PROTAC concentrations saturate the E3 ligase and the POI pmpeding the formation of ternary complexes. Created with Biorender.

1.2.1 PHOTACs: a new class of proximity-inducing tools

As PROTACs have solidified their position as a frontrunner in targeted protein degradation, attention has increasingly turned towards exploring novel methodologies to expand the arsenal of targeted protein degradation. In the pursuit of broadening the scope of protein degraders, innovative methodologies such as hydrophobic tags (HyTs), molecular glues, LYTACs (lysosomal-targeting chimeras), AbTAC (antibody-based chimeras) or AUTACs (autophagytageting chimeras) have emerged as compelling avenues (247). Hydrophic tags exploit hydrophic moietys such as adamantane or fluorene to mimic the hydrophic sites of misfolded proteins to induce chaperone-mediated proteasomal degradation. (248) Molecular glues are small molecules that bridge an E3 ligase directly with the POI without the need of a tripartite structure of POI ligand, linker and E3 ligase ligand. (249) LYTACs and antibody-based chimeras induce lysosomal-mediated degradation. This is achieved by simultaneous binding of the LYTAC or the AbTAC to an extracellular domain of the targeted membrane protein and a lysosome-targeting receptor. This ternary complex induces clathrin-mediated internalization and subsequent lysosomal degradation. (250) (251) Autophagy-targeting chimeras (AUTACs) are tripartite molecules with a POI ligand that is tethered by a linker to an autophagy tag. The autophagy tag of the AUTAC triggers polyubiquitination and subsequent lysosomal degradation. (252) While novel methods of targeted protein degradation, such as hydrophobic tags, molecular glues, LYTACs, and others, have significantly expanded the repertoire of targetable proteins, they present inherent limitations in terms of spatial and temporal control over their activity. These methodologies lack the ability to exert precise control over the location and timing of protein degradation. Once administered, these degraders typically exhibit constitutive activity, leading to the degradation of target proteins regardless of their physiological context or cellular compartment, which can often lead to unwanted toxicity. As a result, while these approaches offer unparalleled versatility in targeting a diverse array of proteins, their indiscriminate and continuous action underscores the ongoing challenges in achieving precise modulation of protein function for therapeutic purposes. One method to achieve localized effects of drugs is to control their activity by light. The utility of light in precisely modulating biological pathways has gained recognition in recent years. (253) Optical control methods encompass diverse approaches, such as photocaged compounds and the introduction of synthetic photoswitches. Photoswitches leverage photochemical isomerization and thermal relaxation processes to alter the activity of compounds, allowing for precise temporal and spatial control over their effects. (254) In 2020, the Trauner group presented the first photochemically targeting chimeras (PHOTACs). (255) (256) These molecules consist of an POI ligand, a photoswitch, and an E3 ligase ligand. The conformation of the degrader in the inactive form prevents the formation of a ternary complex presumably by introduction of a steric

clash between the binary complex and the second protein. Upon irradiation with light of the appropriate wavelength the internal photoswitch changes its conformation and the PHOTAC is now able to form a ternary complex and induce the ubiquitinylation and subsequent proteasomal degradation of its target. The active isomer gradually switches back to the inactive conformation through thermal relaxation therefore losing its activity. Alternatively, PHOTACs can also be rapidly inactivated photochemically. This highly reduces the risk of adverse side effects, since they can be selectively activated by light at the desired location and their inactivation is much less dependent on dilution, clearance, and metabolism. As a result, PHOTACs may be able to provide a higher level of spatiotemporal control that cannot be achieved by the established methods of targeted degradation used to date.

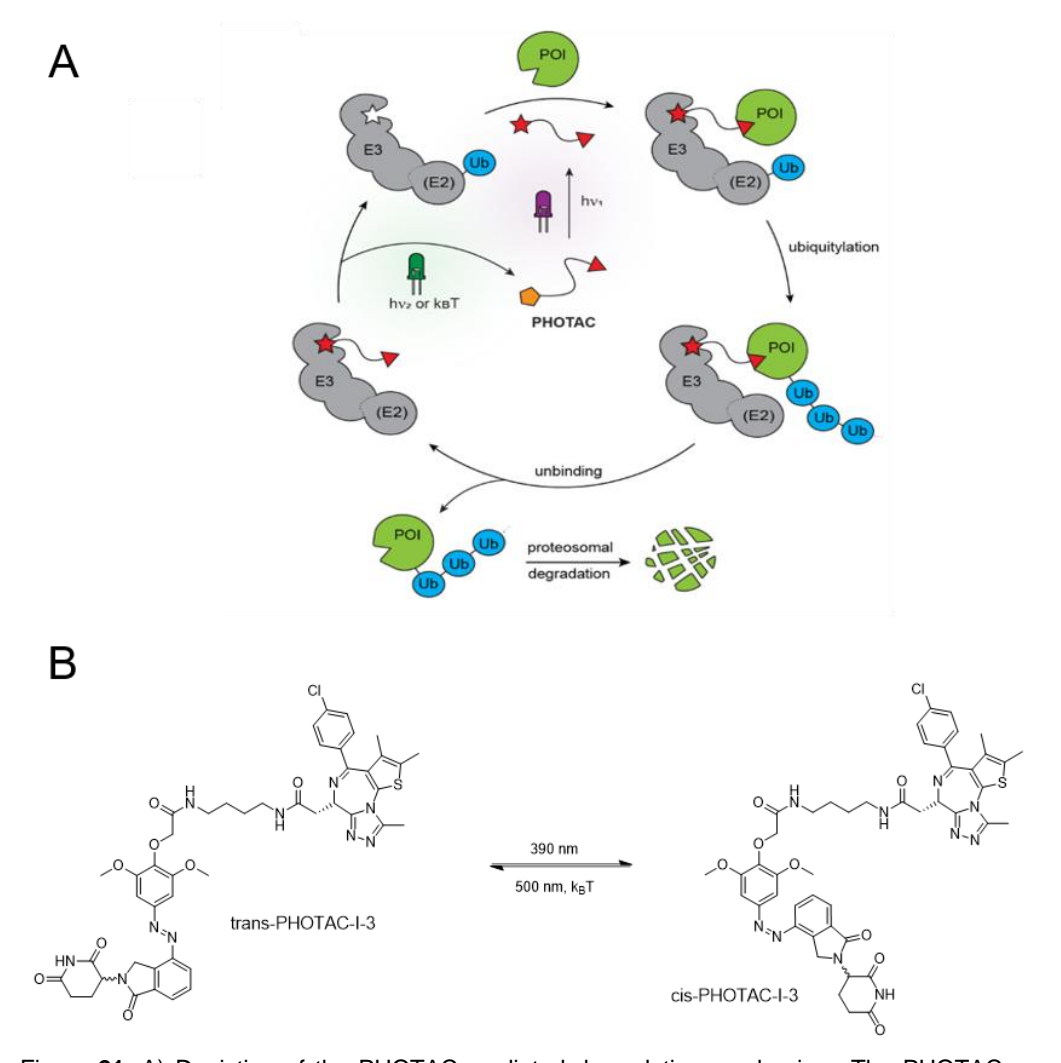


Figure 21. A) Depiction of the PHOTAC-mediated degradation mechanism. The PHOTAC can be switched between the inactive (orange) or active (red) conformation by irradiation with light. The active PHOTAC can then form ternary complexes with the E3 ligase and the POI to induce proteasomal degradation. Reprinted with permission from Ko, T.; Jou, C.; Grau-Perales, A. B.; Reynders, M. Fenton, A. A. and Trauner, D. Photoactivated Protein Degraders for Optical Control of Synaptic Function. ACS Chem. Neurosci. 2023, 3704-3713. (256) B) Switching of a PHOTAC from the *trans*to the *cis*-state with the wavelengths necessary for the switch.

1.3 Scope of the thesis

The aim of this work is the development of novel intracellular allosteric antagonists for the chemokine receptors CXCR1, CXCR2, CCR6, and CCR7. To this end, the squaramide-based scaffold of navarixin as well as the thiadiazole-1,1-dioxide scaffold from Cmpd2105 will be modified in different regions to obtain valuable structure-activity relationship data on the affinity and selectivity of the synthesized antagonists. Additionally, the introduction of a clickable propargylamide handle will be pursued to enable the late-stage functionalization of the synthesized antagonists.

Figure 22. Overview of the residues that will be modified during the synthesis of novel chemokine receptor antagonists.

Firstly, the clickable navarixin- and Cmpd2105-derived building blocks will be functionalized with a TAMRA-fluorophore to enable the establishment of NanoBRET assays. To this end, our cooperation partner will fuse a nanoluciferase to the intracellular part of the respective chemokine receptor. With the help of this assay, it will be possible to distinguish between intracellular and extracellular allosteric antagonists. The intracellular antagonists will compete for binding with the fluorescent tracer, thereby reducing the measured BRET signal and indicating their binding to the IABS. This NanoBRET platform can then be used to evaluate the binding affinities of the synthesized antagonists to their chemokine receptor. Additionally, the selectivity of the synthesized compounds between a selection of chemokine receptors will be investigated.

The best performing compound from each scaffold will then be used as the POI ligand in the synthesis of PROTACs targeting the different chemokine receptors. To this end, two different sets of PROTACs will be synthesized. The first set will focus on the effect of different cereblon targeting thalidomide derivatives to better understand the effect of the E3 ligase ligand on the degradation of the chemokine receptors. The second set of PROTACs will focus on variations regarding the linker flexibility and their physicochemical properties.

The final project aims to exploit the innovative PHOTAC approach as a powerful tool to achieve precise spatiotemporal control of protein degradation. To this end, three PHOTACs will be designed targeting histone deacetylase 6 (HDAC6), based on the established HDAC6-PROTAC A6 previously developed by the Hansen group. The thalidomide moiety will be replaced with a photoswitchable, lenalidomide-based cereblon recruiter to create light-responsive PHOTACs. These PHOTACs will then be evaluated for their ability to switch from the *trans*- to the *cis*-state. Finally, western blot experiments will be performed to assess their degradation efficiency in both photostates.

2. Fluorescent ligands enable target engagement studies for the intracellular allosteric binding site of the chemokine receptor CXCR2

Max. E. Huber, Silas Wurnig, Lara Toy, Corinna Weiler, Nicole Merten, Evi Kostenis, Finn K. Hansen and Matthias Schiedel

J. Med. Chem. 2023, 66, 9916-9933.

*These authors contributed equally.

Please refer to Appendix I for the publication's full text and Supporting Information.

2.1 Publication summary

The chemokine receptor CXCR2 is highly expressed on the surface of inflammatory cells and is implicated in trafficking and recruitment of neutrophilic cells. (204) Therefore CXCR2 overexpression is associated with the pathogenesis of various diseases including inflammatory diseases like ulcerative colitis, psoriasis, chronic obstructive pulmonary disease (COPD), bronchial asthma as well as various types of cancer. (257)

Consequently, significant efforts have been devoted to the discovery and development of CXCR2 antagonists. (258) The most notable discovery was identifying an intracellular allosteric binding site of CXCR2 by cocrystallizing the compound 00767013 with the receptor. (204) This led to the development of navarixin, an intracellular antagonist that progressed to phase II clinical trials. However, like other developed CXCR2 antagonists such as elubrixin (6) and danirixin (7), navarixin showed limited therapeutic efficacy and the development was terminated after phase II clinical trials. Therefore, new approaches are urgently needed for the development of novel intracellular allosteric antagonists and to determine their binding affinities. In 2020, Salchow *et. al.* reported a radioligand binding assay using [³H]Sch527123 as a molecular tool to measure the binding affinities of allosteric CXCR2 antagonists. (259) Although this was considered a breakthrough, radioligand binding assays have several disadvantages, including high infrastructural requirements for radiation protection, heterogeneous assay protocols, and the accumulation of radioactive waste. In addition, the necessary washing steps to remove unbound radioligand before assay measurement hinder

the use of this assay in high-throughput screenings for novel antagonists. Hence, developing new methods for high-throughput screening is of utmost importance.

The previously used approach to develop fluorescent tracers for the IABS of CCR2 and CCR9 has proven to be a viable option for the development of high-throughput assays for chemokine receptors. (218) (219) For this purpose, we employed a structure-based design starting from the previously cocrystallized CXCR2 ligand 00767013. (106) These studies showed that the dimethylbenzamide moiety of 00767013 and navarixin is sufficiently solvent exposed to enable the installation of a linker unit while retaining the necessary affinity towards the IABS of CXCR2. Therefore, a synthetic route based on the work of Tavares et. al was established to obtain a squaramide-based fluorescent CXCR2 ligand. (260) To enable the late-stage functionalization of the CXCR2 ligand with a cell-permeable TAMRA-based fluorophore for NanoBRET assays via a Cu(I)-catalyzed azide-alkyne cycloaddition (CuAAC), the dimethylamide moiety was replaced with a propargylamide in a first step. First, 3-nitrosalicylic acid was activated using PyBroP prior to its reaction with the clickable propargylamine handle. The nitro group was then reduced using tin(II)chloride monohydrate to obtain the free amine 12, which was directly coupled with dimethyl squarate to afford the monosubstituted squaramide **13**. The optically pure (*R*)-2,2-dimethyl-1-(5-methylfuran-2-yl)propan-1-amine (**18**) was obtained by a diastereoselective chiral addition route using Ellman's sulfinimide ((S)-2methylpropane-2-sulfinamide, 15) and 5-methylfurfuryl aldehyde (14) to obtain the imine intermediate (16), which was directly treated with tert-butyl magnesium chloride to obtain the sulfinamide 17. (261) (262) ¹H NMR, ¹³C NMR, and HPLC experiments confirmed that 17 was obtained as a diastereoselective addition product. The free amine 18 was obtained by cleavage of the chiral auxiliary using HCl in diethyl ether. Subsequent coupling with the monosubstituted squaramide compound 13 provided the clickable ligand 19. Finally, the cycloaddition reaction of 19 with the azido-functionalized TAMRA analogues yielded the final fluorescent CXCR2 probes 9a-c.

To evaluate the binding affinities of the synthesized fluorescent probes **9a-c**, a NanoBRET-based binding assay was developed. To this end, CXCR2 was fused at its intracellular C-terminus to a nanoluciferase (Nluc). Saturation binding experiments demonstrated that the synthesized fluorescent tracers **9a-c** possess low nanomolar binding affinities with K_d values ranging from 2.62 to 4.62 nM. In a selectivity study, **9a** also showed a sub-micromolar affinity of towards CXCR1 (K_d (CXCR1) = 198 nM), which was expected given by the low CXCR2/1 selectivity of the parent ligand **3**. However, our fluorescent probe showed over ~ 50-fold selectivity for CXCR2 over CXCR1. Further selectivity screenings showed no significant binding to other chemokine receptors with a reported drugabble IABS such as CCR2, CCR7

and CCR9. To investigate the suitability of 9a as a molecular tool, the binding of published non-fluorescent ligands to the IABS of CXCR2 was examined in a NanoBRET assay. For the known intracellular CXCR2 antagonists 2-4, binding affinities were measured that were in very good agreement with the previously reported picomolar affinities from the aforementioned radioligand assay. To demonstrate the potential of the fluorescent tracer 9a, the NanoBRET binding assay was transferred to a live cell setup. This measurement is crucial because these antagonists target an intracellular binding pocket, requiring them to cross the cell membrane to be biologically effective. For this, HEK293T cells transiently expressing the CXCR2_Nluc construct were used. Using this setup, a Kd of 0.25 nM was determined for our fluorescent tracer 9a, revealing that the fluoresecent ligand can pass through the cell membrane and bind to CXCR2 at the intracellular allosteric binding site. Using the fluorescent tracer 9a, picomolar to low nanomolar K values were determined for the literature known CXCR2 antagonists 2 and 4. These results align with the affinities detected in the cell-free setup showing great agreement between both assays. Lastly, the suitability of 9a as a fluorescent probe to visualize cellular target engagement for ligands targeting the IABS of CXCR2 was proven by fluorescence microscopy. Costaining experiments with a CXCR2-directed fluorescent antibody showed a good overlap with the membrane-associated fluorescence of 9a. Preincubation with the nonfluorescent intracellular antagonists 2 and 3 resulted in a significant reduction in membrane-based fluorescence without a decrease in antibody fluorescence, thereby proving the applicability of **9a** as a tool for live cell imaging.

2.2 Author contribution

Within this project I designed, synthesized, and structurally characterized compounds **8** and **10-19** referring to the numbering within the publication. Apart from that, I contributed to the main text and the Supporting Information.

Development of a NanoBRET assay platform to detect intracellular ligands for the chemokine receptors CCR6 and CXCR1

Max E. Huber,* Silas L. Wurnig,* Aurélien F. A. Moumbock, Lara Toy, Evi Kostenis, Ana A. Bartolomé, Martyna Szpakowska, Andy Chevigné, Stefan Günther, Finn K. Hansen,* Matthias Schiedel*

ChemMedChem 2024, 19, e202400284.

*These authors contributed equally.

Please refer to Appendix II for the publication's full text and Supporting Information.

3.1 Publication summary

G protein-coupled receptors (GPCRs) are crucial for cellular signaling and are important drug targets for various diseases. (3) Most known GPCR ligands bind to the extracellular orthosteric binding site, but recent research has identified additional allosteric binding sites inside the cell. (219) (218) One such site, the intracellular allosteric binding site (IABS), has been discovered in several GPCRs, including chemokine receptors. (218) (219) Ligands that target the IABS offer a new approach to modulate receptor function and may offer better selectivity, particularly for receptors where traditional ligands have shown limited success. However, discovering and optimizing these intracellular allosteric ligands is challenging due to their complex pharmacology. The limitations of traditional radioligand binding assays have prompted researchers to develop innovative techniques, such as small-molecule fluorescent tracers, for more efficient studies of intracellular binding. (218) Emerging tools like NanoBRET-based binding assays offer detailed insights into both the occurrence and location of ligand binding, enhancing drug discovery efforts targeting intracellular GPCR binding sites. Previous research indicated the presence of a druggable IABS at receptors such as CXCR1 and CCR6, thereby providing potential new avenues for therapeutic intervention in inflammation and immunooncology.

Motivated by the off-target inhibition of the previously studied intracellular fluorescent ligands (3-5) with CXCR1, their utility as tracer molecules to monitor the binding of non-fluorescent

ligands to the IABS of CXCR1 was explored in this research. To this end, a NanoBRET-based competition binding assay using membranes from HEK293T cells expressing a C-terminally Nluc-tagged CXCR1 construct (CXCR1_Nluc) was used. Among the fluorescent tracers, LT221 (5) exhibited the highest affinity for CXCR1, making it a prime candidate for further investigations.

This setup was used to determine the binding affinity of the known dual CXCR1/CXCR2 antagonist navarixin (1) and a linker-ligand conjugate XI (6) based on a squaramide scaffold. Interestingly, 6 showed an even higher affinity for CXCR1 compared to 1, suggesting the potential for structural modifications to enhance binding affinity. Importantly, no significant competition with the extracellular orthosteric CXCR1 agonist CXCL8 was observed, confirming the noncompetitive allosteric binding mode of intracellular chemokine receptor antagonists. Docking studies predicted the binding of 1 and 6 to the IABS of CXCR1, consistent with the observed affinities.

Transitioning to live cell assays confirmed that the fluorescent ligand $\mathbf{5}$ can penetrate the cell membrane and bind to CXCR1_Nluc, demonstrating its suitability for studying intracellular ligand binding in physiologically relevant conditions. Moreover, cellular competition binding assays with $\mathbf{5}$ revealed low nanomolar K_i values for $\mathbf{1}$ and $\mathbf{6}$, consistent with the affinities observed in the cell-free setup.

Overall, the results from both membrane-based and live cell experiments agree well, highlighting the potential of **5** as a valuable tool for investigating ligand binding to the IABS of CXCR1 in live cells.

Intrigued by the findings that ligands containing a squaramide motif, a characteristic of intracellular chemokine receptor antagonists, also interact with CCR6, a NanoBRET assay using a CCR6-Nluc fusion protein was set up to explore the potential of previously reported squaramide-based ligands **3-5** as fluorescent tracers for CCR6.

In saturation binding experiments using membranes from HEK293T cells expressing CCR6_Nluc, ligand **5** exhibited the highest binding affinity among the tested ligands, with a K_D value of 38.0 \pm 5.0 nM. The tracer **5** could be completely displaced by the ligand **1** and the linker-conjugate **6**, demonstrating its suitability as a tracer for CCR6. Docking studies supported intracellular CCR6 binding of **6**, with a predicted binding mode similar to that of the squaramide-based ligand 00767013.

After establishing **5** as a reliable fluorescent tracer, the membrane-based assay was used to measure the binding affinities of known intracellular ligands for CXCR2 and CXCR1 such as SB225002 (**9**), cmp24 (**10**) and reparixin (**11**). Additionally, CCR6 ligands such as CCR6

antagonist 1 (12), CCR6 inhibitor 1 (13) and PF-07054894 (2) were tested for their affinities towards CCR6. The screening of compounds for competition with 5 at 10 µM revealed that the diarylurea 8 and squaramide-based compound 10 showed strong competition for intracellular CXCR1 binding, aligning with their known affinity for CXCR1. In contrast, the high-affinity dual CXCR1/CXCR2 antagonist 11 did not compete with 5, suggesting that it binds instead to an extracellular allosteric site. For CCR6 ligands, compounds 12 and 13 showed no competition with 5, suggesting distinct binding sites. In contrast, the squaramide-based compound 2, a potent CCR6 antagonist, exhibited strong competition with 5, suggesting its binding to the IABS of CCR6 and supporting its role in inhibiting CCL20/CCR6-mediated T-cell chemotaxis. Interestingly, the screening revealed an overlap between intracellular CXCR1 and CCR6 ligands, especially among squaramides. Notably, the CCR6-targeting 2 also showed binding to CXCR1, whereas the dual CXCR1/CXCR2 antagonist 10 exhibited significant affinity for CCR6.

Intrigued by the remarkable 150-fold increase in CCR6 affinity achieved by replacing the ethyl group at the chiral carbon of compound **1** with a *tert*-butyl group in **10**, a systematic exploration of the structure-activity relationships (SARs) at this critical position was performed. For this, various analogues of **1** with different substituents at this position were synthesized and evaluated. The new compounds included linear, branched, and cyclic alkyl groups as well as a phenyl group. The synthesis of these compounds was adapted from the previously reported procedures for the CXCR2-targeted fluorescent probes.

By combining the screening platform for CXCR1 and CCR6 with the previously established CXCR2 assay, the selectivity profiles of the synthesized analogues were investigated, revealing the *tert*-butyl moiety as the sterical sweet spot for enhancing CCR6 affinity. Docking experiments were performed to investigate the significant impact of the *tert*-butyl group on CCR6 affinity, which is facilitated by hydrophobic interactions with an aromatic cage formed by specific amino acids in the IABS CCR6.

In contrast, smaller residues such as hydrogen, methyl, or ethyl groups, as well as flat aliphatic residues, such as cyclopropyl or cyclobutyl exhibited limited hydrophobic interactions necessary for binding to the aromatic cage, leading to reduced CCR6 affinity. However, branched aliphatic groups like isopropyl, isobutyl, and cyclopentyl demonstrated some ability to engage in hydrophobic interactions with the aromatic cage. Aliphatic or aromatic sixmembered rings, such as cyclohexyl and phenyl, appeared to penetrate too deeply into the binding pocket, leading to potential steric clashes and diminished CCR6 affinities.

Overall, the collected SAR data underscored the crucial importance of a bulky hydrophobic substituent at the chiral carbon of the navarixin-based scaffold for achieving CCR6 affinity. This observation was corroborated by the structure of the clinical candidate $\mathbf{2}$, which features a bulky 1-methylcyclopentyl residue at this crucial position. Docking studies further supported this, showing similar interactions between the 1-methylcyclopentyl moiety of $\mathbf{2}$ and the aromatic cage as predicted for the *tert*-butyl group of $\mathbf{10}$. To assess whether the robust low nanomolar CCR6 affinity observed for $\mathbf{10}$ under cell-free conditions translates to cellular activity, a cell-based NanoBRET competition binding assay was performed. The measured K_i value of the cell-based assay was similar to the cell-free assay.

This initial estimation of cellular CCR6 affinity was corroborated by a cellular NanoBiT-based β -arrestin-2 recruitment assay. Here, compound **10** demonstrated a notable inhibition of CCL20-induced β -arrestin-2 recruitment, resulting in a K_i value of 11.4 nM. These findings underscore the potent inhibitory effect of **10** on CCR6 activity, aligning with its low nanomolar CCR6 affinity observed in both cell-free and cell-based assays.

3.2 Author contribution

Within this project, I designed, synthesized, and structurally characterized compounds **20**, **21b**-j, **23-26**, and **27a-j** referring to the numbering within the publication. Apart from that, I created Scheme 1 and contributed to the main text and the Supporting Information.

4. A fluorescent probe enables the discovery of improved antagonists targeting the intracellular allosteric binding site of the chemokine receptor CCR7

Silas L. Wurnig,[‡] Max E. Huber,[‡] Corinna Weiler,[‡] Hanna Baltrukevich, Nicole Merten, Isabel Stötzel, Yinshui Chang, René H. L. Klammer, Dirk Baumjohann, Eva Kiermaier, Peter Kolb, Evi Kostenis,* Matthias Schiedel,* Finn K. Hansen*

J. Med. Chem. 2025, 68, 4308-4333.

[‡]These authors contributed equally.

Please refer to Appendix III for the publication's full text and Supporting Information.

4.1 Publication summary

G-protein coupled receptors (GPCRs) are important drug targets, as they are targeted by more than 30% of currently utilized medications. (1) (2) Traditionally, drug development has focused on the orthosteric site of GPCRs, a conserved area within the helical bundle accessible from the extracellular side of the receptor. However, recent studies have uncovered a conserved intracellular allosteric binding site (IABS) in several GPCRs, opening new avenues for therapeutic intervention. This IABS has been identified through X-ray crystallography in chemokine receptors such as CXCR2, CCR2, CCR7, and CCR9, as well as the beta-2-adrenergic receptor (β_2 AR). (200) (201) (202) (203) (204) (205) The IABS discovery across various GPCRs has sparked interest in its potential as a druggable target, particularly for receptors where orthosteric antagonists have shown limited therapeutic success.

Allosteric binding of ligands to the IABS offers a novel dual-mechanism approach to GPCR modulation. This strategy involves stabilizing the inactive conformation of the receptor, leading to negative cooperativity with orthosteric agonists. In addition, the resulting steric hindrance blocks the binding of intracellular transducers like G-proteins, kinases, and β -arrestins. This approach is especially promising for chemokine receptors, which are involved in cancers with poor prognoses and in non-oncological conditions, such as immune cell trafficking and inflammatory processes. (209) (210) (211) (212)

CCR7, a chemokine receptor that interacts with CCL19 and CCL21, is primarily expressed in lymphoid tissues, where it plays a crucial role in lymphocyte and dendritic cell homing to secondary lymphoid organs. (143) (144) The absence of known orthosteric antagonists for CCR7 has hindered drug development targeting this receptor. However, the recent discovery of Cmp2105, an intracellular allosteric antagonist binding to the IABS of CCR7, offers a promising starting point for the development of novel CCR7 antagonists. Cmp2105's binding mechanism is similar to the binding mode other known IABS-targeting antagonists in different receptors, such as vercirnon in CCR9 and Cmpd-15PA in the β_2 -AR. (205) (216) In addition, studies have shown that navarixin, an established antagonist for CXCR1/CXCR2, also binds to CCR7's IABS, suggesting that these compounds could serve as lead structures for the development of new intracellular CCR7 antagonists.(205)

The characterization of CCR7 ligands has so far primarily relied on thermofluor stability assays and functional assays such as cellular arrestin recruitment assays. Recent advancements have led to the development of squaramide-based fluorescent tracers targeting the IABS of CCR6, CXCR1 and CXCR2, which have been effectively used in cell-free and cellular binding studies as described in the previous chapters. Building on this, the aim of this research was to develop a fluorescent thiadiazoledioxide-based CCR7 ligand derived from Cmp2105 that would allow to study the binding of established and novel ligands to the IABS of CCR7 in both cell-free and cellular environments.

The structure-based design of a fluorescent tracer targeting the IABS of CCR7 was guided by the co-crystal structure of human CCR7 in complex with Cmp2105. By conjugating a TAMRA fluorophore to a Cmp2105 analog, the fluorescent probe Mz437 (4) was synthesized to investigate ligand binding to the IABS of CCR7.

In experiments using membranes from HEK293T cells expressing CCR7, the synthesized probe **4** demonstrated high-affinity as an intracellular CCR7 ligand. Membrane-based kinetic binding experiments showed that **4** binds quickly and with high affinity, making it a valuable tool for studying ligand binding in high-throughput settings. The probe was also effective in live cell settings, demonstrating its ability to cross cell membranes and bind to the IABS of CCR7 in live cells.

Molecular modeling studies were performed to rationalize the observed 10-fold increase in binding affinity of the desmethylated derivative of Cmp2105 (compound **10**) compared to Cmp2105. This improvement was attributed to the removal of a methyl group at the benzamide motif, which allowed an energetically favorable water molecule to stabilize the protein-ligand

complex. Modeling studies also highlighted the importance of specific structural features, such as the tertiary amide and the *tert*-butyl moieties, in maintaining high binding affinity for CCR7.

To expand the understanding of structure-activity relationships (SARs) for intracellular CCR7 antagonists, a series of novel Cmp2105 and navarixin analogs was synthesized. The synthesis produced a range of derivatives with modifications to the arylalkylamino and benzamide moieties. The screening of these compounds using a NanoBRET-based binding assay for the IABS of CCR7 provided important insights into the SARs of these antagonists. The two best performing compounds (10 and 21m) and the reference Cmpd2105 were selected for further testing.

The efficacy of the CCR7 inhibitors **10**, **21m**, and Cmp2105 was evaluated in recombinant HEK293T cells and primary bone marrow-derived dendritic cells (BMDCs). In HEK293T cells expressing human CCR7, both **10** and **21m** effectively inhibited CCR7's interaction with G proteins and β-arrestins upon CCL19 stimulation, while Cmp2105 showed minimal inhibitory effects. Compound **21m** demonstrated superior efficacy over **10** in these assays. Label-free dynamic mass redistribution assays confirmed that compounds **10** and **21m** effectively inhibited CCR7 activation, whereas Cmp2105 showed no such effect. In primary BMDCs, both **10** and **21m** significantly reduced CCL19-induced cell shape changes, but not those induced by CXCL12 and prostaglandin E₁, thereby confirming their specificity for CCR7.

In summary, two new CCR7 inhibitors, SLW131 (10) and SLW132 (21m), were identified using the fluorescent probe 4. Both compounds demonstrated improved binding affinities and enhanced antagonistic properties compared to the previous gold standard, Cmp2105.

4.2 Author Contributions

Within this project, I designed, synthesized, and structurally characterized compounds **3**, **6**, **7**, **8**, **9**, **10**, **13a-e**, **14a-g**, **15a-g**, **16a-g**, **17a-c**, **18a-c**, **19a-b**, **20a-e**, and **21a-m** referring to the numbering within the publication. Apart from that, I created Figures **1** and **2**, Scheme **1** and **2**, Table **1** and **2**, Supplementary Scheme **1**, Supplementary Table **1** and contributed to the main text and the Supporting Information.

5. Synthesis of novel squaramide-based CCR7 antagonists targeting the chemokine receptor 7 (CCR7)

5.1 Design of novel squaramide-based CCR7 antagonists

Chapter 3 and 4 showed that the best-performing CCR6 and CCR7 ligands contain a *tert*-butyl side chain at the chiral carbon atom and a dimethylamide on the benzamide. The previously synthesized clickable ligands **SLW007**¹ (1) and compound 9 from chapter 4, which showed lower affinity than the respective dimethylamide counterparts, bear a secondary amide. The aim of this chapter was to further investigate the structure-activity relationships (SARs) of tertiary amides on the benzamide part in regards to CCR7 affinity.

5.1.1 Synthesis of novel CCR7 antagonists

Starting from the already published ligand **SLW007** (1) shown in Figure **23** we wanted to modify the residues R¹, R² (marked in green), and R³ (marked in red) to achieve structural diversity for further SAR studies regarding CCR7 affinity. To confirm the previously shown effects of R³ replacement observed in chapter 4 for sulfadiazole-1,1-dioxide-based CCR7 antagonists, we wanted to replace the *tert*-butyl group of **SLW007** with smaller residues like isopropyl, ethyl, methyl and hydrogen. This was done to replicate the change in affinity as observed with the respective compounds from the sulfadiazole-1,1-dioxide series. Additionally, we combined the R³ replacements with changes in the benzamide moiety to further investigate the observed change of affinity from secondary to tertiary amides. Consequently, different terminal alkyne amines and propylamine were used. To achieve this, the respective left and right parts of the molecule were synthesized separately and applied in subsequent substitution reactions with dimethyl squarate.

Figure 23. Intended structural modifications on the benzamide (green) and the secondary amide (red).

_

¹ SLW007 refers to compound 19 from chapter 2

5.1.1.1 Synthesis of the benzamides

For the synthesis of diversified benzamides, the commercially available 3-nitrosalicylic acid was converted to an amide by means of amide coupling reactions with the corresponding amines shown in table 1. Firstly, the amide coupling was performed by the reaction of 3-nitrosalicylic acid (2) with bromo-tris-pyrrolidino-phosphonium hexafluorophosphate (PyBroP) and *N,N'*-diisopropyl-ethylamine (DIPEA) to convert the free acid into an active ester. After formation of the active ester, observed by the change of color from yellow to orange, the corresponding amine was added dropwise to obtain the benzamides 3a-f (Scheme 1). In the next step, the nitro group was reduced by the addition of tin(II) chloride monohydrate to a refluxed mixture of the corresponding nitro compounds to obtain the free anilines 4a-f (Table

HO
$$NO_2$$
 A R^1 NO_2 D NO_2 NO_2 NO_2 R^2 NO_2 NO_2

Scheme 1. Synthesis of the benzamide part. *Reagents and conditions*: (a) corresponding amine, PyBroP, DIPEA, DCM, rt, overnight; (b) SnCl₂·H₂O, MeOH, reflux, 2 h.

Table 1. Overview of the synthesized intermediates.

R ¹ of the amine	R ² of the amine	product structure	compound
<u> </u>		H ₂ N H	4a
		H ₂ N OH O	4b
		H ₂ N OH O	4c
<u>Н</u>	<i></i>	H ₂ N H	4d
<u>н</u>		H ₂ N H N N	4e
<u>н</u>	/	H_2N OH O OH OH OH OH OH OH	4f

5.1.1.2 Synthesis of the primary amines

The chiral alkyl residue on the furan side chain was diversified in the next step. In addition to the *tert*-butyl group, isopropyl, ethyl and methyl residues were implemented. To achieve this the stereospecific synthesis of the previously established *tert*-butyl side chain from chapters 2, 3, and 4 was adapted as shown in Scheme 2.

Scheme **2.** Synthesis of the primary amines. *Reagents and conditions*: (a) Ti(OEt)₄, DCM, rt, overnight. (b) corresponding alkyl magnesium chloride, tetrahydrofuran (THF), 0 °C to rt, 3 days, 18 - 54% yield over two steps. (c) HCl (in Et₂O), Et₂O, rt, 3 h, quantitative yield.

Starting from the commercially available and optically pure Ellman's sulfinamide ((S)-2-methylpropane-2-sulfinamide, purity confirmed by optical rotation measurement), the imine **7** was obtained by a condensation reaction with the commercially available 5-methylfurfural. Imine formation was performed by dissolving both starting compounds in dichloromethane. Due to a stoichiometric amount of water emerging from the condensation reaction, titanium ethoxide was added to the reaction. This chemical is highly reactive towards water with the reaction proceeding as following: $Ti(OEt)_4 + 2 H_2O \rightarrow TiO_2 + 4$ EtOH. Through this reaction, the water is removed in an irreversible way to push the reaction towards the product side. Without further purification steps, the imine **7** was subjected to a Grignard-like reaction with the respective *tert*-butyl-, isopropyl-, ethyl- or methyl magnesium bromides to obtain the diastereospecific addition products **8a-d**. The stereospecificity of this reaction is attributed to the proposed six-membered cyclic transition state shown in Figure **24** that favors the addition of the alkyl magnesium bromide into the desired *R*-conformation of the newly formed stereocenter due to the steric hindrance caused by the bulky substituent. This stereospecificity cannot be achieved for smaller residues like hydrogen, methyl or ethyl. The formation and

Figure 24. Proposed six-membered cyclic transition state of the Grignard addition reaction with the Ellman's imine intermediate. (262)

Scheme **3**. Convergent synthesis of ligands targeting CCR7. *Reagents and conditions*: (a) anilines **4a-e**, dimethyl squarate, MeOH, rt, overnight. (b) mono-substituted squaramides **10a-e**, primary amine hydrochlorides **9a-d**, DIPEA, MeOH, rt, 3 days.

purification of the correct diastereomer was verified by HPLC and NMR measurements. In the final step, the sulfinyl group was removed by treatment with a stoichiometric amount of HCl in a suitable organic solvent such as diethyl ether or tetrahydrofuran to provide the free amines **9a-d** in near quantitative yields after filtration. The four synthesized furan side chains are shown in Table **2**.

Table 2. Overview of the synthesized furfurylamine intermediates.

R ³ of the Grignard reagent	product structure	compound
Т	O NH ₃	9a
Ţ	NH ₃	9b
Y	NH ₃	9c
<u>\</u>	, CI NH ₃	9d

5.1.1.3 Final assembly of the novel CCR7 antagonists

For the final assembly of the target compounds, dimethyl squarate was subjected to two subsequent substitution reactions as shown in Scheme 3. In terms of the substitution sequence, it is crucial to first introduce the aniline side chain since the first substitution of a methoxy group is lowering the reactivity of the product for the second step due to the lowered partial positive character of the second vinylogous ester. Hence, a benzylic or aliphatic amine

is needed for the second substitution since anilines are not nucleophilic enough to perform the second substitution reaction. In the first step of the assembly, the free anilines **4a-e** and dimethyl squarate were dissolved in methanol and stirred overnight to obtain the corresponding mono-substituted compounds **10a-e**. In the last step, the hydrochloride salts **9a-d** or the commercially 5-methyl-2-furanmethanamine were added to the respective mono-substituted squaramides **10a-e** dissolved in methanol. After the addition of DIPEA, the reaction was stirred for three days. Evaporation of the solvents under reduced pressure afforded the crude products, which were purified by preparative HPLC to obtain the final CCR7 ligands **11a-l** shown in Table **3**.

Table 3. Overview of the synthesized CCR7 ligands.

, o	
compound	product structure
11a	HN OH HN
11b	HN OH HN
11c	HN OH HN
11d	NH HN-O
11e	NH HN
11f	NH HN

5.2 Biological evaluation of the novel CCR7 antagonists

The newly synthesized squaramide-based CCR7 antagonists were tested for their affinity towards the chemokine receptor. For this the NanoBRET assay from chapter 4 was employed. This assay was performed by Max E. Huber from the group of Prof. Dr. Matthias Schiedel at the University of Erlangen-Nürnberg and the results are shown in Table **4**. For experimental procedures see Appendix 3.

Table 4. Affinity data of the synthesized antagonists for the chemokine receptor CCR7.

 $pK_i \pm SEM (K_i [nM]) or comp.^a$

compound	structure	CCR7
11a	HN OH HN	5.21 ± 0.06 (6240)
11b	HN OH HN	5.48 ± 0.01 (3300)
11c	HN OH HN	6.53 ± 0.01 (294)
11d	N OH HN	12% comp. @ 10 μM
11e	N OH HN	0% comp. @ 10 μM
11f	N OH HN	25% comp. @ 10 μM
11g	N OH HN	5.79 ± 0.01 (1620)
11h	N OH HN	7.11 ± 0.06 (80.6)
11 i	NH HN	7.34 ± 0.08 (47.4)

11j
$$\frac{1}{1}$$
 5.58 ± 0.04 (2660)
11k $\frac{1}{1}$ 5.81 ± 0.09 (1610)
11l $\frac{1}{1}$ 5.49 ± 0.06 (3340)

^aComp. = percentual competitive tracer displacement at given concentration.

5.2.1 SAR studies on the R¹ and R² positions

The introduction of a methyl group at the R¹-postion of the benzamide moiety improved the affinity of **11h** approximately 4-fold compared to the corresponding secondary amide **11c**. However, the replacement of the methyl group by a second propargyl residue showed no great change in affinity. Hence, the general introduction of a tertiary amide at the benzamide moiety proved to be favorable for the binding to CCR7. The replacement of the propargylamide by a propylamide, but-3-yn-1-amide or hex-5-yn-1-amide showed no effect on the affinity of these ligands towards CCR7.

5.2.2 SAR studies on the R³ position

In the two sets **11a-c** and **11d-h**, the effect of the residue R³ is evident. For both series steric increase of the side chain showed improved affinity towards CCR7. The *tert*-butyl side chain was in both series favored and the binding affinities decreased in the order isopropyl > ethyl > methyl > hydrogen. This aligns with the observed SARs reported in chapter 3 and 4.

5.3 Conclusion

Within this project a series of twelve compounds was designed and synthesized to further explore the SAR of CCR7 ligands. Starting from the SAR data obtained in chapter 4, the steric effect of the alkyl chain at the chiral carbon atom on the affinity towards CCR7 was investigated by implementing different residues at the chiral center. Shorter alkyl chains like methyl and ethyl showed lower affinity towards CCR7 than bulkier carbon chains such as isopropyl and tert-butyl. This is consistent with the SAR data presented in chapter 4 and therefore proves the

transferability of obtained SAR data between the squaramide- and thiadiazole-1,1-dioxide scaffolds. Furthermore, the replacement of secondary amides with tertiary amides on the benzamide part showed an increase in affinity towards CCR7. Based on these results, the development of novel CCR7 antagonist should focus on the implementation of different tertiary amides such as cyclic amides or tertiary amides bearing two carbon chains to further explore the SAR of the benzamide region.

5.5 Experimental section

5.5.1 General information and chemistry

Chemicals were obtained from abcr GmbH (Karlsruhe, Germany), Acros Organics (Geel, Belgien), Carbolution Chemicals (Sankt Ingberg, Germany), Sigma-Aldrich (Steinheim, Germany,) TCI Chemicals (Eschborn, Germany) or VWR (Langenfeld, Germany) and used without further purification. Technical-grade solvents were distilled prior to use. For all HPLC purposes, acetonitrile in HPLC-grade quality (HiPerSolv CHROMANORM, VWR, Langenfeld, Germany) was used. Water was purified with a PURELAB flex® (ELGA VEOLIA, Celle, Germany). Thin-layer chromatography (TLC) was carried out on prefabricated plates (silica gel 60, F254, Merck). Components were visualized either by irradiation with ultraviolet light (254 nm or 366 nm) or by appropriate staining. Column chromatography was carried out on silica gel (60 Å, 40–60 µm, Acros Organics, Geel, Belgien). If no solvent is stated, an aqueous solution was prepared with demineralized water. Mixtures of two or more solvents are specified as "solvent A"/"solvent B", 3/1, v/v, meaning that 100 mL of the respective mixture consists of 75 mL of "solvent A" and 25 mL of "solvent B". The uncorrected melting points were determined using a Büchi (Essen, Germany) Melting Point M-560 apparatus. Diastereomeric ratios were determined by ¹H NMR spectroscopy.

5.5.1.1 Nuclear magnetic resonance spectroscopy (NMR):

Proton (¹H) and carbon (¹³C) NMR spectra were recorded either on a Bruker AVANCE 500 MHz at a frequency of 500 MHz (¹H) and 126 MHz (¹³C) or a Bruker AVANCE III HD 600 MHz at a frequency of 600 MHz (1H) and 151 MHz (13C). The chemical shifts are given in parts per million (ppm). As solvents, deuterated chloroform (CDCl₃), deuterated methanol (methanol-d₄) and deuterated dimethyl sulfoxide (DMSO-d₆) were used. The residual solvent signal (CDCl₃: ¹H NMR: 7.26 ppm, ¹³C NMR: 77.1 ppm; DMSO-d₆: ¹H NMR: 2.50 ppm, ¹³C NMR: 39.52 ppm; methanol-d₄: ¹H NMR: 3.31 ppm, 4.87 ppm, ¹³C NMR: 49.00 ppm) was used for calibration. The multiplicity of each signal is reported as singlet (s), doublet (d), triplet (t), quartet (q), multiplet (m) or combinations thereof. Multiplicities and coupling constants are reported as measured and might disagree with the expected values.

5.5.1.2 Mass spectrometry

High-resolution electrospray-ionization mass spectra (HRMS-ESI) were acquired with a Bruker Daltonik GmbH micrOTOF coupled to a an LC Packings Ultimate HPLC system and controlled by micrOTOFControl3.4 and HyStar 3.2-LC/MS, with a Bruker Daltonik GmbH ESI-qTOF Impact II coupled to a Dionex UltiMateTM 3000 UHPLC system and controlled by micrOTOFControl 4.0 and HyStar 3.2-LC/MS or with a micrOTOF-Q mass spectrometer (Bruker, Bremen, Germany) with ESI-source coupled with an HPLC Dionex UltiMate 3000 (Thermo Scientific, Heysham, United Kingdom). Low-resolution electrospray-ionization mass spectra (LRMS-ESI) were acquired with an Advion expression® compact mass spectrometer (CMS) coupled with an automated TLC plate reader Plate Express® (Advion, Ithaca, NY, USA).

5.5.1.3 High performance liquid chromatography (HPLC)

A Thermo Fisher Scientific (Heysham, United Kingdom) UltiMateTM 3000 UHPLC system with a Nucleodur 100-5 C18 (250 × 4.6 mm, Macherey Nagel, Düren, Germany) with a flow rate of 1 mL/min and a temperature of 25 °C, or a 100-5 C18 (100 × 3 mm, Macherey Nagel, Düren, Germany) with a flow rate of 0.5 mL/min and a temperature of 25 °C was used with an appropriate gradient. For preparative purposes, an AZURA Prep. 500/1000 gradient system with a Nucleodur 110-5 C18 HTec (150 × 32 mm, Macherey Nagel, Düren, Germany) column with 20 mL/min was used. Detection was implemented with UV absorption measurement at wavelengths of λ = 220 nm and λ = 250 nm. Bidest. H₂O (A) and MeCN (B) were used as eluents with an addition of 0.1% TFA in case of eluent A. Purity: The purity of all final compounds was 95% or higher. Purity was determined via HPLC with the Nucleodur 100-5 C18 (250 × 4.6 mm, Macherey Nagel, Düren, Germany) at 250 nm. After column equilibration for 5 min, a linear gradient from 5% A to 95% B in 7 min followed by an isocratic regime of 95% B for 10 min was used.

5.5.2 Synthesis and compound characterization

2-Hydroxy-3-nitro-N-(prop-2-yn-1-yl)benzamide (SLW062, 3a)

$$\bigvee_{O}^{H} \bigvee_{O \cap H}^{NO_2}$$

2-Hydroxy-3-nitrobenzoic acid (1.50 g, 8.03 mmol, 1.00 eq.), bromotrispyrrolidinophosphonium hexafluorophosphate (4.54 g, 9.63 mmol, 1.20 eq.) and

N,N-diisopropylethylamine (5.59 mL, 32.1 mmol, 4.00 eq.) were dissolved in 30 mL of dichloromethane and stirred at room temperature for 30 min. Propargylamine (734 μL, 11.2 mmol, 1.40 eq.) was added and the resulting mixture was stirred overnight. The reaction was then extracted with 1 N sodium hydroxide solution (3 x 100 mL) and the organic phase was discarded. The aqueous phase was then acidified using 1 M hydrochloric acid (300 mL) and the organic products were extracted using ethyl acetate (3 x 150 mL). The organic phase was then dried over sodium sulfate, filtered and concentrated *in vacuo* to afford the crude product, which was then purified by column chromatography using a mixture of dichloromethane, methanol and trifluoroacetic acid (99/0.9/0.1 (v/v)). The title compound was obtained as a pale yellow solid (1.4 g, 79%). ¹H NMR (600 MHz, DMSO- d_6 δ [ppm]): 13.96 (s, 1H) 9.68-9.63 (m, 1H), 8.20-8.14 (m, 1H), 8.13-8.07 (m, 1H), 7.13-7.06 (m, 1H). 4.17-4.10 (m, 2H), 3.22 (t, J = 2.5 Hz, 1H); ¹³C NMR (151 MHz, DMSO- d_6 δ [ppm]): 168.4, 154.5, 138.4, 132.6, 129.2, 118.1, 117.2, 79.9, 73.7, 28.6; LRMS m/z (ESI+) [Found: 221.1, C₁₀H₉N₂O₄+ requires [M+H]+ 221.1]; Rf: 0.65 (dichloromethane/methanol/trifluoroacetic acid) (99/0.9/0.1) (v/v)); mp: 125-128 °C.

2-Hydroxy-N-methyl-3-nitro-N-(prop-2-yn-1-yl)benzamide (SLW129, 3b)

$$\bigvee_{O \quad OH}^{N} NO_2$$

2-Hydroxy-3-nitrobenzoic acid (1.00 g,5.35 mmol, 1.00 eq.), bromotrispyrrolidinophosphonium hexafluorophosphate (3.02 g, 6.42 mmol, 1.20 eq.) and N,N-diisopropylethylamine (3.78 mL, 21.4 mmol, 4.00 eq.) were dissolved in 30 mL of dichloromethane and stirred at room temperature for 30 min. N-methylpropargylamine (666 µL, 7.49 mmol, 1.40 eq.) was added and the resulting mixture was stirred overnight. The reaction was then extracted with 1 N sodium hydroxide solution (3 x 100 mL) and the organic phase was discarded. The aqueous phase was then acidified using 1 M hydrochloric acid (300 mL) and the organic products were extracted using ethyl acetate (3 x 150 mL). The organic phase was then dried over sodium sulfate, filtered and concentrated in vacuo to afford the crude product, which was then purified by column chromatography using a mixture of cyclohexane and ethyl acetate (6/4 (v/v)). The title compound was obtained as a pale yellow oil (1.2 g, 95%). ¹H NMR (500 MHz, DMSO- $d_6 \delta$ [ppm]): 10.71 (s, 1H), 8.05 (dd, J = 8.3, 1.7 Hz, 1H), 7.56 (dd, J = 7.5, 1.7 Hz, 1H), 7.11 (dd, J = 8.4, 7.4 Hz, 1H), 4.32 (s, 1H), 3.39 – 3.21 (m, 2H), 3.10 - 2.81 (m, 3H); ¹³C NMR (126 MHz, DMSO- d_6 δ [ppm]): 166.0, 148.6, 136.2, 134.3, 134.2, 128.4, 125.9, 120.1, 78.9, 74.6, 35.3; LRMS m/z (ESI+) [Found: 235.1, C₁₁H₁₁N₂O₄+ requires [M+H]⁺ 235.1]; Rf: 0.55 (cyclohexane/ethyl acetate (6/4) (v/v)).

2-Hydroxy-3-nitro-*N,N*-di(prop-2-yn-1-yl)benzamide (SLW412, 3c)

2-Hydroxy-3-nitrobenzoic acid (750 mg, 4.01 mmol, 1.00 eq.), bromotrispyrrolidinophosphonium hexafluorophosphate (2.27 g, 4.82 mmol, 1.20 eq.) and N,N-diisopropylethylamine (2.83 mL, 16.1 mmol, 4.00 eq.) were dissolved in 30 mL of dichloromethane and stirred at room temperature for 30 min. Dipropargylamine (659 µL, 5.62 mmol, 1.40 eq.) was added and the resulting mixture was stirred overnight. The reaction was then extracted with 1 N sodium hydroxide solution (3 x 100 mL) and the organic phase was discarded. The aqueous phase was then acidified using 1 M hydrochloric acid (300 mL) and the organic products were extracted using ethyl acetate (3 x 150 mL). The organic phase was then dried over sodium sulfate, filtered and concentrated in vacuo to afford the crude product, which was then purified by column chromatography using ethyl acetate. The title compound was obtained as an orange oil (589 mg, 58%). ¹H NMR (500 MHz, DMSO-d₆ δ [ppm]): 10.76 (s, 1H), 8.09 (dd, J = 8.3, 1.7 Hz, 1H), 7.57 (dd, J = 7.5, 1.7 Hz, 1H), 7.13 (dd, J = 7.5, 1H), 7.15 (dd, J == 8.3, 7.5 Hz, 1H), 4.50 - 3.96 (m, 4H), 3.29 (t, J = 2.5 Hz, 2H); 13 C NMR (126 MHz, DMSO $d_6\delta$ [ppm]): 166.0, 149.1, 136.3, 134.4, 127.7, 126.4, 120.3, 78.4, 75.9, 75.1, 37.6, 33.5, 20.9; LRMS m/z (ESI⁺) [Found: 259.1, $C_{13}H_{11}N_2O_4$ requires [M+H]⁺ 259.1]; Rf: 0.78 (ethyl acetate).

2-Hydroxy-3-nitro-N-propylbenzamide (SLW413, 3d)

2-Hydroxy-3-nitrobenzoic acid (750 g, 4.01 mmol, 1.00 eq.), bromotrispyrrolidinophosphonium hexafluorophosphate (2.27 g, 4.82 mmol, 1.20 eq.) and *N,N*-diisopropylethylamine (2.83 mL, 16.1 mmol, 4.00 eq.) were dissolved in 30 mL of dichloromethane and stirred at room temperature for 30 min. Propylamine (476 μL, 5.62 mmol, 1.40 eq.) was added and the resulting mixture was stirred overnight. The reaction was then extracted with 1 N sodium hydroxide solution (3 x 100 mL) and the organic phase was discarded. The aqueous phase was then acidified using 1 M hydrochloric acid (300 mL) and the organic products were extracted using ethyl acetate (3 x 150 mL). The organic phase was then dried over sodium sulfate, filtered and concentrated *in vacuo* to afford the crude product, which was then purified by column chromatography using ethyl acetate. The title compound was obtained as a yellow

solid (697 mg, 78%). ¹H NMR (500 MHz, DMSO- d_6 δ [ppm]): 9.22 (s, 1H), 8.18 (dd, J = 8.0, 1.6 Hz, 1H), 8.07 (dd, J = 8.1, 1.6 Hz, 1H), 7.06 (t, J = 8.0 Hz, 1H), 3.30 - 3.26 (m, 2H), 1.61 - 1.53 (m, 2H), 0.90 (t, J = 7.4 Hz, 3H); ¹³C NMR (126 MHz, DMSO- d_6 δ [ppm]): 168.6, 154.9, 138.5, 132.2, 129.1, 117.6, 117.1, 41.0, 21.8, 11.3; LRMS m/z (ESI⁺) [Found: 225.1, $C_{10}H_{13}N_2O_4^+$ requires [M+H]⁺ 225.1]; Rf: 0.48 (ethyl acetate); mp: 106 – 109 °C.

N-(But-3-yn-1-yl)-2-hydroxy-3-nitrobenzamide (SLW414, 3e)

$$\bigvee_{O} \bigvee_{O} \bigvee_{O} \bigvee_{O} \bigvee_{O}$$

2-Hydroxy-3-nitrobenzoic acid (750 mg, 4.01 mmol. 1.00 eq.), bromotrispyrrolidinophosphonium hexafluorophosphate (2.27 g, 4.82 mmol, 1.20 eq.) and N,N-diisopropylethylamine (2.83 mL, 16.1 mmol, 4.00 eq.) were dissolved in 30 mL of dichloromethane and stirred at room temperature for 30 min. But-3-yn-1-amine hydrochloride (502 mg, 4.62 mmol, 1.15 eq.) was added and the resulting mixture was stirred overnight. The reaction was then extracted with 1 N sodium hydroxide solution (3 x 100 mL) and the organic phase was discarded. The aqueous phase was then acidified using 1 M hydrochloric acid (300 mL) and the organic products were extracted using ethyl acetate (3 x 150 mL). The organic phase was then dried over sodium sulfate, filtered and concentrated in vacuo to afford the crude product, which was then purified by column chromatography using ethyl acetate. The title compound was obtained as a pale yellow solid (807 mg, 86%). ¹H NMR (500 MHz, DMSO- d_6 δ [ppm]): 14.27 (s, 1H), 9.38 (t, J = 5.7 Hz, 1H), 8.16 (dd, J = 7.9, 1.6 Hz, 1H), 8.09 (dd, J = 8.2, 1.6 Hz, 1H), 7.08 (t, J = 8.0 Hz, 1H), 3.47 - 3.42 (m, 2H), 2.86 (t, J = 2.6 Hz, 1H),2.50 - 2.43 (m, 2H); ¹³C NMR (126 MHz, DMSO- d_6 δ [ppm]): 168.7, 154.7, 138.5, 132.3, 129.3, 117.8, 117.1, 81.7, 72.4, 38.2, 18.2; LRMS m/z (ESI+) [Found: 235.1, C₁₁H₁₁N₂O₄+ requires [M+H]⁺ 235.1]; Rf: 0.64 (ethyl acetate); mp: 108 – 110 °C.

N-(Hex-5-yn-1-yl)-2-hydroxy-3-nitrobenzamide (SLW415, 3f)

2-Hydroxy-3-nitrobenzoic acid (600 mg, 3.21 mmol, 1.00 eq.), bromotrispyrrolidinophosphonium hexafluorophosphate (1.81 g, 3.85 mmol, 1.20 eq.) and *N,N*-diisopropylethylamine (2.26 mL, 12.8 mmol, 4.00 eq.) were dissolved in 30 mL of dichloromethane and stirred at room temperature for 30 min. Hex-5-yn-1-amine hydrochloride

(509 mg, 3.69 mmol, 1.15 eq.) was added and the resulting mixture was stirred overnight. The reaction was then extracted with 1 N sodium hydroxide solution (3 x 100 mL) and the organic phase was discarded. The aqueous phase was then acidified using 1 M hydrochloric acid (300 mL) and the organic products were extracted using ethyl acetate (3 x 150 mL). The organic phase was then dried over sodium sulfate, filtered and concentrated *in vacuo* to afford the crude product, which was then purified by column chromatography using ethyl acetate. The title compound was obtained as a pale yellow solid (589 mg, 58%). 1 H NMR (500 MHz, DMSO- d_6 δ [ppm]): 14.52 (s, 1H), 9.23 (t, J = 5.7 Hz, 1H), 8.17 (dd, J = 8.0, 1.6 Hz, 1H), 8.07 (dd, J = 8.2, 1.6 Hz, 1H), 7.05 (t, J = 8.0 Hz, 1H), 3.38 - 3.31 (m, 2H), 2.74 (t, J = 2.7 Hz, 1H), 2.24 - 2.17 (m, 2H), 1.70 - 1.63 (m, 2H), 1.55 – 1.46 (m, 2H); 13 C NMR (126 MHz, DMSO- d_6 δ [ppm]): 168.6, 154.9, 138.4, 132.3, 129.1, 117.6, 117.1, 84.2, 71.3, 38.7, 27.7, 25.4, 17.3; LRMS m/z (ESI $^+$) [Found: 263.1, C₁₃H₁₅N₂O₄ $^+$ requires [M+H] $^+$ 263.1]; Rf: 0.78 (ethyl acetate); mp: 99 – 102 $^{\circ}$ C.

3-Amino-2-hydroxy-N-(prop-2-yn-1-yl)benzamide (SLW073, 4a)

$$\bigvee_{O \quad OH}^{H} \bigvee_{NH_2}$$

2-Hydroxy-3-nitro-*N*-(prop-2-yn-1-yl)benzamide (**3a**, 1.00 g, 4.50 mmol, 1.00 *eq.*) and tin(II) chloride dihydrate (5.18 g, 22.5 mmol, 5.00 *eq.*) were dissolved in methanol (20 mL) and heated under reflux for an hour. After cooling, the mixture was extracted with ethyl acetate (4 x 100 mL). After drying over sodium sulfate, filtration and evaporation of the solvent the title compound was obtained as a brown oil in quantitative yield that was used without further purification. LRMS m/z (ESI+) [Found: 191.3, $C_{10}H_{11}N_2O_2$ + requires [M+H]+ 191.2].

3-Amino-2-hydroxy-N-methyl-N-(prop-2-yn-1-yl)benzamide (SLW133, 4b)

$$\bigvee_{O \quad OH}^{N} \mathsf{NH}_2$$

2-Hydroxy-*N*-methyl-3-nitro-*N*-(prop-2-yn-1-yl)benzamide (**3b**, 1.15 g, 4.86 mmol, 1.00 *eq*.) and tin(II) chloride dihydrate (5.48 g, 24.3 mmol, 5.00 *eq*.) were dissolved in methanol (25 mL) and heated under reflux for an hour. After cooling, the mixture was extracted with ethyl acetate (4 x 100 mL). After drying over sodium sulfate, filtration and evaporation of the solvent the title

compound was obtained as a brown oil in quantitative yield that was used without further purification. LRMS m/z (ESI⁺) [Found: 205.1, C₁₁H₁₃N₂O₂⁺ requires [M+H]⁺ 205.1].

3-Amino-2-hydroxy-*N*,*N*-di(prop-2-yn-1-yl)benzamide (SLW416, 4c)

2-Hydroxy-3-nitro-N,N-di(prop-2-yn-1-yl)benzamide (**3c**, 600 mg, 2.30 mmol, 1.00 eq.) and tin(II) chloride dihydrate (2.65 g, 11.5 mmol, 5.00 eq.) were dissolved in methanol (25 mL) and heated under reflux for an hour. After cooling, the mixture was extracted with ethyl acetate (4 x 100 mL). After drying over sodium sulfate, filtration and evaporation of the solvent the title compound was obtained as a brown oil in quantitative yield that was used without further purification. LRMS m/z (ESI+) [Found: 229.1, $C_{13}H_{13}N_2O_2$ + requires [M+H]+ 229.1].

3-Amino-2-hydroxy-N-propylbenzamide (SLW417, 4d)

2-Hydroxy-3-nitro-*N*-propylbenzamide (**3d**, 550 mg, 2.43 mmol, 1.00 *eq.*) and tin(II) chloride dihydrate (2.80 g, 12.2 mmol, 5.00 *eq.*) were dissolved in methanol (25 mL) and heated under reflux for an hour. After cooling, the mixture was extracted with ethyl acetate (4 x 100 mL). After drying over sodium sulfate, filtration and evaporation of the solvent the title compound was obtained as a brown oil in quantitative yield that was used without further purification. LRMS m/z (ESI+) [Found: 195.1, $C_{10}H_{14}N_2O_2^+$ requires [M+H]+ 195.1].

3-Amino-N-(but-3-yn-1-yl)-2-hydroxybenzamide (SLW418, 4e)

N-(But-3-yn-1-yl)-2-hydroxy-3-nitrobenzamide (**3e**, 550 g, 2.33 mmol, 1.00 eq.) and tin(II) chloride dihydrate (2.68 g, 11.6 mmol, 5.00 eq.) were dissolved in methanol (25 mL) and heated under reflux for an hour. After cooling, the mixture was extracted with ethyl acetate (4 x 100 mL). After drying over sodium sulfate, filtration and evaporation of the solvent the title

compound was obtained as a brown oil in quantitative yield that was used without further purification. LRMS m/z (ESI⁺) [Found: 205.1, C₁₁H₁₃N₂O₂⁺ requires [M+H]⁺ 205.1].

3-Amino-N-(hex-5-yn-1-yl)-2-hydroxybenzamide (SLW419, 4f)

N-(Hex-5-yn-1-yl)-2-hydroxy-3-nitrobenzamide (**3f**, 550 g, 2.08 mmol, 1.00 *eq*.) and tin(II) chloride dihydrate (2.39 g, 10.4 mmol, 5.00 *eq*.) were dissolved in methanol (25 mL) and heated under reflux for an hour. After cooling, the mixture was extracted with ethyl acetate (4 x 100 mL). After drying over sodium sulfate, filtration and evaporation of the solvent the title compound was obtained as a brown oil in quantitative yield that was used without further purification. LRMS m/z (ESI⁺) [Found: 233.1, C₁₃H₁₆N₂O₂⁺ requires [M+H]⁺ 233.1].

2-Hydroxy-3-[(2-methoxy-3,4-dioxocyclobut-1-en-1-yl)amino]-*N*-(prop-2-yn-1-yl)benzamide (SLW081, 10a)

3-Amino-2-hydroxy-N-(prop-2-yn-1-yl)benzamide (**4a**, 250 mg, 1.31 mmol, 1.00 *eq*.) and 3,4-dimethoxycyclobut-3-ene-1,2-dione (187 mg, 1.31 mmol, 1.00 *eq*.) were dissolved in methanol (10 mL) and stirred overnight. Filtration of the solids and drying under reduced pressure afforded the title compound as a green gum (240 mg, 61% yield) that was used without further purification. LRMS m/z (ESI⁺) [Found: 301.2, $C_{15}H_{13}N_2O_5^+$ requires [M+H]⁺ 301.3].

2-Hydroxy-3-[(2-methoxy-3,4-dioxocyclobut-1-en-1-yl)amino]-*N*-methyl-*N*-(prop-2-yn-1-yl)benzamide (SLW135, 10b)

3-Amino-2-hydroxy-*N*-methyl-*N*-(prop-2-yn-1-yl)benzamide (**4b**, 230 mg, 1.13 mmol, 1.00 *eq*.) and 3,4-dimethoxycyclobut-3-ene-1,2-dione (176 mg, 1.24 mmol, 1.10 *eq*.) were dissolved in methanol (10 mL) and stirred overnight. Filtration of the solids and drying under reduced

pressure afforded the title compound as a green gum (550 mg, 72% yield) that was used without further purification. LRMS m/z (ESI⁺) [Found: 315.3, $C_{16}H_{15}N_2O_5^+$ requires [M+H]⁺ 315.3].

2-Hydroxy-3-[(2-methoxy-3,4-dioxocyclobut-1-en-1-yl)amino]-*N,N*-di(prop-2-yn-1-yl)benzamide (SLW421, 10c)

3-Amino-2-hydroxy-N,N-di(prop-2-yn-1-yl)benzamide (**4c**, 438 mg, 1.92 mmol, 1.00 eq.) and 3,4-dimethoxycyclobut-3-ene-1,2-dione (273 mg, 1.92 mmol, 1.00 eq.) were dissolved in methanol (10 mL) and stirred overnight. Filtration of the solids and drying under reduced pressure afforded the title compound as a green gum (407 mg, 63% yield) that was used without further purification. LRMS m/z (ESI⁺) [Found: 339.2, $C_{18}H_{15}N_2O_5^+$ requires [M+H]⁺ 339.3].

2-Hydroxy-3-[(2-methoxy-3,4-dioxocyclobut-1-en-1-yl)amino]-*N*-propylbenzamide (SLW422, 10d)

3-Amino-2-hydroxy-*N*-propylbenzamide (**4d**, 472 mg, 2.43 mmol, 1.00 *eq*.) and 3,4-dimethoxycyclobut-3-ene-1,2-dione (345 mg, 2.43 mmol, 1.00 *eq*.) were dissolved in methanol (10 mL) and stirred overnight. Filtration of the solids and drying under reduced pressure afforded the title compound as a green gum (431 mg, 58% yield) that was used without further purification. LRMS m/z (ESI⁺) [Found: 305.3, $C_{15}H_{17}N_2O_{5}^+$ requires [M+H]⁺ 305.3].

N-(But-3-yn-1-yl)-2-hydroxy-3-[(2-methoxy-3,4-dioxocyclobut-1-en-1-yl)amino]benzamide (SLW423, 10e)

3-Amino-*N*-(but-3-yn-1-yl)-2-hydroxybenzamide (**4e**, 280 mg, 1.37 mmol, 1.00 *eq*.) and 3,4-dimethoxycyclobut-3-ene-1,2-dione (292 mg, 2.06 mmol, 1.50 *eq*.) were dissolved in methanol (10 mL) and stirred overnight. Filtration of the solids and drying under reduced pressure afforded the title compound as a green gum (410 mg, 62% yield) that was used without further purification. LRMS m/z (ESI⁺) [Found: 315.3, $C_{16}H_{15}N_2O_5^+$ requires [M+H]⁺ 315.3].

N-(Hex-5-yn-1-yl)-2-hydroxy-3-[(2-methoxy-3,4-dioxocyclobut-1-en-1-yl)amino]benzamide (SLW424, 10f)

3-Amino-*N*-(hex-5-yn-1-yl)-2-hydroxybenzamide (**4f**, 438 mg, 1.89 mmol, 1.00 *eq*.) and 3,4-dimethoxycyclobut-3-ene-1,2-dione (268 mg, 1.89 mmol, 1.00 *eq*.) were dissolved in methanol (10 mL) and stirred overnight. Filtration of the solids and drying under reduced pressure afforded the title compound as a green gum (378 mg, 59% yield) that was used without further purification. LRMS m/z (ESI⁺) [Found: 343.4, $C_{18}H_{19}N_2O_5^+$ requires [M+H]⁺ 343.4].

(S,E)-2-Methyl-N-[(5-methylfuran-2-yl)methylene]propane-2-sulfinamide (SLW076, 7)

(S)-2-Methylpropane-2-sulfinamide (2.00 g, 16.2 mmol, 1.00 eq.) was dissolved in dichloromethane (10 mL). 5-Methylfuran-2-carboxaldehyde (1.69 mL, 16.2 mmol, 1.00 eq.), titanium ethoxide (7.46 mL, 35.6 mmol, 2.20 eq.) and sodium sulfate (2 g) were added under stirring. The reaction mixture was stirred at room temperature overnight, filtered through celite, and rinsed with dichloromethane. Evaporation of the solvent gave the crude product in quantitative yield, which was used without further purification.

(S)-2-Methyl-N-[(R)-1-(5-methylfuran-2-yl)ethyl]propane-2-sulfinamide (SLW358, 8a)

A 250 mL flask was sealed with a septum flushed with N_2 and filled with THF (20 mL). A 3 M methylmagnesium chloride solution in THF (5.83 mL, 17.5 mmol, 2.20 eq.) was added and the solution was cooled to 0 °C. (S,E)-2-Methyl-N-[(5-methylfuran-2-yl)methylene]propane-2-

sulfinamide (**7**, 1.70 g, 8.00 mmol, 1.00 eq.) was dissolved in 20 mL THF and added dropwise to the vigorously stirred solution. After addition the mixture was stirred for 72 h. The reaction mixture was then quenched by the addition of saturated ammonium chloride solution (50 mL) and extracted using ethyl acetate (3 x 100 mL). Drying over sodium sulfate, filtration, and evaporation of the solvent resulted in the crude product, which was purified by column chromatography using a gradient of dichloromethane, and ethyl acetate (dichloromethane to dichloromethane/ethyl acetate (8/2) to dichloromethane/ethyl acetate (5/5) (v/v)). The title compound was obtained as a dark orange to red oil (330 mg, 18%). ¹H NMR (500 MHz, DMSO-d₆ δ [ppm]) 6.16 & 6.09 (d, J = 3.1 Hz, 1H), 5.99 -5.94 (m, 1H), 5.49 & 5.32 (d, J = 7.1 Hz, 1H), 4.37 - 4.29 (m, 1H), 2.23 - 2.19 (m, 3H), 1.45 & 1.41 (d, J = 6.8 Hz, 3H), 1.10 & 1.09 (s, 9H); ¹³C NMR (126 MHz, DMSO-d₆ δ [ppm]) 155.1, 154.9, 150.3, 106.7, 106.4, 106.1, 106.1, 55.0, 49.3, 48.5, 22.5, 22.4, 22.3, 21.9, 21.3, 20.9, 13.2; LRMS m/z (ESI⁺) [Found: 230.5, C₁₁H₂₂NO₂S⁺ requires [M+H]⁺ 230.3]; R_f: 0.24 (dichloromethane/ethyl acetate (1/1) (v/v)); Diastereomeric ratio: dr = 3:1

(S)-2-Methyl-N-[(R)-1-(5-methylfuran-2-yl)propyl]propane-2-sulfinamide (SLW164, 8b)

A 250 mL flask was sealed with a septum flushed with N₂ and filled with THF (20 mL). A 2 M ethylmagnesium chloride solution in THF (5.15 mL, 17.5 mmol, 2.20 eq.) was added and the solution was cooled to 0 °C. (S,E)-2-Methyl-N-[(5-methylfuran-2-yl)methylene]propane-2sulfinamide (7, 1.70 g, 8.00 mmol, 1.00 eq.) was dissolved in 20 mL THF and added dropwise to the vigorously stirred solution. After addition the mixture was stirred for 72 h. The reaction mixture was then quenched by the addition of saturated ammonium chloride solution (50 mL) and extracted using ethyl acetate (3 x 100 mL). Drying over sodium sulfate, filtration, and evaporation of the solvent resulted in the crude product, which was purified by column chromatography using a gradient of dichloromethane, and ethyl acetate (dichloromethane to dichloromethane/ethyl acetate (8/2) to dichloromethane/ethyl acetate (5/5) (v/v)). The title compound was obtained as a dark orange to red oil (520 mg, 27%). ¹H NMR (600 MHz, DMSO- $d_6 \delta$ [ppm]) 6.10 (d, J = 3.1 Hz, 1H), 5.97 – 5.94 (m, 1H), 5.26 (d, J = 6.0 Hz, 1H), 4.08 (q, J = 6.7 Hz, 1H), 2.20 (s, 3H), 1.84 - 1.76 (m, 2H), 1.09 (s, 9H), 0.86 (t, J = 7.4 Hz, 3H);NMR (151 MHz, DMSO-*d*₆ δ [ppm]) 153.8, 150.3, 107.2, 106.0, 55.5, 55.0, 27.6, 22.5, 13.2, 10.5; LRMS m/z (ESI⁺) [Found: 244.5, $C_{12}H_{22}NO_2S^+$ requires [M+H]⁺ 244.4]; R_f : 0.24 (dichloromethane/ethyl acetate (1/1) (v/v)); Diastereomeric ratio: dr = 1:0

(S)-2-Methyl-N-[(R)-2-methyl-1-(5-methylfuran-2-yl)propyl]propane-2-sulfinamide (SLW163, 8c)

A 250 mL flask was sealed with a septum flushed with N₂ and filled with THF (20 mL). A 2 M isopropylmagnesium chloride solution in THF (5.15 mL, 10.3 mmol, 2.20 eq.) was added and the solution was cooled to 0 °C. (S,E)-2-Methyl-N-[(5-methylfuran-2-yl)methylene]propane-2sulfinamide (7, 1.0 g, 4.7 mmol, 1.0 eq.) was dissolved in 20 mL THF and added dropwise to the vigorously stirred solution. After addition the mixture was stirred for 72 h. The reaction mixture was then guenched by the addition of saturated ammonium chloride solution (50 mL) and extracted using ethyl acetate (3 x 100 mL). Drying over sodium sulfate, filtration, and evaporation of the solvent resulted in the crude product, which was purified by column chromatography using a gradient of dichloromethane and ethyl acetate (dichloromethane to dichloromethane/ethyl acetate (8/2) to dichloromethane/ethyl acetate (5/5) (v/v)). The title compound was obtained as a dark orange to red oil (220 mg, 18%). ¹H NMR (600 MHz, DMSO- d_6 δ [ppm]) 6.08 (d, J = 3.1 Hz, 1H), 5.98 - 5.94 (m, 1H), 5.10 (d, J = 6.1 Hz, 1H), 3.97 (t, J = 6.3 Hz, 1H), 2.20 (s, 3H), 2.12 - 2.03 (m, J = 6.8 Hz, 1H), 1.07 (s, 9H), 0.91 (d, J = 6.8 Hz, 1H)6.8 Hz, 3H), 0.82 (d, J = 6.8 Hz, 3H); ¹³C NMR (151 MHz, DMSO- d_6 δ [ppm]) 152.9, 150.2, 107.9, 106.0, 59.7, 55.2, 32.0, 22.5, 19.4, 18.6, 13.3; LRMS m/z (ESI+) [Found: 258.1, $C_{13}H_{24}NO_2S^+$ requires [M+H]⁺ 258.4]; R_f: 0.14 (dichloromethane/ethyl acetate (7/3) (ν/ν)); Diastereomeric ratio: dr = 1:0

(*S*)-*N*-[(*R*)-2,2-Dimethyl-1-(5-methylfuran-2-yl)propyl]-2-methylpropane-2-sulfinamide (SLW077, 8d)

A 250 mL flask was sealed with a septum flushed with N_2 and filled with THF (20 mL). A 2 M tert-butylmagnesium chloride solution in THF (5.15 mL, 10.3 mmol, 2.20 eq.) was added and the solution was cooled to 0 °C. (S,E)-2-Methyl-N-[(5-methylfuran-2-yl)methylene]propane-2-sulfinamide ($\mathbf{7}$, 1.0 g, 4.7 mmol, 1.0 eq.) was dissolved in 20 mL THF and added dropwise to the vigorously stirred solution. After addition the mixture was stirred for 72 h. The reaction

mixture was then quenched by the addition of saturated ammonium chloride solution (50 mL) and extracted using ethyl acetate (3 x 100 mL). Drying over sodium sulfate, filtration, and evaporation of the solvent resulted in the crude product which was purified by column chromatography using a gradient of dichloromethane, and ethyl acetate (dichloromethane to dichloromethane/ethyl acetate (8/2) to dichloromethane/ethyl acetate (5/5) (v/v)). The title compound was obtained as a dark orange to red oil (690 mg, 54%). ¹H NMR (500 MHz, DMSO- d_6 δ [ppm]) 6.11 (d, J = 3.1 Hz, 1H), 5.98 – 5.95 (m, 1H), 4.64 (d, J = 6.3 Hz, 1H), 3.94 (d, J = 6.3 Hz, 1H), 2.21 (s, 3H), 1.05 (s, 9H), 0.92 (s, 9H); ¹³C NMR (126 MHz, DMSO- d_6 δ [ppm]) 152.5, 149.9, 108.5, 106.0, 62.9, 55.3, 35.3, 26.5, 22.2, 13.2; LRMS m/z (ESI⁺) [Found: 272.5, $C_{14}H_{26}NO_2S^+$ requires [M+H]⁺ 272.4]; R_f : 0.28 (cyclohexane/ethyl acetate (7/3) (v/v)); Diastereomeric ratio: dr = 1:0

(R)-1-(5-Methylfuran-2-yl)ethan-1-amine hydrochloride (SLW371, 9a)

(*S*)-2-Methyl-*N*-[(*R*)-1-(5-methylfuran-2-yl)ethyl]propane-2-sulfinamide (**8a**, 85 mg, 0.40 mmol, 1.0 *eq.*) was dissolved in diethyl ether (10 mL) and cooled to 0 °C. After addition of 2 M HCl in diethyl ether (0.45 mL, 0.90 mmol, 2.5 *eq.*) the mixture was stirred for 1 h. After evaporation of the solvents **9a** was obtained as a reddish oil that was used in the next step without further purification. LRMS m/z (ESI+) [Found: 126.2, $C_7H_{12}NO^+$ requires [M+H]+ 126.2].

(R)-1-(5-Methylfuran-2-yl)propan-1-amine hydrochloride (SLW166, 9b)

(*S*)-2-Methyl-*N*-[(*R*)-1-(5-methylfuran-2-yl)propyl]propane-2-sulfinamide (**8b**, 300 mg, 1.20 mmol, 1.00 *eq*.) was dissolved in diethyl ether (10 mL) and cooled to 0 °C. After addition of 2 M HCl in diethyl ether (1.6 mL, 3.0 mmol, 2.5 *eq*.) the mixture was stirred for 1 h. After evaporation of the solvents **9b** was obtained as a reddish oil that was used in the next step without further purification. LRMS m/z (ESI⁺) [Found: 140.2, $C_8H_{15}NO^+$ requires [M+H]⁺ 140.2].

(R)-2-Methyl-1-(5-methylfuran-2-yl)propan-1-amine hydrochloride (SLW165, 9c)

(*S*)-2-Methyl-*N*-[(*R*)-2-methyl-1-(5-methylfuran-2-yl)propyl]propane-2-sulfinamide (8c, 300 mg, 1.17 mmol, 1.00 *eq.*) was dissolved in diethyl ether (10 mL) and cooled to 0 °C. After addition of 2 M HCl in diethyl ether (1.5 mL, 2.9 mmol, 2.5 *eq.*) the mixture was stirred for 1 h. After evaporation of the solvents 9c was obtained as a reddish oil that was used in the next step without further purification. LRMS m/z (ESI⁺) [Found: 154.4, C₉H₁₆NO⁺ requires [M+H]⁺ 154.2].

(R)-2,2-Dimethyl-1-(5-methylfuran-2-yl)propan-1-amine hydrochloride (SLW079, 9d)

(*S*)-*N*-[(*R*)-2,2-Dimethyl-1-(5-methylfuran-2-yl)propyl]-2-methylpropane-2-sulfinamide (8d, 845 mg, 3.10 mmol, 1.00 *eq.*) was dissolved in diethyl ether (10 mL) and cooled to 0 °C. After addition of 2 M HCl in diethyl ether (1.5 mL, 2.9 mmol, 2.5 *eq.*) the mixture was stirred for 1 h. After evaporation of the solvents 9d was obtained as a reddish oil that was used in the next step without further purification. LRMS m/z (ESI+) [Found: 168.3, $C_{10}H_{18}NO^+$ requires [M+H]+ 168.2].

(*R*)-2-Hydroxy-3-[(2-{[1-(5-methylfuran-2-yl)propyl]amino}-3,4-dioxocyclobut-1-en-1-yl)amino]-*N*-(prop-2-yn-1-yl)benzamide (SLW170, 11a)

2-Hydroxy-3-[(2-methoxy-3,4-dioxocyclobut-1-en-1-yl)amino]-N-(prop-2-yn-1-yl)benzamide (**10a**, 0.10 g, 0.33 mmol, 1.0 eq.) and (R)-1-(5-Methylfuran-2-yl)propan-1-amine hydrochloride (**9b**, 70 mg, 0.50 mmol, 1.5 eq.) were dissolved in methanol (10 mL). After the addition of N,N-diisopropylethylamine (0.12 mL, 0.66 mmol, 2.0 eq.), the reaction was stirred for 3 days. Extraction between water and ethyl acetate (3 × 50 mL), drying over sodium sulfate, filtration, and evaporation of the solvent gave the crude product that was purified by preparative HPLC (acetonitrile/water (0.1% TFA): gradient 5–95%) to obtain the title compound as a white-brown amorphous solid (81 mg, 60%). 1 H NMR (600 MHz, DMSO- d_6 , δ [ppm]): 13.62 (s, 1H), 9.47 (t, J = 5.6 Hz, 1H), 9.35 (s, 1H), 8.69 (d, J = 9.0 Hz, 1H), 8.00 (d, J = 8.2 Hz, 1H), 7.54 (d, J = 8.2 Hz, 1H), 6.90 (t, J = 8.1 Hz, 1H), 6.26 (d, J = 3.1 Hz, 1H), 6.05 (d, J = 3.1 Hz, 1H), 5.14 (q,

J = 7.8 Hz, 1H), 4.13 - 4.10 (m, 2H), 3.20 (t, J = 2.5 Hz, 1H), 2.26 (s, 3H), 1.99 - 1.95 (m, 1H), 1.93 - 1.83 (m, 1H), 0.92 (t, J = 7.3 Hz, 3H); ¹³C NMR (151 MHz, DMSO-d₆, δ [ppm]): 184.1, 180.2, 169.8, 168.6, 163.1, 152.0, 151.4, 150.9, 128.0, 123.4, 120.6, 118.3, 113.5, 107.6, 106.4, 80.3, 73.4, 52.8, 28.4, 27.2, 13.3, 10.2; HRMS m/z (ESI⁺) [found: 407.1554, C₂₂H₂₂N₃O₅⁺ requires [M + H]⁺ 407.1481]; HPLC retention time 12.60 min, purity: 95.3%.

(*R*)-2-Hydroxy-3-[(2-{[2-methyl-1-(5-methylfuran-2-yl)propyl]amino}-3,4-dioxocyclobut-1-en-1-yl)amin]-*N*-(prop-2-yn-1-yl)benzamide (SLW168, 11b)

2-Hydroxy-3-[(2-methoxy-3,4-dioxocyclobut-1-en-1-yl)amino]-*N*-(prop-2-yn-1-yl)benzamide (**10a**, 0.10 g, 0.33 mmol, 1.0 *eq*.) and (*R*)-2-Methyl-1-(5-methylfuran-2-yl)propan-1-amine hydrochloride (**9c**, 51 mg, 0.33 mmol, 1.0 *eq*.) were dissolved in methanol (10 mL). After the addition of *N*,*N*-diisopropylethylamine (0.12 mL, 0.66 mmol, 2.0 *eq*.), the reaction was stirred for 3 days. Extraction between water and ethyl acetate (3 × 50 mL), drying over sodium sulfate, filtration, and evaporation of the solvent gave the crude product that was purified by preparative HPLC (acetonitrile/water (0.1% TFA): gradient 5–95%) to obtain the title compound as a white-brown amorphous solid (75 mg, 53%). ¹H NMR (600 MHz, DMSO- d_6 , δ [ppm]): 13.66 - 13.62 (m, 1H), 9.57 – 9.38 (m, 2H), 8.73 - 8.68 (m, 1H), 8.01 - 7.98 (m, 1H), 7.56 - 7.53 (m, 1H), 6.90 (t, *J* = 8.1 Hz, 1H), 6.25 - 6.22 (m, 1H), 6.05 (s, 1H), 5.27 – 4.97 (m, 1H), 4.13 - 4.10 (m, 2H), 3.21 - 3.18 (m, 1H), 2.27 - 2.26 (m, 3H), 2.20 - 2.15 (m, 1H), 1.94 – 1.29 (m, 1H), 1.01 – 0.86 (m, 6H); ¹³C NMR (151 MHz, DMSO- d_6 , δ [ppm]): 184.1, 180.2, 169.8, 168.7, 163.1, 152.3, 151.4, 151.2, 128.0, 123.5, 120.7, 118.3, 113.4, 107.9, 106.4, 80.3, 73.4, 57.3, 51.1, 35.9, 32.1, 28.4, 19.1, 18.6, 18.2, 13.3; HRMS m/z (ESI+) [found: 422.1710, C₂₃H₂₄N₃O₅+ requires [M + H]+ 422.1638]; HPLC retention time 12.82 min, purity: 96.6%.

(*R*)-3-[(2-{[2,2-Dimethyl-1-(5-methylfuran-2-yl)propyl]amino}-3,4-dioxocyclobut-1-en-1-yl)amino]-2-hydroxy-*N*-(prop-2-yn-1-yl)benzamide (SLW090, 11c)

2-Hydroxy-3-[(2-methoxy-3,4-dioxocyclobut-1-en-1-yl)amino]-*N*-(prop-2-yn-1-yl)benzamide (**10a**, 0.13 g, 0.43 mmol, 1.0 *eq.*) and (*R*)-2,2-Dimethyl-1-(5-methylfuran-2-yl)propan-1-amine hydrochloride (**9d**, 88 mg, 0.43 mmol, 1.0 *eq.*) were dissolved in methanol (10 mL). After the addition of *N*,*N*-diisopropylethylamine (0.23 mL, 1.3 mmol, 3.0 *eq.*), the reaction was stirred for 3 days. Extraction between water and ethyl acetate (3 × 50 mL), drying over sodium sulfate, filtration, and evaporation of the solvent gave the crude product that was purified by preparative HPLC (acetonitrile/water (0.1% TFA): gradient 5–95%) to obtain the title compound as a white-brown amorphous solid (120 mg, 64%). ¹H NMR (500 MHz, MeOD-*d*₄, δ [ppm]): NH and OH signals were not detectable due to proton exchange, 8.11 (dd, *J* = 8.1, 1.3 Hz, 1H), 7.41 (dd, *J* = 8.1, 1.4 Hz, 1H), 6.86 (t, *J* = 8.1 Hz, 1H), 6.15 (d, *J* = 3.1 Hz, 1H), 5.99 - 5.96 (m, 1H), 5.19 (s, 1H), 4.16 (d, *J* = 2.5 Hz, 2H), 2.62 (t, *J* = 2.5 Hz, 1H), 2.29 (s, 3H), 1.05 (s, 9H); ¹³C NMR (126 MHz, MeOD-*d*₄, δ [ppm]): 185.4, 182.1, 171.5, 170.4, 164.7, 152.9, 152.5, 152.1, 129.3, 124.9, 122.1, 119.6, 115.3, 109.8, 107.1, 80.5, 72.2, 62.6, 36.9, 29.5, 26.8, 13.5; HRMS m/z (ESI⁺) [found: 458.1686, C₂₇H₃₃N₆O₆⁺ requires [M + Na]⁺ 458.1794]; HPLC retention time 13.02 min, purity: 96.0%.

2-Hydroxy-*N*-methyl-3-[(2-{[(5-methylfuran-2-yl)methyl]amino}-3,4-dioxocyclobut-1-en-1-yl)amino]-*N*-(prop-2-yn-1-yl)benzamide (SLW482, 11d)

2-Hydroxy-3-[(2-methoxy-3,4-dioxocyclobut-1-en-1-yl)amino]-*N*-methyl-*N*-(prop-2-yn-1-yl)benzamide (**10b**, 90 mg, 0.29 mmol, 1.0 eq.) and 5-methyl-2-furanmethanamine (32 μL, 0.29 mmol, 1.0 eq.) were dissolved in methanol (10 mL). After the addition of *N*,*N*-diisopropylethylamine (0.10 mL, 0.58 mmol, 2.0 eq.), the reaction was stirred for 3 days. Extraction between water and ethyl acetate (3 × 50 mL), drying over sodium sulfate, filtration, and evaporation of the solvent gave the crude product that was purified by preparative HPLC (acetonitrile/water (0.1% TFA): gradient 5–95%) to obtain the title compound as a white-brown amorphous solid (80 mg, 64%). ¹H NMR (500 MHz, DMSO- d_6 , δ [ppm]): 9.82 (s, 1H), 9.26 (s, 1H), 8.61 (t, J = 5.9 Hz, 1H), 7.79 (d, J = 7.8 Hz, 1H), 6.95 – 6.84 (m, 2H), 6.28 (d, J = 3.1 Hz, 1H), 6.05 (d, J = 3.1 Hz, 1H), 4.77 (d, J = 5.9 Hz, 2H), 4.19 (s, 2H), 3.28 (s, 1H), 2.95 (s, 3H), 2.26 (s, 3H); ¹³C NMR (126 MHz, DMSO- d_6 , δ [ppm]): 184.2, 180.4, 168.9, 168.0, 163.6, 151.7, 149.5, 143.2, 128.9, 124.1, 122.0, 121.2, 120.1, 108.9, 106.6, 79.1, 74.9, 40.1, 13.3; HRMS

m/z (ESI⁺) [found: 394.3175, $C_{21}H_{20}N_3O_5^+$ requires [M + H]⁺ 394.1325]; HPLC retention time 11.91 min, purity: 97.6%.

(*R*)-2-Hydroxy-*N*-methyl-3-[(2-{[1-(5-methylfuran-2-yl)ethyl]amino}-3,4-dioxocyclobut-1-en-1-yl)amino]-*N*-(prop-2-yn-1-yl)benzamide (SLW483, 11e)

2-Hydroxy-3-[(2-methoxy-3,4-dioxocyclobut-1-en-1-yl)amino]-*N*-methyl-*N*-(prop-2-yn-1-yl)benzamide (**10b**, 90 mg, 0.29 mmol, 1.0 eq.) and (*R*)-1-(5-Methylfuran-2-yl)ethan-1-amine hydrochloride (**9a**, 60 mg, 0.37 mmol, 1.3 eq.) were dissolved in methanol (10 mL). After the addition of *N*,*N*-diisopropylethylamine (0.10 mL, 0.58 mmol, 2.0 eq.), the reaction was stirred for 3 days. Extraction between water and ethyl acetate (3 × 50 mL), drying over sodium sulfate, filtration, and evaporation of the solvent gave the crude product that was purified by preparative HPLC (acetonitrile/water (0.1% TFA): gradient 5–95%) to obtain the title compound as a white-brown amorphous solid (34 mg, 29%). ¹H NMR (500 MHz, DMSO- d_6 , δ [ppm]): 9.83 (s, 1H), 9.23 (s, 1H), 8.66 (d, J = 8.6 Hz, 1H), 7.80 (d, J = 8.0 Hz, 1H), 6.95 – 6.84 (m, 2H), 6.26 (d, J = 3.1 Hz, 1H), 6.05 (d, J = 3.1 Hz, 1H), 5.33 (p, J = 7.3 Hz, 1H), 4.18 (s, 2H), 3.30 – 3.25 (m, 1H), 2.95 (s, 3H), 2.26 (s, 3H), 1.56 (d, J = 6.9 Hz, 3H); ¹³C NMR (126 MHz, DMSO- d_6 , δ [ppm]): 184.0, 180.2, 168.2, 168.0, 163.5, 153.0, 151.4, 143.1, 128.9, 124.1, 122.0, 121.1, 120.1, 107.0, 106.4, 79.1, 74.9, 47.0, 40.1, 20.3, 13.3; HRMS m/z (ESI⁺) [found: 408.1521, $C_{22}H_{22}N_3O_5^+$ requires [M + H]⁺ 408.1481]; HPLC retention time 12.11 min, purity: 96.9%.

(*R*)-2-Hydroxy-*N*-methyl-3-[(2-{[1-(5-methylfuran-2-yl)propyl]amino}-3,4-dioxocyclobut-1-en-1-yl)amino]-*N*-(prop-2-yn-1-yl)benzamide (SLW484, 11f)

2-Hydroxy-3-[(2-methoxy-3,4-dioxocyclobut-1-en-1-yl)amino]-N-methyl-N-(prop-2-yn-1-yl)benzamide (**10b**, 90 mg, 0.29 mmol, 1.0 eq.) and (R)-1-(5-Methylfuran-2-yl)propan-1-amine hydrochloride (**9b**, 75 mg, 0.43 mmol, 1.5 eq.) were dissolved in methanol (10 mL). After the addition of N,N-diisopropylethylamine (0.10 mL, 0.58 mmol, 2.0 eq.), the reaction was stirred for 3 days. Extraction between water and ethyl acetate (3 × 50 mL), drying over sodium sulfate,

filtration, and evaporation of the solvent gave the crude product that was purified by preparative HPLC (acetonitrile/water (0.1% TFA): gradient 5–95%) to obtain the title compound as a white-brown amorphous solid (65 mg, 54%). 1 H NMR (500 MHz, DMSO- d_{6} , δ [ppm]): 9.83 (s, 1H), 9.26 (s, 1H), 8.62 (d, J = 9.0 Hz, 1H), 7.80 (d, J = 7.9 Hz, 1H), 6.94 – 6.82 (m, 2H), 6.25 (d, J = 3.1 Hz, 1H), 6.04 (d, J = 3.1 Hz, 1H), 5.13 (q, J = 7.7 Hz, 1H), 4.18 (s, 2H), 3.30 - 3.26 (m, 1H), 2.95 (s, 3H), 2.26 (s, 3H), 1.99 - 1.94 (m, 1H), 1.92 - 1.81 (m, 1H), 0.92 (t, J = 7.3 Hz, 3H); 13 C NMR (126 MHz, DMSO- d_{6} , δ [ppm]): 184.0, 180.2, 168.6, 168.0, 163.4, 152.1, 151.3, 143.1, 129.0, 124.1, 122.0, 121.2, 120.1, 107.5, 106.4, 79.1, 74.9, 52.8, 40.1, 27.2, 13.3, 10.2; HRMS m/z (ESI+) [found: 422.1694, $C_{23}H_{24}N_{3}O_{5}$ + requires [M + H]+ 422.1638]; HPLC retention time 12.36 min, purity: 97.4%.

(*R*)-2-Hydroxy-*N*-methyl-3-[(2-{[2-methyl-1-(5-methylfuran-2-yl)propyl]amino}-3,4-dioxocyclobut-1-en-1-yl)amino}-*N*-(prop-2-yn-1-yl)benzamide (SLW485, 11g)

2-Hydroxy-3-[(2-methoxy-3,4-dioxocyclobut-1-en-1-yl)amino]-*N*-methyl-*N*-(prop-2-yn-1-yl)benzamide (**10b**, 90 mg, 0.29 mmol, 1.0 eq.) and (*R*)-2-Methyl-1-(5-methylfuran-2-yl)propan-1-amine hydrochloride (**9c**, 65 mg, 0.34 mmol, 1.2 eq.) were dissolved in methanol (10 mL). After the addition of *N*,*N*-diisopropylethylamine (0.10 mL, 0.58 mmol, 2.0 eq.), the reaction was stirred for 3 days. Extraction between water and ethyl acetate (3 × 50 mL), drying over sodium sulfate, filtration, and evaporation of the solvent gave the crude product that was purified by preparative HPLC (acetonitrile/water (0.1% TFA): gradient 5–95%) to obtain the title compound as a white-brown amorphous solid (52 mg, 42%). ¹H NMR (500 MHz, DMSO- d_6 , δ [ppm]): 9.85 (s, 1H), 9.36 (s, 1H), 8.66 (d, J = 9.6 Hz, 1H), 7.79 (d, J = 7.8 Hz, 1H), 6.95 – 6.84 (m, 2H), 6.22 (d, J = 3.1 Hz, 1H), 6.05 (d, J = 3.1 Hz, 1H), 5.07 - 5.03 (m, 1H), 4.19 (s, 2H), 3.30 - 3.28 (m, 1H), 2.96 (s, 3H), 2.27 (s, 3H), 2.23 - 2.14 (m, 1H), 0.97 (d, J = 6.7 Hz, 3H), 0.90 (d, J = 6.7 Hz, 3H); ¹³C NMR (126 MHz, DMSO- d_6 , δ [ppm]): 184.0, 180.2, 168.7, 168.0, 163.4, 151.5, 151.3, 151.2, 143.2, 128.9, 124.2, 122.0, 121.3, 120.1, 107.9, 106.4, 106.3, 79.1, 57.2, 40.1, 32.1, 19.1, 18.2, 13.3; HRMS m/z (ESI+) [found: 436.1810, C₂₄H₂₆N₃O₅+ requires [M + H]+ 436.1794]; HPLC retention time 12.59 min, purity: 98.5%.

(*R*)-3-[(2-{[2,2-Dimethyl-1-(5-methylfuran-2-yl)propyl]amino}-3,4-dioxocyclobut-1-en-1-yl)amino]-2-hydroxy-*N*-methyl-*N*-(prop-2-yn-1-yl)benzamide (SLW137, 11h)

2-Hydroxy-3-[(2-methoxy-3,4-dioxocyclobut-1-en-1-yl)amino]-*N*-methyl-*N*-(prop-2-yn-1-yl)benzamide (**10b**, 50 mg, 0.16 mmol, 1.0 eq.) and (*R*)-2,2-Dimethyl-1-(5-methylfuran-2-yl)propan-1-amine hydrochloride (**9d**, 40 mg, 0.24 mmol, 1.5 eq.) were dissolved in methanol (10 mL). After the addition of *N*,*N*-diisopropylethylamine (57 μL, 0.32 mmol, 2.0 eq.), the reaction was stirred for 3 days. Extraction between water and ethyl acetate (3 × 50 mL), drying over sodium sulfate, filtration, and evaporation of the solvent gave the crude product that was purified by preparative HPLC (acetonitrile/water (0.1% TFA): gradient 5–95%) to obtain the title compound as a white-brown amorphous solid (43 mg, 60%). ¹H NMR (500 MHz, DMSO- d_6 , δ [ppm]): 9.87 (s, 1H), 9.48 (s, 1H), 8.73 (d, J = 10.1 Hz, 1H), 7.76 (d, J = 7.9 Hz, 1H), 6.95 – 6.85 (m, 2H), 6.19 (d, J = 3.1 Hz, 1H), 6.05 (d, J = 3.1 Hz, 1H), 5.12 (d, J = 10.1 Hz, 1H), 4.20 (s, 2H), 3.28 (s, 1H), 2.96 (s, 3H), 2.28 (s, 3H), 0.98 (s, 9H); ¹³C NMR (126 MHz, DMSO- d_6 , δ [ppm]): 184.1, 180.3, 168.7, 168.1, 163.4, 151.0, 150.8, 143.3, 128.9, 124.2, 122.1, 121.5, 120.1, 108.5, 106.3, 79.1, 74.9, 60.2, 40.1, 35.7, 26.2, 13.4; HRMS m/z (ESI*) [found: 450.1983, $C_{25}H_{28}N_3O_5^+$ requires [M + H]* 450.1951]; HPLC retention time 12.85 min, purity: 97.8%.

(*R*)-3-[(2-{[2,2-Dimethyl-1-(5-methylfuran-2-yl)propyl]amino}-3,4-dioxocyclobut-1-en-1-yl)amino]-2-hydroxy-*N,N*-di(prop-2-yn-1-yl)benzamide (SLW426, 11i)

2-Hydroxy-3-[(2-methoxy-3,4-dioxocyclobut-1-en-1-yl)amino]-N,N-di(prop-2-yn-1-yl)benzamide (10c, 60 mg, 0.18 mmol, 1.0 eq.) and (R)-2,2-Dimethyl-1-(5-methylfuran-2-yl)propan-1-amine hydrochloride (9d, 39 mg, 0.23 mmol, 1.3 eq.) were dissolved in methanol (10 mL). After the addition of N,N-diisopropylethylamine (63 μ L, 0.36 mmol, 2.0 eq.), the reaction was stirred for 3 days. Extraction between water and ethyl acetate (3×50 mL), drying over sodium sulfate, filtration, and evaporation of the solvent gave the crude product that was purified by preparative HPLC (acetonitrile/water (0.1% TFA): gradient 5–95%) to obtain the

title compound as a white-brown amorphous solid (70 mg, 83%). ¹H NMR (500 MHz, DMSO- d_6 , δ [ppm]): 9.86 (s, 1H), 9.48 (s, 1H), 8.73 (d, J = 10.0 Hz, 1H), 7.77 (d, J = 8.0 Hz, 1H), 6.99 – 6.85 (m, 2H), 6.19 (d, J = 3.1 Hz, 1H), 6.05 (d, J = 3.1 Hz, 1H), 5.12 (d, J = 10.1 Hz, 1H), 4.24 (s, 4H), 3.31 (s, 2H), 2.28 (s, 3H), 0.98 (s, 9H); ¹³C NMR (126 MHz, DMSO- d_6 , δ [ppm]): 184.1, 180.3, 168.7, 167.8, 163.4, 151.0, 150.8, 143.3, 129.1, 123.8, 122.0, 121.9, 120.3, 108.5, 106.3, 78.5, 75.4, 60.2, 40.1, 35.7, 26.2, 13.4; HRMS m/z (ESI+) [found: 474.2009, $C_{27}H_{28}N_3O_5^+$ requires [M + H]+ 474.1951]; HPLC retention time 13.98 min, purity: 98.3%.

(*R*)-3-[(2-{[2,2-Dimethyl-1-(5-methylfuran-2-yl)propyl]amino}-3,4-dioxocyclobut-1-en-1-yl)amino]-2-hydroxy-*N*-propylbenzamide (SLW427,11j)

2-Hydroxy-3-[(2-methoxy-3,4-dioxocyclobut-1-en-1-yl)amino]-N-propylbenzamide (10d, 60 mg, 0.20 mmol, 1.0 eq.) and (R)-2,2-Dimethyl-1-(5-methylfuran-2-yl)propan-1-amine hydrochloride (9d, 43 mg, 0.26 mmol, 1.3 eq.) were dissolved in methanol (10 mL). After the addition of N,N-diisopropylethylamine (70 µL, 0.40 mmol, 2.0 eq.), the reaction was stirred for 3 days. Extraction between water and ethyl acetate (3 x 50 mL), drying over sodium sulfate, filtration, and evaporation of the solvent gave the crude product that was purified by preparative HPLC (acetonitrile/water (0.1% TFA): gradient 5-95%) to obtain the title compound as a whitebrown amorphous solid (62 mg, 71%). ¹H NMR (500 MHz, DMSO-*d*₆, δ [ppm]): 14.12 (s, 1H), 9.54 (s, 1H), 9.00 (t, J = 5.7 Hz, 1H), 8.78 (d, J = 10.1 Hz, 1H), 7.96 (d, J = 8.0 Hz, 1H), 7.56 (d, J = 8.1 Hz, 1H), 6.87 (t, J = 8.0 Hz, 1H), 6.18 (d, J = 3.1 Hz, 1H), 6.04 (d, J = 3.1 Hz, 1H),5.12 (d, J = 10.1 Hz, 1H), 3.30 - 3.26 (m, 2H), 2.28 (s, 3H), 1.62 - 1.54 (m, 2H), 0.97 (s, 9H), 0.90 (t, J = 7.4 Hz, 3H); ¹³C NMR (126 MHz, DMSO- d_6 , δ [ppm]): 184.1, 180.2, 169.8, 168.6, 163.1, 151.1, 151.0, 150.7, 127.9, 123.3, 120.6, 117.9, 113.8, 108.5, 106.3, 60.2, 40.8, 35.7, 26.2, 22.0, 13.4, 11.3; HRMS m/z (ESI⁺) [found: 440.2115, $C_{24}H_{30}N_3O_5^+$ requires [M + H]⁺ 440.2107]; HPLC retention time 13.53 min, purity: 98.4%.

(R)-N-(But-3-yn-1-yl)-3-[(2-{[2,2-dimethyl-1-(5-methylfuran-2-yl)propyl]amino}-3,4-dioxocyclobut-1-en-1-yl)amino]-2-hydroxybenzamide (SLW428, 11k)

N-(But-3-yn-1-yl)-2-hydroxy-3-[(2-methoxy-3,4-dioxocyclobut-1-en-1-yl)amino]benzamide (**10e**, 60 mg, 0.19 mmol, 1.0 *eq.*) and (*R*)-2,2-Dimethyl-1-(5-methylfuran-2-yl)propan-1-amine hydrochloride (**9d**, 42 mg, 0.25 mmol, 1.3 *eq.*) were dissolved in methanol (10 mL). After the addition of *N*,*N*-diisopropylethylamine (68 μL, 0.38 mmol, 2.0 *eq.*), the reaction was stirred for 3 days. Extraction between water and ethyl acetate (3 × 50 mL), drying over sodium sulfate, filtration, and evaporation of the solvent gave the crude product that was purified by preparative HPLC (acetonitrile/water (0.1% TFA): gradient 5–95%) to obtain the title compound as a white-brown amorphous solid (54 mg, 63%). ¹H NMR (500 MHz, DMSO- d_6 , δ [ppm]): 13.89 (s, 1H), 9.55 (s, 1H), 9.16 (t, J = 5.7 Hz, 1H), 8.78 (d, J = 10.0 Hz, 1H), 7.97 (d, J = 8.1 Hz, 1H), 7.54 (d, J = 8.1 Hz, 1H), 6.89 (t, J = 8.1 Hz, 1H), 6.19 (d, J = 3.1 Hz, 1H), 6.05 (d, J = 3.1 Hz, 1H), 5.12 (d, J = 10.1 Hz, 1H), 3.46 - 3.42 (m, 2H), 2.86 - 2.85 (m, 1H), 2.50 - 2.45 (m, 2H), 2.28 (s, 3H), 0.98 (s, 9H); ¹³C NMR (126 MHz, DMSO- d_6 , δ [ppm]): 184.1, 180.2, 170.0, 168.6, 163.1, 151.0, 151.0, 150.7, 127.9, 123.5, 120.6, 118.1, 113.6, 108.5, 106.3, 81.8, 72.3, 60.2, 38.1, 35.7, 26.2, 18.3, 13.4; HRMS m/z (ESI+) [found: 450.2007, C₂₅H₂₈N₃O₅+ requires [M + H]+ 450.1951]; HPLC retention time 13.28 min, purity: 98.1%.

(*R*)-3-[(2-{[2,2-Dimethyl-1-(5-methylfuran-2-yl)propyl]amino}-3,4-dioxocyclobut-1-en-1-yl)amino]-*N*-(hex-5-yn-1-yl)-2-hydroxybenzamide (SLW429, 11l)

N-(Hex-5-yn-1-yl)-2-hydroxy-3-[(2-methoxy-3,4-dioxocyclobut-1-en-1-yl)amino]benzamide (**10f**, 60 mg, 0.18 mmol, 1.0 *eq.*) and (R)-2,2-Dimethyl-1-(5-methylfuran-2-yl)propan-1-amine hydrochloride (**9d**, 38 mg, 0.23 mmol, 1.3 *eq.*) were dissolved in methanol (10 mL). After the addition of N,N-diisopropylethylamine (62 μ L, 0.35 mmol, 2.0 *eq.*), the reaction was stirred for 3 days. Extraction between water and ethyl acetate (3 × 50 mL), drying over sodium sulfate, filtration, and evaporation of the solvent gave the crude product that was purified by preparative

HPLC (acetonitrile/water (0.1% TFA): gradient 5–95%) to obtain the title compound as a white-brown amorphous solid (28 mg, 33%). 1 H NMR (500 MHz, DMSO- d_6 , δ [ppm]): 14.08 (s, 1H), 9.54 (s, 1H), 9.02 (t, J = 5.7 Hz, 1H), 8.78 (d, J = 10.1 Hz, 1H), 7.96 (d, J = 8.1 Hz, 1H), 7.55 (d, J = 8.1 Hz, 1H), 6.81 (t, J = 8.1 Hz, 1H), 6.19 (d, J = 3.1 Hz, 1H), 6.05 (d, J = 3.1 Hz, 1H), 5.12 (d, J = 10.1 Hz, 1H), 3.39 – 3.28 (m, 8H), 2.75 (t, J = 2.6 Hz, 1H), 2.28 (s, 3H), 2.23 - 2.19 (m, 2H), 1.70 – 1.61 (m, 2H), 1.55 – 1.46 (m, 2H), 0.98 (s, 9H); 13 C NMR (126 MHz, DMSO- d_6 , δ [ppm]): 184.1, 180.2, 169.8, 168.6, 163.1, 151.1, 151.0, 150.7, 127.9, 123.3, 120.6, 118.0, 113.8, 108.5, 106.3, 84.3, 71.3, 60.2, 38.5, 35.7, 27.8, 26.2, 25.4, 17.3, 13.4; HRMS m/z (ESI+) [found: 478.2312, $C_{27}H_{32}N_3O_5$ + requires [M + H]+ 478.2264]; HPLC retention time 13.59 min, purity: 97.5%.

6. Development of PROTACs targeting the chemokine receptor CCR7

6.1 Design of PROTACs targeting CCR7

For a proof-of-concept study to investigate whether targeted protein degradation of CCR7 is possible, we designed PROTACs hijacking cereblon (CRBN) as the E3 ligase, since it is the most widely used E3 ligase. (263) In 2015, the first CRBN-recruiting PROTACs were designed with the aid of immunomodulatory imide drugs (IMiDs) like thalidomide and pomalidomide. However, these compounds exhibited hydrolytic stability issues with respect to the phthalimide and glutarimide rings. (264) To overcome these difficulties, intense efforts have been dedicated towards exploring new CRBN ligands with enhanced affinity and stability. One of these newly developed ligands is the phenylglutarimide scaffold shown in Figure 25. (263) Compound SLW89² from chapter 4 and SLW007³ were chosen as the CCR7 ligands since they already contain the propargyl group than can be leveraged for a coupling reaction in the last step using a copper-catalyzed azide-alkyne cycloaddition (CuAAC) reaction.

Figure 25. Common IMiDs and the novel CRBN phenylglutarimide template for the recruitment of the E3 ligase CRBN.

6.1.1 Synthesis of the E3 ligase ligands

In this study, we used the thalidomide and phenylglutarimide scaffolds as the E3 ligase warheads to develop of CCR7-targeting PROTACs. For ligand attachment these two scaffolds had to be modified to enable that the corresponding linker could be introduced in a single reaction step. In the case of thalidomide, introduction of a fluorine atom at the 4-,

Figure 26. Commercially available thalidomide derivatives.

² SLW089 refers to compound 9 from chapter 4

³ SLW007 refers to compound 19 from chapter 2

5-, or the 5- and 6-position proved to be a viable option as this halogen atom allows for a simple nucleophilic aromatic substitution reaction (S_NAr) with an appropriate amino-functionalized linker. In the case of the phenylglutarimide ligand, a switch from the phenyl to a phenol moiety enabled the introduction of a tert-butylacetate handle. Since 2-(2,6-dioxopiperidin-3-yl)-4fluoroisoindoline-1,3-dione (1) and 2-(2,6-dioxopiperidin-3-yl)-5-fluoroisoindoline-1,3-dione (2) (Figure 26) are commercially available only 2-(2,6-dioxopiperidin-3-yl)-5,6-difluoroisoindoline-1,3-dione (5) and the modified phenylglutarimide tert-butyl 2-[4-(2,6-dioxopiperidin-3yl)phenoxy]acetate (9) had to be synthesized as shown in Scheme 4. The synthesis of the E3 ligase ligand 5 was performed by refluxing 4,5-difluorophthalic anhydride (3) together with the hydrochloride of 3-aminopiperidine-2,6-dione (4) in the presence of acetic acid to obtain 2-(2,6dioxopiperidin-3-yl)-5,6-difluoroisoindoline-1,3-dione (5) after filtration. The synthesis of the phenylglutarimide derivative was performed in three steps. In the first step, 2,6-bis(benzyloxy)-3-bromopyridine (6) was reacted with (4-hydroxyphenyl)boronic acid in a Suzuki-coupling reaction using tribasic potassium phosphate and bis(diphenylphosphino)ferrocenepalladium(II)dichloride-dichloromethane as a catalyst to obtain compound 7. In the next step, the phenol group was deprotonated using potassium carbonate to perform a nucleophilic substitution reaction with tert-butyl bromoacetate yielding the product 8. Lastly hydrogenolytic deprotection of the benzyl-protecting group, followed by a lactam-lactim tautomerism of the phenolic alcohols gave the final E3 ligase ligand 9 bearing the glutarimide structure necessary for binding to CRBN.

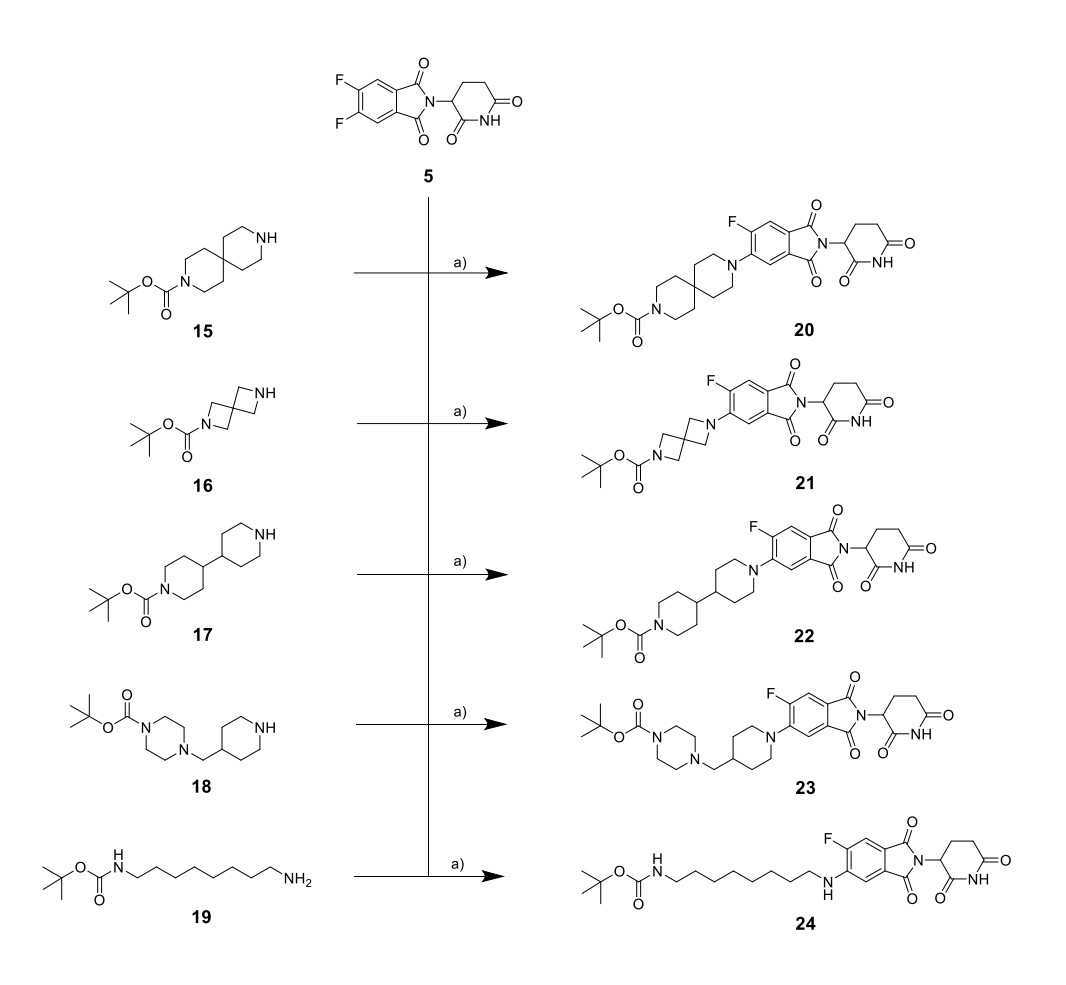
Scheme **4.** Synthesis of E3 ligase ligands. Reagents and conditions: (a) NaOAc, AcOH, reflux, 4 h; (b) (4-hydroxyphenyl)boronic acid, K_3PO_4 , $Pd(dppf)Cl_2 \cdot CH_2Cl_2$, dioxane/ H_2O , 100 °C, 16 h; (c) tert-butyl bromoacetate, K_2CO_3 , DMF, rt, 4 h; (d) Pd/C, EtOH, rt, 16 h.

6.1.2 Synthesis of functionalized PROTAC-linker precursors

To investigate the effect of the CRBN ligand and the corresponding linker length and their respective physicochemical characteristics, two different sets of precursors were synthesized. For the first set a particular focus was set on the effect of the four designated CRBN binders 1, 2, 5 and 9. For this all four CRBN ligands were subjected to a nucleophilic aromatic substitution reaction with 2-[2-(2-azidoethoxy)ethoxy]ethanamine (10). This α,ω -functionalized linker is perfectly suited because the α-amine reacts readily with the fluorine of the thalidomide derivatives to afford the desired PROTAC precursors, while the ω-azide is needed as the counterpart to the alkyne function already present in the respective CCR7 ligands SLW089 and **SLW007**. This strategy should enable a quick conjugation between the precursors and the CCR7 ligands in the last step via CuAAC. For the thalidomide derivatives 1, 2, and 5, the synthesis (Scheme 5) was performed in one step by addition of DIPEA to a solution of the respective fluorothalidomides and 2-[2-(2-azidoethoxy)ethoxy]ethanamine in DMSO under reflux to obtain the PROTAC-linker precursors 11-13. In the case of the phenylglutarimide, acidolytic Boc-deprotection using TFA was performed before the subsequent PyBroP mediated amide coupling with 2-[2-(2-azidoethoxy)ethoxy]ethanamine yielded the PROTAClinker precursor 14.

Scheme **5.** Synthesis of the 2-[2-(2-azidoethoxy)ethoxy]ethanamine based PROTAC-linker precursors. *Reagents and conditions*: (a) DIPEA, DMSO, reflux, 16 h; (b) TFA, DCM, rt, 4 h; (c) PyBroP, DIPEA, DCM, rt, overnight.

The second set of PROTAC-linker precursors focused on the physicochemical characteristics and rigidity of the respective linkers and their possible effect on the observed degradation of the target protein. To this end the CRBN ligand $\bf 5$ was chosen and a set of five precursors were synthesized as outline in Scheme 6. Starting from the commercially available α,ω -mono-Boc-protected diamine linkers $\bf 15-19$, a nucleophilic aromatic substitution reaction ($\bf S_NAr$) of one of the fluorine atoms of $\bf 5$ gave the mono-substituted PROTAC-linker precursors $\bf 20-24$. Substitution of both fluorine atoms of $\bf 5$ was observed in small amounts for some linkers but the mono- and di-substituted derivatives were easily separated by column chromatography.



Scheme **6.** Synthesis of the PROTAC-linker precursors based on the 5,6-difluorothalidomide CRBN ligand. *Reagents and conditions*: (a) DIPEA, DMSO, reflux, 16 h.

6.1.3 Final assembly of the CCR7 PROTACs

For the final conjugation of PROTAC precursors with the protein of interest (POI) ligands, 'click' chemistry reactions like the CuAAC, the alkene and tetrazine inverse-electron-demand Diels-Alder reaction, and the strain-promoted azide alkyne cycloaddition (SPAAC) have been extensively used. (265) (266) (267) These reactions show high modularity of the starting materials, high yields of product formation and a generally high atom economy while simultaneously avoiding harsh reaction conditions and complex purification methods. The CuAAC was used for the synthesis of all PROTACs in this study. This catalytic version of the Huisgen 1,3-dipolar cycloaddition enables a regiospecific formation of 1,4-disubstituted 1,2,3triazoles. The functional groups required for this reaction are alkynes (present in the chosen POI ligands) and azides, which were introduced during the synthesis of the CRBN ligand-linker precursors. The hypothesized reaction mechanism of this CuAAC reaction starts by in situ generation of the Cu(I) acetylene II by addition of a Cu(I) species to the terminal alkyne I. A second Cu(I) species coordinates to the alkyne to give the complex III. This copper ion is needed to guide the azide towards the alkyne. The alignment of the azide (intermediate IV) enables the formation of the first carbon nitrogen bond to yield the six-membered meta-stable ring V. After the formation of the second carbon-nitrogen bond and the release of a Cu(I) species, the five-membered ring VI is generated. Upon addition of the previously released proton, the 1,4-disubstituted-1,2,3-triazole is formed and the Cu(I) species can enter a new

$$R^{2}$$

$$R^{1}$$

$$R^{1}$$

$$R^{1}$$

$$R^{2}$$

$$R^{2}$$

$$R^{1}$$

$$R^{2}$$

$$R^{2}$$

$$R^{1}$$

$$R^{2}$$

$$R^{2}$$

$$R^{1}$$

$$R^{2}$$

Scheme 7. Hypothesized mechanism of the CuAAC reaction. Modified from Worrel, Malik and Fokin. (278)

catalytic cycle. These 1,2,3-triazoles are assumed to be amide surrogates due to their dipole moment and innate ability to act as hydrogen bond acceptors and show high chemical and hydrolytic stability. (268) The crucial point in performing this reaction is the challenge of maintaining the appropriate concentration of the Cu(I) species, which can easily be oxidized to Cu(II) by oxygen from the air. To circumvent this challenge Cu(II) salts are used in combination with reductants like sodium ascorbate. To further stabilize the reactive Cu(I) species all CuAAC reaction were performed under an argon atmosphere.

Scheme **8.** Assembly of CCR7 PROTACs using **SLW089** as the POI ligand. Reagents and conditions: (+)-sodium L-ascorbate, CuSO₄, TBTA, H_2O , THF, rt, overnight.

Finally, the reaction of the alkyne-terminal thiadiazole-1,1-dioxide-based CCR7 ligand **SLW089** and the squaramide-based CCR7 ligand **SLW007** with the azido-terminal CRBN-adressing PROTAC precursors **11-14** (Scheme 8 and 9) afforded the desired CCR7 PROTACs **25-32** (Table 5).

Scheme **9**. Assembly of CCR7 PROTACs using **SLW007** as the POI ligand. *Reagents and conditions*: (a) (+)-sodium L-ascorbate, $CuSO_4$, TBTA, H_2O , THF, rt, 16 h.

Table 5. Overview of the synthesized PROTACs 25-32.

compound	product structure			
25	O NH NH O			
26	OPES NH			
27	OH NH OF NH			
28	NH N			
29	NH N=N			

The second set of CCR7 PROTACs focused on the variation of the linker moiety. To this end, the synthesized PROTAC precursors **20-24** were selected as they show variations regarding the length, rigidity, and heteroatoms present within the linker compared to the the linkers present in the first generation of PROTACs. This variation is critical, as linker influence on degradation efficiency is highly target-dependent, and optimizing linkers for PROTACs still relies heavily on trial and error. All four precursors share the same Boc-protected amine. To transfer this functionality, the Boc-protection group was removed by treatment with TFA in DCM followed by a PyBroP-mediated amide coupling with azidoacetic acid (see Scheme 10). The resulting amide intermediate contains the azide moiety required to perform the CuAAC reaction in the same fashion as mentioned earlier to obtain the final PROTACs **33-37** (see Table **6**).

Scheme **10**. Synthesis of CCR7 PROTACs with variations in the linker region. *Reagents and conditions*: (a) TFA, DCM, rt, 4 h; (b) azidoacetic acid, PyBroP, DIPEA, DCM, rt, 16 h; (c) (+)-sodium L-ascorbate, CuSO₄, H₂O, TBTA, THF, rt, 16 h.

 $\label{thm:continuous} \textbf{Table 6. Overview of the synthesized PROTACs based on the squaramide scaffold.}$

compound	product structure
33	NH OH HN NH OH NH
34	NH OH HN OH HN OH
35	O H N N N N N N N N N N N N N N N N N N
36	HO NH N=N O NH N=N O NH

6.2 Biological evaluation of the CCR7 PROTACs

6.2.1 NanoBRET target engagement assays

For all synthesized PROTACs NanoBRET-based target engagement assays for CCR6, CCR7, CXCR1, and CXCR2 were performed by Max E. Huber in the group of Prof. Dr. Matthias Schiedel at the University of Erlangen-Nürnberg. Surprisingly, all synthesized PROTACs demonstrated very low affinities towards CCR7. However, the thiadiazole-1,1-dioxide-based PROTACs showed high affinity towards CCR6 and CXCR2 but limited affinity towards the CXCR1 receptor. The squaramide-based PROTACs, however, exhibited a high affinity towards CXCR2 and good affinity towards CCR6 and CXCR1 but showed even lower affinity for CCR7 compared to the corresponding thiadiazole-1,1-dioxide-based PROTACs.

Table **7**. Affinity data of the synthesized PROTACs towards CCR6, CCR7, CXCR1 and CXCR2 obtained by NanoBRET target engagement assays.

	POI ligand	$pK_i \pm SEM (K_i [nM]) \text{ or comp.}^a$			
compound		CCR6	CCR7	CXCR1	CXCR2
35	Thiadiazole,1,1-dioxide	8.45 ± 0.07 (3.62)	6.33 ± 0.08 (499)	6.06 ± 0.06 (884)	8.29 ± 0.10 (5.48)
36	Thiadiazole,1,1-dioxide	8.64 ± 0.03 (2.31)	6.34 ± 0.10 (496)	6.20 ± 0.09 (662)	8.17 ± 0.07 (7.09)
37	Thiadiazole,1,1-dioxide	8.56 ± 0.04 (2.76)	6.43 ± 0.09 (395)	6.17 ± 0.05 (689)	8.15 ± 0.01 (7.09)
38	Thiadiazole,1,1-dioxide	8.68 ± 0.06 (2.13)	6.53 ± 0.06 (300)	6.51 ± 0.01 (308)	8.35 ± 0.01 (4.48)
39	Squaramide	7.40 ± 0.08 (41.5)	43% comp. @ 10 μΜ	7.09 ± 0.02 (82.0)	8.78 ± 0.07 (1.69)
40	Squaramide	7.64 ± 0.03 (23.0)	5.65 ± 0.14 (2620)	7.17 ± 0.07 (69.9)	8.77 ± 0.07 (1.75)
41	Squaramide	7.75 ± 0.05 (18.1)	6.01 ± 0.07 (1000)	7.39 ± 0.07 (42.2)	8.90 ± 0.09 (1.31)
42	Squaramide	7.95 ± 0.06 (11.5)	6.38 ± 0.08 (431)	7.70 ± 0.03 (19.8)	9.21 ± 0.02 (0.62)

43	Squaramide	8.16 ± 0.03 (6.92)	6.22 ± 0.06 (609)	7.59 ± 0.09 (26.8)	8.78 ± 0.03 (1.67)
44	Squaramide	8.12 ± 0.04 (7.74)	5.89 ± 0.11 (1380)	7.95 ± 0.03 (11.4)	9.31 ± 0.01 (0.49)
45	Squaramide	7.97 ± 0.03 (10.8)	6.39 ± 0.05 (411)	7.68 ± 0.08 (21.9)	8.87 ± 0.07 (1.38)
46	Squaramide	8.37 ± 0.07 (4.41)	6.56 ± 0.06 (280)	8.12 ± 0.04 (7.75)	9.10 ± 0.09 (0.84)
47	Squaramide	7.71 ± 0.04 (19.7)	52% comp. @ 10 μΜ	7.02 ± 0.03 (97.0)	8.63 ± 0.07 (2.42)

^aComp. = percentual competitive tracer displacement at given concentration.

6.2.2 ELISA assays

The four PROTACs SLW141 (25), SLW142 (28), SLW225 (29), and SLW228 (32) were tested by the group of Prof. Dr. Kostenis (University of Bonn) for their degradation efficiency in CHO-

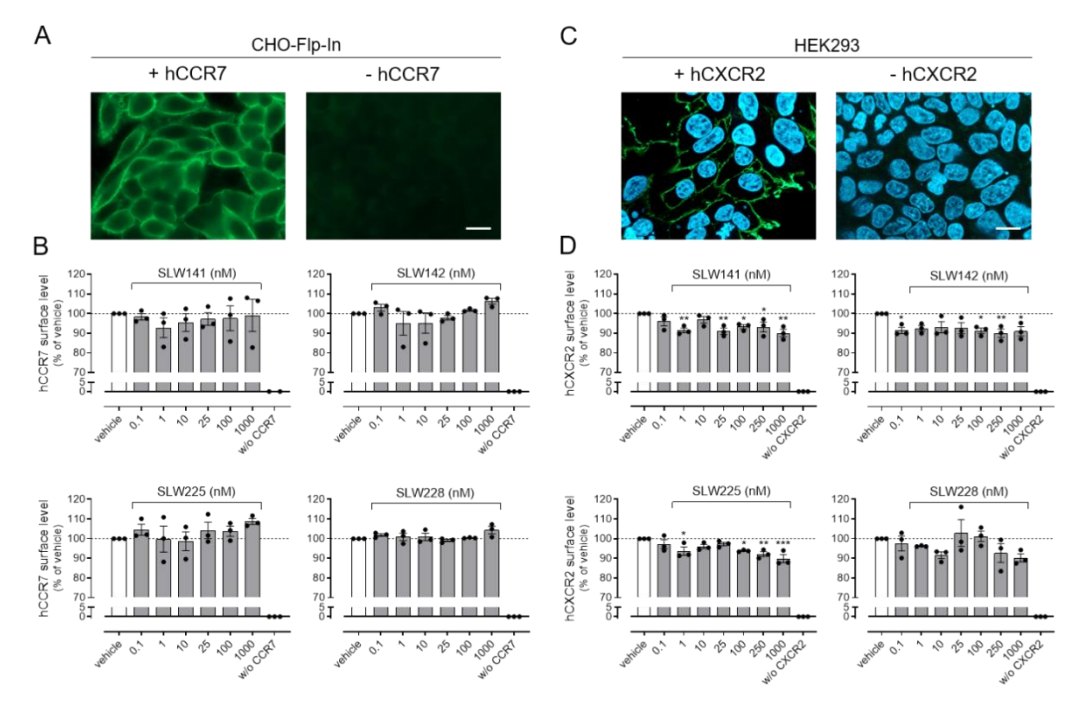


Figure 27. Tested PROTACs do not induce a concentration-dependent reduction of CCR7 or CXCR2 receptor surface level under high cytomegalovirus (CMV)-driven expression per cell. (A) Intact CHO-Flp-In cells stably expressing human CCR7 (hCCR7) were labeled with mouse CCR7 antibody (MAB197). Surface hCCR7 was then visualized with FITC-conjugated goat anti-mouse IgG (green). No membrane fluorescence was observed in parental CHO-Flp-In cells. (B) hCCR7-CHO-Flp-In cells were incubated with vehicle (0.1% DMSO) or PROTAC at the indicated concentrations for 16 h. Plasma-membrane-resident receptor was measured in ELISA using mouse CCR7 antibody (MAB197) and anti-mouse HRP as secondary antibody (n=3 ± SEM, data generated by Max Huber). (C) Nonpermeabilized HEK293 cells stably transfected with human CXCR2 (hCXCR2) were labeled with mouse CXCR2 antibody (MAB331). Surface hCXCR2 was subsequently detected with FITC-conjugated goat anti-mouse IgG (green). No membrane-associated fluorescence was observed in parental HEK293 cells. Nuclei were stained with 4',6-diamidin-2-phenylindole (DAPI, blue). (D) hCXCR2-HEK293 cells were treated with vehicle (0.1% DMSO) or protac at the indicated concentrations for 16 h. Plasma-membrane-localized receptor was detected in ELISA using mouse CXCR2 antibody (MAB331) and anti-mouse HRP as secondary antibody (n=3 ± SEM). Significant differences were determined by one-way ANOVA with Dunnett's multiple-comparison test. Scale bar is 10 μm.

Flp-In cells (for CCR7) and HEK293 cells (for CXCR2) using an ELISA assay. Both cell lines were modified to stably express the desired receptor (seen in Figure 27A/C). All four tested PROTACs were not able to significantly degrade CCR7 (Figure 27B). However, SLW141 and SLW142, were able to degrade CXCR2 to around 80% of residual protein level (Figure 27D). To determine whether CRBN-recruiting PROTACs are useful for degrading the membranebound chemokine receptors CCR7 and CXCR2, their degradation was assessed using benchmark degraders to rule out the possibility that the synthesized degraders may not exhibit sufficient affinity towards the targeted receptors. To this end the protein FKBP12 was fused to the C-terminus of CCR7 and CXCR2 to enable the use of dTAG13. This CRBN-recruiting degrader can induce degradation of FKBP12. By fusing FKBP12 to CCR7 or CXCR2, dTAG13 should induce degradation of the chemokine receptor-FKBP12 constructs. The second benchmark degrader is the NanoTAC NC4. This CRBN-recruiting PROTAC is capable of degrading Nluc. To this end, the two receptors were fused C-terminally to a nanoluciferase. The FKBP12-targeting PROTAC dTAG13 was only able to degrade the CXCR2 receptor to a residual protein level of around 90%, while the Nluc-targeting degrader NC4 was able to degrade both receptors by 20%. Of note, the maximum degradation achieved by the benchmark degrader NC4 is comparable to that observed with the synthesized PROTACs. In summary, to date, the degradation of the chemokine receptors CCR7 and CXCR2 by CRBNrecruiting PROTACs has only achieved a maximum of approximately 20%.

6.3 Conclusion

Within this chapter two sets of potential CCR7 PROTACs were synthesized. The first set used the same PEG-based linker with variations regarding the chemokine receptor and CRBN ligands. The second set focused on linker diversification, which is often crucial to form a productive ternary complex. Many of the synthesized PROTACs showed promising affinities towards the chemokine receptors CXCR1, CXCR2, and CCR6 but unfortunately none of them showed sufficient affinity towards CCR7. The synthesized PROTACs were able to achieve a maximum degradation of around 20% for both CCR7 and CXCR2. The benchmark degraders achieved the same maximum degradation. Therefore, CRBN-recruiting PROTACs might not be the best choice for the degradation of chemokine receptors. Future studies should evaluate the degradation efficiency of the synthesized PROTACs against CCR6 and CXCR1 to determine whether either receptor can be degraded to a greater extent. Additionally, novel degradation technologies like LYTACs or AbTACs could be utilized to see if these degrader classes are able to degrade chemokine receptors to a greater level. Furthermore, the development of selective degraders for individual chemokine receptors, as well as potent degraders capable of efficiently targeting CCR7, should be prioritized.

6.4 Experimental section

6.4.1 General information and chemistry

Chemicals were obtained from abcr GmbH (Karlsruhe, Germany), Acros Organics (Geel, Belgien), Carbolution Chemicals (Sankt Ingberg, Germany), Sigma-Aldrich (Steinheim, Germany,) TCI Chemicals (Eschborn, Germany) or VWR (Langenfeld, Germany) and used without further purification. Technical-grade solvents were distilled prior to use. For all HPLC purposes, acetonitrile in HPLC-grade quality (HiPerSolv CHROMANORM, VWR, Langenfeld, Germany) was used. Water was purified with a PURELAB flex® (ELGA VEOLIA, Celle, Germany). Thin-layer chromatography (TLC) was carried out on prefabricated plates (silica gel 60, F254, Merck). Components were visualized either by irradiation with ultraviolet light (254 nm or 366 nm) or by appropriate staining. Column chromatography was carried out on silica gel (60 Å, 40–60 µm, Acros Organics, Geel, Belgien). If no solvent is stated, an aqueous solution was prepared with demineralized water. Mixtures of two or more solvents are specified as "solvent A"/"solvent B", 3/1, v/v, meaning that 100 mL of the respective mixture consists of 75 mL of "solvent A" and 25 mL of "solvent B". The uncorrected melting points were determined using a Büchi (Essen, Germany) Melting Point M-560 apparatus. Diastereomeric ratios were determined by ¹H NMR spectroscopy.

6.4.1.1 Nuclear magnetic resonance spectroscopy (NMR):

Proton (¹H) and carbon (¹³C) NMR spectra were recorded either on a Bruker AVANCE 500 MHz at a frequency of 500 MHz (¹H) and 126 MHz (¹³C) or a Bruker AVANCE III HD 600 MHz at a frequency of 600 MHz (1H) and 151 MHz (¹³C). The chemical shifts are given in parts per million (ppm). As solvents, deuterated chloroform (CDCl₃), deuterated methanol (methanol-d₄) and deuterated dimethyl sulfoxide (DMSO-d₆) were used. The residual solvent signal (CDCl₃: ¹H NMR: 7.26 ppm, ¹³C NMR: 77.1 ppm; DMSO-d₆: ¹H NMR: 2.50 ppm, ¹³C NMR: 39.52 ppm; methanol-d₄: ¹H NMR: 3.31 ppm, 4.87 ppm, ¹³C NMR: 49.00 ppm) was used for calibration. The multiplicity of each signal is reported as singlet (s), doublet (d), triplet (t), quartet (q), multiplet (m) or combinations thereof. Multiplicities and coupling constants are reported as measured and might disagree with the expected values.

6.4.1.2 Mass spectrometry

High-resolution electrospray-ionization mass spectra (HRMS-ESI) were acquired with a Bruker Daltonik GmbH micrOTOF coupled to a an LC Packings Ultimate HPLC system and controlled by micrOTOFControl3.4 and HyStar 3.2-LC/MS, with a Bruker Daltonik GmbH ESI-qTOF Impact II coupled to a Dionex UltiMateTM 3000 UHPLC system and controlled by

micrOTOFControl 4.0 and HyStar 3.2-LC/MS or with a micrOTOF-Q mass spectrometer (Bruker, Bremen, Germany) with ESI-source coupled with an HPLC Dionex UltiMate 3000 (Thermo Scientific, Heysham, United Kingdom). Low-resolution electrospray-ionization mass spectra (LRMS-ESI) were acquired with an Advion expression® compact mass spectrometer (CMS) coupled with an automated TLC plate reader Plate Express® (Advion, Ithaca, NY, USA).

6.4.1.3 High performance liquid chromatography (HPLC)

A Thermo Fisher Scientific (Heysham, United Kingdom) UltiMateTM 3000 UHPLC system with a Nucleodur 100-5 C18 (250 × 4.6 mm, Macherey Nagel, Düren, Germany) with a flow rate of 1 mL/min and a temperature of 25 °C, or a 100-5 C18 (100 × 3 mm, Macherey Nagel, Düren, Germany) with a flow rate of 0.5 mL/min and a temperature of 25 °C was used with an appropriate gradient. For preparative purposes, an AZURA Prep. 500/1000 gradient system with a Nucleodur 110-5 C18 HTec (150 × 32 mm, Macherey Nagel, Düren, Germany) column with 20 mL/min was used. Detection was implemented with UV absorption measurement at wavelengths of λ = 220 nm and λ = 250 nm. Bidest. H₂O (A) and MeCN (B) were used as eluents with an addition of 0.1% TFA in case of eluent A. Purity: The purity of all final compounds was 95% or higher. Purity was determined via HPLC with the Nucleodur 100-5 C18 (250 × 4.6 mm, Macherey Nagel, Düren, Germany) at 250 nm. After column equilibration for 5 min, a linear gradient from 5% A to 95% B in 7 min followed by an isocratic regime of 95% B for 10 min was used.

6.4.2 Synthesis and compound characterization

2-(2,6-Dioxopiperidin-3-yl)-5,6-difluoroisoindoline-1,3-dione (SLW175, 5)

3-Aminopiperidine-2,6-dione hydrochloride (586 mg, 3.50 mmol, 1.00 eq.) and 5,6-difluorobenzofuran-1,3-dione (986 mg, 5.25 mmol, 1.50 eq.) were suspended in 20 mL of glacial acetic acid. After addition of sodium acetate (234 mg, 2.80 mmol, 0.800 eq.) the reaction mixture was stirred at reflux for 6 hours. After cooling the solution was poured into ice cold water and the solids were filtered off and washed with ice cold water (2 x 25 mL). Drying under reduced pressure afforded the title compound as a pale violet solid (1.0 g, 97%). ¹H NMR (600 MHz, DMSO- d_6 δ [ppm]): 11.13 (s, 1H), 8.14 (t, J = 7.6 Hz, 2H), 5.16 (dd, J = 13.0, 5.4 Hz, 1H), 2.92 - 2.86 (m, 1H), 2.64 - 2.58 (m, 1H), 2.57 - 2.51 (m, 1H), 2.09 - 2.05 (m, 1H);

¹³C NMR (151 MHz, DMSO- d_6 δ [ppm]): 172.7, 169.6, 165.4, 153.8 (dd, J = 258.0, 15.3 Hz), 134.1 – 108.9 (m), 49.4, 40.1, 30.9, 21.9; ¹⁹F NMR (565 MHz, DMSO- d_6 δ [ppm]): 127.0; LRMS m/z (ESI⁺) [Found: 295.2, C₁₃H₉F₂N₂O₄⁺ requires [M+H]⁺ 295.2]; Rf: 0.34 (cyclohexane /ethyl acetate (1/1 (v/v))); mp: 215 – 218 °C.

4-[2,6-Bis(benzyloxy)pyridin-3-yl]phenol (SLW119, 7)

2,6-Bis(benzyloxy)-3-bromopyridine (500 mg, 1.32 mmol, 1.00 eq.), (4-hydroxyphenyl)boronic acid (373 ,g, 2.65 mmol, 2.00 eq.) and tribasic potassium phosphate (411 mg, 2.91 mmol, 2.20 eq.) in a mixture of dioxane and water (7 mL (6:1 (VV)) were degassed under Argon. 1,1-Bis(diphenylphosphino)ferrocene-palladium(II)dichloride dichloromethane complex (0.11 g, 0.13 mmol, 0.10 eq.) was then added and the reaction mixture was stirred at 100 °C for 16 hours, cooled to room temperature and then filtered through a short bed of celite. The filtrate was diluted with ethyl acetate (25 mL), washed with water (50 mL), dried over anhydrous sodium sulfate and concentrated under reduced pressure. The crude product was purified by column chromatography using a mixture of cyclohexane and ethyl acetate (1/1 (VV)) to afford the title compound as an orange gum (480 mg, 95%). ¹H NMR (600 MHz, DMSO- d_6 δ [ppm]): 9.41 (s, 1H), 7.69 – 7.54 (m, 1H), 7.50 – 7.22 (m, 12H), 6.83 – 6.72 (m, 2H), 6.51 (d, J= 8.0 Hz, 1H), 5.43 - 5.32 (m, 4H); ¹³C NMR (151 MHz, DMSO- d_6 δ [ppm]): 160.1, 157.5, 156.3, 141.6, 137.4, 129.8, 128.7, 128.3, 127.7, 127.5, 127.3, 126.6, 125.9, 115.5, 114.9, 102.1, 67.1; LRMS m/z (ESI+) [Found: 384.6, $C_{25}H_{22}NO_3$ + requires [M+H]+ 384.5]; Rf: 0.73 (cyclohexane/ethyl acetate (7/3 (VV)).

tert-Butyl 2-{4-[2,6-bis(benzyloxy)pyridin-3-yl]phenoxy}acetate (SLW121, 8)

4-[2,6-Bis(benzyloxy)pyridin-3-yl]phenol (**7**, 0.40 g, 0.99 mmol, 1.0 eq.) and potassium carbonate (210 mg, 1.49 mmol, 1.50 eq.) were dissolved in dimethylformamide (10 mL). After dropwise addition of *tert*-butylbromoacetate (156 μ L, 1.04 mmol, 1.05 eq) the reaction mixture

was stirred at room temperature for 4 hours. The reaction was then quenched by the addition of water (50 mL) and extracted with ethyl acetate (3 x 50 mL). After drying over sodium sulfate, filtration and evaporation of the solvent the crude product was purified by column chromatography using a mixture of cyclohexane and ethyl acetate (9/1 (v/v)) to afford the title compound as a clear gum (340 mg, 69%). ¹H NMR (600 MHz, DMSO- d_6 δ [ppm]): 7.70 (d, J = 8.1 Hz, 1H), 7.53 – 7.45 (m, 2H), 7.46 – 7.42 (m, 2H), 7.41 – 7.24 (m, 8H), 6.94 – 6.89 (m, 2H), 6.53 (d, J = 8.1 Hz, 1H), 5.40 (s, 2H), 5.37 (s, 2H), 4.66 (s, 2H), 1.43 (s, 9H); ¹³C NMR (151 MHz, DMSO- d_6 δ [ppm]): 167.8, 160.4, 157.6, 156.6, 141.8, 137.5, 129.7, 128.9, 128.3, 127.7, 127.7, 127.5, 127.3, 115.0, 114.1, 102.2, 81.3, 67.2, 65.0, 27.7; LRMS m/z (ESI⁺) [Found: 498.6, $C_{31}H_{32}NO_5^+$ requires [M+H]⁺ 498.6]; Rf: 0.48 (cyclohexane/ethyl acetate (9/1 (v/v)).

tert-Butyl 2-[4-(2,6-dioxopiperidin-3-yl)phenoxy]acetate (SLW128, 9)

tert-Butyl 2-{4-[2,6-bis(benzyloxy)pyridin-3-yl]phenoxy}acetate (**8**, 0.21 g, 0.42 mmol, 1.0 eq.) was dissolved in ethanol (10 mL). After addition of 10% Pd/C (21 mg, 0.21 mmol, 0.50 eq.) the flask was sealed and stirred at room temperature under a hydrogen atmosphere for 16 hours. The reaction mixture was then filtered through a short pad of celite, washed with ethyl acetate (25 mL) and dried under high vacuum to afford the title compound as a clear gum (85 mg, 64%). ¹H NMR (600 MHz, DMSO- d_6 δ [ppm]): 10.76 (s, 1H), 7.16 – 7.10 (m, 2H), 6.88 – 6.82 (m, 2H), 4.62 (s, 2H), 3.79 (dd, J = 11.5, 4.9 Hz, 1H), 2.68 - 2.61 (m, 1H), 2.49 – 2.43 (m, 1H), 2.20 - 2.12 (m, 1H), 2.06 – 1.97 (m, 1H), 1.43 (s, 9H); ¹³C NMR (151 MHz, DMSO- d_6 δ [ppm]): 174.3, 173.3, 167.8, 156.6, 131.6, 129.5, 114.2, 81.3, 65.0, 46.4, 31.3, 27.7, 25.9; LRMS m/z (ESI+) [Found: 320.5, C₁₇H₂₂NO₅+ requires [M+H]+ 320.4]; Rf: 0.34 (cyclohexane/ethyl acetate (9/1 (v/v)).

2-[4-(2,6-Dioxopiperidin-3-yl)phenoxy]acetic acid (SLW138)

tert-Butyl 2-[4-(2,6-dioxopiperidin-3-yl)phenoxy]acetate (**9**, 80 mg, 0.30 mmol, 1.0 eq.) was dissolved in a mixture of dichloromethane and trifluoroacetic acid (2 mL (1/1 (v/v))) and stirred at room temperature for 2 hours. The solvents were evaporated under reduced pressure to afford the title compound that was used without further purification in the next step.

tert-Butyl-9-[2-(2,6-dioxopiperidin-3-yl)-6-fluoro-1,3-dioxoisoindolin-5-yl]-3,9-diazaspiro[5.5]undecane-3-carboxylate (SLW201, 20)

2-(2,6-Dioxopiperidin-3-yl)-5,6-difluoroisoindoline-1,3-dione (5, 380 mg, 1.23 mmol, 1.00 eg.) and tert-Butyl-3-9-diazaspiro[5.5]undecane-3-carboxylate (322 mg, 1.23 mmol, 1.00 eq.) were dissolved in DMSO (10 mL). After the addition of DIPEA (439 µL. 2.46 mmol, 2.00 eq.) the reaction was stirred at reflux overnight. After the addition of water (50 mL) the mixture was extracted using ethyl acetate (3 x 50 mL). Drying over sodium sulfate, filtration, evaporation of the solvent the crude product was purified by column chromatography using a mixture of cyclohexane and ethyl acetate (1/1 (v/v)) to give the title compound as yellow gum (307 mg, 47%). ¹H NMR (600 MHz, DMSO- d_6 δ [ppm]): 11.08 (s, 1H), 7.68 (d, J = 11.4 Hz, 1H), 7.44 (d, J = 7.4 Hz, 1H), 5.09 (dd, J = 12.9, 5.4 Hz, 1H), 3.34 - 3.33 (m, 4H), 3.26 - 3.21 (m, 4H), 2.91 - 2.85 (m, 1H), 2.64 - 2.51 (m, 2H), 2.05 - 2.01 (m, 1H), 1.63 - 1.58 (m, 4H), 1.46 - 1.41 (m, 4H), 1.40 (s, 9H); 13 C NMR (151 MHz, DMSO- d_6 δ [ppm]): 172.7, 169.9, 166.7, 166.2 (d, J=2.3 Hz), 158.0, 156.3, 154.0, 145.7 (d, J = 8.8 Hz), 128.8 (d, J = 2.2 Hz), 122.7 (d, J = 9.7 Hz), 113.6 (d, J = 4.9 Hz), 111.9, 111.7, 78.4, 49.0, 45.4 (d, J = 4.7 Hz), 40.1, 34.6, 30.9, 29.3, 28.1, 22.1; ¹⁹F NMR (565 MHz, DMSO- d_6 δ [ppm]): 113.0; LRMS m/z (ESI+) [Found: 529.6, $C_{27}H_{34}FN_4O_6^+$ requires [M+H]⁺ 529.6]; Rf: 0.53 (cyclohexane/ethyl acetate (1/1 (ν/ν))); mp: 233 - 236 °C.

tert-Butyl-6-[2-(2,6-dioxopiperidin-3-yl)-6-fluoro-1,3-dioxoisoindolin-5-yl]-2,6-diazaspiro[3.3]heptane-2-carboxylate (SLW217, 21)

2-(2,6-Dioxopiperidin-3-yl)-5,6-difluoroisoindoline-1,3-dione (**5**, 0.12 g, 0.39 mmol, 1.0 *eq.*) and *tert*-Butyl-2-6-diazaspiro[3.3]heptane-2-carboxylate (77 mg, 0.39 mmol, 1.0 *eq.*) were dissolved in DMSO (10 mL). After the addition of DIPEA (0.13 mL. 0.78 mmol, 2.0 *eq.*) the reaction was stirred at reflux overnight. After the addition of water (50 mL) the mixture was extracted using ethyl acetate (3 x 50 mL). Drying over sodium sulfate, filtration, evaporation of the solvent the crude product was purified by column chromatography using a mixture of cyclohexane and ethyl acetate (1/1 (ν/ν)) to give the title compound as yellow gum (211 mg, 73%). H NMR (600 MHz, DMSO- d_6 δ [ppm]): 11.06 (s, 1H), 7.59 (d, J = 11.1 Hz, 1H), 6.90 (d, J = 7.6 Hz, 1H), 5.06 (dd, J = 12.9, 5.4 Hz, 1H), 4.29 (s, 4H), 4.04 (s, 4H), 2.90 - 2.84 (m, 1H), 2.65 - 2.51 (m, 2H), 2.05 - 1.97 (m, 1H), 1.38 (s, 9H); 13 C NMR (151 MHz, DMSO- d_6 δ [ppm]): 172.7, 169.9, 166.7, 166.3 (d, J = 2.7 Hz), 155.3, 154.6, 153.0, 143.7 (d, J = 12.0 Hz), 129.2, 118.9 (d, J = 8.3 Hz), 111.2 (d, J = 22.1 Hz), 108.2 (d, J = 6.6 Hz), 78.6, 63.0, 48.9, 40.1, 33.4 (d, J = 2.7 Hz), 30.9, 28.0, 22.1; 19 F NMR (565 MHz, DMSO- d_6 δ [ppm]): 128.4; LRMS m/z (ESI*) [Found: 473.6, C_{23} H₂₆FN₄O₆* requires [M+H]* 473.5]; Rf: 0.37 (cyclohexane/ethyl acetate (1/1 (ν/ν)); mp: 244 - 248 °C.

tert-Butyl-4-{1-[2-(2,6-dioxopiperidin-3-yl)-6-fluoro-1,3-dioxoisoindolin-5-yl]piperidin-4-yl}piperazine-1-carboxylate (SLW278, 22)

2-(2,6-Dioxopiperidin-3-yl)-5,6-difluoroisoindoline-1,3-dione (**5**, 0.28 g, 0.90 mmol, 1.0 e*q*.) and *tert*-Butyl-4-(piperidin-4-yl)piperazine-1-carboxylate (326 mg, 1.18 mmol, 1.30 *eq*.) were dissolved in DMSO (10 mL). After the addition of DIPEA (324 μ L. 1.80 mmol, 2.00 *eq*.) the reaction was stirred at reflux overnight. After the addition of water (50 mL) the mixture was extracted using ethyl acetate (3 x 50 mL). Drying over sodium sulfate, filtration, evaporation of the solvent the crude product was purified by column chromatography using a mixture of cyclohexane and ethyl acetate (1/1 (ν / ν)) to give the title compound as yellow gum (444 mg, 90%). H NMR (600 MHz, DMSO- d_6 δ [ppm]): 11.09 (s, 1H), 7.69 (d, J = 11.4 Hz, 1H), 7.44 (d, J = 7.5 Hz, 1H), 5.09 (dd, J = 12.9, 5.4 Hz, 1H), 3.65 (d, J = 12.2 Hz, 2H), 3.34 – 3.26 (m, 2H, under the water peak), 2.93 – 2.83 (m, 4H), 2.63 – 2.51 (m, 2H), 2.48 – 2.41 (m, 6H), 2.06 – 1.99 (m, 1H), 1.88 – 1.81 (m, 2H), 1.61 – 1.51 (m, 2H), 1.39 (s, 9H); ¹³C NMR (151 MHz, DMSO- d_6 δ [ppm]): 172.6, 169.8, 166.6, 166.1, 158.2, 156.2, 153.7, 145.4 (d, J = 8.9 Hz), 128.7, 122.9 (d, J = 9.7 Hz), 113.6 (d, J = 4.8 Hz), 111.8 (d, J = 25.3 Hz), 78.6, 60.4, 49.3 (d,

J = 4.8 Hz), 49.0, 48.5, 40.1, 30.9, 28.0, 27.7, 22.0; ¹⁹F NMR (565 MHz, DMSO- d_6 δ [ppm]): 112.9; LRMS m/z (ESI⁺) [Found: 544.5, C₂₇H₃₅FN₅O₆⁺ requires [M+H]⁺ 544.6]; Rf: 0.22 (cyclohexane/ethyl acetate (1/1 (v/v)); mp: 213 – 216 °C.

tert-Butyl 4-({1-[2-(2,6-dioxopiperidin-3-yl)-6-fluoro-1,3-dioxoisoindolin-5-yl]piperidin-4-yl}methyl)piperazine-1-carboxylate (SLW295, 23)

$$0 \xrightarrow{HN} N \xrightarrow{N} N$$

2-(2,6-Dioxopiperidin-3-yl)-5,6-difluoroisoindoline-1,3-dione (5, 0.27 g, 0.87 mmol, 1.0 eq.) and tert-Butyl-4-(piperazin-1-ylmethyl)piperidine-1-carboxylate (331 mg, 1.13 mmol, 1.30 eq.) were dissolved in DMSO (10 mL). After the addition of DIPEA (312 µL. 1.74 mmol, 2.00 eg.) the reaction was stirred at reflux overnight. After the addition of water (50 mL) the mixture was extracted using ethyl acetate (3 x 50 mL). Drying over sodium sulfate, filtration, evaporation of the solvent the crude product was purified by column chromatography using a mixture of cyclohexane and ethyl acetate (1/1 (v/v)) to give the title compound as yellow gum (350 mg, 72%). H NMR (600 MHz, DMSO-d₆ δ [ppm]): two protons are not detectable due to the solvent peak, 11.08 (s, 1H), 7.70 (d, J = 11.4 Hz, 1H), 7.44 (d, J = 7.4 Hz, 1H), 5.10 (dd, J = 12.9, 5.4 Hz, 1H), 3.92 (d, J = 13.0 Hz, 2H), 3.28 - 3.23 (m, 4H), 2.94 - 2.85 (m, 1H), 2.70 (s, 3H), 2.65 - 2.51 (m, 2H), 2.18 (d, J = 6.8 Hz, 2H), 2.09 - 1.96 (m, 1H), 1.75 - 1.66 (m, 3H), 1.39 (s, 9H), 1.02 - 0.89 (m, 2H); 13 C NMR (151 MHz, DMSO- d_6 δ [ppm]): 172.7, 169.8, 166.6, 166.1 (d, J = 2.3 Hz), 158.3, 156.3, 153.9, 145.3 (d, J = 8.9 Hz), 128.7 (d, J = 2.3 Hz), 123.3 (d, J = 2.3 Hz), 123.9.8 Hz), 113.6 (d, J = 5.1 Hz), 111.9 (d, J = 25.3 Hz), 78.3, 63.6, 52.8, 49.5 (d, J = 4.5 Hz), 49.0, 40.1, 32.6, 30.9, 30.2, 28.1, 22.0; ¹⁹F NMR (565 MHz, DMSO-d₆ δ [ppm]): 112.8; LRMS m/z (ESI+) [Found: 558.6, C₂₈H₃₇FN₅O₆+ requires [M+H]+ 558.6]; Rf: 0.64 (cyclohexane/ethyl acetate (1/1 (v/v)); mp: 242 – 246 °C.

tert-Butyl (8-{[2-(2,6-dioxopiperidin-3-yl)-6-fluoro-1,3-dioxoisoindolin-5-yl]amino}octyl)carbamate (SLW181, 24)

2-(2,6-Dioxopiperidin-3-yl)-5,6-difluoroisoindoline-1,3-dione (5, 400 mg, 1.29 mmol, 1.00 eq.) and tert-Butyl-(8-aminooctyl)carbamate (332 mg, 1.29 mmol, 1.00 eq.) were dissolved in DMSO (10 mL). After the addition of DIPEA (462 µL. 2.58 mmol, 2.00 eq.) the reaction was stirred at reflux overnight. After the addition of water (50 mL) the mixture was extracted using ethyl acetate (3 x 50 mL). Drying over sodium sulfate, filtration, evaporation of the solvent the crude product was purified by column chromatography using a mixture of cyclohexane and ethyl acetate (1/1 (v/v)) to give the title compound as yellow gum (471 mg, 70%). H NMR (600 MHz, DMSO- d_6 δ [ppm]): 11.05 (s, 1H), 7.54 (d, J = 10.3 Hz, 1H), 7.08 (d, J = 7.2 Hz, 1H), 6.88 - 6.86 (m, 1H), 6.72 - 6.71 (m, 1H), 5.04 (dd, J = 12.9, 5.5 Hz, 1H), 3.25 (q, J =6.7 Hz, 2H), 2.93 - 2.83 (m, 3H), 2.63 - 2.50 (m, 2H), 2.07 - 1.94 (m, 1H), 1.59 - 1.55 (m, 2H), 1.36 (s, 9H), 1.36 – 1.20 (m, 10H); 13 C NMR (151 MHz, DMSO- d_6 δ [ppm]): 173.2, 170.5, 167.6, 167.1 (d, J = 2.7 Hz), 165.8, 156.0, 154.3, 152.7, 143.4 (d, J = 13.2 Hz), 130.5, 116.6 (d, J = 8.4 Hz), 110.3 (d, J = 22.0 Hz), 105.4 (d, J = 6.2 Hz), 77.7, 60.2, 49.3, 42.8, 40.6, 31.5,29.9, 29.2, 28.7, 26.8, 22.7, 21.2, 14.6; ¹⁹F NMR (565 MHz, DMSO-d₆ δ [ppm]): 127.4; LRMS m/z (ESI⁺) [Found: 519.6, $C_{26}H_{36}FN_4O_6^+$ requires [M+H]⁺ 519.6]; Rf: 0.47 (cyclohexane/ethyl acetate (1/1 (v/v)); mp: 135 - 139 °C.

 $3-[(4-\{[(R)-2,2-Dimethyl-1-(5-methylfuran-2-yl)propyl]amino}-1,1-dioxido-1,2,5-thiadiazol-3-yl)amino]-$ *N* $-[(1-{2-[2-(2-{[2-(2,6-dioxopiperidin-3-yl)-1,3-dioxoisoindolin-4-yl]amino}ethoxy)ethoxy]ethyl}-1$ *H*-1,2,3-triazol-4-yl)methyl]-2-hydroxybenzamide (SLW141, 25)

2-(2,6-Dioxopiperidin-3-yl)-4-fluoroisoindoline-1,3-dione (40 mg, 0.10 mmol, 1.0 eq.) and 2-[2 -(2 -azidoethoxy)ethoxy]ethan-1-amine(19 μ L, 0.10 mmol, 1.0 eq.) were dissolved in DMSO (5 mL). After the addition of DIPEA (49 μ L. 0.30 mmol, 3.0 eq.) the reaction was stirred at reflux overnight. After the addition of water (50 mL) the mixture was extracted using ethyl acetate (3 x 50 mL). Drying over sodium sulfate, filtration, evaporation of the solvent and a quick column chromatography using a mixture of cyclohexane and ethyl acetate (1/1 (2 - 2) gave the intermediate 2 -(2 - 2 - 2 -azidoethoxy)ethoxy]ethyl}amino)-2-(2 - 2 -dioxopiperidin-3-

yl)isoindoline-1,3-dione. The intermediate (30 mg, 0.10 mmol, 1.0 eq.) and (R)-3-[(4-{[2,2-Dimethyl-1-(5-methylfuran-2-yl)propyl]amino}-1,1-dioxido-1,2,5-thiadiazol-3-yl)amino]-2hydroxy-N-(prop-2-yn-1-yl)benzamide (SLW089, 34 mg, 0.10 mmol, 1.0 eg.) were dissolved (3 mL, in mixture of DMF, *tert*-butanol and water 1/1/1 (v/v). Tris(benzyltriazolylmethyl)amine (5.3 mg, 0.020 mmol, 0.20 eq.) a 0.1M copper(II)sulfate solution (0.5 mL, 0.05 mmol, 0.5 eq.) and an 0.1M ascorbic acid solution (0.5 mL, 0.05 mmol, 0.5 eq.) were added in that order. After the last addition the reaction was stirred overnight. After completion of the reaction the mixture was quenched by the addition of water (5 mL) and extracted using ethyl acetate (3 x 50 mL). Drying over sodium sulfate, filtration and evaporation of the solvents gave the crude product that was purified by preparative HPLC (acetonitrile/water (0.1% TFA): gradient 5-95%) to obtain the title compound as a yellow amorphous solid (24 mg, 53%). ¹H NMR (600 MHz, DMSO-*d*₆, δ [ppm]): 13.73 (s, 1H), 11.07 (s, 1H), 10.58 (s, 1H), 9.61 (t, J = 5.8 Hz, 1H), 9.25 (d, J = 9.1 Hz, 1H), 8.00 (s, 1H), 7.88 -7.83 (m, 2H), 7.57 - 7.54 (m, 1H), 7.09 (d, J = 8.6 Hz, 1H), 7.04 - 6.96 (m, 2H), 6.56 (s, 1H), 6.31 (d, J = 3.1 Hz, 1H), 6.07 (dd, J = 3.1, 1.3 Hz, 1H), 5.04 (dd, J = 12.9, 5.5 Hz, 1H), 4.87 (d, J = 9.0 Hz, 1H), 4.56 (d, J = 5.7 Hz, 2H), 4.49 (t, J = 5.2 Hz, 2H), 3.81 (t, J = 5.2 Hz, 2H), 3.58 -3.48 (m, 6H), 3.41 (s, 2H), 2.90 - 2.84 (m, 1H), 2.62 - 2.52 (m, 2H), 2.29 (s, 3H), 2.04 - 1.99 (m, 1H), 1.01 (s, 9H); 13 C NMR (151 MHz, DMSO- d_6 , δ [ppm]): 172.7, 170.0, 169.3, 168.9, 167.2, 158.0, 155.8, 154.0, 153.4, 151.3, 149.3, 146.3, 143.8, 136.2, 132.0, 129.5, 125.2, 123.5, 118.1, 117.3, 114.9, 110.6, 109.7, 109.2, 106.4, 69.6, 69.5, 68.8, 68.7, 61.8, 49.3, 48.5, 41.6, 35.7, 34.6, 30.9, 26.5, 22.1, 13.4; HRMS m/z (ESI+) [Found: 902.3246, C₄₁H₄₈N₁₁O₁₁S+ requires [M+H]⁺ 902.3177]; HPLC retention time 12.55 min, purity: 95.0%.

3-[(4-{[(R)-2,2-Dimethyl-1-(5-methylfuran-2-yl)propyl]amino}-1,1-dioxido-1,2,5-thiadiazol-3-yl)amino]-N-[(1-{2-[2-(2-{[2-(2,6-dioxopiperidin-3-yl)-1,3-dioxoisoindolin-5-yl]amino}ethoxy)ethoxy]ethyl}-1H-1,2,3-triazol-4-yl)methyl]-2-hydroxybenzamide (SLW223, 26)

2-(2,6-dioxopiperidin-3-yl)-5-fluoroisoindoline-1,3-dione (30 mg, 0.10 mmol, 1.0 eq.) and 2-[-2-(2-azidoethoxy)ethoxy]ethan-1-amine (19 μ L, 0.10 mmol, 1.0 eq.) were dissolved in DMSO (5 mL). After the addition of DIPEA (37 μ L. 0.20 mmol, 2.0 eq.) the reaction was stirred at reflux

overnight. After the addition of water (50 mL) the mixture was extracted using ethyl acetate (3 x 50 mL). Drying over sodium sulfate, filtration, evaporation of the solvent and a quick column chromatography using a mixture of cyclohexane and ethyl acetate (1/1 (v/v)) gave the intermediate 5-({2-[2-(2-azidoethoxy)ethoxy]ethyl}amino)-2-(2,6-dioxopiperidin-3yl)isoindoline-1,3-dione. The intermediate (39 mg, 0.10 mmol, 1.0 eq.) and (R)-3-[(4-{[2,2-Dimethyl-1-(5-methylfuran-2-yl)propyl]amino}-1,1-dioxido-1,2,5-thiadiazol-3-yl)amino]-2hydroxy-N-(prop-2-yn-1-yl)benzamide (SLW089, 44 mg, 0.10 mmol, 1.0 eq.) were dissolved in а mixture DMF, *tert*-butanol and water (3 mL, 1/1/1 (v/v). Tris(benzyltriazolylmethyl)amine (9.4 mg, 0.050 mmol, 0.50 eq.) a 0.1M copper(II)sulfate solution (0.5 mL, 0.05 mmol, 0.5 eq.) and an 0.1M ascorbic acid solution (0.5 mL, 0.05 mmol, 0.5 eq.) were added in that order. After the last addition the reaction was stirred overnight. After completion of the reaction the mixture was quenched by the addition of water (5 mL) and extracted using ethyl acetate (3 x 50 mL). Drying over sodium sulfate, filtration and evaporation of the solvents gave the crude product that was purified by preparative HPLC (acetonitrile/water (0.1% TFA): gradient 5-95%) to obtain the title compound as a yellow amorphous solid (22 mg, 27%). ¹H NMR (600 MHz, DMSO-*d*₆, δ [ppm]): 13.72 (s, 1H), 11.03 (s, 1H), 10.59 (s, 1H), 9.62 (t, J = 5.7 Hz, 1H), 9.25 (d, J = 9.1 Hz, 1H), 8.01 (s, 1H), 7.91 – 7.83 (m, 2H), 7.55 (d, J = 8.4 Hz, 1H), 7.03 – 6.95 (m, 2H), 6.87 (dd, J = 8.4, 2.2 Hz, 1H), 6.31 (d, J = 3.1 Hz, 1H), 6.07 (dd, J = 3.1, 1.2 Hz, 1H), 5.02 (dd, J = 12.7, 5.4 Hz, 1H), 4.87 (d, J = 12.7, 1.2 Hz, 1.4 Hz)9.1 Hz, 1H), 4.57 (d, J = 5.5 Hz, 2H), 4.49 (t, J = 5.3 Hz, 2H), 3.80 (t, J = 5.3 Hz, 2H), 3.56 – 3.46 (m, 6H), 3.31 (t, J = 5.4 Hz, 2H), 2.91 - 2.83 (m, 1H), 2.68 - 2.51 (m, 2H), 2.29 (s, 3H), 2.03 - 1.94 (m, 1H), 1.01 (s, 9H); 13 C NMR (151 MHz, DMSO- d_6 , δ [ppm]): 172.7, 170.0, 169.3, 167.6, 167.1, 155.8, 154.4, 153.9, 153.4, 151.2, 149.3, 143.8, 134.1, 129.5, 125.5, 125.2, 124.9, 123.4, 118.0, 116.1, 115.5, 114.9, 109.6, 106.4, 105.4, 69.6, 69.5, 68.7, 61.8, 49.3, 48.6, 42.4, 40.1, 35.6, 34.6, 30.9, 26.5, 22.2, 13.3; HRMS *m/z* (ESI⁺) [Found: 902.3283, C₄₁H₄₇N₁₁O₁₁S⁺ requires [M+H]⁺ 902.3177]; HPLC retention time 12.29 min, purity: 99.6%.

3-[(4-{[(R)-2,2-Dimethyl-1-(5-methylfuran-2-yl)propyl]amino}-1,1-dioxido-1,2,5-thiadiazol-3-yl)amino]-N-[(1-{2-[2-(2-{[2-(2,6-dioxopiperidin-3-yl)-6-fluoro-1,3-dioxoisoindolin-5-yl]amino}ethoxy)ethoxy]ethyl}-1H-1,2,3-triazol-4-yl)methyl]-2-hydroxybenzamide (SLW224, 27)

2-(2,6-Dioxopiperidin-3-yl)-5,6-difluoroisoindoline-1,3-dione (5, 30 mg, 0.10 mmol, 1.0 eq.) and 2-[-2-(2-azidoethoxy)ethoxy]ethan-1-amine (17 µL, 0.10 mmol, 1.0 eq.) were dissolved in DMSO (5 mL). After the addition of DIPEA (35 µL. 0.20 mmol, 2.0 eq.) the reaction was stirred at reflux overnight. After the addition of water (50 mL) the mixture was extracted using ethyl acetate (3 x 50 mL). Drying over sodium sulfate, filtration, evaporation of the solvent and a quick column chromatography using a mixture of cyclohexane and ethyl acetate (1/1 (v/v)) gave the intermediate 5-({2-[2-(2-azidoethoxy)ethoxy]ethyl}amino)-2-(2,6-dioxopiperidin-3-yl)-6-fluoroisoindoline-1,3-dione. The intermediate (37 mg, 0.10 mmol, 1.0 eg.) and (R)-3-[(4-{[2,2-Dimethyl-1-(5-methylfuran-2-yl)propyl]amino}-1,1-dioxido-1,2,5-thiadiazol-3-yl)amino]-2hydroxy-N-(prop-2-yn-1-yl)benzamide (SLW089, 40 mg, 0.10 mmol, 1.0 eq.) were dissolved DMF, tert-butanol mixture of and water (3 mL, 1/1/1 (v/v). Tris(benzyltriazolylmethyl)amine (8.6 mg, 0.050 mmol, 0.50 eq.) a 0.1M copper(II)sulfate solution (0.5 mL, 0.05 mmol, 0.5 eq.) and an 0.1M ascorbic acid solution (0.5 mL, 0.05 mmol, 0.5 eq.) were added in that order. After the last addition the reaction was stirred overnight. After completion of the reaction the mixture was quenched by the addition of water (5 mL) and extracted using ethyl acetate (3 x 50 mL). Drying over sodium sulfate, filtration and evaporation of the solvents gave the crude product that was purified by preparative HPLC (acetonitrile/water (0.1% TFA): gradient 5-95%) to obtain the title compound as a yellow amorphous solid (35 mg, 47%). ¹H NMR (600 MHz, DMSO-*d*₆, δ [ppm]): 13.72 (s, 1H), 11.05 (s, 1H), 10.59 (s, 1H), 9.61 (t, J = 5.8 Hz, 1H), 9.25 (d, J = 9.1 Hz, 1H), 8.00 (s, 1H), 7.86 (td, J = 8.3, 1.5 Hz, 2H, 7.55 (dd, J = 10.3, 1.4 Hz, 1H), 7.19 (d, J = 7.2 Hz, 1H), 6.99 (t, J = 8.0 Hz, 1Hz)1H), 6.75 (s, 1H), 6.31 (d, J = 3.1 Hz, 1H), 6.07 (dd, J = 3.1, 1.3 Hz, 1H), 5.04 (dd, J = 12.9, 5.4 Hz, 1H), 4.87 (d, J = 9.0 Hz, 1H), 4.57 (d, J = 5.6 Hz, 2H), 4.47 (t, J = 5.3 Hz, 2H), 3.79 (t, J = 5.3 Hz, 2H), 3.55 (t, J = 5.6 Hz, 2H), 3.52 – 3.50 (m, 4H), 3.44 - 3.38 (s, 2H), 2.91 – 2.82 (m, 1H), 2.64 – 2.51 (m, 2H), 2.29 (s, 3H), 2.02 - 1.97 (m, 1H), 1.01 (s, 9H); ¹³C NMR (151 MHz, DMSO-d₆, δ [ppm]): 172.7, 170.0, 169.3, 167.1, 166.6, 166.6, 158.2, 158.0, 155.8, 154.0, 153.4, 152.2, 151.3, 149.3, 143.8, 142.8 (d, J = 13.0 Hz), 129.7 (d, J = 39.3 Hz), 125.5, 125.2, 123.5, 118.1, 116.5, 116.5, 114.9, 109.9 (d, J = 22.0 Hz), 109.7, 106.4, 105.6, 105.5, 69.6 (d, J = 22.0 Hz), 68.8 (d, J = 25.0 Hz), 61.9, 49.3, 48.8, 42.2, 40.1, 40.1, 35.7, 34.6, 31.0, 26.5, 22.2, 13.4; ¹⁹F NMR (565 MHz, DMSO-d₆, δ [ppm]:-74.7; HRMS m/z (ESI+) [Found: 920.3183, C₄₁H₄₇FN₁₁O₁₁S+ requires [M+H]+ 920.3083]; HPLC retention time 12.39 min, purity: 99.5%.

3-[(4-{[2,2-Dimethyl-1-(5-methylfuran-2-yl)propyl]amino}-1,1-dioxido-1,2,5-thiadiazol-3-yl)amino]-N-[(1-{2-[2-(2-{2-[4-(2,6-dioxopiperidin-3-yl)phenoxy]acetamido}ethoxy)ethoxy]ethyl}-1H-1,2,3-triazol-4-yl)methyl]-2-hydroxybenzamide (SLW142, 28)

2-[4-(2,6-Dioxopiperidin-3-yl)phenoxy]acetic acid (SLW138, 30 mg, 0.10 mmol, 1.0 eq.) and 2-[-2-(2-azidoethoxy)ethoxy]ethan-1-amine (19 µL, 0.10 mmol, 1.0 eq.) were dissolved in DMF (5 mL). After the addition of DIPEA (78 µL. 0.40 mmol, 4.0 eq.) and PyBroP (0.12 g, 0.26 mmol, 1.2 eq.) the reaction was stirred overnight. After the addition of water (50 mL) the mixture was extracted using ethyl acetate (3 x 50 mL). Drying over sodium sulfate, filtration, evaporation of the solvent and a quick column chromatography using a mixture of cyclohexane and ethyl acetate (1/1 (v/v)) gave the intermediate N-{2-[2-(2-azidoethoxy)ethoxy]ethyl}-2-[4-(2,6-dioxopiperidin-3-yl)phenoxylacetamide. The intermediate (40 mg, 0.10 mmol, 1.0 eq.) and (R)-3-[(4-{[2,2-Dimethyl-1-(5-methylfuran-2-yl)propyl]amino}-1,1-dioxido-1,2,5-thiadiazol-3-yl)amino]-2-hydroxy-*N*-(prop-2-yn-1-yl)benzamide (**SLW089**, 46 mg, 0.10 mmol, 1.0 eg.) were dissolved in a mixture of DMF, tert-butanol and water (3 mL, 1/1/1 (v/v)). Tris(benzyltriazolylmethyl)amine (5.0 mg, 0.020 mmol, 0.20 eq.) a 0.1M copper(II)sulfate solution (0.5 mL, 0.05 mmol, 0.5 eq.) and an 0.1M ascorbic acid solution (0.5 mL, 0.05 mmol, 0.5 eq.) were added in that order. After the last addition the reaction was stirred overnight. After completion of the reaction the mixture was quenched by the addition of water (5 mL) and extracted using ethyl acetate (3 x 50 mL). Drying over sodium sulfate, filtration and evaporation of the solvents gave the crude product that was purified by preparative HPLC (acetonitrile/water (0.1% TFA): gradient 5-95%) to obtain the title compound as a white amorphous solid (35 mg, 42%). ¹H NMR (600 MHz, DMSO-*d*₆, δ [ppm]): 13.73 (s, 1H), 10.77 (s, 1H), 10.60 (s, 1H), 9.62 (t, J = 5.8 Hz, 1H), 9.26 (d, J = 9.1 Hz, 1H), 8.03 - 8.01 (m, 2H), 7.88 - 7.86 (m, 2H), 7.13 (d, J = 8.6 Hz, 2H), 7.00 (t, J = 8.0 Hz, 1H), 6.94 - 6.87 (m, 2H), 6.32 (d, J = 3.1 Hz, 1H), 6.07 (d, J = 3.0 Hz, 1H), 4.87 (d, J = 9.0 Hz, 1H), 4.58 (d, J = 5.5 Hz, 2H), 4.52 - 4.44 (m, 4H), 3.86 - 3.77 (m, 2H partially under the water peak), 3.50 (dd, J = 6.1, 3.5 Hz, 2H), 3.45 (dd, J = 6.1, 3.5 Hz, 2H), 3.40 (t, J = 5.9 Hz, 2H), 3.27 (q, J = 5.9 Hz, 2H), 2.68 - 2.61 (m, 1H), 2.48 - 2.38 (m, 1H), 2.29 (s, 3H), 2.19 - 2.11 (m, 1H), 2.02 - 1.97 (m, 1H), 1.04 (d, J = 6.1 Hz, 1H), 1.01 (s, 9H); ¹³C NMR (151 MHz, DMSO-d₆, δ [ppm]): 174.3, 173.3, 169.3, 167.7, 156.6, 155.8, 153.9, 153.3, 151.2, 149.3, 143.8, 131.8, 129.5, 129.5, 125.5, 125.2, 123.4, 118.0, 114.9, 114.5, 109.6, 106.4, 69.4, 69.3, 68.7, 68.6, 67.0, 61.8, 49.3, 46.4, 38.2, 35.6, 34.6, 31.3, 26.5, 25.9, 25.4, 13.3; HRMS m/z (ESI+) [Found: 891.3451, C₄₁H₅₁N₁₀O₁₁S+ requires [M+H]+ 891.3381]; HPLC retention time 12.15 min, purity: 97.8%.

 $3-[(2-\{[(R)-2,2-Dimethyl-1-(5-methylfuran-2-yl)propyl]amino}-3,4-dioxocyclobut-1-en-1-yl)amino]-<math>N-[(1-\{2-[2-(2-\{[2-(2,6-dioxopiperidin-3-yl)-1,3-dioxoisoindolin-4-yl]amino}ethoxy)ethoxy]ethyl}-1$ H-1,2,3-triazol-4-yl)methyl]-2-hydroxybenzamide (SLW225, 29)

2-(2,6-Dioxopiperidin-3-yl)-4-fluoroisoindoline-1,3-dione (40 mg, 0.10 mmol, 1.0 eq.) and 2-[2-(2-azidoethoxy)ethoxy]ethan-1-amine(19 μ L, 0.10 mmol, 1.0 eq.) were dissolved in DMSO (5 mL). After the addition of DIPEA (49 μ L. 0.30 mmol, 3.0 eq.) the reaction was stirred at reflux overnight. After the addition of water (50 mL) the mixture was extracted using ethyl acetate (3 x 50 mL). Drying over sodium sulfate, filtration, evaporation of the solvent and a quick column chromatography using a mixture of cyclohexane and ethyl acetate (1/1 (ν / ν)) gave the intermediate 4-({2-[2-(2-azidoethoxy)ethoxy]ethyl}amino)-2-(2,6-dioxopiperidin-3-yl)isoindoline-1,3-dione. The intermediate (30 mg, 0.10 mmol, 1.0 eq.) and (R)-3-[(2-{[2,2-dimethyl-1-(5-methylfuran-2-yl)propyl]amino}-3,4-dioxocyclobut-1-en-1-yl)amino]-2-hydroxy-N-(prop-2-yn-1-yl)benzamide (**SLW007**, 45 mg, 0.10 mmol, 1.0 eq.) were dissolved in a mixture of DMF, tert-butanol and water (3 mL, 1/1/1 (ν / ν)). Tris(benzyltriazolylmethyl)amine (10.6 mg, 0.0200 mmol, 0.200 eq.) a 0.1M copper(II)sulfate solution (1.5 mL, 0.15 mmol, 1.5 eq.) and an 0.1M ascorbic acid solution (0.5 mL, 0.05 mmol, 0.5 eq.) were added in that

order. After the last addition the reaction was stirred overnight. After completion of the reaction the mixture was quenched by the addition of water (5 mL) and extracted using ethyl acetate (3 x 50 mL). Drying over sodium sulfate, filtration and evaporation of the solvents gave the crude product that was purified by preparative HPLC (acetonitrile/water (0.1% TFA): gradient 5–95%) to obtain the title compound as a yellow amorphous solid (66 mg, 73%). ¹H NMR (600 MHz, DMSO- d_6 , δ [ppm]): 13.89 (s, 1H), 11.07 (s, 1H), 9.56 (t, J = 5.8 Hz, 1H), 9.53 (s, 1H), 8.78 (d, J = 10.1 Hz, 1H, 7.99 (s, 1H), 7.95 (dd, J = 8.0, 1.3 Hz, 1H), 7.60 - 7.50 (m, 2H), 7.05 (d, J = 8.0, 1.3 Hz, 1H)7.8 Hz, 1H), 7.00 (dd, J = 7.0, 1.4 Hz, 1H), 6.86 (t, J = 8.1 Hz, 1H), 6.54 (s, 1H), 6.19 (d, J =3.1 Hz, 1H), 6.05 (dd, J = 3.1, 1.3 Hz, 1H), 5.11 (d, J = 10.1 Hz, 1H), 5.04 (dd, J = 9.9, 5.5 Hz, 1H), 4.55 (d, J = 5.7 Hz, 2H), 4.49 (t, J = 5.2 Hz, 2H), 3.80 (t, J = 5.3 Hz, 2H), 3.56 - 3.45 (m, 6H), 3.39 - 3.35 (m, 2H), 2.91 - 2.84 (m, 1H), 2.63 – 2.51 (m, 2H), 2.28 (s, 3H), 2.05 - 1.99 (m, 1H), 0.97 (s, 9H); ¹³C NMR (151 MHz, DMSO-d₆, δ [ppm]): 184.1, 180.2, 172.8, 172.7, 170.0, 168.9, 168.6, 167.2, 163.1, 158.3, 151.0, 150.7, 146.3, 143.9, 136.1, 132.0, 127.9, 123.5, 120.8, 118.1, 117.3, 113.6, 110.6, 109.2, 108.5, 106.3, 69.6, 69.5, 68.8, 68.7, 60.2, 50.0, 49.4, 48.5, 41.6, 35.7, 34.6, 31.0, 26.2, 22.1, 13.4; HRMS *m/z* (ESI+) [Found: 866.3497, $C_{43}H_{48}N_9O_{11}^+$ requires [M+H]⁺ 866.3395]; HPLC retention time 12.71 min, purity: 99.3%.

 $3-[(2-\{[(R)-2,2-dimethyl-1-(5-methylfuran-2-yl)propyl]amino}-3,4-dioxocyclobut-1-en-1-yl)amino]-N-[(1-\{2-[2-(2-\{[2-(2,6-dioxopiperidin-3-yl)-1,3-dioxoisoindolin-5-yl]amino}ethoxy)ethoxy]ethyl}-1<math>H$ -1,2,3-triazol-4-yl)methyl]-2-hydroxybenzamide (SLW226, 30)

2-(2,6-dioxopiperidin-3-yl)-5-fluoroisoindoline-1,3-dione (30 mg, 0.10 mmol, 1.0 eq.) and 2-[-2-(2-azidoethoxy)ethoxy]ethan-1-amine (19 μ L, 0.10 mmol, 1.0 eq.) were dissolved in DMSO (5 mL). After the addition of DIPEA (37 μ L. 0.20 mmol, 2.0 eq.) the reaction was stirred at reflux overnight. After the addition of water (50 mL) the mixture was extracted using ethyl acetate (3 x 50 mL). Drying over sodium sulfate, filtration, evaporation of the solvent and a quick column chromatography using a mixture of cyclohexane and ethyl acetate (1/1 (ν / ν)) gave the intermediate 5-({2-[2-(2-azidoethoxy)ethoxy]ethyl}amino)-2-(2,6-dioxopiperidin-3-yl)isoindoline-1,3-dione. The intermediate (32 mg, 0.10 mmol, 1.0 eq.) and (R)-3-[(2-{[2,2-dimethyl-1-(5-methylfuran-2-yl)propyl]amino}-3,4-dioxocyclobut-1-en-1-yl)amino]-2-hydroxy-

N-(prop-2-yn-1-yl)benzamide (SLW007, 36 mg, 0.10 mmol, 1.0 eq.) were dissolved in a mixture of DMF, tert-butanol and water (3 mL, 1/1/1 (v/v)). Tris(benzyltriazolylmethyl)amine (7.7 mg, 0.020 mmol, 0.20 eq.) a 0.1M copper(II)sulfate solution (1.5 mL, 0.15 mmol, 1.5 eq.) and an 0.1M ascorbic acid solution (0.5 mL, 0.05 mmol, 0.5 eq.) were added in that order. After the last addition the reaction was stirred overnight. After completion of the reaction the mixture was guenched by the addition of water (5 mL) and extracted using ethyl acetate (3 x 50 mL). Drying over sodium sulfate, filtration and evaporation of the solvents gave the crude product that was purified by preparative HPLC (acetonitrile/water (0.1% TFA): gradient 5-95%) to obtain the title compound as a yellow amorphous solid (34 mg, 52%). ¹H NMR (600 MHz, DMSO- d_6 , δ [ppm]): 13.89 (s, 1H), 11.03 (s, 1H), 9.60 – 9.53 (m, 2H), 8.78 (d, J = 10.1 Hz, 1H), 8.00 (s, 1H), 7.96 (d, J = 8.0 Hz, 1H), 7.59 - 7.53 (m, 2H), 6.99 (d, J = 2.2 Hz, 1H), 6.91 -6.83 (m, 2H), 6.18 (d, J = 3.1 Hz, 1H), 6.04 (d, J = 3.0 Hz, 1H), 5.11 (d, J = 10.1 Hz, 1H), 5.02 (dd, J = 12.7, 5.5 Hz, 1H), 4.56 (d, J = 5.6 Hz, 3H), 4.50 - 4.48 (t, J = 5.2 Hz, 3H), 3.80 (t, J = 5.3 Hz, 2H), 3.54 - 3.50 (m, 6H), 3.30 (t, J = 5.5 Hz, 2H), 2.90 - 2.83 (m, 1H), 2.66 - 2.51 (m, 2H), 2.28 (s, 3H), 2.02 - 1.96 (m, 1H), 0.97 (s, 9H); 13 C NMR (151 MHz, DMSO- d_6 , δ [ppm]): 184.1, 172.7, 170.0, 169.9, 167.6, 167.0, 163.1, 158.3, 154.3, 151.0, 150.9, 150.7, 143.9, 134.1, 127.9, 124.9, 123.5, 123.4, 118.1, 116.1, 115.4, 113.6, 108.5, 106.2, 105.4, 69.6, 69.5, 68.7, 60.2, 49.3, 48.6, 42.4, 40.1, 35.6, 34.6, 30.9, 26.2, 22.2, 13.3; HRMS *m/z* (ESI+) [Found: 866.3460, C₄₃H₄₈N₉O₁₁⁺ requires [M+H]⁺ 866.3395]; HPLC retention time 12.39 min, purity: 95.7%.

 $3-[(2-\{[(R)-2,2-dimethyl-1-(5-methylfuran-2-yl)propyl]amino}-3,4-dioxocyclobut-1-en-1-yl)amino]-<math>N-[(1-\{2-[2-(2-\{[2-(2,6-dioxopiperidin-3-yl)-6-fluoro-1,3-dioxoisoindolin-5-yl]amino}ethoxy)ethoxy]ethyl}-1<math>H-1,2,3-triazol-4-yl)$ methyl]-2-hydroxybenzamide (SLW227, 31)

2-(2,6-Dioxopiperidin-3-yl)-5,6-difluoroisoindoline-1,3-dione (**5**, 30 mg, 0.10 mmol, 1.0 *eq.*) and 2-[-2-(2-azidoethoxy)ethoxy]ethan-1-amine (17 μ L, 0.10 mmol, 1.0 *eq.*) were dissolved in DMSO (5 mL). After the addition of DIPEA (35 μ L. 0.20 mmol, 2.0 *eq.*) the reaction was stirred at reflux overnight. After the addition of water (50 mL) the mixture was extracted using ethyl acetate (3 x 50 mL). Drying over sodium sulfate, filtration, evaporation of the solvent and a

quick column chromatography using a mixture of cyclohexane and ethyl acetate (1/1 (v/v)) gave the intermediate 5-({2-[2-(2-azidoethoxy)ethoxy]ethyl}amino)-2-(2,6-dioxopiperidin-3-yl)-6-fluoroisoindoline-1,3-dione. The intermediate (35 mg, 0.10 mmol, 1.0 eg.) and (R)-3-[(2-{[2,2-dimethyl-1-(5-methylfuran-2-yl)propyl]amino}-3,4-dioxocyclobut-1-en-1-yl)amino]-2hydroxy-N-(prop-2-yn-1-yl)benzamide (**SLW007**, 37 mg, 0.10 mmol, 1.0 eq.) were dissolved mixture of DMF, tert-butanol and water (3 mL, 1/1/1 (v/v). Tris(benzyltriazolylmethyl)amine (8.6 mg, 0.050 mmol, 0.50 eq.) a 0.1M copper(II)sulfate solution (1.5 mL, 0.15 mmol, 1.5 eq.) and an 0.1M ascorbic acid solution (0.5 mL, 0.05 mmol, 0.5 eq.) were added in that order. After the last addition the reaction was stirred overnight. After completion of the reaction the mixture was quenched by the addition of water (5 mL) and extracted using ethyl acetate (3 x 50 mL). Drying over sodium sulfate, filtration and evaporation of the solvents gave the crude product that was purified by preparative HPLC (acetonitrile/water (0.1% TFA): gradient 5-95%) to obtain the title compound as a yellow amorphous solid (32 mg, 45%). ¹H NMR (600 MHz, DMSO-d₆, δ [ppm]): two protons are not detectable due to the water peak, 13.88 (s, 1H), 11.05 (s, 1H), 9.56 (t, J = 5.8 Hz, 1H), 9.53 (s, 1H), 8.78 (d, J = 10.1 Hz, 1H), 7.99 (s, 1H), 7.95 (dd, J = 8.0, 1.3 Hz, 1H), 7.57 (dd, J = 8.2, 1H), 7.57 (dd, J = 8.2,1.4 Hz, 1H), 7.53 (d, J = 10.3 Hz, 1H), 7.17 (d, J = 7.3 Hz, 1H), 6.86 (t, J = 8.1 Hz, 1H), 6.74 (s, 1H), 6.18 (d, J = 3.1 Hz, 1H), 6.05 (dd, J = 3.1, 1.3 Hz, 1H), 5.11 (d, J = 10.1 Hz, 1H), 5.04 (dd, J = 12.9, 5.4 Hz, 1H), 4.56 (d, J = 5.6 Hz, 2H), 4.48 (t, J = 5.3 Hz, 2H), 3.79 (t, J = 5.3 Hz, 2H)2H), 3.57 - 3.47 (m, 6H), 2.90 - 2.84 (m, 1H), 2.65 - 2.52 (m, 2H), 2.28 (d, J = 1.0 Hz, 3H), 2.28 - 1.98 (m, 1H), 0.97 (s, 9H); ¹³C NMR (151 MHz, DMSO-d₆, δ [ppm]): 172.7, 170.0, 169.3, 167.1, 166.6, 166.6, 158.1 (d, J = 36.3 Hz), 155.8, 153.7 (d, J = 87.5 Hz), 152.2, 150.3 (d, J = 87.5 Hz), 152.2, 150.3 (d, J = 87.5 Hz) 300.3 Hz), 143.8, 142.8 (d, J = 13.0 Hz), 129.7 (d, J = 39.3 Hz), 125.5, 125.2, 123.5, 118.1, 116.5, 116.5, 114.9, 109.9 (d, J = 22.0 Hz), 109.7, 106.4, 105.6, 105.5, 69.6 (d, J = 22.0 Hz), 68.8 (d, J = 25.0 Hz), 61.9, 49.3, 48.8, 42.2, 40.1, 40.1, 35.7, 34.6, 31.0, 26.5, 22.2, 13.4; ¹⁹F NMR (565 MHz, DMSO- d_6 , δ [ppm]:-75.3; HRMS m/z (ESI+) [Found: 884.3373, C₄₃H₄₇FN₉O₁₁+ requires [M+H]⁺ 884.3301]; HPLC retention time 12.50 min, purity: 96.7%.

 $3-[(2-\{[(R)-2,2-dimethyl-1-(5-methylfuran-2-yl)propyl]amino}-3,4-dioxocyclobut-1-en-1-yl)amino]-$ *N* $-[(1-{2-[2-(2-{2-[4-(2,6-dioxopiperidin-3-yl)phenoxy]acetamido}ethoxy)ethoxy]ethyl}-1$ *H*-1,2,3-triazol-4-yl)methyl]-2-hydroxybenzamide (SLW228, 32)

2-[4-(2,6-Dioxopiperidin-3-yl)phenoxy]acetic acid (SLW138, 30 mg, 0.10 mmol, 1.0 eq.) and 2-[-2-(2-azidoethoxy)ethoxy]ethan-1-amine (19 µL, 0.10 mmol, 1.0 eq.) were dissolved in DMF (5 mL). After the addition of DIPEA (78 µL. 0.40 mmol, 4.0 eg.) and PyBroP (122 mg, 0.480 mmol, 1.20 eq.) the reaction was stirred overnight. After the addition of water (50 mL) the mixture was extracted using ethyl acetate (3 x 50 mL). Drying over sodium sulfate, filtration, evaporation of the solvent and a quick column chromatography using a mixture of cyclohexane and ethyl acetate (1/1 (v/v)) gave the intermediate N-{2-[2-(2-azidoethoxy)ethoxy]ethyl}-2-[4-(2,6-dioxopiperidin-3-yl)phenoxy]acetamide. The intermediate (30 mg, 0.10 mmol, 1.0 eq.) (R)-3-[(2-{[2,2-dimethyl-1-(5-methylfuran-2-yl)propyl]amino}-3,4-dioxocyclobut-1-en-1and yl)amino]-2-hydroxy-*N*-(prop-2-yn-1-yl)benzamide (**SLW007**, 32 mg, 0.10 mmol, 1.0 *eq.*) were dissolved in a mixture of DMF, tert-butanol and water (3 mL, 1/1/1 (v/v)). Tris(benzyltriazolylmethyl)amine (7.4 mg, 0.020 mmol, 0.20 eq.) a 0.1M copper(II)sulfate solution (1.5 mL, 0.15 mmol, 1.5 eq.) and an 0.1M ascorbic acid solution (0.5 mL, 0.05 mmol, 0.5 eq.) were added in that order. After the last addition the reaction was stirred overnight. After completion of the reaction the mixture was quenched by the addition of water (5 mL) and extracted using ethyl acetate (3 x 50 mL). Drying over sodium sulfate, filtration and evaporation of the solvents gave the crude product that was purified by preparative HPLC (acetonitrile/water (0.1% TFA): gradient 5-95%) to obtain the title compound as a white amorphous solid (20 mg, 32%). ¹H NMR (600 MHz, DMSO-*d*₆, δ [ppm]): 13.89 (s, 1H), 10.77 (s, 1H), 9.60 - 9.54 (m, 2H), 8.79 (d, J = 10.1 Hz, 1H), 8.02 - 7.98 (m, 2H), 7.96 (dd, J = 8.1, 1.3 Hz, 1H), 7.58 (dd, J = 8.2, 1.4 Hz, 1H), 7.15 – 7.11 (m, 2H), 6.93 – 6.85 (m, 3H), 6.19 (d, J = 3.1 Hz, 1H), 6.04 (dd, J = 3.1, 1.3 Hz, 1H), 5.11 (d, J = 10.1 Hz, 1H), 4.57 (d, J = 5.6 Hz, 2H), 4.49 (t, J = 5.3 Hz, 2H), 4.45 (s, 2H), 3.82 - 3.74 (m, 2H), 3.51 - 3.49 (m, 2H), 3.47 - 3.44(m, 2H), 3.40 (t, J = 5.9 Hz, 2H), 3.26 (q, J = 5.9 Hz, 2H), 2.67 - 2.61 (m, 1H), 2.49 - 2.43 (m,

1H), 2.28 (s, 3H), 2.17 - 2.11 (m, 1H), 2.02 - 1.97 (m, 1H), 1.04 (d, J = 6.1 Hz, 1H), 0.97 (s, 9H); ¹³C NMR (151 MHz, DMSO- d_6 , δ [ppm]): 184.1, 180.2, 174.3, 173.4, 169.9, 168.6, 167.7, 163.1, 158.0, 156.6, 151.0, 150.7, 143.9, 131.8, 129.5, 127.9, 123.5, 123.5, 120.8, 118.1, 114.5, 113.7, 108.5, 106.3, 69.5, 69.4, 68.8, 68.7, 67.0, 62.0, 60.2, 49.3, 46.5, 40.1, 38.2, 35.7, 34.6, 31.3, 26.2, 25.5, 13.4; HRMS m/z (ESI+) [Found: 855.3671, $C_{43}H_{51}N_8O_{11}$ + requires [M+H]+ 855.3599]; HPLC retention time 12.23 min, purity: 99.2%.

3-[(2-{[(R)-2,2-dimethyl-1-(5-methylfuran-2-yl)propyl]amino}-3,4-dioxocyclobut-1-en-1-yl)amino]-N-{[1-(2-{9-[2-(2,6-dioxopiperidin-3-yl)-6-fluoro-1,3-dioxoisoindolin-5-yl]-3,9-diazaspiro[5.5]undecan-3-yl}-2-oxoethyl)-1H-1,2,3-triazol-4-yl]methyl}-2-hydroxybenzamide (SLW408, 33)

tert-Butyl 9-[2-(2,6-dioxopiperidin-3-yl)-6-fluoro-1,3-dioxoisoindolin-5-yl]-3,9diazaspiro[5.5]undecane-3-carboxylate (20, 50 mg, 0.10 mmol, 1.0 eq.) was dissolved in a mixture of dichloromethane and trifluoroacetic acid (2 mL (1/1 (v/v))) and stirred at room temperature for 2 hours. The solvents were evaporated under reduced pressure to afford the intermediate 2-(2,6-dioxopiperidin-3-yl)-5-fluoro-6-(3,9-diazaspiro[5.5]undecan-3yl)isoindoline-1,3-dione as a trifluoroacetic acid salt. The intermediate (50 mg, 0.10 mmol, 1.0 eq.) and azidoacetic acid (9.0 µL, 0.12 mmol, 1.2 eq.) were dissolved in DMF (5 mL). After the addition of DIPEA (64 µL. 0.36 mmol, 4.0 eq.) and PyBroP (51 mg, 0.11 mmol, 1.2 eq.) the reaction was stirred overnight. After the addition of water (50 mL) the mixture was extracted using ethyl acetate (3 x 50 mL). Drying over sodium sulfate, filtration, evaporation of the solvent and a quick column chromatography using a mixture of cyclohexane and ethyl acetate (1/1 (v/v)) gave the intermediate 5-[9-(2-azidoacetyl)-3,9-diazaspiro[5.5]undecan-3-yl]-2-(2,6dioxopiperidin-3-yl)-6-fluoroisoindoline-1,3-dione. This intermediate (50 mg, 0.10 mmol, 1.0 eq.) and (R)-3-[(2-{[2,2-dimethyl-1-(5-methylfuran-2-yl)propyl]amino}-3,4-dioxocyclobut-1en-1-yl)amino]-2-hydroxy-*N*-(prop-2-yn-1-yl)benzamide (**SLW007**, 43 mg, 0.10 mmol, 1.0 *eq.*) were dissolved in a mixture of DMF, tert-butanol and water (3 mL, 1/1/1 (v/v)). Tris(benzyltriazolylmethyl)amine (5.1 mg, 0.01 mmol, 0.10 eq.) a 0.1M copper(II)sulfate solution (1.5 mL, 0.15 mmol, 1.5 eq.) and an 0.1M ascorbic acid solution (0.5 mL, 0.05 mmol,

0.5 eq.) were added in that order. After the last addition the reaction was stirred overnight. After completion of the reaction the mixture was quenched by the addition of water (5 mL) and extracted using ethyl acetate (3 x 50 mL). Drying over sodium sulfate, filtration and evaporation of the solvents gave the crude product that was purified by preparative HPLC (acetonitrile/water (0.1% TFA): gradient 5-95%) to obtain the title compound as a yellow amorphous solid (42 mg, 46%). ¹H NMR (600 MHz, DMSO- d_6 , δ [ppm]): 13.91 (s, 1H), 11.09 (s, 1H), 9.62 (t, J = 5.5 Hz, 1H), 9.56 (s, 1H), 8.79 (d, J = 10.0 Hz, 1H), 8.00 – 7.95 (m, 1H), 7.92 (s, 1H), 7.69 (d, J = 11.4 Hz, 1H), 7.60 (d, J = 8.2 Hz, 1H), 7.45 (d, J = 7.4 Hz, 1H), 6.89 (t, J = 8.1 Hz, 1H), 6.19 (d, J = 3.1 Hz, 1H), 6.05 (d, J = 3.1 Hz, 1H), 5.42 (s, 2H), 5.14 - 5.06(m, 2H), 4.59 (d, J = 5.5 Hz, 2H), 3.49 - 3.47 (m, 4H), 3.28 - 3.23 (m, 4H), 2.91 - 2.85 (m, 1H),2.63 – 2.50 (m, 2H), 2.28 (s, 3H), 2.06 - 2.01 (m, 1H), 1.66 – 1.59 (m, 4H), 1.57 - 1.54 (m, 2H), 1.48 - 1.46 (m, 2H), 0.97 (s, 9H); ¹³C NMR (151 MHz, DMSO-*d*₆, δ [ppm]): 184.6, 180.7, 173.2, 170.4 (d, J = 12.3 Hz), 169.1, 167.1, 166.7, 166.6, 164.4, 163.6, 158.5, 156.8, 151.6, 151.5, 151.2, 151.2, 146.2 (d, J = 8.8 Hz), 144.3, 129.2, 129.2, 128.4, 125.2, 124.0, 123.3 (d, J =9.8 Hz), 121.2, 118.6, 114.2, 114.1, 112.3 (d, J = 25.3 Hz), 109.0, 106.8, 60.7, 51.1, 49.5, 45.9, 45.8, 40.5, 37.9, 36.1, 35.6, 35.1, 35.1, 34.9, 31.4, 30.0, 26.7, 22.5, 13.8; ¹⁹F NMR (565 MHz, DMSO-d₆, δ [ppm]:-74.8; HRMS m/z (ESI⁺) [Found: 947.3821, C₄₈H₅₂FN₁₀O₁₀⁺ requires [M+H]⁺ 947.3774]; HPLC retention time 12.95 min, purity: 95.7%.

 $3-[(2-\{[(R)-)2,2-dimethyl-1-(5-methylfuran-2-yl)propyl]amino}-3,4-dioxocyclobut-1-en-1-yl)amino]-$ *N* $-{[1-(2-{6-[2-(2,6-dioxopiperidin-3-yl)-6-fluoro-1,3-dioxoisoindolin-5-yl]-2,6-diazaspiro[3.3]heptan-2-yl}-2-oxoethyl)-1$ *H* $-1,2,3-triazol-4-yl]methyl)}2-hydroxybenzamide (SLW409, 34)$

tert-Butyl-6-[2-(2,6-dioxopiperidin-3-yl)-6-fluoro-1,3-dioxoisoindolin-5-yl]-2,6-

diazaspiro[3.3]heptane-2-carboxylate (21, 50 mg, 0.10 mmol, 1.0 eq.) was dissolved in a mixture of dichloromethane and trifluoroacetic acid (2 mL (1/1 (v/v))) and stirred at room temperature for 2 hours. The solvents were evaporated under reduced pressure to afford the intermediate 2-(2,6-dioxopiperidin-3-yl)-5-fluoro-6-(2,6-diazaspiro[3.3]heptan-2-yl)isoindoline-1,3-dione as a trifluoroacetic acid salt. The intermediate (50 mg, 0.10 mmol, 1.0 eq.) and

azidoacetic acid (10 µL, 0.13 mmol, 1.3 eq.) were dissolved in DMF (5 mL). After the addition of DIPEA (71 µL. 0.40 mmol, 4.0 eq.) and PyBroP (57 mg, 0.12 mmol, 1.2 eq.) the reaction was stirred overnight. After the addition of water (50 mL) the mixture was extracted using ethyl acetate (3 x 50 mL). Drying over sodium sulfate, filtration, evaporation of the solvent and a quick column chromatography using a mixture of cyclohexane and ethyl acetate (1/1 (v/v)) gave intermediate 5-[6-(2-azidoacetyl)-2,6-diazaspiro[3.3]heptan-2-yl]-2-(2,6dioxopiperidin-3-yl)-6-fluoroisoindoline-1,3-dione. This intermediate (45 mg, 0.10 mmol, 1.0 eq.) and (R)-3-[(2-{[2,2-dimethyl-1-(5-methylfuran-2-yl)propyl]amino}-3,4-dioxocyclobut-1en-1-yl)amino]-2-hydroxy-N-(prop-2-yn-1-yl)benzamide (**SLW007**, 44 mg, 0.10 mmol, 1.0 eq.) were dissolved in a mixture of DMF, tert-butanol and water (3 mL, 1/1/1 (v/v)). Tris(benzyltriazolylmethyl)amine (5.1 mg, 0.01 mmol, 0.10 eq.) a 0.1M copper(II)sulfate solution (1.5 mL, 0.15 mmol, 1.5 eq.) and an 0.1M ascorbic acid solution (0.5 mL, 0.05 mmol, 0.5 eq.) were added in that order. After the last addition the reaction was stirred overnight. After completion of the reaction the mixture was quenched by the addition of water (5 mL) and extracted using ethyl acetate (3 x 50 mL). Drying over sodium sulfate, filtration and evaporation of the solvents gave the crude product that was purified by preparative HPLC (acetonitrile/water (0.1% TFA): gradient 5-95%) to obtain the title compound as a yellow amorphous solid (35 mg, 41%). ¹H NMR (600 MHz, DMSO-d₆, δ [ppm]): 13.89 (s, 1H), 11.07 (s, 1H), 9.61 (t, J = 5.5 Hz, 1H), 9.56 (s, 1H), 8.79 (d, J = 10.1 Hz, 1H), 8.00 – 7.93 (m, 2H), 7.63 - 7.57 (m, 2H), 6.94 (d, J = 7.6 Hz, 1H), 6.88 (t, J = 8.1 Hz, 1H), 6.19 (d, J = 3.1 Hz, 1H), 6.05 (d, J = 3.0 Hz, 1H), 5.21 - 5.09 (m, 3H), 5.06 (dd, J = 12.9, 5.5 Hz, 1H), 4.59 (d, J = 12.9, 5.5 Hz, 1H), 4.50 (d, J = 12.9, 5.5 Hz, 1H), 4.50 (d, J = 12.9, 5.6 Hz, 2H), 4.41 (s, 2H), 4.39 - 4.29 (m, 4H), 4.14 (s, 2H), 3.02 - 2.84 (m, 1H), 2.64 - 2.52 (m, 2H), 2.29 (s, 3H), 2.04 - 2.00 (m, 1H), 0.98 (s, 9H); 13 C NMR (151 MHz, DMSO- d_6 , δ [ppm]): 184.1, 180.2, 172.7, 169.9 (d, J = 3.8 Hz), 168.6, 166.7, 166.3 (d, J = 2.7 Hz), 165.1, 163.1, 154.7, 153.0, 151.1, 151.0, 150.7, 144.0, 143.7 (d, J = 12.0 Hz), 129.2, 127.9, 124.6, 123.5, 120.8, 119.0 (d, J = 8.3 Hz), 118.2, 113.6, 111.3 (d, J = 22.2 Hz), 108.5, 108.4 (d, J = 6.6 Hz), 106.3, 63.0, 60.2, 60.1, 59.4, 58.1, 49.0 (d, J = 10.0 Hz), 45.8 (d, J = 4.1 Hz), 40.1, 35.7, 34.6, 34.0, 34.0, 30.9, 26.2, 25.9 (d, J = 7.7 Hz), 22.1, 13.4; ¹⁹F NMR (565 MHz, DMSO- d_6 , δ [ppm]:-74.5; HRMS m/z (ESI+) [Found: 891.3164, C₄₄H₄₄FN₁₀O₁₀+ requires [M+H]+ 891.3148]; HPLC retention time 12.37 min, purity: 95.6%.

 $3-[(2-\{[(R)2,2-dimethyl-1-(5-methylfuran-2-yl)propyl]amino}-3,4-dioxocyclobut-1-en-1-yl)amino]-$ *N* $-({1-[2-(4-{1-[2-(2,6-dioxopiperidin-3-yl)-6-fluoro-1,3-dioxoisoindolin-5-yl]piperidin-4-yl}piperazin-1-yl)-2-oxoethyl]-1$ *H* $-1,2,3-triazol-4-yl}methyl)-2-hydroxybenzamide (SLW410, 35)$

tert-Butyl-4-{1-[2-(2,6-dioxopiperidin-3-yl)-6-fluoro-1,3-dioxoisoindolin-5-yl]piperidin-4yl}piperazine-1-carboxylate (22, 50 mg, 0.090 mmol, 1.0 eg.) was dissolved in a mixture of dichloromethane and trifluoroacetic acid (2 mL (1/1 (v/v))) and stirred at room temperature for 2 hours. The solvents were evaporated under reduced pressure to afford the intermediate 2-(2,6-dioxopiperidin-3-yl)-5-fluoro-6-[4-(piperazin-1-yl)piperidin-1-yl]isoindoline-1,3-dione as a trifluoroacetic acid salt. The intermediate (50 mg, 0.090 mmol, 1.0 eg.) and azidoacetic acid (9.0 μL, 0.11 mmol, 1.3 eq.) were dissolved in DMF (5 mL). After the addition of DIPEA (62 μL. 0.35 mmol, 4.0 eq.) and PyBroP (50 mg, 0.11 mmol, 1.2 eq.) the reaction was stirred overnight. After the addition of water (50 mL) the mixture was extracted using ethyl acetate (3 x 50 mL). Drying over sodium sulfate, filtration, evaporation of the solvent and a quick column chromatography using a mixture of cyclohexane and ethyl acetate (1/1 (v/v)) gave the intermediate 5-{4-[4-(2-azidoacetyl)piperazin-1-yl]piperidin-1-yl}-2-(2,6-dioxopiperidin-3-yl)-6fluoroisoindoline-1,3-dione. This intermediate (52 mg, 0.10 mmol, 1.0 eq.) and (R)-3-[(2-{[2,2dimethyl-1-(5-methylfuran-2-yl)propyllamino}-3,4-dioxocyclobut-1-en-1-yl)amino]-2-hydroxy-N-(prop-2-yn-1-yl)benzamide (SLW007, 44 mg, 0.10 mmol, 1.0 eq.) were dissolved in a mixture of DMF, tert-butanol and water (3 mL, 1/1/1 (v/v)). Tris(benzyltriazolylmethyl)amine (5.1 mg, 0.01 mmol, 0.10 eq.) a 0.1M copper(II)sulfate solution (1.5 mL, 0.15 mmol, 1.5 eq.) and an 0.1M ascorbic acid solution (0.5 mL, 0.05 mmol, 0.5 eq.) were added in that order. After the last addition the reaction was stirred overnight. After completion of the reaction the mixture was quenched by the addition of water (5 mL) and extracted using ethyl acetate (3 x 50 mL). Drying over sodium sulfate, filtration and evaporation of the solvents gave the crude product that was purified by preparative HPLC (acetonitrile/water (0.1% TFA): gradient 5-95%) to obtain the title compound as a yellow amorphous solid (20 mg, 21%). ¹H NMR (600 MHz,

DMSO- d_6 , δ [ppm]): 13.88 (s, 1H), 11.10 (s, 1H), 9.63 (t, J = 5.4 Hz, 1H), 9.56 (s, 1H), 8.78 (d, J = 10.1 Hz, 1H), 7.96 (d, J = 7.93 Hz, 1H), 7.88 (s, 1H), 7.76 (d, J = 11.2 Hz, 1H), 7.60 (d, J = 8.2 Hz, 1H), 7.51 (d, J = 7.4 Hz, 1H), 6.90 (t, J = 8.1 Hz, 1H), 6.19 (d, J = 3.1 Hz, 1H), 6.05 (d, J = 3.1 Hz, 1H), 5.66 – 5.40 (m, 2H), 5.14 – 5.08 (m, 2H), 4.60 (d, J = 5.5 Hz, 3H), 3.78 (d, J = 12.2 Hz, 3H), 3.13 – 2.93 (m, 3H), 2.92 - 2.87 (m, 1H), 2.64 – 2.50 (m, 4H), 2.28 (s, 3H), 2.18 - 2.10 (m, 3H), 2.08 – 2.00 (m, 1H), 1.87 – 1.77 (m, 3H), 1.03 - 0.93 (m, 11H); ¹³C NMR (151 MHz, DMSO- d_6 , δ [ppm]): 184.1, 180.2, 172.7, 170.0, 169.8, 168.7, 166.6, 166.1 (d, J = 2.4 Hz), 164.6, 163.1, 158.1, 158.0, 157.8, 156.5, 151.1, 151.0, 150.7, 144.6, 144.0, 128.7, 128.7 (d, J = 2.3 Hz), 127.9, 127.9, 124.6, 123.6, 120.8, 118.2, 114.2, 113.6, 112.0 (d, J = 25.2 Hz), 108.5, 106.3, 62.1, 60.2, 50.5, 49.1, 48.4, 47.9, 44.9, 40.1, 35.7, 34.6, 30.9, 26.2, 26.1, 25.9, 23.6, 22.0, 13.4; ¹⁹F NMR (565 MHz, DMSO- d_6 , δ [ppm]:-73.7; HRMS m/z (ESI+) [Found: 962.3912, $C_{48}H_{53}FN_{11}O_{10}^{+}$ requires [M+H]+ 962.3883]; HPLC retention time 11.28 min, purity: 98.9%.

 $3-[(2-\{[(R)-2,2-dimethyl-1-(5-methylfuran-2-yl)propyl]amino}-3,4-dioxocyclobut-1-en-1-yl)amino]-$ *N* $-[(1-{2-[4-({1-[2-(2,6-dioxopiperidin-3-yl)-6-fluoro-1,3-dioxoisoindolin-5-yl]piperidin-4-yl}methyl)piperazin-1-yl]-2-oxoethyl}-1$ *H*-1,2,3-triazol-4-yl)methyl]-2-hydroxybenzamide (SLW411, 36)

tert-Butyl 4-($\{1-[2-(2,6-dioxopiperidin-3-yl)-6-fluoro-1,3-dioxoisoindolin-5-yl]$ piperidin-4-yl}methyl)piperazine-1-carboxylate (**23**, 50 mg, 0.090 mmol, 1.0 eq.) was dissolved in a mixture of dichloromethane and trifluoroacetic acid (2 mL (1/1 (v/v))) and stirred at room temperature for 2 hours. The solvents were evaporated under reduced pressure to afford the intermediate 2-(2,6-dioxopiperidin-3-yl)-5-fluoro-6-[4-(piperazin-1-ylmethyl)piperidin-1-yl]isoindoline-1,3-dione as a trifluoroacetic acid salt. The intermediate (50 mg, 0.090 mmol, 1.0 eq.) and azidoacetic acid (9.0 μ L, 0.11 mmol, 1.3 eq.) were dissolved in DMF (5 mL). After the addition of DIPEA (62 μ L. 0.35 mmol, 4.0 eq.) and PyBroP (50 mg, 0.11 mmol, 1.2 eq.) the reaction was stirred overnight. After the addition of water (50 mL) the mixture was extracted using ethyl acetate (3 x 50 mL). Drying over sodium sulfate, filtration, evaporation of the solvent and a quick column chromatography using a mixture of cyclohexane and ethyl acetate (1/1

(v/v)) gave the intermediate 5-(4-{[4-(2-azidoacetyl)piperazin-1-yl]methyl}piperidin-1-yl)-2-(2,6-dioxopiperidin-3-yl)-6-fluoroisoindoline-1,3-dione. This intermediate (53 mg, 0.10 mmol, 1.0 eq.) and (R)-3-[(2-{[2,2-dimethyl-1-(5-methylfuran-2-yl)propyl]amino}-3,4-dioxocyclobut-1en-1-yl)amino]-2-hydroxy-N-(prop-2-yn-1-yl)benzamide (**SLW007**, 44 mg, 0.10 mmol, 1.0 eq.) were dissolved in a mixture of DMF, tert-butanol and water (3 mL, 1/1/1 (v/v)). Tris(benzyltriazolylmethyl)amine (5.1 mg, 0.01 mmol, 0.10 eq.) a 0.1M copper(II)sulfate solution (1.5 mL, 0.15 mmol, 1.5 eq.) and an 0.1M ascorbic acid solution (0.5 mL, 0.05 mmol, 0.5 eq.) were added in that order. After the last addition the reaction was stirred overnight. After completion of the reaction the mixture was quenched by the addition of water (5 mL) and extracted using ethyl acetate (3 x 50 mL). Drying over sodium sulfate, filtration and evaporation of the solvents gave the crude product that was purified by preparative HPLC (acetonitrile/water (0.1% TFA): gradient 5-95%) to obtain the title compound as a yellow amorphous solid (18 mg, 19%). ¹H NMR (600 MHz, DMSO-*d*₆, δ [ppm]): 13.90 (s, 1H), 11.10 (s, 1H), 9.63 (t, J = 5.9 Hz, 1H), 9.56 (s, 1H), 8.79 (d, J = 10.1 Hz, 1H), 7.97 (d, J = 8.0 Hz, 1H), 7.91 (s, 1H), 7.82 (d, J = 11.0 Hz, 1H), 7.60 (d, J = 8.0 Hz, 2H), 6.89 (t, J = 8.0 Hz, 1H), 6.19 (d, J = 3.1 Hz, 1H), 6.05 (d, J = 3.1 Hz, 1H), 5.48 (d, J = 16.7 Hz, 1H), 5.40 (d, J = 16.7 Hz, 1H), 5.15 - 5.09 (m, 2H), 4.60 (d, J = 5.5 Hz, 2H), 4.30 (d, J = 13.0 Hz, 1H), 3.93 (d, J =13.3 Hz, 1H), 3.82 - 3.78 (m, 2H), 3.67 - 3.62 (m, 2H), 3.38 - 3.20 (m, 6H), 3.14 - 3.10 (m, 3H), 2.92 -2.86 (m, 1H), 2.71 - 2.66 (m, 1H), 2.64 - 2.50 (m, 3H), 2.17 - 2.10 (m, 1H), 2.08 -2.03 (m, 1H), 1.81 - 1.78 (m, 2H), 1.33 – 1.19 (m, 1H), 1.13 - 1.08 (m, 1H), 0.97 (s, 9H); ¹³C NMR (151 MHz, DMSO- d_6 , δ [ppm]): 184.1, 180.2, 172.7 (d, J = 2.4 Hz), 170.0 (d, J = 2.4 Hz), 169.8, 168.7, 166.5, 166.0, 164.0, 163.1, 158.2, 158.0, 157.8, 156.6, 151.1, 151.0, 150.7, 143.8, 128.6, 127.9, 124.7, 123.6, 120.8, 118.2, 114.5, 113.7, 112.2 (d, J = 25.0 Hz), 108.5, 106.3, 60.5, 60.2, 51.2, 50.6, 49.1, 46.3, 43.7, 41.0, 40.1, 35.7, 34.6, 30.9, 30.1, 29.7, 29.0, 26.2, 26.1, 22.0, 13.4; ¹⁹F NMR (565 MHz, DMSO-d₆, δ [ppm]:-73.8; HRMS m/z (ESI⁺) [Found: 976.4064, C₄₉H₅₅FN₁₁O₁₀+ requires [M+H]+ 976.4039]; HPLC retention time 11.28 min, purity: 98.9%.

 $3-[(2-\{[(R)-2,2-dimethyl-1-(5-methylfuran-2-yl)propyl]amino}-3,4-dioxocyclobut-1-en-1-yl)amino]-$ *N* $-[(1-{2-[(8-{[2-(2,6-dioxopiperidin-3-yl)-6-fluoro-1,3-dioxoisoindolin-5-yl]amino}octyl)amino]-2-oxoethyl}-1$ *H*-1,2,3-triazol-4-yl)methyl]-2-hydroxybenzamide (SLW491, 37)

tert-Butyl (8-{[2-(2,6-dioxopiperidin-3-yl)-6-fluoro-1,3-dioxoisoindolin-5yl]amino}octyl)carbamate (24, 50 mg, 0.10 mmol, 1.0 eq.) was dissolved in a mixture of dichloromethane and trifluoroacetic acid (2 mL (1/1 (v/v))) and stirred at room temperature for 2 hours. The solvents were evaporated under reduced pressure to afford the intermediate 5-[(8-aminooctyl)amino]-2-(2,6-dioxopiperidin-3-yl)-6-fluoroisoindoline-1,3-dione as а trifluoroacetic acid salt. The intermediate (50 mg, 0.10 mmol, 1.0 eq.) and azidoacetic acid (11 µL, 0.13 mmol, 1.3 eq.) were dissolved in DMF (5 mL). After the addition of DIPEA (68 µL. 0.40 mmol, 4.0 eq.) and PyBroP (54 mg, 0.12 mmol, 1.2 eq.) the reaction was stirred overnight. After the addition of water (50 mL) the mixture was extracted using ethyl acetate (3 x 50 mL). Drying over sodium sulfate, filtration, evaporation of the solvent and a quick column chromatography using a mixture of cyclohexane and ethyl acetate (1/1 (v/v)) gave the intermediate 2-azido-N-(8-{[2-(2,6-dioxopiperidin-3-yl)-6-fluoro-1,3-dioxoisoindolin-5yl]amino}octyl)acetamide. This intermediate (53 mg, 0.10 mmol, 1.0 eq.) and (R)-3-[(2-{[2,2dimethyl-1-(5-methylfuran-2-yl)propyl]amino}-3,4-dioxocyclobut-1-en-1-yl)amino]-2-hydroxy-N-(prop-2-yn-1-yl)benzamide (SLW007, 44 mg, 0.10 mmol, 1.0 eq.) were dissolved in a mixture of DMF, tert-butanol and water (3 mL, 1/1/1 (v/v)). Tris(benzyltriazolylmethyl)amine (5.1 mg, 0.01 mmol, 0.10 eq.) a 0.1M copper(II)sulfate solution (1.5 mL, 0.15 mmol, 1.5 eq.) and an 0.1M ascorbic acid solution (0.5 mL, 0.05 mmol, 0.5 eq.) were added in that order. After the last addition the reaction was stirred overnight. After completion of the reaction the mixture was quenched by the addition of water (5 mL) and extracted using ethyl acetate (3 x 50 mL). Drying over sodium sulfate, filtration and evaporation of the solvents gave the crude product that was purified by preparative HPLC (acetonitrile/water (0.1% TFA): gradient 5-95%) to

obtain the title compound as a yellow amorphous solid (30 mg, 55%). ¹H NMR (600 MHz, DMSO- d_6 , δ [ppm]): 13.89 (s, 1H), 11.05 (s, 1H), 9.60 (t, J = 5.8 Hz, 1H), 9.56 (s, 1H), 8.79 (d, J = 10.1 Hz, 1H), 8.26 (t, J = 5.6 Hz, 1H), 7.99 – 7.95 (m, 2H), 7.59 (d, J = 8.1 Hz, 1H), 7.55 (d, J = 10.2 Hz, 1H), 7.09 (d, J = 7.1 Hz, 1H), 6.90 - 6.85 (m, 2H), 6.19 (d, J = 3.1 Hz, 1H), 6.04 (d, J = 3.1 Hz, 1H), 5.12 (d, J = 10.0 Hz, 1H), 5.07 – 5.01 (m, 3H), 4.58 (d, J = 5.5 Hz, 2H), 3.25 (t, J = 7.3 Hz, 3H), 3.09 - 3.07 (m, 2H), 2.90 - 2.84 (m, 1H), 2.62 - 2.54 (m, 2H), 2.28 (s, 3H), 2.03 -2.00 (m, 1H), 1.59 -1.54 (m, 2H), 1.45 - 1.38 (m, 3H), 1.36 - 1.20 (m, 6H), 0.97 (s, 9H); ¹³C NMR (151 MHz, DMSO- d_6 , δ [ppm]): 184.1, 180.2, 172.7, 170.0, 169.9, 168.7, 167.2, 166.6, 166.6, 165.1, 163.1, 158.2, 157.0, 153.8, 152.2, 151.1, 151.0, 150.7, 143.8, 142.8 (d, J = 13.1 Hz), 130.0, 127.9, 124.6, 123.5, 120.8, 118.1, 116.1 (d, J = 8.5 Hz), 113.6, 109.9, 109.8 (d, J = 22.0 Hz), 106.3, 104.9 (d, J = 5.9 Hz), 60.2, 51.6, 48.8, 42.2, 40.1, 38.7, 35.7, 34.6, 31.0, 28.8, 28.7, 28.6, 28.1, 26.3, 26.3, 26.2, 22.2, 13.4; ¹⁹F NMR (565 MHz, DMSO- d_6 , δ [ppm]:-74.7; HRMS m/z (ESI+) [Found: 937.4010, C₄₇H₅₄FN₁₀O₁₀+ requires [M+H]+ 937.3930]; HPLC retention time 12.89 min, purity: 97.1%.

7. Light-Activatable Photochemically Targeting Chimeras (PHOTACs) Enable the Optical Control of Targeted Protein Degradation of HDAC6

Silas L. Wurnig,[‡] Maria Hanl,[‡] Thomas M. Geiger, Shiyang Zhai, Ina Dressel, Dominika E. Pieńkowska, Radosław P. Nowak, Finn K. Hansen*

RSC Med. Chem., 2025, 16, 2452-2459

[‡]These authors contributed equally.

Please refer to Appendix IV for the publication's full text and Supporting Information

7.1 Publication summary

Proteolysis targeting chimeras (PROTACs) have emerged as a groundbreaking approach in targeted protein degradation, a rapidly advancing field with significant potential to selectively eliminate disease-associated proteins. PROTACs are bifunctional molecules consisting of three primary components: a ligand that binds to the protein of interest (POI), an E3 ubiquitin ligase ligand, and a linker that connects these two parts. (225) The PROTAC mode of action works by bringing the POI in close proximity to the E3 ligase, thereby facilitating polyubiquitination of the POI, which marks it for degradation by the proteasome. (225) This mechanism is catalytic, allowing PROTACs to repeatedly induce the degradation of the target protein, offering significant advantages over traditional therapeutic approaches that rely on high-affinity binding to the POI to inhibit its function. (229) (230)

One of the key advantages of PROTACs is that they do not require high affinity binding to the POI. This is because their mode of action is catalytic rather than occupancy-driven. Additionally, the POI ligand in a PROTAC does not need to bind to the active site of a protein. Instead, it can target any pocket on the protein that is accessible to a small molecule, thereby reducing competition with endogenous ligands. This flexibility allows PROTACs to degrade proteins that were previously considered "undruggable" by traditional small molecule inhibitors.

As the first PROTACs have advanced into late-stage clinical trials, interest has grown in expanding the scope of targeted protein degradation. New approaches such as molecular glues, lysosome-targeting chimeras (LYTACs), autophagy-targeting chimeras (AUTACs), and antibody-targeting chimeras (AbTACs) have been developed. (247) These methods aim to

target a wider range of proteins, but are limited in terms of spatial and temporal control. The continuous activity of these degraders, independent of the physiological context, can lead to unwanted toxicity, posing a significant challenge for therapeutic applications.

To address the need for more precise control of protein degradation, light-controllable degraders, specifically photochemically targeting chimeras (PHOTACs), have been developed. PHOTACs are light-activatable PROTACs that incorporate a photoswitch, allowing them to be activated by specific wavelengths of light. In their inactive state, PHOTACs prevent the formation of the ternary complex necessary for degradation. Upon irradiation, the photoswitch changes its conformation, allowing the ternary complex to form, leading to polyubiquitination and subsequent degradation of the POI. The photoswitch also allows for the reversible inactivation of the PHOTAC, providing unprecedented spatiotemporal control of protein degradation, potentially minimizing off-target effects and toxicity. (254) (255) (256)

In this work, a set of three PHOTACs was synthesized for the targeted degradation of histone deacetylase 6 (HDAC6). These PHOTACs were designed based on the previously developed HDAC6 degrader **A6**. The design involved replacing the thalidomide moiety in **A6** with a photoswitchable lenalidomide-based cereblon (CRBN) recruiter. The synthesis of the photoswitch was achieved starting from lenalidomide. The diazotation and reaction with 2,6-dimethoxyphenol yielded the intermediate **3**. Subsequent reaction with *tert*-butyl bromoacetate resulted in the photoswitchable CRBN ligand **4**. The HDAC ligand was synthesized separately on a solid support following a previously published procedure The diversification of the linker length was introduced in the final steps to create three different PHOTACs (**11-13**).

The photochemical properties of the synthesized PHOTACs were evaluated to confirm their ability to switch between the *trans*- and *cis*-states. The UV spectra of the PHOTACs were measured before and after illumination with light of a specific wavelength at room temperature and at the physiological temperature of 37 °C, confirming their ability to switch states independent of temperature. The half-life of the *cis*-state PHOTACs was measured to determine the stability of the PHOTACs, with **12** having the longest half-life of 10.30 hours. Additionally, the photochemical stability of the PHOTACs was tested by rapidly switching them between the *cis*- and *trans*-states, with all three PHOTACs demonstrating stability over 20 switching cycles.

The ability of the PHOTACs to degrade HDAC6 was evaluated in MM.1S multiple myeloma cells and by immunoblot analysis. PHOTAC **11** induced HDAC6 degradation under both light and dark conditions, likely due to its long and flexible linker. In contrast, PHOTAC **13**, which

lacked a linker, failed to degrade HDAC6 under both condition. Notably, PHOTAC **12**, which contains a short γ-aminobutyric acid linker, selectively degraded HDAC6 upon light activation, suggesting that its *cis*-state is an active degrader while the *trans*-state is inactive.

To further understand the differential activity of PHOTAC **12** in its *cis*- and *trans*-states, ternary complex modeling studies were conducted. These studies revealed that in the *cis*-state, PHOTAC **12** forms key interactions with CRBN that are necessary for its recruitment and subsequent degradation of HDAC6. However, in the *trans*-state, due to a conformational change in the linker, these interactions are reduced, explaining the lower activity of the *trans*-state.

In conclusion, the successful synthesis and characterization of a series of PHOTACs targeting HDAC6 were performed. Physicochemical and biological assays were conducted to demonstrate their potential use in therapeutic applications where spatiotemporal control is critical. The results highlight the importance of linker design and the role of photochemical properties in determining the efficacy of PHOTACs, paving the way for further exploration of light-activatable degraders in biomedical research. Overall, the development of PHOTAC 12 represents a significant advancement in the field of targeted protein degradation of HDAC6, allowing precise control of the degradation process through light activation.

7.2 Author contributions

Within this project, I synthesized and characterized compounds **1-13** referring to the numbering within the publication. I performed all the photophysical assays, created Figures **1-3** and Scheme **1**. Additionally, I contributed to the main text and the Supporting Information.

8. Summary and perspective

The main aim of this work was to develop of novel intracellular allosteric antagonists and fluorescent probes for the chemokine receptors CXCR1, CXCR2, CCR6, and CCR7. The focus was set on elucidating the effect of side chain modifications on the published antagonists navarixin and Cmpd2105 and to explore the structure-activity relationships (SARs) by synthesizing focused libraries of squaramide- and thiadiazoledioxide-based analogs.

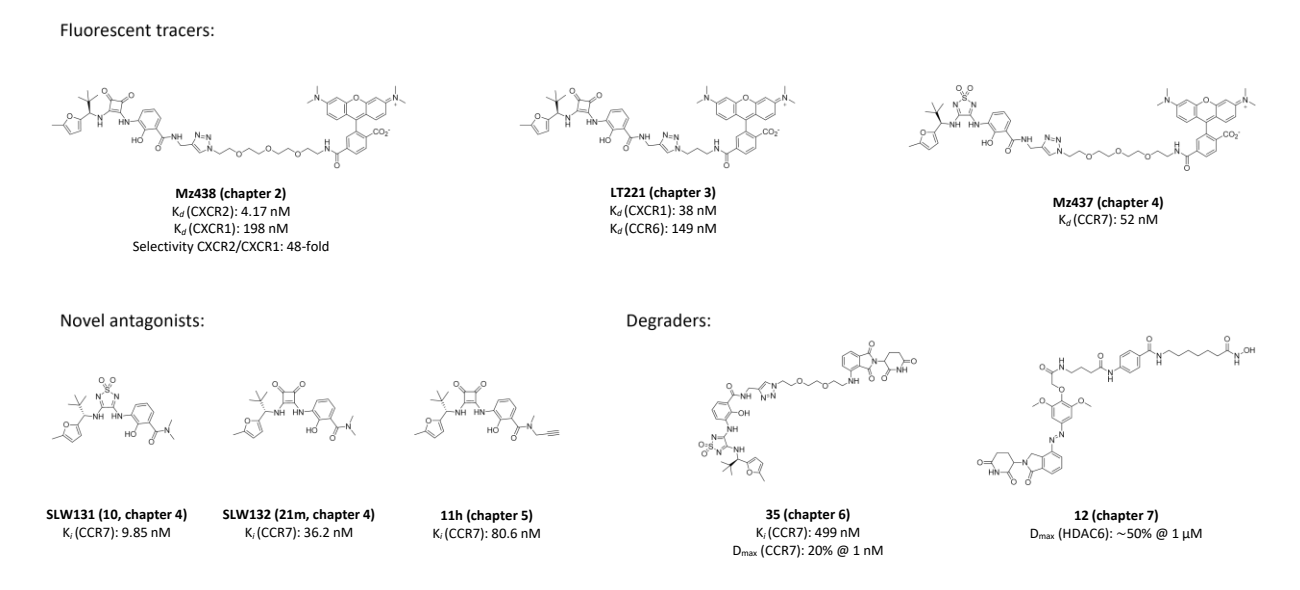


Figure 28. Overview of the most important compounds from chapters 2-7.

The first chapter focused on the chemokine receptor CXCR2. Previous CXCR2 antagonists, such as navarixin, showed promise but failed in clinical trials, highlighting the need for new approaches to develop effective CXCR2 inhibitors. (204) (258) Therefore, a novel fluorescent tracer for CXCR2 was designed to specifically bind to the intracellular allosteric binding site (IABS) of the receptor. This tracer (Mz438), derived from the structure of a known CXCR2 ligand, was synthesized via a multi-step process incorporating a TAMRA-based fluorophore, enabling its application in NanoBRET assays for real-time monitoring of ligand–receptor interactions in live cells. The fluorescent tracer showed a high binding affinity to CXCR2 with good preference over CXCR1. The suitability of this tracer for membrane-based and cellular applications was then demonstrated by displacement assays and live-cell staining. Overall, this research provided a new tool for studying CXCR2 and developing new antagonists targeting its IABS, with potential applications in high-throughput drug screening and live-cell imaging.

The next chapter focused on the use of the synthesized fluorescent tracer LT221 as a fluorescent probe for the chemokine receptors CXCR1 and CCR6. Although LT221 displayed

a greater affinity for CXCR2 than for CXCR1 and CCR6, it was shown that the tracer could be used for both membrane-based and live-cell displacement assays targeting CXCR1 and CCR6. The assay results indicated that the published ligands danirixin and cmpd24 bind to the IABS of CXCR1. In addition, PF-07054984 was shown to bind to the IABS of CCR6. Furthermore, a series of ten new potential allosteric antagonists for CXCR1 and CCR6 featuring structural modifications at the chiral carbon atom were synthesized to investigate the SAR of this position. The results revealed that a bulky hydrophobic group, such as a *tert*-butyl substituent, is critical for enhancing CCR6 affinity. Docking studies supported these insights, highlighting favorable binding interactions for bulkier residues. Cellular assays further validated these findings, identifying compound SLW131 (10) as a novel and promising CCR6 antagonist, positioning it as an excellent candidate for further optimization studies.

The third chapter explored the intracellular allosteric binding site of the CCR7 receptor, a key target in immune response modulation. (143) (144) To this end, a fluorescent probe based on a Cmp2105-derived CCR7 antagonist was developed. This tracer was found to be effective in both cell-free and cellular NanoBRET-based binding studies, as well as in live-cell imaging applications. The results of these assays validated the intracellular allosteric binding of both Cmp2105 and its desmethyl derivative SLW131 (10) at CCR7. Docking studies revealed that the methyl group of Cmp2105 displaces an energetically favorable water molecule, explaining the lower affinity of Cmp2105 compared to SLW131 (10). To further elucidate the SARs, a series of five thiadiazoledioxide- and thirteen squaramide-based antagonists were synthesized. Using the newly developed NanoBRET assay, the two antagonists SLW131 (10) and SLW132 (21m) were identified as the most promising CCR7 ligands, demonstrating improved binding affinity compared to the prior gold standard intracellular CCR7 ligand Cmpd2105. The improved antagonistic properties of these compounds was further demonstrated in functional assays. These newly identified antagonists are promising lead compounds for future studies of CCR7 pharmacology and function in both recombinant and primary cell settings. It is anticipated that these molecular tools will significantly advance our understanding of CCR7 functionality.

The next project focused on expanding the SARs of CCR7 ligands. For this purpose, twelve new compounds were designed and synthesized. Building on the SAR data from chapter 4, the steric influence of the alkyl chain at the chiral carbon on CCR7 affinity was explored by incorporating different residues at the chiral center. NanoBRET-based displacement assays showed that shorter alkyl chains such as methyl and ethyl had lower affinity for CCR7 compared to bulkier chains such as isopropyl and *tert*-butyl, confirming the consistency of the SAR data obtained in the last chapter across both the squaramide and thiadiazole-1,1-dioxide

scaffolds. Additionally, replacing the secondary amides with tertiary amides in the benzamide moiety resulted in increased affinity for CCR7. Based on these findings, future optimization studies of novel CCR7 antagonists should focus on incorporating different tertiary amides, such as cyclic amides or tertiary amides with two different carbon chains, to further explore the SARs of the benzamide region.

In the next chapter, two sets of potential CCR7-targeting proteolysis targeting chimeras (PROTACs) were synthesized. The first set employed a consistent PEG-based linker while varying the chemokine receptor and CRBN ligands. The second set focused on linker diversification, a key factor in the formation of an effective POI:PROTAC:E3 ligase ternary complex. Although many of the synthesized PROTACs exhibited promising affinities for the chemokine receptors CXCR1, CXCR2, and CCR6, none showed sufficient affinity for CCR7. Both the synthesized PROTACs and two benchmark degraders achieved a maximum degradation of approximately 20% for CCR7 and CXCR2, suggesting that CRBN-recruiting PROTACs may not be the most effective option for degrading chemokine receptors. Future studies should test the degradation efficiency of the synthesized PROTACs on CCR6 and CXCR1 to determine if higher levels of degradation can be achieved for these receptors. Additionally, the exploration of novel degradation technologies such as lysosomal-targeting chimeras (LYTACs) or antibody-based chimeras (AbTACs) could potentially enhance the degradation of chemokine receptors.

The final chapter explored the use of a photoswitchable moiety in PROTACs. Since degradation of chemokine receptors proved to be unsuitable, histone deacetylase 6 (HDAC6) was used as an already established target for PROTACs. In this chapter a series of three photochemically targeting chimeras (PHOTACs), each with a different in linker length were designed and developed to degrade HDAC6 under precise control by light activation. The design of the PHOTACs was based on a photoswitch developed by the Trauner group and the HDAC6 degrader **A6** developed in our group. (255) (256) The three synthesized PHOTACs were then tested for their photophysical properties. All PHOTACs showed a switch from the *trans*- to the *cis*-isomer upon exposure to light of 390 nm wavelength with half-lifes ranging from 4 to approximately 10 hours. Additionally, all three PHOTACs showed photochemical stability after 20 switching cycles. Among them, PHOTAC **12** with a short γ-aminobutyric acid linker demonstrated selective HDAC6 degradation upon light activation, with its *cis*-state being active and the *trans*-state inactive, while PHOTAC **11** also showed degradation in the dark as well and PHOTAC **13** demonstrated inferior degradation compared to PHOTAC **12**. These results underscore the critical role of linker design and photochemical properties in generating

efficient PHOTACs and highlight their potential for therapeutic applications requiring spatiotemporal control.

In summary, in this work several fluorescent probes were developed to enable NanoBRET-based displacement assays for the profiling of intracellular allosteric antagonists targeting the chemokine receptors CXCR1, CXCR2, CCR6, and CCR7. In addition, novel hit compounds for CCR6 and CCR7 were identified. Based on the SAR data generated in this work, the development of novel improved CCR7 antagonists should focus on squaramide- or thiadiazoledioxide-based antagonists bearing the *tert*-butyl moiety at the chiral carbon atom and tertiary amides at the benzamide moiety. For the development of targeted protein degraders for chemokine receptors, CRBN-based PROTACs have been shown to achieve limited degradation. Therefore, future efforts should focus on novel targeted protein degradation methods such as LYTACs or AbTACs to demonstrate that chemokine receptor degradation is achievable. Furthermore, developing selective degraders that recruit alternative E3 ligases for the targeted degradation of specific chemokine receptors, especially those achieving efficient CCR7 degradation, should be prioritized in future research efforts.

References

- 1. Sriram, K. and Insel, P. A. G Protein-Coupled Receptors as Targets for Approved Drugs: How Many Targets And How Many Drugs? *Mol. Pharmacol.* **2018**, 93(4), 251-258.
- 2. Ma, F. and Zemmel, R. Value of Novelty? Nat. Rev. Drug Discov. 2002, 1, 571-572.
- 3. Yang, D., Zhou, Q., Labroska, V., Qin, S., Darbalaei, S., Wu, Y., Yuliantie, E., Xie, L., Tao, H., Cheng, J., Liu, Q., Zhao, S., Shui, W. and Wang, M.-W. G protein-coupled receptors: structure- and function-based drug discovery. *Sig. Transduct. Target. Ther.* **2020**, 6(1), 1-27.
- 4. Cheng, L., Xia, F., Li, Z., Shen, C., Yang, Z., Hou, H., Sun, S., Feng, Y., Yong, X., Tian, X., Qin, X., Yan, W. and Shao, Z. Structure, function and drug discovery of GPRC signaling. *Mol. Biomed.* **2023**, 4(46), 1-39.
- 5. Kobilka, B. G Protein Coupled Receptor Structure and Activation. *Biochim. Biophys. Acta.* **2007**, 1768(4), 794-807.
- 6. Moro, S., Deflorian, F., Spalluto, G., Cacciari, B., Kim, S.-Y. and Jacobson, K. A. Demystifying the three dimensional structure of G protein coupled receptors (GPCRs) with the aid of molecular modeling. *Chem. Comm.* **2003**, 2949–2956.
- 7. Jones, A. J. Y., Gabriel, F., Tandale A. and Nietlispach, D. Structure and Dynamics of GPCRs in Lipid Membranes: Physical Principles and Experimental Approaches. *Molecules* **2020**, 25(20), 1-39.
- 8. Calebiro, D., Koszegi, Z., Lanoiselée, Y., Miljus, T. and O'Brian, S. G Protein-Coupled Receptor-G Protein Interactions: A Single-Molecule Perspective. *Physiol. Rev.* **2021**, 101(3), 857-906.
- 9. Weis, W. I. and Kobilka, B. A. The Molecular basis of G Protein-Coupled Receptor Activation. *Annu. Rev. Biochem.* **2018**, 87, 897-919.
- 10. Syrovatkina, V., Alegre, K. O. und Dey, R. and Huang, X.-Y. Regulation, signaling, and physiological functions of G-proteins. *J. Mol. Biol.* **2016**, 428(19), 3850-3868.
- 11. Hepler, J. R. and Gilman, A. G. G proteins. *TIBS.* **1992**, 17(10), 383-387.
- 12. Kamato, D.; Thach, L.; Bernard, R.; Chan, V.; Zheng, W.; Kaur, H.; Brimble, M.; Osman, N. and Little, P. J. Structure, function, pharmacology, and therapeutic potential of the G protein Gaq/11. *Front. Cardiovasc. Med.* **2015**, 2(14), 1-11.
- 13. Flock, T.; Hauser, A. E.; Lund, N.; Gloriam, D. E.; Balaji, S. and Babu, M. M. Selectivity determinants of GPCR-G protein binding. *Nature* **2017**, 545(7654), 317-322.
- 14. Xiao, R.P. Beta-adrenergic signaling in the heart: dual coupling of the Beta2-adrenergic receptor to Gs and Gi proteins. *Sci. STKE.* **2001**, 104, re15.

- 15. Voss, J.H.; Mahardhika, A. B.; Inoue, A.; Müller, C. E. Agonist-dependent coupling of the promiscuous adenosine A2B receptor to Ga protein subunits. *ACS Pharmacol. Transl. Sci.* **2022**, 5(5), 373-386.
- 16. Milligan, G. and Kostenis, E. Heterotrimeric G-proteins: a short history. *Br. J. Pharmacol.* **2006**, 147, 62(3), 46-55.
- 17. Downes, G. B. and Gautam, N. The G protein subunit gene families. *Genomics* **1999**; 62(3), 544-552.
- 18. Hilger, D., Masureel, M. und Kobilka, B. K. Structure and dynamics of GPCR signaling complexes. *Nat. Struct. Mol. Biol.* **2018**, 25(1), 4-12.
- 19. Katritch, V., Cherezov, V. and Stevens, R. C. Diversity and modularity of G protein-coupled receptor structures. *Trends Pharmacol. Sci.* **2012**, 33(1), 17-27.
- 20. Hu, G.-M., Mai, T.-L. and Chen, C.-M. Visualizing the GPCR Network: Classification and Evolution. *Sci. Rep.* **2017**, 7(1), 15495.
- 21. Schiöth, H. B. and Fredriksson, R. The GRAFS classiWcation system of G-protein coupled receptors in comparative perspective. *Gen. Comp. Endocrinol.* **2005**, 142(1-2), 94-101.
- 22. Isberg, V.; de Graaf, C.; Bortolato, A.; Cherezov, V.; Katritch, V.; Marshall, F. H.; Mordalski, S.; Pin, J.-P.; Stevens, R. C.; Vriend, G. and Gloriam, D. E. Generic GPCR Residue Numbers Aligning Topology Maps Minding The Gaps. *Trends Pharmacol. Sci.* **2015**, 36(1), 22-31.
- 23. Wright, S. C. and Bouvier, M. Illuminating the complexity of GPCR pathway selectivity advances in biosensensor development. *Curr. Opin. Struct. Biol.* **2021**, 69, 142-149.
- 24. Smith, J. S., Lefkowitz, R. J. and Rajagopal, S. Biased signalling: from simple switches to allosteric microprocessors. *Nat. Rev. Drug Discov.* **2018**, 17(4), 243-260.
- 25. Hinz, S.; Navarro, G.; Borroto-Escuela, D.; Seibt, B. F.; Ammon, Y.-C.; Filippo, E.; Danish, A.; Lacher, S. K.; Červinková, B.; Rafehi, M.; Fuxe, K.; Schiedel, A. C.; Franco, R. and Müller, C. E. Adenosine A2A receptor ligand recognition and signaling is blocked by A2B receptors. *Oncotarget*. **2018**, 9(17), 13593-13611.
- 26. Calebiro, D. and Koszegi, Z. The subcellular dynamics of GPCR signaling. *Mol. Cell. Endocrinol.* **2019**, 483, 24-30.
- 27. Gao, Z.-G., Inoue, A. and Jacobson, K. A. On the G protein-coupling selectivity of the native A2B adenosine receptor. *Biochem. Pharmacol.* **2018**, 151, 201-213.
- 28. Sriram, K. and Insel, P. A. G protein-coupled receptors as targets for approved drugs. How many targets and how many drugs? *Mol. Pharmacol.* **2018**, 93(4), 251-258.
- 29. Singh, A., Nunes, J. and Ateeq, B. Role and therapeutic potential of G-protein coupled receptors in breast cancer progression and metastases. *Eur. J. Pharmacol.* **2015**, 763, 178-183.

- 30. Katritch, V., Cherezov, V. and Stevens, R. C. Structure-function of the G protein-coupled receptor superfamily. *Annu. Rev. Pharmacol. Toxicol.* **2013**, 53, 531-556.
- 31. Latorraca, N. R., Venkatakrishnan, A. J. and Dror, R. O. GPCR dynamics: Structures in motion. *Chem. Rev.* **2017**, 117(1), 139-155.
- 32. García-Nafría, J.; Lee, Y.; Bai, X.; Carpenter, B. and Tate, C. G. Cryo-EM structure of the adenosine A2A receptor coupled to an engineered heterotrimeric G protein. *eLife* **2018**, 7, e35946.
- 33. Glukhova, A.; Draper-Joyce, C. J.; Sunahara, R. K.; Christopoulos, A.; Wooten, D. and Sexton, P. M. Rules of Engagement: GPCRs and G Proteins. *ACS Pharmacol. Transl. Sci.* **2018**, 1(2), 73-83.
- 34. Zhou, Q.; Yang, D.; Wu, M.; Guo, Y.; Guo, W.; Zhong, L.; Cai, X.; Dai, A.; Jang, W.; Shakhnovich, E. I.; Liu, Z.-J.; Stevens, R. C.; Lambert, N. A.; Babu, M. M.; Wang, M.-W. and Zhao, S. Common activation mechanism of class A GPCRs. *eLife* **2019**, *8*, e50279.
- 35. Filipek, S. Molecular switches in GPCRs. Curr. Opin. Struct. Biol. 2019, 55, 114-120.
- 36. Katritch, V.; Fenalti, G.; Abola, E. E.; Roth, B. L.; Cherezov, V. and Stevens, R. C. Allosteric sodium in class A GPCR signaling. *Trends Biochem. Sci.* **2014**, 39(5), 233-244.
- 37. Huang, H. and Tao, Y.-X. Function of the DRY motif and intracellular loop 2 of human melanocortin 3 receptor. *J. Mol. Endocrinol.* **2014**, 53(3), 319-330.
- 38. Fritze, O.; Filipek, S.; Kuksa, V.; Palczewski, K.; Hofmann, K. P. and Ernst, O. P. Role of the conserved NPxxY(x)5,6F motif in the rhodopsin ground state and during activation. *Proc. Natl. Acad. Sci. USA.* **2003**, 100(5), 2290-2295.
- 39. Schneider, E. H.; Schnell, D.; Strasser, A.; Dove, S. and Seifert, R. Impact of the DRY motif and the missing "ionic lock" on constitutive activity and G-protein coupling of the human histamine H4 receptor. *J. Pharmacol. Exp. Ther.* **2010**, 333(2), 382-392.
- 40. Flock, T.; Ravarani, C. N. J.; Sun, D.; Venkatakrishnan, A. J.; Kayikci, M.; Tate, C. G.; Veprintsev, D. B. and Babu, M. M. Universal allosteric mechanism for $G\alpha$ activation by GPCRs. *Nature* **2015**, 524(7564), 173-179.
- 41. Sun, D.; Flock, T.; Deupi, X.; Maeda, S.; Matkovic, M.; Mendieta, S.; Mayer, D.; Dawson, R.; Schertler, G. F. X.; Madan Babu, M. and Veprintsev, D. B. Probing Gαi1 protein activation at single-amino acid resolution. *Nat. Struct. Mol. Biol.* **2015**, 22(9), 686-694.
- 42. Chung, Y. K. and Wong, Y. H. Re-examining the 'Dissociation Model' of G protein activation from the perspective of Gβγ signaling. *FEBS J.* **2021**, 288(8), 2490-2501.
- 43. Hamm, H. E. How activated receptors couple to G proteins. *Proc. Natl. Acad. Sci. USA.* **2001**, 98(9), 4819-4821.

- 44. Park, P. S.-H.; Lodowski, D. T. and Palczewski, K. Activation of G Protein—Coupled Receptors: Beyond Two-State Models and Tertiary Conformational Changes. *Annu. Rev. Pharmacol. Toxicol.* **2008**, 48, 107-141.
- 45. Wettschureck, N. and Offermanns, S. Mammalian G Proteins and Their Cell Type Specific Functions. *Physiol. Rev.* **2005**, 85(4), 1159-1204.
- 46. Wright, P. T.; Schobesberger, S. and Gorelik, J. Studying GPCR/cAMP pharmacology from the perspective of cellular structure. *Front. Pharmacol.* **2015**, 6(148), 1-10.
- 47. Syrovatkina, V.; Alegre, K. O. and Huang, X.-Y. Regulation, Signaling, and Physiological Functions of G-Proteins. *J. Mol. Biol.* **2016**, 428(19), 3850-3868.
- 48. Sassone-Corsi, P. The Cyclic AMP Pathway. Cold Spring Harb. Perspect. Biol. 2012, 4(12), 1-3.
- 49. Mizuno, N. and Itoh, H. Functions and regulatory mechanisms of Gq-signaling pathways . *Neurosignals* **2009**, 17(1), 42-54.
- 50. Kamato, D.; Thach, L.; Bernard, R.; Chan, V.; Zheng, W.; Kaur, H.; Brimble, M.; Osman, N. and Little, P. J. Structure, function, pharmacology, and therapeutic potential of the G protein, $G\alpha/q$,11. *Front. Cardiovasc. Med.* **2015**, 2(14), 1-11.
- 51. Guo, P.; Tai, Y.; Wang, M.; Sun, H.; Zhang, L.; Wei, W.; Xiang, Y. K. and Wang, Q. Gα12 and Gα13: Versatility in Physiology and Pathology. *Front. Cell. Dev. Biol.* **2022**, 10, 1-19.
- 52. Yang, Y. M.; Kuen, D.-S.; Chung, Y.; Kurose, H. and Kim, S. G. $G\alpha 12/13$ signaling in metabolic diseases. *Exp. Mol. Med.* **2020**, 52, 896-910.
- 53. Smrcka, A. V. G protein βγ subunits: Central mediators of G protein-coupled receptor signaling. *Cell Mol. Life Sci.* **2008**, 65(14), 2191-2214.
- 54. Gutkind, J. S. The Pathways Connecting G Protein-coupled Receptors to the Nucleus through Divergent Mitogen-activated Protein Kinase Cascades. *J. Biol. Chem.* **1998**, 273(4), 1839-1842.
- 55. Sulon, S. M. and Benovic, J. L. Targeting G protein-coupled receptor kinases (GRKs) to G protein-coupled receptors. *Curr. Opin. Endocr. Metab. Res.* **2021**, 16, 56-65.
- 56. Ribas, C.; Penela, P.; Murga, C.; Salcedo, A.; García-Hoz, C.; Jurado-Pueyo, M.; Aymerich, I. and Mayor Jr., F. The G protein-coupled receptor kinase (GRK) interactome: Role of GRKs in GPCR regulation and signaling. *BBA* **2007**, 1768(4), 913-922.
- 57. Premont, R. T. und Inglese, J. and Lefkowitz, R. J. Protein kinases that phosphorylate activated G protein-coupled receptors. *FASEB J.* **1995**, 9(2), 175-182.
- 58. Latorraca, N. R.; Masureel, M.; Hollingsworth, S. A.; Heydenreich, F. M.; Suomivuori, C.-M.; Brinton, C.; Townshend, R. J. L.; Bouvier, M.; Kobilka, B. K. and Dror, R. O. How GPCR Phosphorylation Patterns Orchestrate Arrestin-Mediated Signaling. *Cell* **2020**, 183(7), 1813-1825.

- 59. Shukla, A. K. and Dwivedi-Agnihotri, H. Structure and function of β -arrestins, their emerging role in breast cancer, and potential opportunities for therapeutic manipulation. *Adv. Cancer Res.* **2020**, 145, 139-156.
- 60. Gurevich, V. V. and Gurevich, E. V. GPCR Signaling Regulation: The Role of GRKs and Arrestins. *Front. Pharmacol.* **2019**, 10, 1-11.
- 61. Zhuo, Y.; Crecelius, J. M. and Marchese, A. G protein—coupled receptor kinase phosphorylation of distal C-tail sites specifies βarrestin1-mediated signaling by chemokine receptor CXCR4. *J. Biol. Chem.* **2022**, 298(9), 1-13.
- 62. Tian, X.; Kang, D. S. and Benovic, J. L. β -arrestins and G Protein-Coupled Receptor Trafficking. *Handb. Exp. Pharmacol.* **2014**, 219, 173-186.
- 63. Sprang, S. R. Activation of G proteins by GTP and the mechanism of $G\alpha$ -catalyzed GTP hydrolysis. *Biopolymers* **2016**, 105(8), 449-462.
- 64. Lambert, N. A., Johnston, C. A.; Cappel, S. D. and Siderovski, D. P. Regulators of G-protein Signaling accelerate GPCR signaling kinetics and govern sensitivity solely by accelerating GTPase activity. *Proc. Natl. Acad. Sci. USA.* **2010**, 109(6), 7066-7071.
- 65. Coleman, B. D.; Marivin, A.; Parag-Sharma, K.; DiGiacomo, V.; Kim, S.; Pepper, J. S.; Casler, J.; Nguyen, L. T.; Koelle, M. R. and Garcia-Marcos, M. Evolutionary Conservation of a GPCR-Independent Mechanism of Trimeric G Protein Activation. *Mol. Biol. Evol.* **2016**, 33(3), 820-837.
- 66. Allen, S. J.; Crown, S. E. and Handel, T. M. Chemokine: Receptor Structure, Interactions and Antagonism. *Annu. Rev. Immunol.* **2007**, 25, 787-820.
- 67. Griffith, J. W.; Sokol, C. L. and Luster, A. D. Annu. Rev. Immunol. 2014, 32, 659-702.
- 68. Kulkarni, N.; Pathak, M. and Lal, G. Role of chemokine receptors and intestinal epithelial cells in the mucosal inflammation and tolerance. *J. Leukoc. Biol.* **2017**, 101(2), 377-394.
- 69. Beck, L. A.; Tancowny, B.; Brummet, M. E.; Asaki, S. Y.; Curry, S. L.; Penno, M. B.; Foster, M.; Bahl, A. and Stellato, C. Functional analysis of the chemokine receptor CCR3 on airway epithelial cells. *J. Immunol.* 2006, 177(5), 3344-3354.
- 70. López-Cotarelo, P.; Gómez-Moreira, C.; Criado-García, O.; Sánchez, L. and Rodríguez_Fernández, J. L Beyond chemoattraction: multifunctionality of chemokine receptors in leukocytes. *Trends Immunol.* **2017**, 38(12), 927-941.
- 71. Torres-Palomino, D. C. and Marti, L. C. Chemokines and immunity. *Einstein* **2015**, 13(3), 469-473.
- 72. Sokol, C. L. and Luster, A. D. The Chemokine System in Innate Immunity . *Cold Spring Harb. Perspect. Biol.* **2015**, 7(5), a016303.
- 73. Esche, C.; Stellato, C. and Beck, L. A. Chemokines: Key Players in Innate and Adaptive Immunity. *JID* **2005**, 125(4), 615-628.

- 74. Williams, J. L.; Holman, D. W. and Klein, R. S. Chemokines in the balance: maintenance of homeostasis and protection at CNS barriers. *Front. Cell. Neurosci.* **2014**, 8, 154.
- 75. Koelink, P. J.; Overbeek, S. A.; Braber, S.; de Kruijf, P.; Folkerts, G.; Smit, M. J. and Kraneveld, A. D. Targeting chemokine receptors in chronic inflammatory diseases: An extensive review. *Pharmacol. Ther.* **2012**, 133(1), 1-18.
- 76. Poeta, V. M., Massara, M. und Capucetti, A. and Bonecchi, R. Chemokines and Chemokine Receptors: New Targets for Cancer Immunotherapy. *Front. Immunol.* **2019**, 10, 1-10.
- 77. Liu, C.; Zhang, X.; Xiang, Y.; Qu, X.; Liu, H.; Liu, C.; Tan, M.; Jiang, J. and Qin, X. Role of epithelial chemokines in the pathogenesis of airway inflammation in asthma (Review). *Mol. Med. Rep.* **2018**, 17(5), 6935-6941.
- 78. Zdanowska, N., Kasprowicz-Furmanczyk, M.; Placek, W. and Owczarczyk-Saczonek, A. The Role of Chemokines in Psoriasis. An Overview. *Medicina* **2021**, 57(8), 754.
- 79. Lederman, M. M., Penn-Nicholson, A.; Cho, M. and Mosier, D. Biology of CCR5 and Its Role in HIV Infection and Treatment. *JAMA* **2006**, 296(7), 815-826.
- 80. Lowoski, D. T. and Palczewski, K. Chemokine receptors and other GPCRs. *Curr. Opin. HIV AIDS.* **2009**, 4(2), 88-95.
- 81. Zhang, D.; Zhao, Q. and Wu, B. Structural Studies of G Protein-Coupled Receptors. *Mol. Cells.* **2015**, 38(10), 836-842.
- 82. Arimont, M.; Sun, S.-L.; Leurs, R.; Smit, M.; de Esch, I. J. P. and de Graaf, C. Structural Analysis of Chemokine Receptor–Ligand Interactions. *J. Med. Chem.* **2017**, 60(12), 4735-4779.
- 83. Hughes, C. E. and Nibbs, R. J. B. A guide to chemokines and their receptors. *FEBS J.* **2018**, 285(16), 2944-2971.
- 84. Zlotnik, A. and Yoshie, O. Chemokines: A New Classification System and Their Role in Immunity. *Immunity* **2000**, 12(2), 121-127.
- 85. Rajagopalan, L. and Rajarathnam, K. Structural Basis of Chemokine Receptor Function—A Model for Binding Affinity and Ligand Selectivity. *Biosci. Rep.* **2006**, 26(5), 325-339.
- 86. Mantovani, A.; Locati, M.; Vecchi, A.; Sozzani, S. and Allavena, P. Decoy receptors: a strategy to regulate inflammatory cytokines and chemokines. *Trends Immunol.* **2001**, 22(6), 328-336.
- 87. Bonecchi, R.; Savino, B.; Borroni, E. M.; Mantovani, A. and Locati, M. Chemokine decoy receptors: structure-function and biological properties. *Curr. Top. Microbiol. Immunol.* **2010**, 341, 15-36.
- 88. Rollins, B. J. Chemokines. *Blood* **1997**, 90(3), 909-928.
- 89. Turner, M. D., Nedjai, B.; Hurst, T. and Pennington, D. J. Cytokines and chemokines: At the crossroads of cell signalling and inflammatory disease. *BBA* **2014**, 1843(11), 2563-2582.

- 90. Arimont, M., Hoffmann, C.; de Graaf, C. and Leurs, R. Chemokine Receptor Crystal Structures: What Can Be Learned from Them? *Mol. Pharmacol.* **2019**, 96(6), 756-777.
- 91. Miller, M. C. and Mayo, K. H. Chemokines from a Structural Perspective. *Int. J. Mol. Sci.* **2017**, 18(10), 2088.
- 92. Rostène, W.; Kitagbi, P. and Parsadaniantz, S. M. Chemokines: a new class of neuromodulator? *Nat. Rev. Neurosci.* **2007**, 8(11), 895-904.
- 93. Ishimoto, N.; Park, J.-H.; Kawakami, K.; Tajiri, M.; Mizutani, K.; Akashi, S.; Tame, J. R. H.; Inoue, A. and Park, S.-Y. Structural basis of CXC chemokine receptor 1 ligand binding and activation. *Nat. Comm.* **2023**, 14(1), 4107.
- 94. Taddese, B.; Deniaud, M.; Garnier, A.; Tiss, A.; Guissouma, H.; Abdi, H.; Henrion, D. and Chabbert, M. Evolution of chemokine receptors is driven by mutations in the sodium binding site. *PLoS Comput. Biol.* **2018**, 14(6), e1006209.
- 95. Dyer, D. P.; Migliorini, E.; Salanga, C. L.; Thakar, D.; Handel, T. M. and Richter, R. P. Differential structural remodelling ofheparan sulfate by chemokines: the roleof chemokine oligomerization. *Open Biol.* **2017**, 7(1), 160286.
- 96. Wang, X., Sharp, J. S.; Handel, T. M. and Prestegard, J. H. Chemokine Oligomerization in Cell Signaling and Migration. *Prog. Mol. Biol. Transl. Sci.* **2013**, 117, 31-578.
- 97. Proudfoot, A. E. I.; Handel, T. M.; Johnson, Z.; Lau, E. K.; Liwang, P.; Clark-Lewis, I.; Borlat, F.; Wells, T. N. C. and Kosco-Vilbois, M. H. Glycosaminoglycan binding and oligomerization are essential for the in vivo activity ofcertain chemokines. *Proc. Natl. Acad. Sci. USA.* **2003**, 100(4), 1885-1890.
- 98. Quast, T.; Zölzer, K.; Guu, D.; Alvarez, L.; Küsters, C.; Kiermaier, E.; Kaupp, U. B. and Kolanus, W. A Stable Chemokine Gradient Controls Directional Persistence of Migrating Dendritic Cells. *Front. Cell Dev. Biol.* **2022**, 10, 943041.
- 99. Rajarathnam, K.; Prado, G. N.; Fernando, H.; Clark-Lewis, I. and Navarrao, J. Probing Receptor Binding Activity of Interleukin-8 Dimer Using a Disulfide Trap. *Biochemistry* **2006**, 274(1), 7882-7888.
- 100. Larsen, C. G., Anderson, A. O.; Oppenheim, J. J. and Matsushima, K. Production of interleukin-8 by human dermal fibroblasts and keratinocytes in response to interleukin-1 or tumour necrosis factor. *Immunology* **1989**, 68(1), 31-36.
- 101. Wang, Y.; Wang, W.; Wang, X. and Xia, J. Regulatory mechanisms of interleukin-8 production induced by tumour necrosis factor- α in human hepatocellular carcinoma cells. *J. Cell. Mol. Med.* **2012**, 16(3), 496-506.
- 102. Park, S. H., et al. Interaction of Monomeric Interleukin-8 with CXCR1 Mapped by Proton-Detected Fast MAS Solid-State NMR. *Biophys. J.* **2017**, 113(12), 2695-2705.

- 103. Fernando, H., Chin, C.; Rösgen, J. and Rajarathnam, K. Dimer dissociation is essential for interleukin-8 (IL-8) binding to CXCR1 receptor. *J. Biol. Chem.* **2004**, 279(35), 36175-8.
- 104. Butterfield, T. A.; Best, T. M. and Merrick, M. A. The Dual Roles of Neutrophils and Macrophages in Inflammation: A Critical Balance Between Tissue Damage and Repair. *J. Athl. Tain.* **2006**, 41(4), 457-465.
- 105. Hess, C.; Means, T. K.; Autissier, P.; Woodberry, T.; Altfeld, M.; Addo, M. M.; Frahm, N.; Brander, C.; Walker, B. D. and Luster, A. D. IL-8 responsiveness defines a subset of CD8 T cells poised to kill. *Blood* **2004**, 104(12), 3463-3471.
- 106. Liu, K.; Wu, L.; Yuan, S.; Wu, M.; Xu, Y.; Sun, Q.; Li, S.; Zhao, S.; Hua, T. and Liu, Z.-J. Structural basis of CXC chemokine receptor 2 activation and signalling . *Nature* **2020**, 585, 135-140.
- 107. Raghuwanshi, S. K.; Su, Y.; Singh, V.; Hayes, K.; Richmond, A. and Richardson, R. M. The chemokine receptors CXCR1 and CXCR2 couple to distinct G protein-coupled receptor kinases to mediate and regulate leukocyte functions. *J. Immunol.* **2012**, 189(6), 2824-2832.
- 108. Veenstra, M. and Ransohoff, R. M. Chemokine receptor CXCR2: physiology regulator and neuroinflammation controller? *J. Neuroimmunol.* **2012**, 246(1-2), 1-9.
- 109. Zhang, X.; Guo, R.; Kambara, H.; Ma, F. and Luo, H. R. The role of CXCR2 in acute inflammatory responses and its antagonists as anti-inflammatory therapeutics. *Curr. Opin. Hematol.* **2019**, 26(1), 28-33.
- 110. Pease, J. E. and Sabroe, I. The Role of Interleukin-8 and its Receptors in Inflammatory Lung Disease. *Am. J. Respir. Med.* **2002**, 1(1), 19-25.
- 111. Dhayni, K.; Zibara, K.; Issa, H.; Kamel, S. and Bennis, Y. Targeting CXCR1 and CXCR2 receptors in cardiovascular diseases. *Pharmacol. Ther.* **2022**, 237, 108257.
- 112. Miyabe, Y., Miyabe, C.; Iwai, Y. and Luster, A. D. Targeting the Chemokine System in Rheumatoid Arthritis and Vasculitis. *JMA J.* **2020**, 3(3), 182-192.
- 113. Henrot, P., Prevel, R.; Berger, P. and Dupin, I. Chemokines in COPD: From Implication to Therapeutic Use. *Int. J. Mol. Sci.* **2019**, 20(11), 2785.
- 114. Korbecki, J.; Kupnicka, P.; Chlubek, M.; Goracy, J.; Gutowska, I. and Baranowska-Bosiacka, I. CXCR2 Receptor: Regulation of Expression, Signal Transduction, and Involvement in Cancer. *Int. J. Mol. Sci.* **2022**, 23(4), 2168.
- 115. Ha, H.; Debnath, B. and Neamati, N. Role of the CXCL8-CXCR1/2 Axis in Cancer and Inflammatory Diseases. *Theranostics* **2017**, 7(6), 1543-1588.
- 116. Molczyk, C. and Singh, R. K. CXCR1: A Cancer Stem Cell Marker and Therapeutic Target in Solid Tumors. *Biomedicine*. **2023**, 11(2), 576.

- 117. Bishayi, B.; Adhikary, R.; Sultana, S.; Dey, R. and Nandi, A. Altered expression of CXCR1 (IL-8R) in macrophages utilizing cell surface TNFR1 and IL-1 receptor during Staphylococcus aureus infection. *Microb. Patho.* **2017**, 113, 460-471.
- 118. Del Rio, L., Bennouna, S.; Salinas, J. and Denkers, E. Y. CXCR2 deficiency confers impaired neutrophil recruitment and increased susceptibility during Toxoplasma gondii infection. *J. Immunol.* **2001**, 167(11), 6503-6509.
- 119. Boff, D.; Oliveira, V. L. S.; Queiroz Junior, C. M.; Silva, T. A.; Allegretti, M.; Verri Jr., W. A.; Proost, P.; Teixera, M. M. and Amaral, F. A. CXCR2 is critical for bacterial control and development of joint damage and pain in Staphylococcus aureus-induced septic arthritis in mouse. *Eur. J. Immunol.* **2018**, 30(12), 454-463.
- 120. Zhu, F.; He, H.; Fan, L.; Ma, C.; Xu, X.; Xue, Y.; Wang, Y.; Zhang, C. and Zhou, G. Blockade of CXCR2 suppresses proinflammatory activities of neutrophils in ulcerative colitis. *Am. J. Transl. Res.* **2020**, 12(9), 5237-5251.
- 121. Hartl, D.; Lehmann, N.; Hoffmann, F.; Jansson, A.; Hector, A.; Notheis, G.; Roos, D.; Belohradsky, B. H. and Wintergerst, U. Dysregulation of innate immune receptors on neutrophils in chronic granulomatous disease. *J. Allergy Cli. Immunol.* **2008**, 121(2), 375-382.
- 122. Gómez-Melero, S. and Caballero-Villaraso, J. CCR6 as a Potential Target for Therapeutic Antibodies for the Treatment of Inflammatory Diseases. *Antibodies* **2023**, 12(2), 30.
- 123. Kondo, T.; Takata, H. and Takiguchi, M. Functional expression of chemokine receptor CCR6 on human effector memory CD8+ T cells. *Eur. J. Pharmacol.* **2007**, 37(1), 54-65.
- 124. Lyu, M.; Li, Y.; Hao, Y.; Lyu, C.; Huang, Y.; Sun, B.; Li, H.; Xue, F.; Liu, X. and Yang, R. CCR6 defines a subset of activated memory T cells of Th17 potential in immune thrombocytopenia. *Clin. Exp. Immunol.* **2019**, 195(3), 345-357.
- 125. Aziz, N., Detels, R.; Chang, L. C. and Butch, A. W. Macrophage Inflammatory Protein-3 Alpha (MIP- 3α)/CCL20 in HIV-1-Infected Individuals. *J. AIDS Clin. Res.* **2016**, 7(7), 587.
- 126. Zhao, L., Xia, J.; Wang, X. and Xu, F. Transcriptional regulation of CCL20 expression. *Microbes Infect.* **2014**, 16(10), 864-870.
- 127. Ranasinghe, R. and Eri, R. CCR6–CCL20-Mediated Immunologic Pathways in Inflammatory Bowel Disease. *Gastrointest. Disord.* **2019**, 1(1), 15-29.
- 128. Tan, J.; Xu, T.; Gou, Y.; Wang, H.; Liang, Z.; Cao, Y.; Wang, H.; Yu, Y.; Jiao, N. and Zhang, Z. CCL20/CCR6 axis mediates macrophages to promote proliferation and migration of ESCs by blocking autophagic flux in endometriosis. *Stem Cell Res. Ther.* **2022**, 13, 294.
- 129. Lörchner, H.; Esteve, L. C.; Góes, M. E.; Harzenetter, R.; Brachmann, N.; Gajawada, P.; Günther, S.; Doll, N.; Pöling, J. and Braun, T. Neutrophils for Revascularization Require Activation of CCR6 and CCL20 by TNFα. *Circulation Res.* **2023**, 133(7), 592-610.

- 130. Korona, B.; Korona, D.; Zhao, W.; Wotherspoon, A. C. and Du, M.-Q. CCR6 activation links innate immune responses to mucosa-associated lymphoid tissue lymphoma development. *Haematologica* **2022**, 107(6), 1384-1396.
- 131. Schiavo, R.; Baatar, D.; Olkhanud, P.; Indig, F. E.; Restifo, N.; Taub, D. and Biragyn, A. Chemokine receptor targeting efficiently directs antigens to MHC class I pathways and elicits antigen-specific CD8+ T-cell responses. *Blood* **2006**, 107(12), 4597-4605.
- 132. Izadpanah, A.; Dwinell, M. B.; Eckmann, L.; Varki, N. M. and Kagnoff, M. F. Regulated MIP-3alpha/CCL20 production by human intestinal epithelium: mechanism for modulating mucosal immunity. *Am. J. Physiol. Gastrointest. Liver Physiol.* **2001**, 280(4), 710-719.
- 133. Dalod, M., Chelbi, R.; Malissen, B. and Lawrence, T. Dendritic cell maturation: functional specialization through signaling specificity and transcriptional programming. *EMBO J.* **2014**, 33(10), 1104-1116.
- 134. Lee, G. R. The Balance of Th17 versus Treg Cells in Autoimmunity. Int. J. Mol. Sci. 2018, 19(3), 730.
- 135. Yamazaki, T.; Yang, X. O.; Chung, Y.; Fukunaga, A.; Nurieva, R.; Pappu, B.; Martin-Orozco, N.; Kang, H. S.; Ma, L.; Panopoulos, A. D.; Craig, S.; Watowich, S. S.; Jetten, A. M.; Tian, Q. and Dong, C. CCR6 Regulates the Migration of Inflammatory and Regulatory T Cells. *J. Immunol.* **2008**, 181(12), 8391-8401.
- 136. Kondelkova, K.; Vokurkova, D.; Krejsek, J.; Borska, L.; Fiala, Z. and Ctirad, A. Regulatory T cells (TREG) and their roles in immune system with respect to immunopathological disorders. *Acta Medica* **2010**, 53(2), 73-77.
- 137. Ouyang, W.; Kolls, J. K. and Zheng, Y. The Biological Functions of T Helper 17 Cell Effector Cytokines in Inflammation. *Immunity* **2008**, 28(4), 454-467.
- 138. Zhang, S., et al. The Alterations in and the Role of the Th17/Treg Balance in Metabolic Diseases. *Front. Immunol.* **2021**, 12, 678355.
- 139. Omenetti, S. and Pizzaro, T. T. The Treg/Th17 Axis: A Dynamic Balance Regulated by the Gut Microbiome. *Front. Immunol.* **2015**, 6, 00639.
- 140. Eisenstein, E. M. and Williams, C. B. The Treg/Th17 Cell Balance: A New Paradigm for Autoimmunity. *Ped. Res.* **2009**, 65(5), 26-31.
- 141. Yan, J.-B., Luo, M.-M.; Chen, Z.-Y. and He, B.-H. The Function and Role of the Th17/Treg Cell Balance in Inflammatory Bowel Disease. *J. Immunol. Res.* **2020**, 2020, 8813558.
- 142. Tesmer, L. A., Lundy, S. K.; Sarkar, S. and Fox, D. A. Th17 cells in human disease. *Immunol. Rev.* **2008**, 223, 87-113.
- 143. Alrumaihi, F. The Multi-Functional Roles of CCR7 in Human Immunology and as a Promising Therapeutic Target for Cancer Therapeutics. *Front. Mol. Biosci.* **2022**, 9, 834149.

- 144. Yan, Y.; Chen, R.; Wang, X.; Hu, K.; Huang, L.; Lu, M. and Hu, Q. CCL19 and CCR7 Expression, Signaling Pathways, and Adjuvant Functions in Viral Infection and Prevention. *Front. Cell Dev. Biol.* **2019**, 7, 212.
- 145. Lewandowski, E. M.; Kroeck, K. G.; Jacobs, L. M. C.; Fenske, T. G.; Witt, R. N.; Hintz, A. M.; Ramsden, E. R.; Zhang, X.; Peterson, F.; Volkman, B. F.; Veldkamp, C. T. and Chen, Y. Structural Insights into Molecular Recognition by Human Chemokine CCL19. *Biochemistry* **2022**, 61(5), 311-318.
- 146. Kozai, M.; Kubo, Y.; Katakai, T.; Kondo, H.; Kiyonari, H.; Schaeuble, K.; Luther, S. A.; Ishimaru, N.; Ohigashi, I. and Takahama, Y. Essential role of CCL21 in establishment of central self-tolerance in T cells. *J. Exp. Med.* **2017**, 214(7), 1925-1935.
- 147. Pickens, S. R.; Chamberlain, N. D.; Volin, M. V.; Pope, R. M.; Mandelin II, A. M. and Shahrara, S. Characterization of CCL19 and CCL21 in Rheumatoid Arthritis. *Arthritis Rheum.* **2011**, 63(4), 914-922.
- 148. Comerford, I.; Harata-Lee, Y.; Bunting, M. D.; Gregor, C.; Kara, E. E. and McColl, S. R. A myriad of functions and complex regulation of the CCR7/CCL19/CCL21 chemokine axis in the adaptive immune system. *Cytokine & Growth Factor Reviews* **2013**, 24(3), 269-283.
- 149. Riol-Blanco, L.; Sanchez-Sanchez, N.; Torres, A.; Tejedor, A.; Narumiya, S.; Corbi, A. L.; Sanchez-Mateos, P. and Rodriguez-Fernandez, J. L. The chemokine receptor CCR7 activates in dendritic cells two signaling modules that independently regulate chemotaxis and migratory speed. *J. Immunol.* **2005**, 174(7), 4070-4080.
- 150. Rodriguez-Fernandez, J. L. and Criado-Garcia, O. The Chemokine Receptor CCR7 Uses Distinct Signaling Modules With Biased Functionality to Regulate Dendritic Cells. *Front. Immunol.* **2020**, 11, 00528.
- 151. Hong, W.; Yang, B.; He, Q.; Wang, J. and Weng, Q. New Insights of CCR7 Signaling in Dendritic Cell Migration and Inflammatory Diseases. *Front. Pharmacol.* **2022**, 13, 841687.
- 152. Hunter, M. C.; Teijeira, A. and Halin, C. T Cell Trafficking through Lymphatic Vessels. *Front. Immunol.* **2016**, 7, 613.
- 153. Kumar, B. V.; Connors, T. and Farber, D. L. Human T cell development, localization, and function throughout life. *Immunity* **2018**, 48(2), 202-213.
- 154. Waldmann, A. D.; Fritz, J. M. and Lenardo, M. J. A guide to cancer immunotherapy: from T cell basic science to clinical practice. *Nat. Rev. Immunol.* **2020**, 20(11), 651-668.
- 155. Debes, G. F.; Arnold, C. N.; Young, A. J.; Krautwald, S.; Lipp, M.; Hay, J. B. and Butcher, E. C. CC chemokine receptor 7 required for T lymphocyte exit from peripheral tissues. *Nat. Immunol.* **2005**, 6(9), 889-894.
- 156. Förster, R.; Davalos-Misslitz, A. C. and Rot, A. CCR7 and its ligands: balancing immunity and tolerance. *Nat. Rev. Immunol.* **2008**, 8(5), 362-371.

- 157. Goto, T.; Michiue, T. and Shibuya, H. CCR7 affects both morphogenesis and differentiation during early Xenopus embryogenesis. *Dev. Growth Differ.* 2022, 64(5), 254-260.
- 158. Han, L. and Zhang, L. CCL21/CCR7 axis as a therapeutic target for autoimmune diseases. *Int. Immunopharmacol.* **2023**, 121, 110431.
- 159. Van Raemdonck, K.; Umar, S. and Shahrara, S. The pathogenic importance of CCL21 and CCR7 in rheumatoid arthritis. *Cytokine & Growth Factor Reviews.* **2020**, 55, 86-93.
- 160. Liu, Z.; Li, F.; Pan, A.; Xue, H.; Jiang, S.; Zhu, C.; Jin, M.; Fang, J.; Zhu, X.; Brown, M. A. and Wang, X. Elevated CCL19/CCR7 Expression During the Disease Process of Primary Sjögren's Syndrome. *Front. Immunol.* **2019**, 10, 795.
- 161. Liu, J., Zhang, X.; Cheng, Y. and Cao, X. Dendritic cell migration in inflammation and immunity. *Cell. Mol. Immunol.* **2021**, 18(11), 2461-2471.
- 162. Bill, C. A.; Allen, C. M. and Vines, C. M. C-C Chemokine Receptor 7 in Cancer. *Cells* 11(4), 2022, 656.
- 163. Salem, A.; Alotaibi, M.; Mroueh, R.; Basheer, H. A. and Afarinkia, K. CCR7 as a therapeutic target in Cancer. *BBA* **2021**, 1875(1), 188499.
- 164. Tutunea-Fatan, E., Majumder, M.; Xin, X. and Lala, P. K. The role of CCL21/CCR7 chemokine axis in breast cancer-induced lymphangiogenesis. *Mol. Canc.* **2015**, 14, 35.
- 165. Legler, D. F.; Uetz-von-Almen, E. and Hauser, M. A. CCR7: roles in cancer cell dissemination, migration and metastasis formation. *Int. J. Biochem. Cell Biol.* **2014**, 54, 78-82.
- 166. Lai, W. Y. and Mueller, A. Latest update on chemokine receptors as therapeutic targets. *Biochem. Soc. Trans.* **2021**, 49(3), 1385-1395.
- 167. Sun, D.; Sun, Y.; Janezic, E.; Zhou, T.; Johnson, M.; Azumaya, C.; Noreng, S.; Chiu, C.; Ski, A.; Arenzana, T.L.; Nicoludis, J. M.; Shi, Y.; Wang, B.; Ho, H.; Joshi, P.; Tam, C.; Payandeh, J.; Comps-Agrar, L.; Wang, J.; Rutz, S.; Koerber, J.T. Masureel, M. Structural basis of antibody inhibition and chemokine activation of the human CC chemokine receptor 8. *Nat. Comm.* **2023**, 14, 7940.
- 168. Gong, J. H., Uguccioni, M.; Baggiolini, M. and Clark-Lewis, I. RANTES and MCP-3 antagonists bind multiple chemokine receptors. *J. Bio. Chem.* **1996**, 271(18), 10521-10527.
- 169. Reilly, R. M.; Domingo, R. and Sandhu, J. Oral delivery of antibodies. Future pharmacokinetic trends. *Clin. Pharmacokinet.* **1997**, 32(4), 313-323.
- 170. Pitiot, A.; Heuzé-Vourc'h, N. and Sécher, T. Alternative Routes of Administration for Therapeutic Antibodies—State of the Art. *Antibodies* **2022**, 11(3), 56.
- 171. Emmelkamp, J. M. and Rockstroh, J. K. CCR5 antagonists: comparison of efficacy, side effects, pharmacokinetics and interactions-review of the literature. *Eur. J. Med. Res.* **2007**, 12(9), 409-417.

- 172. Wheeler, C.; Furniss, D.; Galal-Edeen, G. H.; Blandford, A. and Franklin, B. D. Patients' Perspectives on the Quality and Safety of Intravenous Infusions: A Qualitative Study. *J. Patient Exp.* **2020**, 7(3), 380-385.
- 173. Pease, J. E. and Horuk, R. Recent progress in the development of antagonists to the chemokine receptors CCR3 and CCR4. *Expert Opin. Drug, Discov.* **2014**, 9(5), 467-483.
- 174. Isberg, V.; Mordalski, S.; Munk, C.; Rataj, K.; Harpsoe, K.; Hauser, A. S.; Vroling, A.; Vriend, G. and Gloriam, D. E. GPCRdb: an information system for G protein-coupled receptors. *Nucleic Acids Res.* **2016**, 45(5), 356-364.
- 175. Gladue, R. P.; Brown, M. F. and Zwilich, S. H. CCR1 antagonists: what have we learned from clinical trials. *Curr. Top. Med. Chem.* **2010**, 10(13), 1268-1277.
- 176. Pease, J. and Horuk, R. Chemokine Receptor Antagonists. J. Med. Chem. 2012, 55(22), 9363-9392.
- 177. Horuk, R. Chemokine receptor antagonists: overcoming developmental hurdles. *Nat. Rev. Drug Discov.* **2009**, 8(1), 23-33.
- 178. http://clinicaltrials.gov/ct2/show/NCT00185341?term=CCR1&rank=1., Study To Investigate the Efficacy of a Non-Hormonal Drugagainst Endometriosis Associated Pelvic Pain. [Online]
- 179. Carson, K. G., Jaffee, B. D. and Harriman, G. B. CCR1 Antagonists. *Annu. Rep. Med. Chem.* **2004**, 149–158.
- 180. Vergunst, C. E.; Gerlag, D. M.; von Moltke, L.; Karol, M.; Wyant, T.; Chi, X.; Matzkin, E.; Leach, T.; Tak, P. P. MLN3897 plusmethotrexate in patients with rheumatoid arthritis: safety, efficacy, pharmacokinetics, and pharmacodynamics of an oral CCR1 antagonistin a phase IIa, double-blind, placebo-controlled, randomized, proof-of-concept study. *Arthritis Rheum.* **2009**, 48, 3572–3581.
- 181. Hang, P.; Pennell, A. M. K.; Wright, J. J. K.; Wei, C.; Leleti, M.R.; Li, Y.; Li, L.; Xu, Y. (2006). Azaindazole Compounds and Methods of Use. US 2007/0010524A1. https://patentimages.storage.googleapis.com/b9/01/cc/c02bf041a0669a/US20070010524A1.pdf
- 182. Dairaghi, D. J.; Zhang, P.; Wang, Y.; Seitz, L. C.; Johnson, D.A.; Miao, S.; Ertl, L. S.; Zeng, Y.; Powers, J. P.; Pennell, A. M.; Bekker, P.; Schall, T. J.; Jaen, J. C. P harmacokinetic and pharmacodynamicevaluation of the novel CCR1 antagonist CCX354 in healthy humansubjects: implications for selection of clinical dose. *Clin. Pharmacol. Ther.* **2011**, 89(5), 726-734.
- 183. Dak, P. P.; Balanescu, A.; Tseluyko, V.; Bojin, S.; Drescher, E.; Dairaghi, D.; Miao, S.; Marchesin, V.; Jaen, J.; Bekker, P.; Schall, T. J. Safety and Efficacy of Oral Chemokine Receptor 1 AntagonistCCX354-C in a Phase 2 Rheumatoid Arthritis Study. Presented at the2011 American College of Rheumatology/Association of ReproductiveHealth Professionals (ACR/ARHP) Annual Meeting, Chicago, IL,2011. https://acr.confex.com/acr/2011/webprogram/Paper24548.html.
- 184. Moore, J. P.; Trkola, A. and Dragic, T. Co-receptors for HIV-1entry. *Curr. Opin. Immunol.* **1997**, 9(4), 551-562.

- 185. Rao, P. K. S. CCR5 inhibitors: Emerging promising HIV therapeutic strategy. *Indian J. Sex. Transm. Dis. AIDS* **2009**, 30(1), 1-9.
- 186. Wood, A. and Armour, D. he discovery of the CCR5 receptorantagonist, UK-427,857, a new agent for the treatment of HIVinfection and AIDS. *Prog. Med. Chem.* **2005**, 43, 239-271.
- 187. Lieberman-Blum, S. S., Fung, H. B. and Bandres, J. C. Maraviroc: aCCR5-receptor antagonist for the treatment of HIV-1 infection. *Clin. Ther.* **2008**, 30(7), 1228-1250.
- 188. Dorr, P.; Westby, M.; Dobbs, S.; Griffin, P.; Irvine, B.; Macartney, M.; Mori, J.; Rickett, G.; Smith-Burchnell, C.; Napier, C.; Webster, R.; Armour, D.; Price, D.; Stammen, B.; Wood, A.; Perros, M. Maraviroc (UK-427,857), a potent, orally bioavailable, and selectivesmall-molecule inhibitor of chemokine receptor CCR5 with broad-spectrum anti-human immunodeficiency virus type 1 activity. *Antimicrob. Agents Chemother.* **2005**, 49(11), 4721-4732.
- 189. Fatkenheuer, G.; Pozniak, A.L.; Johnson, M.A.; Plettenberg, A.; Staszewski, S.; Hoepelman, A.I.; Saag, M.S.; Goebel, F.D.; Rockstroh, J.K.; Dezube, B.J.; Jenkins, T. M.; Medhurst, C.; Sullivan, J.F.; Ridgway, C.; Abel, S.; James, I.T.; Youle, M.; van der Ryst, E. Efficacy of short-term monotherapy with maraviroc, a new CCR5antagonist, in patients infected with HIV-1. *Nat. Med.* **2005**, 11(11), 1170-1172.
- 190. Este, J. A. CH-351125 and SCH-350634. Schering-Plough. *Curr. Opin. Invest. Drugs.* **2002**, 3(3), 379-383.
- 191. Nichols, W. G.; Steel, H. M.; Bonny, T.; Adkison, K.; Curtis, L.; Millard, J.; Kabeya, K.; Clumeck, N. Hepatotoxicity observed inclinical trials of aplaviroc (GW873140). *Antimicrob. Agents Chemother.* **2008**, 52, 858-865.
- 192. Baba, M.; Takashima, K.; Miyake, H.; Kanzaki, N.; Teshima, K.; Wang, X.; Shiraishi, M.; Iizawa, Y. AK-652 inhibits CCR5-mediated human immunodeficiency virus type 1 infection in vitro andhas favorable pharmacokinetics in humans. *Antimicrob. Agents Chemother.* **2005**, 49(11), 4584-4591.
- 193. **Takeda.** Takeda To License CCR5 Antagonists for Treatment of HIVInfection to Tobira Therapeutics, Inc. http://www.takeda.com/press/article_27377.html.
- 194. Mirza, M. U.; Saadabadi, A.; Vanmeert, M.; Salo-Ahen, O. M. H.; Abdullah, I.; Claes, S.; De Jonghe, S.; Schols, D.; Ahmad, S. and Froeyen, M. Discovery of HIV entry inhibitors via a hybrid CXCR4 and CCR5 receptor pharmacophore-based virtual screening approach. *Eur. J. Pharm. Sci.* **2020**, 155, 105537.
- 195. De Clercq, E. he AMD3100 story: the path to the discovery of a stem cell mobilizer (Mozobil). *Biochem. Pharmacol.* **2008**, 77(11), 1655-1664.
- 196. Zhang, Y.; Dépond, M.; He, L.; Foudi, A.; Kwarteng, E. O.; Lauret, E.; Plo, I.; Desterke, C.; Dessen, P.; Fujii, N.; Opolon, P.; Herault, O.; Solary, E.; Vainchenker, W.; Joulin, V.; Louache, F. and Wittner, M. CXCR4/CXCL12 axis counteracts hematopoietic stem cell exhaustion through selective protection against oxidative stress. *Sci. Rep.* **2016**, 6, 37827.

- 197. Pillay, J.; Tregay, N.; Juzenaite, G.; Carlin, L. M.; Pirillo, C.; Gaboriau, D. C. A.; Farahi, N.; Summers, C.; Lo Celso, C.; Chilvers, E. R.; Rankin, S. and De Filippo, K. Effect of the CXCR4 antagonist plerixafor on endogenous neutrophil dynamics in the bone marrow, lung and spleen. *J. Leukoc. Biol.* **2020**, 107(6), 1175-1185.
- 198. Brave, M.; Farrell, A.; Ching Lin, S.-C.; Ocheltree, T.; Miksinski, S. P.; Lee, S.-L.; Saber, H.; Fourie, J.; Tornoe, C.; Booth, B.; Yuan, W.; He, K.; Justice, R.; and Pazdur, R. FDA review summary: Mozobil in combination with granulocyte colony-stimulating factor tomobilize hematopoietic stem cells to the peripheral blood forcollection and subsequent autologous transplantation. *Oncology* **2010**, 78(3-4), 282-288.
- 199. Shia, K. S.; Hakimelahi, G.; Zhu, J.-L.; Yen, C.-F.; Huang, Y.-H.; Xiang, Y.; Chen, H.-C. and wang, C.-C.(2005) *Polyamine Compoundsfor Treating Chemokine Receptor Mediated Diseases. 20050043366 https://patents.justia.com/patent/20050043366#history*.
- 200. Kobayashi, K. Kawakami, K.; Kusakizako, T.; Tomita, A.; Nishimura, M.; Sawada, K.; Okamoto, H. H.; Hiatsuka, S.; Nakamura, R.; Noda, H.; Muramatsu, H.; Shimizu, M.; Taguchi, T.; Inoue, A.; Murata, T. and Nureki, O. Class B1 GPCR activation by an intracellular agonist. *Nature* **2023**, 618, 1085-1093.
- 201. Oswald, C.; Rappas, M.; Kean, J.; Doré, A. S.; Errey, J. C.; Bennet, K.; Deflorian, F.; Christopher, J. A.; Jazayeri, A.; Mason, J. S.; Congreve, M.; Cooke, R. M. and Marshall, F. H. Intracellular allosteric antagonism of the CCR9. *Nature* **2016**, 540, 462-465.
- 202. Liu, X.; Masoudi, A.; Kahsai, A. W.; Huang, L.-Y.; Pani, B.; Staus, D. P.; Shim, P. J.; Hirata, K.; Simhal, R. K.; Schwalb, A. M.; Rambarat, P. K.; Ahn, S.; Lefkowitz, R. J. and Kobilka, B. Mechanism ofb2AR regulationby an intracellular positive allosteric modulator. *Science* **2019**, 364(6447), 1283-1287.
- 203. Zheng, Y.; Qin, L.; Ortiz-Zacarias, N.V.; de Vries, H.; Han, G.W.; Gustavsson, M.; Dabros, M.; Zhao, C.; Cherney, R.J.; Carter, P.; Stamos, D.; Abagyan, R.; Cherezov, V.; Stevens, R.C.; Ijzerman, A.P.; Heitman, L.H.; Tebben, A.; Kufareva, I. and Handel, T Structure of CC chemokine receptor 2 with orthosteric and allosteric antagonists. *Nature* **2016**, 540(7633), 458-461
- 204. Liu, K.; Wu, L.; Yuan, S.; Wu, M.; Xu, Y.; Sun, Q.; Li, S.; Zhao, S.; Hua, T. and Liu, Z.-J. Structural basis of CXC chemokine receptor 2 activation and signalling. *Nature* **2020**, 585, 135-140.
- 205. Jaeger, K.; Bruenle, S.; Weinert, T.; Guba, W.; Muehle, J.; Miyazaki, T.; Weber, M.; Furrer, A.; Haenggi, N.; Tetaz, T.; Huang, C.-Y.; Mattle, D.; Vonach, J.-M.; Gast, A.; Kuglstatter, A.; Rudolph, M.G.; Nogly, P.; Benz, J.; Dawson, R.J.P. and Standfuss, J. Structural Basis for Allosteric Ligand Recognition in the Human CC Chemokine Receptor 7. *Cell* **2019**, 178(5), 1222-1230.
- 206. Andrews, G.; Jones, C. and Wreggett, K. A. An Intracellular Allosteric Site for a Specific Class of Antagonists of the CC Chemokine G Protein-Coupled Receptors CCR4 and CCR5. *Mol. Pharmacol.* **2008**, 73(3),855-867.
- 207. Ortiz-Zacarias, N. V.; Lenselink, F. B.; Ijzerman, A. P.; Handel, T. M. and Heitman, L. H. Intracellular receptor modulation: Novel approach to target GPCRs. *Trends Pharmacol. Sci.* **2018**, 39(6), 547-559.

- 208. Malik, F. and Li, Z. Is there a common allosteric binding site for G-protein coupled receptors? *J. Comput. Aided Mol. Des.* **2022**, 36(6), 405-413.
- 209. Wold, E. A. and Zhou, J. GPCR Allosteric Modulators: Mechanistic Advantages and Therapeutic Applications. *Curr. Top. Med. Chem.* **2018**, 18(23), 2002-2006.
- 210. Han, B.; Salituro, F. G. and Blanca, M.-J. Impact of Allosteric Modulation in Drug Discovery: Innovation in Emerging Chemical Modalities. *ACS Med. Chem. Lett.* **2020**, 11(10), 1810-1819.
- 211. Reyes-Alcaraz, A., Garcia-Rojas, E. Y. L.; Bond, A. and McConnell, B. K. Allosteric Modulators for GPCRs as a Therapeutic Alternative with High Potential in Drug Discovery. *Mol. Pharmacol.* **2020**, 5(1), 1-14.
- 212. Cao, A.-M.; Quast, R. B.; Fatemi, F.; Rondard, P.; Pin, J.-P. and Margeat, E. Allosteric modulators enhance agonist efficacy by increasing the residence time of a GPCR in the active state. *Nat. Comm.* **2021**, 12(1), 5426.
- 213. Jin, Q.; Nie, H.; McCleland, B. W.; Widdowson, K. L.; Palovich, M. R.; Elliot, J. D.; Goodman, R. M.; Burman, M.; Sarau, H. M.; Ward, K. W.; Nord, M.; Orr, B. O.; Gorycki, P. D. and Busch-Petersen, J. Discovery of potent and orally bioavailable N,N'-diarylurea antagonists for the CXCR2 chemokine receptor. *Bioorg. Med. Chem. Lett.* **2004**, 14(17), 4375-4378.
- 214. Madan, A.; Chen, S.; Yates, P.; Washburn, M. L.; Roberts, G.; Peat, A. J.; Tao, Y.; Parry, M. P.; Barnum, O.; McClain, M. T. and Roy-Ghanta, S. Efficacy and Safety of Danirixin (GSK1325756) Coadministered With Standard-of-Care Antiviral (Oseltamivir): A Phase 2b, Global, Randomized Study of Adults Hospitalized With Influenza. *Open Forum Infect. Dis.* **2019**, 6(4), ofz163.
- 215. Mozzafari, S.; Nikfar, S. and Abdollahi, M. Inflammatory bowel disease therapies discontinued between 2009 and 2014. *Expert Opin. Investig. Drugs.* 2015, 24(7), 949-956.
- 216. Taveras, A. G.; Chao, J.; Biju, P. J.; Aki, C. J.; Merritt, J. R.; Li, G.; Baldwin, J. J.; Lai, G.; Wu, M. and Hecker, E. A. (2010) THIADIAZOLEDIOXIDES AND THIADIAZOLEOXIDES AS CXC- AND CC-CHEMOKINE RECEPTOR LIGANDS. US 7/691/856 B2.
- 217. van Hoof, M.; Claes, S.; Proj, M.; van Loy, T.; Schols, D.; Gobec, S.; Dehaen, W. and de Jonghe, S. Optimization of triazolo[4,5-d]pyrimidines towards human CC chemokine receptor 7 (CCR7) antagonists. *Eur. J. Med. Chem.* **2023**, 251, 115240.
- 218. Toy, L.; Huber, M. E.; Schmidt, M. F.; Weikert, D. and Schiedel, M. Fluorescent Ligands Targeting the Intracellular Allosteric Binding Site of the Chemokine Receptor CCR2. *ACS Chem. Biol.* **2022**, 17(8), 2142-2152.
- 219. Toy, L.; Huber, M. E.; Schmidt, M. F.; Weikert, D. and Schiedel, M. A Chemical Biology Toolbox Targeting the Intracellular Binding Site of CCR9: Fluorescent Ligands, New Drug Leads and PROTACs. *Angew. Chem. Int. Ed.* **2022**, 61(12), e202116782.

- 220. Lipinski, C. A., Lombardo, F.; Dominy, B. W. and Feeney, P. J. Experimental and Computational Approaches to Estimate Solubility and Permeability in Drug Discovery and Development Settings. *Adv. Drug. Deliv. Rev.* **1997**, 46(1-3), 3-25.
- 221. Ramirez, M.; Rajaram, S.; Steininger, R. J.; Osipchuk, D.; Roth, M. A.; Morinishi, L. S.; Evans, L.; Ji, W.; Hsu, C.-H.; Thurley, K.; Zhou, A.; Koduru, P. R.; Posner, B. A.; Wu, L. F. and Altschuler, S. J. Diverse drug-resistance mechanisms can emerge from drug-tolerant cancer persister cells. *Nat. Comm.* **2016**, 7, 10690.
- 222. Finan, C.; Gaulton, A.; Kruger, F. A.; Lumbers, R. T.; Shah, T.; Engmann, J.; Galver, L.; Kelley, R.; Karlsson, A.; Santos, R.; Overington, J. P.; Hingorani, A. D. and Casas, J. P. The druggable genome and support for target identification and validation in drug development. *Sci. Transl. Med.* **2017**, 9, 383.
- 223. Lu, R.-M.; Hwang, Y.-C.; Liu, I.-J.; Lee, C.-C.; Tsai, H.-Z.; Li, H.-J. and Wu, H.-C. Development of Therapeutic Antibodies for the Treatment of Diseases. *J. Biomed. Sci.* **2020**, 27(1), 1.
- 224. Keefe, A. D.; Pai, S. and Ellington, A. Aptamers as Therapeutics. *Nat. Rev. Drug Discov.* **2010**, 9, 537-550.
- 225. Sakamoto, K. M.; Kim, K. B.; Kumagai, A.; Mercurio, F.; Crews, C. M. and Deshaies R. J. Protacs: Chimeric Molecules That Target Proteins to the Skp1-Cullin-F Box Complex for Ubiquitination and Degradation. *Proc. Natl. Acad. Sci.* **2001**, 98(15), 8554-8559.
- 226. Burov, A. V., Rodin, A. A.; Karpov, V. L. and Morozov, A. V. The Role of Ubiquitin-Proteasome System in the Biology of Stem Cells. *Biochemistry* **2023**, 88(12), 2043-2053.
- 227. Bedford, L.; Lowe, J.; Dick, L. R.; Mayer, R. J. and Brownell, J. E. Ubiquitin-like protein conjugation and the ubiquitin–proteasome system as drug targets. *Nat. Rev. Drug Discov.* 2011, 10(1), 29-46.
- 228. Kliza, K. and Husnjak, K. Resolving the Complexity of Ubiquitin Networks. *Front. Mol. Biosci.* **2020**, 7, 21.
- 229. Graham, H. The mechanism of action and clinical value of PROTACs: A graphical review. *Cell. Sign.* **2022**, 99, 110446.
- 230. Sun, X.; Gao, H.; Yang, Y.; He, M.; Wu, Y.; Song, Y.; Tong, Y. and Rao, Y. PROTACs: great opportunities for academia and industry. *Signal Transduct. Target. Ther.* 2019, 4, 64.
- 231. Sincere, N. I.; Anand, K.; Ashique, S.; Yang, J. and You, C. PROTACs: Emerging Targeted Protein Degradation Approaches for Advanced Druggable Strategies. *Molecules* **2023**, 28(10), 4014.
- 232. Schneekloth, J. S.; Fonseca, F. N.; Koldobskiy, M.; Mandal, A.; Sakamoto, K and Crews, C. M. Chemical Genetic Control of Protein Levels: Selective in Vivo Targeted Degradation. *J. Am. Chem. Soc.* **2004**, 126(12), 3748-3754.
- 233. Lopez-Girona, A.; Mendy, D.; Ito, T.; Miller, K.; Gandhi, A.K.; Kang, J.; Karasawa, S.; Carmel, G.; Jackson, P.; Abbasian, M.; Mahmoudi, A.; Cathers, B.; Rychak, E.; Gaidarova, S.; Chen, R.; Schafer, P.

- H.; Handa, H.; Daniel, T.O.; Evans, J.F. and Chopra, R. Cereblon is a direct protein target for immunomodulatory and antiproliferative activities of lenalidomide and pomalidomide. *Nature* **2012**, 26(11), 2326-2335.
- 234. Vargesson, N. Thalidomide-induced teratogenesis: History and mechanisms. *Birth Defects Res. C. Embryo Today* **2015**, 105(2), 140-156.
- 235. Knoche, B. and Blaschke, G. Investigations on the in vitro racemization of thalidomide by high-performance liquid chromatography. *J. Chromatogr. A.* **1994**, 666(1-2), 235-240.
- 236. Bricelj, A.; Steinebach, C.; Kuchta, R.; Gütschow, M. and Sosic, I. E3 Ligase Ligands in Successful PROTACs: An Overview of Syntheses and Linker Attachment Points. *Front. Chem.* **2021**, 9, 707317.
- 237. Lee, J.; Lee, Y.; Jung, Y. M.; Park, J. H.; Yoo, H. S. and Park, J. Discovery of E3 Ligase Ligands for Target Protein Degradation. *Molecules* **2022**, 27(19), 6515.
- 238. Wang, X.; Qin, Z.-L.; Li, N.; Jia, M.-Q.; Liu, Q.-G.; Bai, Y.-R.; Song, J.; Yuan, S. and Zhang, S.-Y. Annual review of PROTAC degraders as anticancer agents in 2022. *Eur. J. Med. Chem.* **2024**, 267(5), 116166.
- 239. Xie, H., Liu, J.; Glison, D. M. A. and Fleming, J. B. The clinical advances of proteolysis targeting chimeras in oncology. *Explor. Target. Antitumor Ther.* **2021**, 2(6), 511-521.
- 240. Ariazi, E. A., Ariazi, J. L.; Cordero, F. and Jordan, V. C. Estrogen receptors as therapeutic targets in breast cancer. *Curr. Top. Med. Chem.* **2006**, 6(3), 181-202.
- 241. Michmerhuizen, A. R., Spratt, D. E.; Pierce, L. J. and Speers, C. W. ARe we there yet? Understanding androgen receptor signaling in breast cancer. *npj Breast Cancer*. **2020**, 6, 47.
- 242. Gadd, M. S.; Testa, A.; Lucas, X.; Chan, K.-H.; Chen, W.; Lamont, D. J.; Zengerle, M. and Ciulli, A. Structural basis of PROTAC cooperative recognition for selective protein degradation. *Nat. Chem. Biol.* **2017**, 13(5), 514-521.
- 243. Roy, M. J.; Winkler, S.; Hughes, S. J.; Whitworth, C.; Galant, M.; Farnaby, W.; Rumpel, K. and Ciulli, A. SPR-Measured Dissociation Kinetics of PROTAC Ternary Complexes Influence Target Degradation Rate. *ACS Chem. Biol.* **2019**, 14(3), 361-368.
- 244. Mai, H.; Zimmer, M. H. and Miller III, T. F. Exploring PROTAC Cooperativity with Coarse-Grained Alchemical Methods. *J. Phys. Chem. B.* **2023**, 127(2), 446-455.
- 245. Nowak, R. P.; DeAngelo, S. L.; Buckley, D.; He, Z.; Donovan, K. A.; An, J.; Safaee, N.; Jedrychowski, M. P.; Ponthier, C. M.; Ishoey, M.; Zhang, T.; Mancias, J. D.; Gray, N. S.: Bradner, J. E. and Fischer, E. S. Plasticity in Binding Confers Selectivity in Ligand-Induced Protein Degradation. *Nat. Chem. Biol.* **2018**, 14(7), 706-714.
- 246. Douglass, E. F.; Miller, C. J.; Sparer, G.; Shapiro, H. and Spiegel, D. A. A Comprehensive Mathematical Model for Three-Body Binding Equilibria . *J. Am. Chem. Soc.* **2013**, 135(16), 6092-6099.

- 247. Zhao, L.; Zhao, L.; Zhong, K.; Tong, A. and Jia, D.Targeted protein degradation: mechanisms, strategies and application. *Signal Transduct. Tar. Ther.* **2022**, 7(1), 113.
- 248. Xie, S.; Zhu, J.; Li, J.; Zhan, F.; Yao, H.; Xu, J. and Xu, S. Small-Molecule Hydrophobic Tagging: A Promising Strategy of Druglike Technology for Targeted Protein Degradation. *J. Med. Chem.* **2023**, 66(16), 10917-10933.
- 249. Sasso, J. M.; Tenchov, R.; Wang, D.; Johnson, L. S.; Wang, X. and Zhou, Q. A. Molecular Glues: The Adhesive Connecting Targeted Protein Degradation to the Clinic. *Biochemistry* **2023**, 62(3), 601-623.
- 250. Cotton, A. D.; Nguyen, D. P.; Gramespacher, J. A.; Seiple, I. B. and Wells, J. A. Development of Antibody-Based PROTACs for the Degradation of the Cell-Surface Immune Checkpoint Protein PD-L1. *J. Am. Chem. Soc.* **2021**, 143(2), 593-598.
- 251. Deane, C. It's a trap! Nat. Chem. Biol. 2020, 16, 291-297.
- 252. Takahashi, D.; Moriyama, J.; Nakamura, T.; Miki, E.; Takahashi, E.; Sato, A.; Akaike, T.; Itto-Nakama, K. and Arimoto, H. AUTACs: Cargo-Specific Degraders Using Selective Autophagy. *Mol. Cell.* 2019, 76(5), 797-810.
- 253. Fan, L. Z. and Lin, M. Z. Optical control of biological processes by light-switchable proteins. *Wiley Interdiscip. Rev. Dev. Biol.* 2015, 4(5), 545-554.
- 254. Ankenbruck, N., Courtney, T. Naro, Y. and Deiters, A. Optochemical Control of Biological Processes in Cells and Animals. *Angew. Chem. Int. Ed.* 2018, 57(11), 2768-2798.
- 255. Reynders, M.; Matsuura, B. S.; Bérouti, M.; Simoneschi, D.; Marzio, A.; Pagano, M. and Trauner, D. PHOTACs enable optical control of protein degradation. *Sci. Adv.* 2020, 6(8), eaay5064.
- 256. Ko, T.; Jou, C.; Grau-Perales, A. B.; Reynders, M.; Fenton, A. A. and Trauner, D. Photoactivated Protein Degrader for Optical Control of Synaptic Function. *ACS Chem. Neurosci.* **2023**, 14(19), 3704-3713.
- 257. Kraus, S:, Kolmann, T.; Yeung, A. and Deming, D. Chemokine reeptor antagonists: role in oncology. *Curr. Oncol. Rep.* **2021**, 23(11), 131.
- 258. Billen, M.; Schols, D. and Verwilst, P. Targeting chemokine receptors from the inside-out: discovery and development of small-molecule intracellular antagonists. *Chem. Commun.* **2022**, 58(26), 4132-4148.
- 259. Salchow, K., et al. A common intracellular allosteric binding site for antagonists of the CXCR2 receptor. *Br. J. Pharmacol.* **2010**, 159(7), 1429-1439.
- 260. Taveras, A. G.; Aki, C. J.; Bond, R. W.; Dwyer, M.; Ferreira, J. A.; Chao, J.; Yu, Y.; Baldwin, J. J.; Kaiser, B.; Merrit, J. R.; Biju, P. J.; Nelson JR, L.; Rokosz, L. L.; Jakway, J. P.; Lai, G.; Wu, M.; Hecker, E. A.; Lundell, D. and Fine, J. S. (2002). 3,4,-DI-SUBSTITUTED CYCLOBUTENE-1,2-DIONES AS CXC-CHEMOKINE RECEPTOR LIGANDS. WO2002083624A1.

- 261. Ellman, J. A. Applications of tert-butanesulfinamide in the asymmetric synthesis of amines. *Pure Appl. Chem.* **2003**, 75(1), 39-46.
- 262. Robak, M. T.; Herbage, M. A. and Ellman, J. A. Synthesis and Applications of tert-Butanesulfinamide. *Chem. Rev.* **2009**, 110(6), 3600-3740.
- 263. Békés, M.; Langley, D. R. and Crews, C. M. PROTAC targeted protein degraders: the past is prologue. *Nat. Rev. Drug Discov.* **2022**, 21(3), 181-200.
- 264. Schuhmacher, H.; Smith, R. L. and Williams, R. T. The Metabolism of Thalidomide: The Spontaneous Hydrolysis of Thalidomide in Solution. *Br. J. Pharmaco. Chemother.* **1965**, 25(2), 324-337.
- 265. Zhang, J.; Shukla, V. and Boger, D. L. Inverse Electron Demand Diels–Alder Reactions of Heterocyclic Azadienes, 1-Aza-1,3-Butadienes, Cyclopropenone Ketals, and Related Systems. A Retrospective. *J. Org. Chem.* **2019**, 84(15), 9397-9445.
- 266. Haldón, E.; Nicasio, M. C. and Pérez, P. J. Copper-catalysed azide—alkyne cycloadditions (CuAAC): an update. *Org. Biomol. Chem.* **2015**, 13, 9528-9550.
- 267. Mbua, N. E., Guo, J.; Wolfert, M. A., Street, R. and Boons, G.-J. Strain-promoted alkyne-azide cycloadditions (SPAAC) reveal new features of glycoconjugate biosynthesis. *Chembiochem.* **2011**, 12(12), 1912-1921.
- 268. Hein, J. E. and Vokin V. V. Copper-Catalyzed Azide-Alkyne Cycloaddition (CuAAC) and Beyond: New Reactivity of Copper(I) Acetylides. *Chem. Soc. Rev.* **2010**, 39, 1302-1315.

Appendix

This section contains the full-length publications and supporting information of the chapters 2, 3, 4, and 7. Please note that the copyright of the publications belongs to the publishers of the respective journals, as indicated by the copyright statements denoted before each paper.

Appendix I. Publication I: Fluorescent Ligands Enable Target Engagement Studies for the Intracellular Allosteric Binding Site of the Chemokine Receptor CXCR2

The following pages include the article "Fluorescent Ligands Enable Target Engagement Studies for the Intracellular Allosteric Binding Site of the Chemokine Receptor CXCR2" as it was published in Journal of Medicinal Chemistry by ACS Publications.

This article is reprinted with permission from:

Max E. Huber, Silas Wurnig, Lara Toy, Corinna Weiler, Nicole Merten, Evi Kostenis, Finn K. Hansen and Matthias Schiedel. Fluorescent Ligands Enable Target Engagement Studies for the Intracellular Allosteric Binding Site of the Chemokine Receptor CXCR2. *J. Med. Chem.* **2023**, *66*, 9916-9933.

Copyright © 2023 The Authors. Published by American Chemical Society. This publication is licensed under CC-BY 4.0.

This article has been removed from the appendix for legal reasons. The full text can be found here:

DOI: https://doi.org/10.1021/acs.jmedchem.3c00769

Link: Fluorescent Ligands Enable Target Engagement Studies for the Intracellular Allosteric Binding Site of the Chemokine Receptor CXCR2 | Journal of Medicinal Chemistry

Appendix II. Publication II: Development of a NanoBRET assay platform to detect intracellular ligands for the chemokine receptors CCR6 and CXCR1

The following pages include the article "Development of a NanoBRET assay platform to detect intracellular ligands for the chemokine receptors CCR6 and CXCR1" as it was published in ChemMedChem by Wiley-VCH.

This article is reprinted with permission from:

Max E. Huber, Silas L. Wurnig, Aurélien F. A. Moumbock, Lara Toy, Evi Kostenis, Ana Alonso Bartolomé, Martyna Szpakowska, Andy Chevigné, Stefan Günther, Finn K. Hansen and Matthias Schiedel. Development of a NanoBRET assay platform to detect intracellular ligands for the chemokine receptors CCR6 and CXCR1. *ChemMedChem* **2024**, e202400284.

Copyright © 2024. The Authors. ChemMedChem Published by Wiley-VCH GmbH. This publication is licensed under CC BY-NC-ND 4.0

This article has been removed from the appendix for legal reasons. The full text can be found here:

DOI: https://doi.org/10.1002/cmdc.202400284

Link: https://chemistry-europe.onlinelibrary.wiley.com/doi/epdf/10.1002/cmdc.202400284

Appendix III. Publication III: A fluorescent probe enables the discovery of improved antagonists targeting the intracellular allosteric binding site of the chemokine receptor CCR7

The following pages include the article "A fluorescent probe enables the discovery of improved antagonists targeting the intracellular allosteric binding site of the chemokine receptor CCR7" as it was published in the Journal of Medicinal Chemistry by ACS Publications.

This article is reprinted with permission from:

Silas L. Wurnig, Max E. Huber, Corinna Weiler, Hanna Baltrukevich, Nicole Merten, Isabel Stötzel, Yinshui Chang, René H. L. Klammer, Dirk Baumjohann, Eva Kiermaier, Peter Kolb, Evi Kostenis, Matthias Schiedel and Finn K. Hansen. A fluorescent probe enables the discovery of improved antagonists targeting the intracellular allosteric binding site of the chemokine receptor CCR7 *J. Med. Chem.* **2025**, *68*, 4, 4308–4333.

Copyright © 2025 American Chemical Society. This publication is licensed under CC-BY 4.0.

This article has been removed from the appendix for legal reasons. The full text can be found here:

DOI: https://doi.org/10.1021/acs.jmedchem.4c02102

Link: A Fluorescent Probe Enables the Discovery of Improved Antagonists Targeting the Intracellular Allosteric Site of the Chemokine Receptor CCR7 | Journal of Medicinal Chemistry

Appendix IV. Publication IV: Light-Activatable Photochemically Targeting Chimeras (PHOTACs) Enable the Optical Control of Targeted Protein Degradation of HDAC6

The following pages include the article "Light-Activatable Photochemically Targeting Chimeras (PHOTACs) Enable the Optical Control of Targeted Protein Degradation of HDAC6" as it was published in.

This article is reprinted with permission from:

Silas L. Wurnig,[‡] Maria Hanl,[‡] Thomas M. Geiger, Shiyang Zhai, Ina Dressel, Dominika E. Pieńkowska, Radosław P. Nowak, Finn K. Hansen* Light-Activatable Photochemically Targeting Chimeras (PHOTACs) Enable the Optical Control of Targeted Protein Degradation of HDAC6 *RSC Med. Chem.*, **2025**, 16, 2452-2459

Copyright © 2025 Royal Society of Chemistry.

This article has been removed from the appendix for legal reasons. The full text can be found here:

DOI: https://doi.org/10.1039/D4MD00972J

Link: <u>Light-activatable photochemically targeting chimeras (PHOTACs) enable the optical control of targeted protein degradation of HDAC6 - RSC Medicinal Chemistry (RSC Publishing)</u>